

# Quidico Bay

Design proposal for a new fishing harbour in the bay of Quidico

Falko Noortman  
Mark Ruessink  
Mathijs Mann  
Ronald Verlinde  
Wouter Sonnema



Universidad  
de Concepción

TU Delft



# Quidico Bay

Design proposal for a new fishing harbour in the bay of Quidico

Falko Noortman	4218213
Mathijs Mann	4224434
Mark Ruessink	4237137
Ronald Verlinde	4251547
Wouter Sonnema	4239695

Group number: MP240

Project duration: November 13, 2017 – January 19, 2018

Project supervisors:	Ir. L.J.M. Houben,	TU Delft
	Dr. ir. D.J.M. Ngan-Tillard,	TU Delft
	Ir. H.J. Verhagen,	TU Delft
	Dr. M.A. Pradena Miquel,	UdeC



March 4<sup>th</sup> 1835

*"The next day I landed at Talcahuano, and afterwards rode to Concepcion. Both towns presented the most awful yet interesting spectacle I ever beheld. To a person who had formerly know them, it possibly might have been still more impressive; for the ruins were so mingled together, and the whole scene possessed so little the air of a habitable place, that it was scarcely possible to imagine its former condition. The earthquake commenced at half-past eleven o'clock in the forenoon. If it had happened in the middle of the night, the greater number of the inhabitants (which in this one province must amount to many thousands) must have perished, instead of less than a hundred: as it was, the invariable practice of running out of doors at the first trembling of the ground, alone saved them. In Concepcion each house, or row of houses, stood by itself, a heap or line of ruins; but in Talcahuano, owing to the great wave, little more than one layer of bricks, tiles, and timber with here and there part of a wall left standing, could be distinguished. From this circumstance Concepcion, although not so completely desolated, was a more terrible, and if I may so call it, picturesque sight. The first shock was very sudden. The mayor-domo at Quiriquina told me, that the first notice he received of it, was finding both the horse he rode and himself, rolling together on the ground. Rising up, he was again thrown down. He also told me that some cows which were standing on the steep side of the island were rolled into the sea. The great wave caused the destruction of many cattle; on one low island near the head of the bay, seventy animals were washed off and drowned. It is generally thought that this has been the worst earthquake ever recorded in Chile; but as the very severe ones occur only after long intervals, this cannot easily be known; nor indeed would a much worse shock have made any difference, for the ruin was now complete. Innumerable small tremblings followed the great earthquake, and within the first twelve days no less than three hundred were counted."*

Charles Robert Darwin

# Preface

This report is a design proposal for the fishing harbour in the bay of Quidico, located in South Central Chile. The report is part of a Multidisciplinary Project conducted by a group of five master students from Delft University of Technology. Within the group three different master specialisations are represented, including Geo-Engineering, Hydraulic Engineering and Structural Engineering. Throughout the project the group has been able to combine the individual acquired knowledge and to gain practical experience by executing an actual civil project.

The project is commissioned by the Department of Ports, one of the six executive departments of the Ministry of Public Works. The improvement of the fishing harbour in Quidico Bay is part of the objective of the Ministry to redevelop ports and coastal infrastructure along the whole coast of Chile.

The new design of the fishing harbour at Quidico Bay should offer the possibility for fishermen to unload their goods, store their equipment, berth safely and accommodate their offices. In the current situation high waves, a strong current and significant sediment transport hamper the effectiveness of the bay as fishing harbour. Also qualitative onshore structures to facilitate housing for onshore activities contribute to the functionality of the harbour.

In cooperation with the Department of Ports and Universidad de Concepción the group analysed the current situation and formulated a design proposal. From the 13<sup>th</sup> of November 2017 till the 19<sup>th</sup> of January 2018 the three parties worked closely together, under the guidance of Dr. M.A. Pradena Miquel. As part of this collaboration several site visits, meetings, discussions and presentations have been organised.

Falko Johannes Noortman  
Mark Ruessink  
Mathijs Mann  
Ronald Paul Verlinde  
Wouter Sonnema

Structural Engineering  
Hydraulic Engineering  
Hydraulic Engineering  
Structural Engineering  
Geo and- Structural Engineering



# Acknowledgements

We would like to express our deep gratitude to Dr. Mauricio A. Pradena Miquel for his effort in setting up this project. His willingness to invest his time in the project and our well-being has been very much appreciated. It started with an email conversation back in October 2016, right from the start Mauricio not only enthused us for the project itself but also for Chile, Concepcion and for the Universidad de Concepción. Throughout the past year we have been in close contact, Mauricio supported us in finding accommodation, prepared us for our stay and introduced us at the Universidad de Concepción. During our stay in Concepción the logistics and project set-up was organised smoothly. Now, at the end of January 2018 and 15 months after our first contact, we would like to thank Mauricio for all he did for us.

The project has been realised in cooperation with the Department of Ports, a department of the Ministry of Public Works. We are particularly grateful for the technical support given by and hospitality of Cristian Figueroa de la Hoz and Fernando Matamala Cabezas. Their will to get us involved in this interesting and challenging project made our cooperation to a success. We appreciated the possibility to work in an actual project and enjoyed learning from these experienced engineers of the DoP.

Our office was based at the Civil Engineering department of Universidad de Concepción. Throughout the project we have been assisted by several professors and experts from the UdeC, we wish to acknowledge the help provided by Dr. Peter Dechent, Ing. Mario Valenzuela, Dr. Rodrigo Silva and Alfonso Neumann.

During the preparations and the actual project, the support and guidance provided by our supervisors from the Delft University of Technology have been of great value. We would like to express our very great appreciation to Ir. Henk Jan Verhagen, Dr. Ir. Dominique Ngan-Tillard and Ir. Lambert Houben.

Special thanks should be given to Javiera Martin, Boris Trocas Castro Valdes and Alvaro Nicolas Sanhueza Orias. Javiera and Boris have worked extensively on the pavement design and Alvaro has been of great value for the breakwater design. They also introduced us to the Chilean way of Engineering and made our stay at the UdeC comfortable. It has been a pleasure to share each others experiences. We would like to extend our thanks to Vilma Silva and José Barrientos of the UdeC, each day we were welcomed with some cake and coffee. In case of any difficulties they were always there for us. Furthermore, we would like to express our gratitude to Andrés Neumann Lira for having us in the beautiful apartment EcoApart.

Lastly, this project would not have been possible without the help of our sponsors and partners. They motivated, stimulated and supported us in all possible ways. We would therefore like to thank BAM International, DIMI, Royal HaskoningDHV, Witteveen+Bos, BMT ARGOSS, Deltares, PLAXIS, Waterbouwfonds and FIS.

## Sponsors



## Partners



# Report outline

This multidisciplinary project is divided into three parts. Similar as the process followed during the project, first the analysis is presented, followed by the different designs. In the final part of the report, the appendices, additional information and calculations are provided.

## **Part 1 - Analysis**

An introduction of Quidico and the adjacent bay is provided within this analysis. The Department of Ports performed a preliminary study for the bay of Quidico to determine the required improvements for the bay as fishing harbour. Based on these requirements the DoP proposed a preliminary design for near-shore and on-shore structures. This process is expanded in the problem analysis.

The proposed preliminary design contains several uncertainties and problems which require a thorough analysis, from which new requirements follow. The problem definition states the different requirements for several specific structures, including the breakwater, onshore facilities, mooring facility and support area.

The problem definition is followed by defining the boundary conditions of Quidico, and more specifically Quidico Bay. These are divided into geo-technical, hydraulic and structural related conditions. The boundary conditions are used during the design phase to ensure the proposed designs fulfill the needs and requirements.

## **Part 2 - Designs**

In the 'Design'-part, designs for the specific structures (breakwater, onshore facilities, mooring facility and support area) are presented in separate chapters. Several alternatives are proposed for each of the structures. Hand-calculations and software models (Delft3D, PLAXIS and ETABS) are used to validate the designs. The calculations, model results and design drawings are presented at the end of each design-chapter. After evaluation of the designs, conclusions and recommendations are presented in the final step.

## **Part 3 - Appendices**

The appendices contain additional calculations and information to complement the main report.

# Summary

Quidico is a small town, approximately 200 kilometers south of Concepcion. In the bay adjacent to Quidico town, a great number of local fishermen are active. In the current situation, high waves, a strong current and significant sediment transport hamper the effectiveness of the bay as fishing harbour. Also qualitative onshore facilities to support onshore activities of the fishermen, are absent. The Department of Ports of the Ministry of Public Works, developed a preliminary design proposal, to solve these problems. However, after consultation with the fishermen, this proposal was declared unsatisfactory. Therefore, an additional study is performed to develop a new integral design for the bay of Quidico. The desired design consists of onshore buildings, a paved support area, mooring facilities and breakwaters to create shelter for safe mooring of the fishing boats. Furthermore, these breakwaters should mitigate the problems related to sediment transport.

To develop a new breakwater orientation and design, wave data is analysed. Waves coming from the south to south-west are most common, but not guiding due to the sheltering factor of Island Mocha, positioned in front of the coast. The guiding wave, which is coming from the north-west, is implemented in models of Delft3D to see what the new orientation of the breakwater should be. Based on the wave analysis, sediment transport analysis and modelling results, a new breakwater orientation is determined, that fulfills all requirements prescribed by the DoP. After defining this new orientation, the influence of the breakwater on sediment and waves is analysed. Due to the new orientation, a new design of the breakwater is made.

The fishing harbour should offer the possibility for the fisherman to unload their goods and berth safely. The DoP proposed the construction of a mooring facility along the south-west shoreline of Quidico Bay. Two types of quay walls for the mooring facilities are proposed, a sheet pile wall and a concrete mass wall. For both types a preliminary design is developed, by making use of the 2D finite element software PLAXIS and hand calculations. The preferred mooring facility design mainly depends on the soil conditions at the specific location. From the boundary conditions it is concluded the bedrock is found at a depth of 60m, the soil above mainly consists of sand. Therefore the construction a sheet pile wall to serve as mooring facility, is recommended.

In the initial design of the Department of Ports, six separate masonry buildings are proposed to accommodate the desired supporting facilities. These buildings cover a large area of the bay and will require a large paved supporting platform. To reduce this paved area, the DoP is interested in a more compact design, that includes all supporting facilities in one multi-storey building. In consultation with the DoP two different designs are developed; a three-storey steel building and a two-storey concrete building. A structural design is developed within the boundaries set by the functional design requirements. Next, a structural analysis is performed by making use of finite element software (ETABS) and a final design is obtained for both buildings. The concrete building is concluded to be the most suitable option for the DoP.

Quick offloading of the boats and smooth transshipment of goods is hindered due to the lack of a good support area and access road. The DoP proposed a design for both pavements in their preliminary study, but it was requested to evaluate different alternatives. Three different pavement technologies are proposed for the access road: surface treatment, asphalt and concrete slabs. For the pavement in the support area concrete slabs are the preferred solution. To achieve an optimal pavement design that fulfills all structural and serviceability requirements throughout the full design life, slab pavements with different dimensions and thicknesses are evaluated. In conclusion, short concrete slabs are the preferred pavement for both areas. Short slab pavement is an upcoming technology that has great advantages in terms of structural performance and costs.

# Contents

## List of Tables

## List of Figures

## List of Symbols

## PART 1: ANALYSIS

<b>1</b>	<b>Introduction</b>	<b>1</b>
1.1	General background . . . . .	1
1.2	Project area . . . . .	1
1.3	Project site . . . . .	2
<b>2</b>	<b>Problem Analysis</b>	<b>3</b>
2.1	Problem analysis current situation . . . . .	3
2.2	Design proposal Department of Ports . . . . .	4
<b>3</b>	<b>Problem Definition</b>	<b>6</b>
3.1	Breakwater . . . . .	6
3.2	Onshore buildings . . . . .	6
3.3	Mooring facility . . . . .	7
3.4	Pavements . . . . .	7
3.5	Schematic overview . . . . .	8
<b>4</b>	<b>Boundary Conditions</b>	<b>9</b>
4.1	Geo-technical conditions . . . . .	9
4.2	Hydraulic conditions . . . . .	18
4.3	Structural conditions . . . . .	28

## PART 2: DESIGNS

<b>5</b>	<b>Breakwater Configuration and Design</b>	<b>29</b>
5.1	Design approach . . . . .	29
5.2	Design requirements . . . . .	29
5.3	Design alternatives . . . . .	30
5.4	Modelling phase . . . . .	31
5.5	Additional analysis . . . . .	35
5.6	Final breakwater orientation . . . . .	37
5.7	Sediment movement around Quidico . . . . .	39
5.8	Breakwater design . . . . .	44
<b>6</b>	<b>Mooring Facility Design</b>	<b>48</b>
6.1	Sheet pile wall . . . . .	48
6.2	Concrete mass wall . . . . .	52
<b>7</b>	<b>Steel Building Design</b>	<b>56</b>
7.1	Design approach . . . . .	56
7.2	Functional design . . . . .	56
7.3	Global structural design . . . . .	57
7.4	Structural analysis . . . . .	61

7.5	Structural design on an element level . . . . .	62
7.6	Summary structural checks . . . . .	66
<b>8</b>	<b>Concrete Building Design</b>	<b>67</b>
8.1	Design approach . . . . .	67
8.2	Functional design . . . . .	68
8.3	Global structural design . . . . .	69
8.4	Structural analysis . . . . .	71
8.5	Structural design on an element level . . . . .	71
<b>9</b>	<b>Pavement Design</b>	<b>75</b>
9.1	Support area . . . . .	75
9.2	Access road . . . . .	77
<b>10</b>	<b>Conclusion and Recommendations</b>	<b>81</b>
10.1	Conclusion . . . . .	81
10.2	Recommendation . . . . .	82
 <b><u>PART 3: APPENDICES</u></b>		
<b>A</b>	<b>Stakeholder Analysis</b>	<b>84</b>
<b>B</b>	<b>Site Visit Quidico</b>	<b>86</b>
<b>C</b>	<b>Geo-Technical Conditions</b>	<b>90</b>
<b>D</b>	<b>Statistical Wave Analysis</b>	<b>99</b>
<b>E</b>	<b>Model Set-Up Delft3D</b>	<b>108</b>
<b>F</b>	<b>Delft3D Model Results</b>	<b>112</b>
<b>G</b>	<b>Sediments</b>	<b>123</b>
<b>H</b>	<b>Breakwater</b>	<b>127</b>
<b>I</b>	<b>Mooring Facility</b>	<b>142</b>
<b>J</b>	<b>Steel Building</b>	<b>148</b>
<b>K</b>	<b>Concrete Building</b>	<b>162</b>
<b>L</b>	<b>Pavement Support Area</b>	<b>168</b>
<b>M</b>	<b>Pavement Access Road</b>	<b>173</b>
<b>N</b>	<b>Meetings, Presentations and Lectures</b>	<b>178</b>
<b>O</b>	<b>Relevant Rules and Regulations</b>	<b>189</b>

# List of Tables

4.1	Descriptive classification of the soil layers. . . . .	12
4.2	The geo-technical properties of the sand in Quidico bay. . . . .	13
4.3	Relation between the number of blow counts and the unconfined compressive strength (Terzaghi and Peck 1948) . . . . .	16
4.4	Values for Sea waves from ARGOSS . . . . .	21
4.5	Values for Swell waves from ARGOSS . . . . .	21
4.6	Swell numbers from the Chilean data . . . . .	21
4.7	Offshore values for a return period of 50 years (ARGOSS) . . . . .	25
4.8	Offshore values for a return period of 50 years (Oleaje Atlas) . . . . .	26
4.9	The guiding wave height and period found for waves coming from 270 till 360 degrees . . . . .	26
4.10	Final values for the hydraulic boundary conditions. . . . .	27
4.11	Equivalent axle factor and traffic load for a 20 year design lifetime . . . . .	28
5.1	Input data for the different models in Delft3D. . . . .	30
5.2	The rules for calculate the dimensions of the filter and core layer . . . . .	44
5.3	All weights for each breakwater layer . . . . .	45
6.1	Section properties of the sheet pile type "LARSEN 601". . . . .	49
6.2	Active and passive earth pressure coefficients for sand and granular backfill. . . . .	49
6.3	The maximum anchor force and maximum bending moment and shear force in the sheet pile wall for the two load-case. . . . .	50
6.4	Unity Check results for the maximum bending moment and maximum shear force in the sheet pile wall, calculated for load-case 1 and 2. . . . .	50
6.5	Anchor capacity for a plate height of 1.0 m for load-case 1 and 2. . . . .	51
6.6	Two possible anchor types ( <i>Sheet Piling Handbook</i> 2010). . . . .	52
6.7	Summary loads concrete mass wall . . . . .	54
6.8	Safety factors concrete mass wall . . . . .	54
6.9	Unity checks concrete mass wall . . . . .	54
7.1	Overview loads steel building . . . . .	60
7.2	LRDF Load Combinations . . . . .	61
7.3	Summary unity checks . . . . .	66
8.1	Overview of load cases for the concrete building design . . . . .	71
8.2	Summary structural components . . . . .	74
9.1	Overview parameters used for traditional slab design equations . . . . .	76
9.2	Calculated slab thickness for traditional slabs . . . . .	76
9.3	Design parameters short slab pavement support area . . . . .	77
9.4	Design verification short slabs support area . . . . .	77
9.5	Final surface treatment design for access road . . . . .	78
9.6	List of design parameters asphalt pavement . . . . .	79
9.7	Final design: layer thickness and characteristics . . . . .	79
9.8	Design parameters short slab pavement access road . . . . .	80
9.9	Design verification short slabs access road . . . . .	80

A.1	Primary Stakeholders . . . . .	84
A.2	Secondary stakeholders . . . . .	85
A.3	Interface stakeholders . . . . .	85
C.1	Densities of the soil types. . . . .	90
C.2	Granulometric analysis of the soil samples. . . . .	91
D.1	Obtained a-values to calculate the wave periods . . . . .	105
D.2	Offshore values for a return period of 50 years, ARGOSS . . . . .	105
D.3	Offshore values for a return period of 50 years, Oleaje . . . . .	105
E.1	Delft3D input for the first models . . . . .	111
H.1	List of used symbols . . . . .	127
H.2	Nominal diameter and weight for the armour layer . . . . .	128
H.3	Design rules to calculate the dimensions of the filter and core layer . . . . .	128
H.4	Stone sizes for all layers of the breakwater . . . . .	128
H.5	Parameters to calculate the stone sizes of the contramolo . . . . .	128
H.6	Stone size and weight for armour layer . . . . .	128
H.7	Stone sizes for the contramolo . . . . .	129
H.8	Parameters used for calculating the toe . . . . .	129
H.9	Values used for the toe . . . . .	130
H.10	Dimensions of the toe . . . . .	130
H.11	Crown wall stability parameters . . . . .	130
H.12	Geometry for the crown wall . . . . .	131
H.13	Values used to fill in the Iribarren formula . . . . .	132
H.14	Calculated values for the run-up and crown-wall heights . . . . .	132
H.15	Pressures . . . . .	132
H.16	Areas and their corresponding weight of the crown wall . . . . .	133
H.17	Safety coefficients used for the crown wall . . . . .	133
H.18	Explanation of the forces and their calculated values . . . . .	133
H.19	Unity check for sliding of the Crown Wall . . . . .	133
H.20	Moments acting on the crown wall to calculate the overturning moment . . . . .	134
H.21	Unity check for the overturning moment . . . . .	134
H.22	Overtopping values used . . . . .	135
H.23	Values used to calculate the overtopping limits . . . . .	135
H.24	Overtopping results . . . . .	135
H.25	Summary of the used stone sizes . . . . .	136
H.26	Geo-technical properties of different types of sand. . . . .	138
H.27	Geo-technical properties of the core, filter and armour. . . . .	139
I.1	Soil properties for definition of the soil stratigraphy at the mooring facility. . . . .	142
I.2	Material properties of the sheet pile wall and the anchor. . . . .	143
I.3	The maximum bending moment and shear force in the sheet pile wall during construction phase.144	
I.4	The values for wall bending moment, wall shear force and anchor force for different anchor depths. . . . .	144
I.5	Capacity of the anchor plate for load-case 1 and load-case 2. . . . .	147
J.1	Design checks beam to beam joint . . . . .	151
J.2	Design checks column to transverse beam joint . . . . .	151
J.3	Design checks column to longitudinal beam joint . . . . .	151
J.4	Design checks column to foundation connection . . . . .	157
K.1	Governing column element details . . . . .	163
K.2	Column: Design axial force and biaxial moment interaction . . . . .	163
K.3	Column: Design shear force and reinforcement . . . . .	163
K.4	Governing beam element details . . . . .	163

K.5	Beam: Flexural design moment and reinforcement . . . . .	163
K.6	Beam: Design shear force and reinforcement . . . . .	164
K.7	Governing wall element details . . . . .	164
K.8	Wall: Design axial force and bi-axial moment interaction . . . . .	165
K.9	Wall: Design shear force and reinforcement . . . . .	165
L.1	Reliability level and value of S0 . . . . .	168
M.1	structural coefficient for bases between 0 and 250 mm . . . . .	173
M.2	Structural coefficients for subbases between 250 and 500 mm . . . . .	173
M.3	Structural coefficients for subgrade between 500 and 900 mm . . . . .	173
M.4	Reliability level and value of S0 for flexible pavements . . . . .	175
M.5	Final design layer thickness and properties . . . . .	176
M.6	Minimum required and provided NE . . . . .	176
M.7	Soil parameters required for short slab design . . . . .	176
N.1	Overview meetings in chronological order . . . . .	178
N.2	Abbreviations of attendees . . . . .	179

# List of Figures

1.1	Schematic timeline of the project . . . . .	1
1.2	Location of Quidico in Chile . . . . .	1
1.3	Impression of Quidico Bay including cocinerias . . . . .	2
1.4	Overview current situation of Quidico Bay . . . . .	2
2.1	Schematic overview design proposal by the Department of Ports. . . . .	4
2.2	Cross section of main breakwater including weight of stone layers . . . . .	4
2.3	Design proposal by the Department of Ports, 3D view . . . . .	5
3.1	Schematic representation of the problem definition. . . . .	8
4.1	Map of geological units in South-Central Chile (Glodny et al. 2008). . . . .	9
4.2	(a) Tectonic plates and their names (USGS 2011). (b) Accretionary prism formation process (Krueger and Gilbert 2009). . . . .	10
4.3	Rock outcrops at Quidico Bay. . . . .	10
4.4	Geological map of Quidico Bay and its surrounding (Sernageomin 2000). P11m and Q1 sedimentary sequence correspond to marine/fluviol sediments and colluvium/alluvium processes respectively. . . . .	11
4.5	Map indicating the positions of the different tests performed (Google-Earth 2017). . . . .	12
4.6	Profile of the number of SPT blow counts over depth. . . . .	13
4.7	Graph of the frequency versus the phase velocity of the combined results of the REMI and MASW test. . . . .	15
4.8	(a) Graph of the H/V spectral ratio. (b) Graph of the shear wave velocity profile over depth. . . . .	15
4.9	Figure 4.1 and table 4.2 from NCh433-1996. . . . .	16
4.10	Vespucio Norte Express bridge, liquefaction was one of the causes for collapse (Maldonado, 2010). . . . .	17
4.11	UTM zone Quidico bay . . . . .	18
4.12	Nautical convention (Deltares 2014) . . . . .	18
4.13	Data from ARGOSS . . . . .	19
4.14	Location Atlas . . . . .	19
4.15	Wind rose, from ARGOSS, offshore of Quidico bay . . . . .	20
4.16	Wind waves, from ARGOSS, offshore of Quidico bay . . . . .	20
4.17	Wave roses from both data bases. . . . .	22
4.18	Oceanic currents (Wikipedia 2017) . . . . .	22
4.19	Tides . . . . .	23
4.20	Tidal system for the bay of Quidico. With: HAT = Highest Astronomical Tide, MSL = Mean Sea Level, LAT = Lowest Astronomical Tide . . . . .	23
4.21	Depth points around Quidico bay . . . . .	24
4.22	Bathymetry offshore and nearshore of Quidico . . . . .	25
4.23	HS 20-44 Truck . . . . .	28
5.1	Foundation consisting of stones in front of the headland . . . . .	29
5.2	(a) The new proposed breakwater orientation. (b) Initial and new proposed breakwater orientation. . . . .	30
5.3	Satellite image from Google Earth plotted over the initial bed file from Delft3D. The white arrow is pointing at the bay of Quidico. . . . .	31

5.4	Model results compared with Google Earth . . . . .	32
5.5	Three configurations of the breakwater . . . . .	32
5.6	Wave height directions plotted with the longest proposed breakwater (indicated in blue) and the initial design from the DoP (indicated in black) . . . . .	33
5.7	Comparison of wave induced currents with the breakwater (black arrows) and without a breakwater (white arrows) . . . . .	34
5.8	Wave diffraction around an object . . . . .	35
5.9	Sommerfeld graph for the wave diffraction . . . . .	36
5.10	The long-term coastal influences of both breakwaters . . . . .	37
5.11	The final orientations of the main breakwater and contramolo . . . . .	38
5.12	(a) Accretion at the left side of a breakwater. (b) Accretion and erosion around a breakwater. (Bosboom and Stive 2015) . . . . .	40
5.13	Sedimentation around a large concrete groyne in Newhaven, East Sussex, England . . . . .	41
5.14	(a) Downdrift accretion in reality. (b) General processes around a headland. (Bosboom and Stive 2015) . . . . .	41
5.15	The coastline indication the main breakwater and contramolo . . . . .	42
5.16	(a) Situation directly after building the breakwater. (b) Longterm situation for the bay of Quidico. . . . .	42
5.17	(a) The proposed guide bund for the river. (b) The initial plan of the Department of Ports. . . . .	43
5.18	Final crown design including dimensions. . . . .	46
5.19	Final breakwater cross-section. . . . .	46
6.1	Overview of the main dimensions and situation of the sheet pile wall. . . . .	48
6.2	The different water levels, measured from the seabed. . . . .	48
6.3	The "LARSSSEN 601" sheet pile profile. . . . .	49
6.4	The design and position of the anchor, anchor plate and sheet pile wall, including dimensions. . . . .	51
6.5	Overview of the main dimensions and situation of the concrete mass wall . . . . .	53
7.1	3D view steel building design (without windows) . . . . .	56
7.2	Structural design steel building . . . . .	57
7.3	Overview geometry in ETABS . . . . .	61
7.4	3D view of structural model . . . . .	62
7.5	Steel section: column/longitudinal beam (left) and transverse beam (right) . . . . .	63
7.6	Steel section: vertical bracing (left) and roof bracing (right) . . . . .	63
7.7	Overview of the final joint designs, including dimensions . . . . .	64
7.8	Composite deck section . . . . .	65
7.9	Foundation for steel building . . . . .	65
7.10	Connection column to foundation . . . . .	66
8.1	Concrete building 3d view . . . . .	67
8.2	Concrete building front view . . . . .	68
8.3	Concrete building floor plans . . . . .	68
8.4	Structural model of concrete building . . . . .	69
8.5	Concrete cross-sections: Outer walls (left), Inner walls (right). Units in mm . . . . .	72
8.6	Concrete cross-sections: Beam (left), Column (right). Units in mm . . . . .	72
8.7	Concrete cross-sections: Roof slab (left), Floor slab (right), Units in mm . . . . .	73
8.8	Concrete slab roof with timber frame . . . . .	73
8.9	Strip foundation plan for concrete building . . . . .	74
8.10	Foundation for concrete building . . . . .	74
9.1	Surface treatment layers . . . . .	78
10.1	Overview of design proposal for Quidico Bay, including contramolo . . . . .	81
B.1	Quidico Bay, photo taken in northern direction . . . . .	86
B.2	Quidico Bay, photo taken in northern direction . . . . .	87
B.3	Quidico Bay, photo taken in eastern direction . . . . .	87
B.4	Quidico Bay, panorama of the whole bay . . . . .	87

B.7	Seismic wave analysis performed at the beach next to Quidico Bay . . . . .	89
B.8	Reference bay and harbour at Tirua, 10km south of Quidico . . . . .	89
C.1	Soil Classification chart from ASTM-International 2006. . . . .	91
C.2	Analysed soil samples from Quidico Bay, the analysis is performed at UdeC. . . . .	93
C.3	The corrected blow counts and the corresponding liquefaction potential over the depth. . . . .	94
C.4	The raw SPT data used for defining the geo-technical boundary conditions. . . . .	95
C.5	(a) Surface wave dispersion in a homogeneous and heterogeneous subsurface. (b) Different shapes of dispersion curves. (Pei 2007) . . . . .	96
C.6	(a) Modes of surface waves. (b) Dispersion curves of different modes of surface waves. (Pei 2007) . . . . .	96
C.7	Schematic representation of the inverse analysis followed during the seismic data analysis. (Pei 2007) . . . . .	97
C.8	Results of the REMI test, with on the left the time versus the amplitude of each of the geophones and on the right the Rayleigh wave dispersion curve. . . . .	97
C.9	Results of the MASW test, with on the left the time versus the amplitude of each of the geophones and on the right the Rayleigh wave dispersion curve. . . . .	98
C.10	Results of the HVSR test, with on the left the Fourier amplitude versus the time of the three principal directions individually and combined and on the right the H/V spectral ratio. . . . .	98
D.1	Data obtained from ARGOSS . . . . .	99
D.2	Location of measurement from Atlas de Oleaje . . . . .	100
D.3	Peak over Threshold analysis for the ARGOSS database . . . . .	101
D.4	Storing of the storms in bins with a bin-width of 0.1 meter . . . . .	101
D.5	Wave height versus the reduced Gumbel variable . . . . .	102
D.6	Wave height versus the reduced Weibull variable . . . . .	103
D.7	Wave height versus the reduced Exponential variable . . . . .	104
D.8	Refraction at a coast . . . . .	107
D.9	Part of the calculation sheet called WAVESHOREF . . . . .	107
E.1	Landboundary . . . . .	109
E.2	Model input . . . . .	109
E.3	Scheme of all steps during modelling. . . . .	110
E.4	Three configurations of the breakwater . . . . .	111
E.5	Three configurations of the breakwater . . . . .	111
E.1	Satellite image from Google Earth plotted over the initial bed file from Delft3D . . . . .	112
E.2	Figures to validate the model and to analyse the processes in Quidico . . . . .	113
E.3	Three wave directions plotted in one figure . . . . .	114
E.4	The current directions without any breakwater . . . . .	115
E.5	The current directions with the 50 m breakwater . . . . .	115
E.6	The current directions with the 100 m breakwater . . . . .	116
E.7	The current directions with the 150 m breakwater . . . . .	116
E.8	Currents due to waves which come from 270 degrees, for all lengths of breakwaters . . . . .	117
E.9	Currents due to waves which come from 292.5 degrees, for all lengths of breakwaters . . . . .	118
E.10	Currents due to waves which come from 315 degrees, for all lengths of breakwaters . . . . .	119
E.11	The wave directions without any breakwater . . . . .	120
E.12	The wave directions with the 50 m breakwater . . . . .	121
E.13	The wave directions with the 100 m breakwater . . . . .	121
E.14	The wave directions with the 150 m breakwater . . . . .	122
G.1	Velocity, concentration and sediment transport profiles (Bosboom and Stive 2015) . . . . .	124
G.2	Influence of waves on the bottom (Bosboom and Stive 2015) . . . . .	124
G.3	Evolution of the coast around the bay of Quidico obtained from Google Earth . . . . .	125
G.4	Influence of the island on the water depths (Navionics 2017) . . . . .	126
G.5	Water depths in front of Quidico due to the island (Navionics 2017) . . . . .	126
H.1	Toe stability formula . . . . .	129

H.2	General crown wall geometry . . . . .	131
H.3	Two different crown wall geometries . . . . .	131
H.4	Total design of the breakwater including toe and crown wall . . . . .	136
H.5	Chosen dimensions for the Crown Wall . . . . .	136
H.6	Costs for the Breakwater and contramolo . . . . .	137
H.7	PLAXIS model of the breakwater. . . . .	138
H.8	Upper settlement limit PLAXIS model. . . . .	139
H.9	Lower settlement limit PLAXIS model. . . . .	140
H.10	(a) Governing failure mechanism and (b) factor of safety calculation for the breakwater using the soft sand conditions. . . . .	140
H.11	(a) Governing failure mechanism and (b) factor of safety calculation for the breakwater using the strong sand conditions. . . . .	141
I.1	Overview of the governing situation during construction of the sheet pile wall. . . . .	144
I.2	The displacements for sheet pile wall load-case 1. . . . .	145
I.3	The shear force (a) and bending moment (b) distribution in and the horizontal displacement (c) of the sheet pile wall for load-case 1. The maximum bending moment is 42.2 kNm/m, the maximum shear force is 59.2 kN/m and the maximum horizontal displacement is 5 mm. . . . .	145
I.4	The deformations for sheet pile wall load-case 2 (scaled up 100 times). . . . .	146
I.5	The shear force (a) and bending moment (b) distribution in and the horizontal displacement (c) of the sheet pile wall for load-case 1. The maximum bending moment is 33.8 kNm/m, the maximum shear force is 53.9 kN/m and the maximum horizontal displacement is 4 mm. . . . .	146
I.6	The active and passive lateral earth pressure working on the anchor plate. . . . .	147
J.1	Unity checks steel structural members . . . . .	160
J.2	Unity checks composite members . . . . .	160
J.3	Unity checks joints side view . . . . .	161
J.4	Unity checks joints front view . . . . .	161
J.5	Unity checks joints top view second floor . . . . .	161
K.1	Column layout of concrete building design . . . . .	162
K.2	Beam layout of concrete building design . . . . .	164
K.3	Concrete floor slab: strip layout . . . . .	165
K.4	Concrete floor slab (strip FS1): geometry, moment diagram and reinforcement . . . . .	166
K.5	Concrete floor slab (strip FS2 and FS3): geometry, moment diagram and reinforcement . . . . .	166
K.6	Concrete roof slab: strip layout . . . . .	167
K.7	Concrete roof slab strips: geometry, moment diagram and reinforcement . . . . .	167
L.1	Crack width design check . . . . .	172
L.2	Mean amount of faulting design check . . . . .	172
L.3	IRI design check . . . . .	172
N.1	All attendees at the first meeting at the DoP . . . . .	180
N.2	Reference building Talcahuano . . . . .	181
N.3	Steel mooring facility Talcahuano . . . . .	182
N.4	Quay wall Tumbes . . . . .	182
N.5	Meeting at the Department of Ports . . . . .	184
N.6	Reference building Coliumo . . . . .	185
N.7	Waves just outside Quidico Bay . . . . .	186
N.8	Final presentation for the DoP . . . . .	187

# List of Symbols

Symbol	Unit	Definition
$\alpha$	-	Fines content parameter
$\beta$	-	Fines content parameter
$\delta$	mm	deflection
$\Delta$	-	Relative density
$\lambda$	-	Slenderness ratio
$\mu$	-	Poisson's coefficient
$\phi$	°	Internal friction angle
$\phi$	-	Resistance factor
$\psi$	°	Dilatancy angle
$\nu$	-	Poisson's ratio
$\rho_w$	kg/m <sup>3</sup>	Density of water
$\rho_s$	kg/m <sup>3</sup>	Density of stones
$\sigma_{vo}$	kN/m <sup>2</sup>	Total vertical overburden pressure
$\sigma'_{vo}$	kN/m <sup>2</sup>	Effective vertical overburden pressure
$\gamma_{sat}$	kN/m <sup>3</sup>	Saturated unit weight
$\gamma_{unsat}$	kN/m <sup>3</sup>	Un-saturated unit weight
$a_{max}$	m/s <sup>2</sup>	Peak horizontal acceleration
$A_0$	g	Design peak ground acceleration
$A$	m <sup>2</sup>	Surface area
$c'_{ref}$	kN/m <sup>2</sup>	Cohesion
$CBR$	%	California bearing ratio
$CRR_M$	-	Liquefaction resistance
$CSR$	-	Cyclic Stress Ratio
$d$	m	Diameter
$D$	mm	Slab thickness
$D_{n50}$	m	Nominal stone diameter
$e_{int}$	-	Initial void ratio
$E$	kN/m <sup>2</sup>	Young's Modulus
$EE$	ESALs	Traffic load
$f$	1/s	Frequency
$f_c$	1/s	Concrete compressive strength
$F$	kN	Force
$F_2$	-	Friction factor
$FoS$	-	Factor of Safety for liquefaction
$F_u$	MPa	Minimum tensile strength
$F_y$	MPa	Minimum yield stress
$g$	m/s <sup>2</sup>	Gravitational acceleration
$G$	kN/m <sup>2</sup>	Shear modulus
$H_{dir}$	degrees	Wave direction
$H_s$	m	Significant wave height
$H_{m0}$	m	Significant wave height from wave spectrum, zero order moment
$I$	mm <sup>4</sup>	Moment of inertia
$IRI$	m/km	International roughness index
$H_{2\%}$	m	Statistical wave height with an exceeding chance of 2%
$J$	mm <sup>4</sup>	Moment of inertia
$k$	-	Subgrade reaction coefficient
$K_a$	-	Active earth pressure coefficient
$K_p$	-	Passive earth pressure coefficient
$L$	m	Length
$L_1$	kN	Single axis load

$L_2$	m	Single axis factor
$M$	kNm	Moment
$M$	-	Earthquake magnitude
$M_r$	MPa	Resilient modulus subgrade
$M_{xy}$	kNm	Torsional Moment
$N_1^{60}$	#	Corrected number of SPT hammer blows
$NE_{tmin}$	mm	Total required structural coefficient
$P_i$	-	Initial serviceability index
$P_f$	-	Final serviceability index
$q$	kN/m	Distributed load
$r_d$	-	Stress reduction coefficient
$R_n$	-	Nominal strength
$R_u$	-	Required strength
$s_u$	kN/m <sup>2</sup>	Unconfined compressive strength
$S_0$	-	Reliability parameter
$S'_c$	MPa	Flexural strength concrete
$t$	m	Thickness
$T$	°C	Temperature
$T_m$	s	Mean wave period
$T_p$	s	Peak period
$U_{dir}$	degrees	Wind direction
$U_w$	m/s	Wind speed at 10 meters above the surface
$UC$	-	Unity Check
$V$	kN	Shear force
$V_{s30}$	m/s	Shear wave velocity at a depth of 30 m
$W_{n50}$	kg	Nominal stone weight
$W$	kN/m	Weight
$W$	m <sup>3</sup>	Section modulus
$Z$	m <sup>3</sup>	Section modulus
$Z_r$	-	Reliability parameter

<b>Abbreviation</b>	<b>Description</b>
AASHTO	American Association of State Highway and Transportation Officials
AISC	American Institute of Steel Construction
CBR	California bearing ratio
CPT	Cone Penetration Test
DoP	Department of Ports
MB	Metabasite
MCV3	Manual de Carreteras, Volumen 3 (Chilean Highway Manual)
MOP	Ministerio de Obras Públicas (Ministry of Public Works)
NCh	National Chilean Building Code
SPT	Standard Penetration Test
TU	Technical University
PSS	Semi-pelitic shale
PSU	Practical Salinity Unit
UdeC	Universidad de Concepción
QGIS	Quantum Geographic Information System

# PART 1: ANALYSIS



# 1 Introduction

## 1.1 General background

The Department of Ports of the Ministry of Public Works is the governing body that is responsible for ports and coastal infrastructure along the whole coast of Chile. This department initiated a project to improve the coastal infrastructure along the entire coastline of Chile. This coastline is 4000 kilometres long. One of the projects is the port infrastructure of Tirúa and Quidico. A special study is executed to determine the appropriate improvements for the coastal infrastructure of these areas. A general design of the port area near Quidico is one of the results of this study. Two separate breakwaters, a supporting area for the fishermen, mooring facilities and several onshore buildings are included in this design. The Department of Ports had some doubts about certain aspects of this design. The goal of this report is to evaluate these problems and to come up with new design proposals which are useful for the Department of Ports. A schematic representation of the timeline is presented in figure 1.1.



Figure 1.1: Schematic timeline of the project

## 1.2 Project area

Quidico is a small fisherman town in the Bío Bio region. The town is located 180 km south of the city of Concepción. The town is bounded on the west by the Pacific Ocean. The nearest city to Quidico is Tirúa, located 5 kilometres south of Quidico. In front of the coast of Quidico an island is located, called Isla Mocha. This island is located 40 kilometres south-west of Quidico. The surface area of Quidico is 0.35 km<sup>2</sup>.

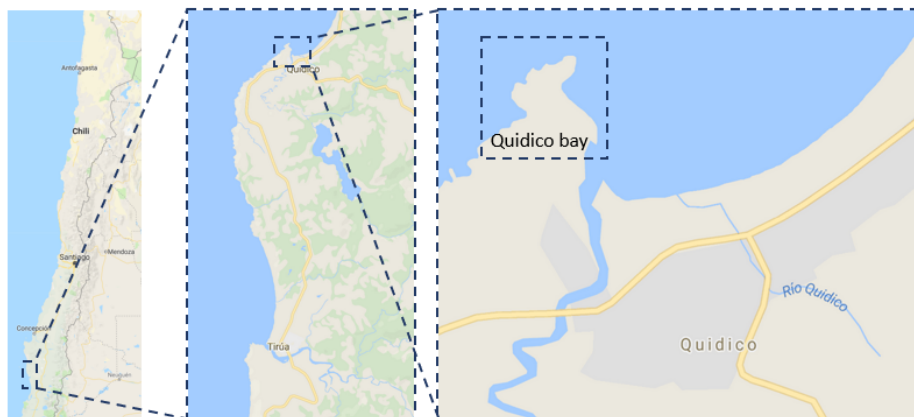


Figure 1.2: Location of Quidico in Chile

Quidico has approximately 3000 inhabitants. The town is known for its beaches which allow for performing various water sports. Accommodation and entertainment areas for touristic purposes are found in the region. Next to the town of Quidico a small bay is located in which a great number of local fishermen are active. Fishing is the main economic activity in the area, twenty percent of the inhabitants have a job related to this bay.

The climate in Quidico is classified as a warm-summer Mediterranean climate. The cool waters of the Pacific Ocean help to maintain the mild temperatures. The temperature almost never exceeds the 30 degrees Celsius or falls below 0 degrees Celsius. The annual precipitation is approximately 1100 mm, but around 80% of this precipitation occurs between May and October.

### 1.3 Project site

The location of this project is Quidico Bay. The bay is located north-west of Quidico town. The bay is located between a small river and a rocky ledge, called La Puntilla. The length of this ledge is approximately 170 meters and provides limited protection against waves from the south-west. The river is regulated upstream and connected to a basin called Laguna Quidico.

Structures to facilitate the fishermen are practically absent. The main structural elements present in the bay are a concrete plaza and a 700 meter long unpaved road. This road connects the plaza in the bay to the main road and therefore with the town of Quidico. On the plaza a set of 20 modules used as cocineras are present (see figure 1.3b), where the local community offer their products which are collected directly from the sea. The surface of this area is 2400 m<sup>2</sup>. On the other side of the plaza the road continues all the way to the end of the bay. At this end a small concrete mooring location is constructed to unload the heavy catches.

A small beach is present next to the cocineras. This small beach is visible next to the cocineras in figure 1.3a. This beach is used by the fishermen to temporarily store their boats and drop off their goods. The fishermen mainly store their boats at the banks of the river. A ramp connects the cocineras with the beach. This ramp only serves people and cars since it is far from the water line. For this reason the fisherman have to drag the boats on the beach. The surface area of this beach greatly depends on the tide. A schematic overview of the current situation of Quidico Bay is presented in figure 1.4.



(a) Quidico Bay overview



(b) The cocineras in Quidico bay

Figure 1.3: Impression of Quidico Bay including cocineras



Figure 1.4: Overview current situation of Quidico Bay

## 2 Problem Analysis

### 2.1 Problem analysis current situation

A preliminary study of the current situation of Quidico Bay is completed by the Department of Ports. From this study several problems and uncertainties, related to the fishing activities within the bay, followed. These problems can be divided into near-shore and onshore problems. In Appendix A the stakeholder analysis can be found, their relation to, impact on and benefit from the project are described.

#### 2.1.1 Near-shore problems

Some near-shore problems are present in the current situation. These problems can be divided into two categories: mooring of the fishing boats and entering the harbour by the boats.

The fisherman are often not able to safely moor their boats due to high waves in the bay. The small rocky ledge is breaking some of the waves, however a significant amount of the waves can enter the bay. Because there is no breakwater the whole bay, including the mooring facility, can be attacked by waves from the open ocean. Another problem related to mooring is caused by the tides. The fishing boats are not able to reach the mooring facility during low tide, due to insufficient draft. Therefore the fishing boats are only able to drop of their goods during high tide. This problem is currently solved by pulling the boats onshore with tractors or other vehicles. On the beach the cargo is offloaded and afterwards the boats are pulled back into the water.

The second near-shore problem is related to entering the harbour with boats. The fishermen are sailing towards the bay in the same direction as the waves. This is mainly from a southwestern direction. Close to the bay the fishermen have to make a change in direction of almost 180 degrees to reach the mooring facility. During high waves, it is quite difficult and unsafe to make this turn. When the weather is relatively rough, this movement might lead to capsizing of the boats. Breaking waves during this movement can increase the danger of capsizing.

Another point of interest is the river, Rio Quidico, which has outflow directly in the bay. This river is coming from a regulated basin, located a few kilometer upstream. The maximum discharge is estimated around 40 m<sup>3</sup>/s. Because there is no data available of this river, this value merely is an estimation. The sediment from the river can cause sedimentation in the bay, however the importance should be analysed.

#### 2.1.2 Onshore problems

In the current situation onshore supporting facilities in Quidico Bay are virtually absent, as described in the project site description of section 1.3. The basic facilities that are present, are mostly constructed by the fishermen themselves and are of poor quality. The wish of the Department of Ports, the fishermen unions and the Tirúa municipality, is to transform Quidico bay into a productive and legal fishery port. To achieve this goal and to improve the efficiency and cost-effectiveness of the bay, the total onshore supporting area should be re-designed.

The office building used by the fishermen unions, is too small, old and in bad condition. Furthermore, sufficient bathrooms and no boxes to safely store the goods of the fishermen, are absent. Quick offloading of the boats and smooth transshipment is hindered due to the lack of a good supporting area. Therefore, a paved support platform is desirable. This platform should be accessible from the beach by a ramp. Another element that needs to be re-designed and improved is the access road connecting the bay to the main road. In the current situation, this unpaved road has insufficient width and does not fulfill the requirements of surface regularity and comfort.

## 2.2 Design proposal Department of Ports

The DoP made a design proposal as a solution to the problems described in section 2.1. A schematic overview of this design proposal is shown in figure 2.1. The design made by the Department of Ports can again be divided in two categories: near-shore and offshore. The design includes two breakwaters, a mooring facility, several onshore buildings, a pavement of the support area and an access road.



Figure 2.1: Schematic overview design proposal by the Department of Ports.

### 2.2.1 Breakwater design

The design proposal of the DoP consists of one breakwater that is roughly projected perpendicular to the headland and a second breakwater that extends from the beach to about 100 meter on sea. The orientations are shown in figure 2.1. The design is proposed by an external consultancy company. This company performed several depth measurements and created different numerical models. Also statistical analyses for the wave and wind data are performed by the company. The numerical model CMS-WAVE is used to model the area. The processes refraction, shoaling, breaking, diffraction and reflection are considered in this model. The environmental conditions are analysed and hydrodynamic models are made to map the processes around Quidico.

#### Main breakwater

Mooring of the fishing boats is unsafe and difficult in the current situation. The primary function of the main breakwater is to break the incoming waves from offshore. This breakwater is designed in a curved way, as shown in figure 2.1, to avoid accretion at the sea-side of the breakwater. It also reduces the wave impact on the breakwater. With this breakwater configuration the movement of the fishing boats into the harbour is relatively smooth.

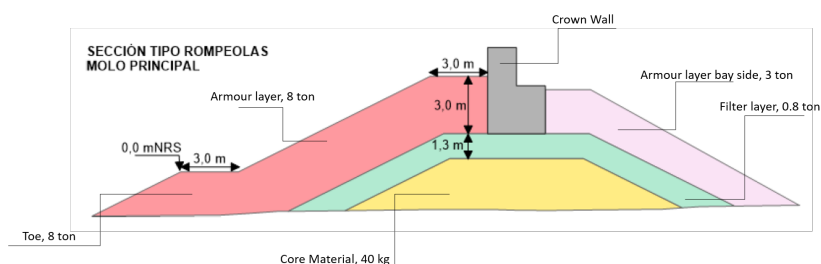


Figure 2.2: Cross section of main breakwater including weight of stone layers

#### Contramolo

The modelling results from the consultancy company showed the presence of a return current within Quidico Bay. This return current could bring sediment into the bay which can cause accretion. A second breakwater (contramolo) is designed, see figure 2.1, to counteract the sediment problems from this return current. In

the design of the DoP this contramolo has a length of 100 m, running from the shore line into the sea. The contramolo is not connected to the main land, a small gap between the main road and the contramolo is maintained. This allows the bay and river to be connected via the beach, as shown in figure 2.3. The secondary function of the contramolo is to guide the sediment transport originating from the river. However, the influence of the river on the total sediment transport is unknown.

## 2.2.2 Onshore structures

The DoP proposed a design for several onshore structures to solve the problems as described in section 2.1.2. These are conceptual designs based on reference projects and do not serve as a final detailed design. A detailed description for each of the supporting facilities in the proposed harbour design are presented below.

### Mooring facilities

Five mooring sites are included in the proposed design, located at the west side of the bay near the origin of the main breakwater. These sites consist of two different elevations to ensure unloading operations during low and high tide. The existing design of the docking sites at the Tirúa harbour are constructed by reinforced concrete L-walls. Depending on the exact soil specifications the L-walls can be replaced by sheet piles. To support the unloading of heavy cargo, two cranes are included in the design of the mooring facility.

### Storage boxes

To allow fishermen to safely store their tools, 24 storage units are proposed. These units have a width of 2.0 meters and a length of 3.0 meters. The walls of this building structure are made of brick masonry, the building has a timber roof structure.

### Bathrooms

Two buildings with in total twelve bathrooms are proposed. The structural design of the building is similar to that of the the masonry and timber structure of the storage building. The bathrooms will include toilets, showers, sinks and additionally several urinals.

### Office spaces

In the proposed design two office spaces are included with a total surface area of about 250 m<sup>2</sup>. These offices will serve as the headquarter of the fishermen unions and will be constructed from masonry and timber.

### Pavement of support area and access road

The pavement of the support area consists of traditional concrete slabs. This area includes a free surface area, a parking and a beaching area for the fishing boats. An asphalt road will connect the supporting area with the main road towards Quidico town.

### Ramp

A ramp will be constructed to allow the fishermen to beach their boats. The ramp is proposed with a slope of 12 percent and dimensions of 10 by 30 meters. The ramp will consist of a reinforced concrete slab that will rest on a filling contained between two reinforced concrete L-walls.

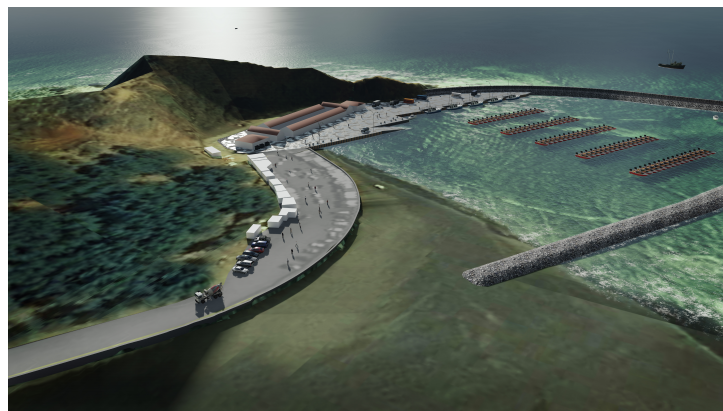


Figure 2.3: Design proposal by the Department of Ports, 3D view

## 3 Problem Definition

A clear problem definition is required to make sure the final design fulfills the needs of the Department of Ports and the other stakeholders. The problems, as described in chapter 2.1, are divided in a few different areas: breakwater, onshore buildings, mooring facility and pavements. A further elaboration of each specific problem can be found in this chapter.

### 3.1 Breakwater

There are still some doubts about the breakwater design made by the external consultancy company, in particular regarding to the entrance of the harbour. They are referring to the project in Tirúa. Problems occurred in Tirúa with entering the harbour, after constructing the breakwaters. By constructing an additional breakwater element, the problems were solved. For Quidico the fishermen have doubts about the point of wave breaking. They expect that this breaking point will occur at the end of the main breakwater. Therefore, the movement into the harbour will be difficult and can cause capsizing of the fishing boats.

Another aspect is the so-called return current. The *contramolo* is designed to counteract the problems of this return current. However, many doubts consist about the presence of this return current and, if present, how strong the influence will be. Furthermore, it is not proven that this *contramolo* will solve the wave- and sediment problems in the bay. The importance of this *contramolo* must be investigated. If this breakwater is not necessary, it reduces the project costs significantly. Also, other alternatives like dredging could be considered.

Considering the prior given problems, different breakwater configurations should be investigated. A sheltered area is necessary to create safe conditions at the mooring facility. Furthermore, a quantitative analysis of the accretion and erosion areas is requested. This analysis gives a good indication about the sediment movements around Quidico Bay. Due to the new proposed breakwater configuration a new cross-sectional design is required.

### 3.2 Onshore buildings

According to the design of the Department of Ports the onshore supporting facilities are divided in six separate masonry buildings. Due to the large area covered by these buildings a large paved area is required. This will affect the natural environment of the bay in a negative way and is not cost-effective. Therefore, the DoP is interested in a more compact design, that includes all supporting facilities in one multi-storey building.

In consultation with the Department of Ports, it is decided that two different building designs should be developed. First, a steel building design was requested by the DoP, including the *cocineras*. However, since the Quidico Bay project is in the preliminary phase, the design process is still ongoing and the exact design requirements are still under discussion. This has the consequence that during the process of the project, the DoP returned on their earlier defined requirements, and requested a concrete building design instead. Other design requirements were adjusted as well and therefore the two building designs are not directly comparably. The exact requirements are given below for each of the two designs.

### **Steel building**

The design requirements for the steel building design are based on the first meeting with the Department of Ports on 24 November 2017. The minutes of the meeting can be found in Appendix N.2.3.

- Steel frame structure
- 24 storage units (3.0×2.0 m)
- Office spaces (200-250 m<sup>2</sup>)
- Public area for cocenerias (200-250 m<sup>2</sup>)
- Sanitary facilities

### **Concrete building**

The design requirements for the second building design are based on the meeting of 1 December 2017. The minutes of this meeting can be found in Appendix N.2.5. The main difference compared to the requirements from the first meeting is the preferred building material. Furthermore, it was concluded that is preferred to not include the cocenerias in the building design, since there is still a lot of discussion about this topic between the different parties involved.

- Reinforced concrete
- 24 storage units (3.0×2.0 m)
- Office spaces (200-250 m<sup>2</sup>)
- Sanitary facilities
- Second floor accessible for disabled people.

Based on these design requirements, a functional design will be developed for the two buildings in consultation with the project managers, engineers and architects of the Department of Ports. Within the boundaries set by this functional design, a structural design should be made which is earthquake resistant and meets all the design criteria set by the Chilean building standards. A preliminary structural design is requested for the building structure, but a detailed design of the foundation is not expected by the DoP. Furthermore, an estimation of costs and a detailed description of the construction process is beyond the scope of this project.

## **3.3 Mooring facility**

Within the bay of Quidico a safe mooring facility is requested by the fishermen. In combination with the required extra support area, the DoP proposed a quay wall construction along the south-west shoreline of the bay. Two types of the quay wall construction are preferred by the DoP, these include a sheet pile wall and a concrete mass wall. The choice of type of quay wall mainly depends on the soil conditions and the available construction space. In the case of a sandy subsurface and little available construction space the sheet pile wall variant is preferred. In the case of a shallow rock basement and enough construction space the concrete mass wall is preferred. The DoP requested a design proposal for both types of quay wall constructions.

## **3.4 Pavements**

A pavement design is required for both the access road and the supporting area that fulfills the structural and serviceability requirements defined by the Department of Ports. The DoP requested to evaluate different alternatives for both the access road and the support area. For the pavement in the supporting area, concrete slabs are the preferred solution. The DoP asked to look into different slab sizes and thicknesses and to create two different designs. For the access road, three pavement technologies will be evaluated: surface treatment, asphalt and concrete slabs.

### 3.5 Schematic overview

During this chapter the general problems for each design are specified. In figure 3.1 a schematic overview is presented, including the new problem definitions. These specific problems definitions are treated in the coming chapters for each design.

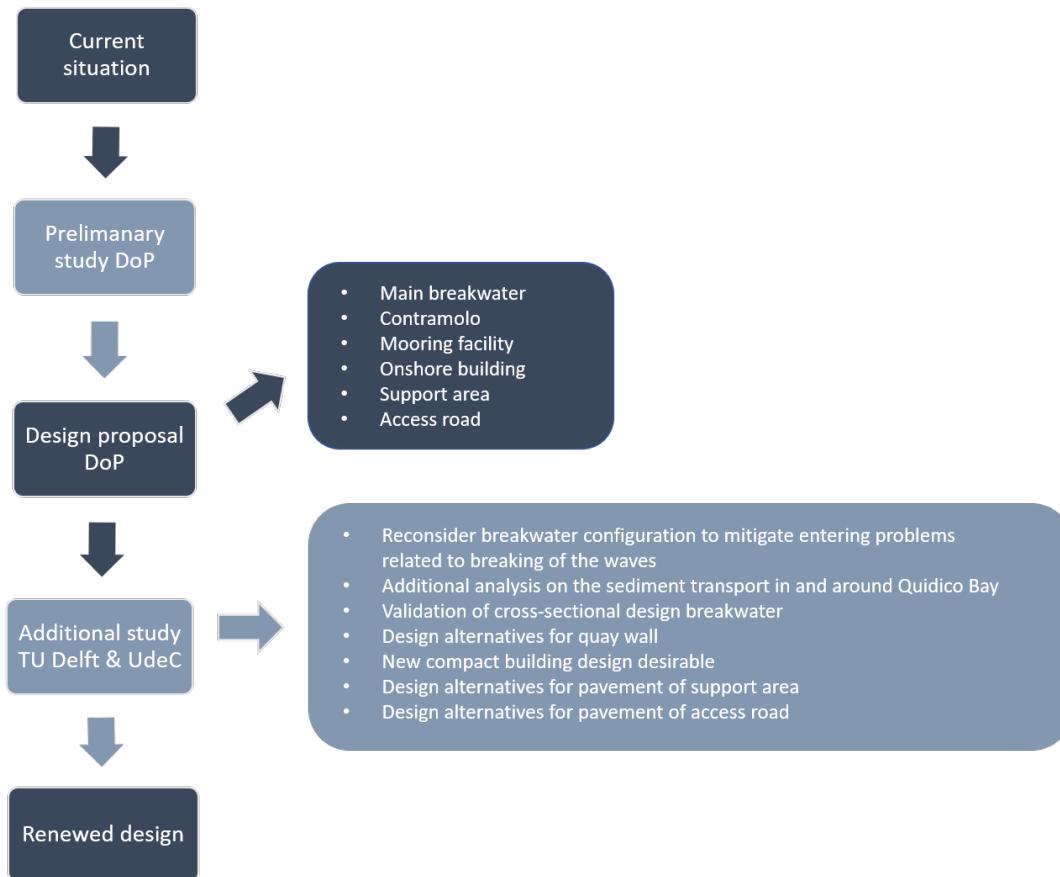


Figure 3.1: Schematic representation of the problem definition.

# 4 Boundary Conditions

Within this chapter the boundary conditions are described. The boundary conditions are divided into (1) geo-technical, (2) hydraulic and (3) structural boundary conditions. In each of these sections the current situation at the bay of Quidico, related to the specific discipline, is analysed and described. The boundary conditions are used during the design phase to ensure the proposed designs fulfill the needs and requirements.

## 4.1 Geo-technical conditions

The geo-technical boundary conditions consist of four different aspects. First, the geological background of south-central Chile and Quidico are expanded (section 4.1.1). This analysis eases the explanation of the occurrence of certain geo-technical characteristics. Second, different types of geo-technical data is analysed and used to define the geo-technical characteristics of the bay (section 4.1.2). Third, the seismic classification of the subsurface is determined. This is an important step in the geo-technical analysis in areas prone to earthquakes, based on this classification the influence of an earthquake on a structure is provided in a descriptive way (4.1.3). Fourth, conclusions can be drawn on the possible geo-technical hazards in the area based on the results of the different tests from section 4.1.2 (section 4.1.4).

### 4.1.1 Geological situation

#### South-Central Chile

Quidico Bay is located in south-central Chile at latitude  $38^{\circ} 15'$ . Quidico and its bay are located to the South-West of the Lanalhue Fault Zone which runs in northwest-southwest direction. The name originates from the Lanalhue Lake which is positioned at the fault trace, positioned 40 km north of Quidico. Northeast of the lineament the so-called 'Eastern Series' are located, southwest the so called 'Western Series' are located (figure 4.1). The fault line is clearly visible due to the lithological differences between both 'Series' and the discontinuity which occurs in the Nahuelbuta mountain range (Glodny et al. 2008).

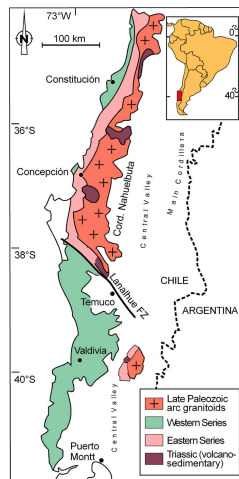


Figure 4.1: Map of geological units in South-Central Chile (Glodny et al. 2008).

Quidico is located where two tectonic plates meet, the tectonic Nazca plate and the South American plate (figure 4.2a). The Nazca plate is positioned on the western side of the South American plate, covering the South American continent. The Nazca Plate has a yearly movement eastwards of 79 mm (The-Geological-Society 2017) and is forced to subduct the South American Plate. As the plates continue to move across each other the surfaces of both plates are deformed and fractured. The earthquakes which occur due to this scraping are relatively shallow, as the process continues the focal depth of the earthquakes increases.

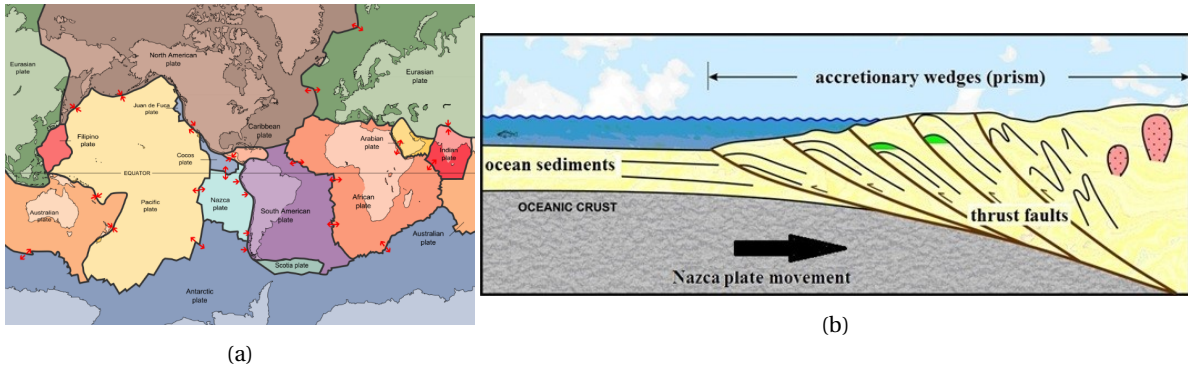


Figure 4.2: (a) Tectonic plates and their names (USGS 2011). (b) Accretionary prism formation process (Krueger and Gilbert 2009).

Due to this subduction-accretion process the sediments on the bottom of the ocean are forced to overtop the South American plate. This process is known as obduction. This results in an accretionary prism (or wedge) where supply of sediments from the ocean and the continent result in continental growth. This process is shown in figure 4.2b. The contact of the two tectonic plates results in deformation of the western edge of the South American plate, rocks are folded. The contact results in uplift and thus the creation of vertical growing rocks and a decreasing width of the lithosphere, this creates mountains (i.e. the Andes).

### Quidico Bay

Towards the coast the Nahuelbuta mountain range shows a sudden fall, this results in the occurrence of outcrops of the metamorphic rock of the Western Series. A discontinuity occurs with the coastal plain which runs from the north along the coast, this is also visible at Quidico Bay. Quidico Bay is founded on the metamorphic rock of the Western Series which forms a rocky basement. This basement is formed during the Late Paleozoic to Triassic period. It is characterised by the presence of mostly calc-alkaline rocks. Other rock types present are granodiorites, tonalities and diorites with minor granites intruded at upper crustal levels (Adriles 2003). These rocks show characteristics of foliation, lineation and folding, this is due to the fact that these rocks deform in a ductile way. The origin of the rocks can be explained by the process subduction-accretion, as described in the previous section. It is expected to find the accretionary wedge along the coast. The metamorphic rocks are formed under high pressure and low temperature. The rocks are composed of pelitic to semi-pelitic shale (PSS) with metabasite inclusions (MB) (Adriles 2003). These outcrops are found at the bay, some indications of these outcrops are shown at the bottom of the picture in figure 4.3.



Figure 4.3: Rock outcrops at Quidico Bay.

The PSS are metasedimentary rocks of coarse grain and dark grey colour and show bands of quartz. The bands of quartz are interrupted by bands of white mica, chlorite, graphite material and porphyroblastic albite. It has clay composition and mineral association dominated by phyllosilicates.

Also coastal deposits and fluvial sediments are found along the north coast of Quidico. These correspond mainly to recent low-lying dunes and current unconsolidated deposits. In addition, on the road connecting Quidico and Canete it is possible to find deposits of wind origin of fine and gray sands. The grains of this sand correspond mainly to fragments of quartz and basement rocks. The topographical arrangement of these deposits points out an age related to the Pleistocene-Holocene. This is also shown in figure 4.4, showing part of the Geological map of Chile (Sernageomin 2000). The P11m sedimentary sequence along the coast around Quidico, formed during the Pleistocene, corresponds to a marine sediments which find its origin in maritime (deposits from sea) and fluvial processes (deposits from rivers and streams). The Q1 sedimentary sequence, formed during the Pleistocene-Holocene, finds its origin in colluvium and alluvium processes.

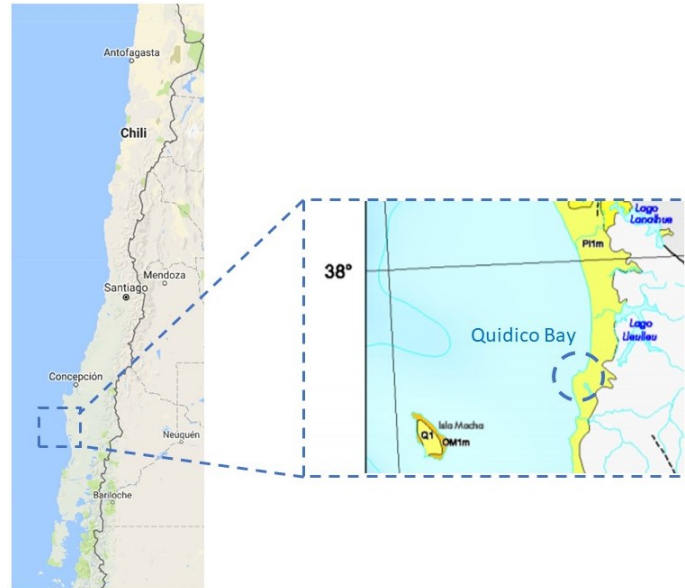


Figure 4.4: Geological map of Quidico Bay and its surrounding (Sernageomin 2000). P11m and Q1 sedimentary sequence correspond to marine/fluvial sediments and colluvium/alluvium processes respectively.

#### 4.1.2 Geo-technical data

In order to classify the soil layers different types of geological data are made available by the DoP. These data include the results of a Standard Penetration Test, several soil samples and a seismic vibration tests.

##### (1) Standard Penetration Test and soil samples

The SPT is performed 500 meter inshore. The SPT data is collected in December 2009 and served for the design of the pedestrian bridge over the river originating from Laguna Quidico. The SPT is performed by the Chilean Ministry of Public Works and its exact location is S 38° 24' 900" and W 73° 49' 080".

Also soil sample data north-east of the bay is provided. These samples are taken in July 2008 in purpose of the design of a new pavement structure along the beach.

##### (2) Seismic vibration tests

The seismic vibration tests are performed during the site visit on the 22nd of November 2017 (B). In total three tests are performed, a REMI, MASW and HVSR test.

The tests are performed at different positions around the bay. Since the SPT and soil samples served as boundary conditions for a pedestrian bridge and a pavement respectively, this data is not from the exact project site. The seismic vibration tests performed during the site visit are performed to collect data regarding the bay, therefore relate to the exact project site. The exact positions of the performed tests and measurements are shown in figure 4.5. Using the results from the tests performed and samples taken, assumptions regarding the soil structure of the bay can be formulated.



Figure 4.5: Map indicating the positions of the different tests performed (Google-Earth 2017).

### (1) Standard Penetration Test

The data obtained with a SPT is very suitable for the determination of the potential of liquefaction. A Standard Penetration Test (SPT) is a simple and low cost soil testing procedure. A standard thick-walled sample tube is driven into the ground by blows from a slide hammer, this can be done at the ground surface or at the bottom of a borehole. The number of blows to drive the sample 150 mm (6 in.) into the ground is recorded, this procedure is performed three times in a row. The SPT blow-count value, N-value, is the number of blows required for the last 12 inch penetration in the procedure described above.

The raw measurement data is shown in Appendix C, figure C.4. From this raw data the descriptive classification of the soil layers is presented in table 4.1.

Table 4.1: Descriptive classification of the soil layers.

Layer boundaries (m)	Description
0 - 1.55	Clay, coffee-like colour
1.55 - 9.55	Stratifications of fine sand
9.95 - 10.85	Clay, grey colour and relatively high humidity
10.85 - 21.2	Stratifications of fine sand

Several sand samples have been taken around the bay (figure 4.5), these samples are analysed using the Unified Soil Classification System (USCS) (table 1 from ASTM D2487 (ASTM-International 2006)). This table is presented in Appendix C, figure C.1. More than 50 percent of the fraction passes sieve no. 4 and less than 5 percent fines (percentage retained on sieve no. 200) are present in all three soil samples. This results in a soil classification indicated by SP: poorly graded sand containing less than 15% of gravel.

The raw SPT data is analysed using the Chilean standard NCh 1508 (2014). Several correction factors should be applied over the raw data in order to get the final use-able number of hammer blows,  $(N_1)_{60}$ . With this number the geo-technical properties and the liquefaction potential of the soil are determined. This analysis is performed in Appendix C. The profile of the corrected number of blow counts over depth is shown in figure 4.6.

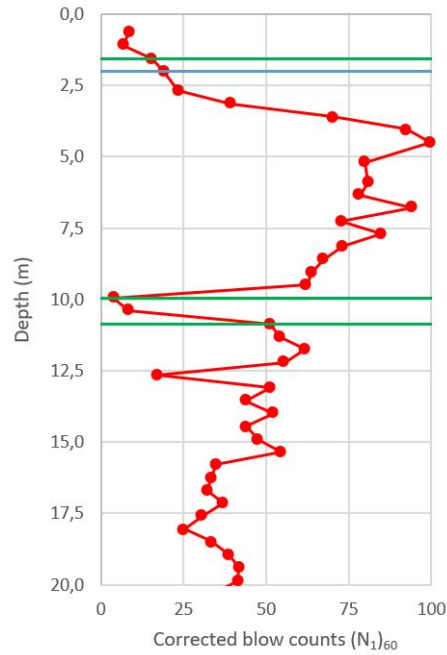


Figure 4.6: Profile of the number of SPT blow counts over depth.

Based on the advise of the engineers of the DoP and experts at UdeC, values are assigned to the geo-technical properties of the sand. Table 4.2 shows the values assigned to the different geo-technical properties.

Table 4.2: The geo-technical properties of the sand in Quidico bay.

$\gamma_{unsat}$ (kg/m <sup>3</sup> )	1850
$\gamma_{sat}$ (kg/m <sup>3</sup> )	2000
$E$ (kN/m <sup>2</sup> )	42000
$c_{ref}$	10
$\phi$ (°)	36
$\psi$ (°)	6

In order to ensure a safe design, regarding earthquake resistance, liquefaction of the soil should be estimated. Liquefaction results in a loss of shear strength due to an increase of pore water pressures. This could result in deformations in the soil profile, which is a risk for the structures on top.

According to the Chilean standard NCh 1508 (2014) the liquefaction potential is analysed with a specific methodology using the cyclic stress ratio and the cyclic resistance ratio (Seed and Idriss 1971). This analysis is performed in Appendix C, with this analysis the plasticity index for the liquefaction potential is determined. In general a soil with a plasticity index value below 1.2 is classified as susceptible to liquefy. The values for the liquefaction potential are obtained for a magnitude 7.5 earthquake and a magnitude 8.8 earthquake over a depth of 21.2 m, this is shown in figure C.3. As said earlier in this section soil with values of  $(N_1)_{60}$  higher than 30 are too dense to liquefy and is classed as non-liquefiable. From the results it is obtained the first 1.5 m of the thick sand layer is susceptible to liquefy. Also some deeper thin sand layers are susceptible for liquefaction according the test results, however these layers are assumed to have no impact on the liquefaction intensity.

According to the SPT, a clay layer of 1.5 m is present at the top of the subsurface. The location of the SPT however, should be taken into account: 500 m inshore next to the river running through Quidico (see figure 4.5). The top clay layer could originate from the deposits transported by the river. In that case the clay layer is not expected to be found directly around the bay. Furthermore, a study for the construction of pavements at the edge of the beach in Quidico contains the analysis of several soil samples. The study, Soil Mechanics in Quidico performed by DICTUC in 2008, contains the descriptive and technical results of six soil samples. The soil samples are taken along the coast of Quidico, north-east of the bay (figure 4.5). In five of the samples the column

consists of stratifications of compacted sand. Only one sample contained a top clayey sand with a height of 0.3 m. Based on the location of the SPT and the soil sample results as described above, it is assumed no clay layer will be present at the project site location. Liquefaction as geo-technical hazard is further described in section 4.1.4.

## **(2) Seismic vibration tests**

During the Quidico Bay site visit on the 22nd of November 2017 (Appendix B) three tests are performed in order to determine the speed of the seismic Rayleigh waves. Rayleigh waves and Love waves are the two types of surface waves, distinguished by the direction and trajectories of particle motion as waves pass by. Surface waves are formed by constructive interference of body waves travelling between the ground surface and various underlying boundaries. The Rayleigh waves propagate along the axis perpendicular to the Earth's surface and are formed by particles rotating in the vertical plane parallel to the direction of wave propagation.

The average shear wave (or Rayleigh wave) velocity at a depth of 30 m is used in the Chilean codes in order to determine the ground-type of a specific location, this analysis is performed in section 4.1.3. The specific ground-type will be used for design or hazard analyses.

In total three tests are performed to measure the Rayleigh wave velocity. During these tests the shear wave velocity profiles are determined. All tests are performed on the ground surface and offer the possibility for relatively cheap measurements.

The tests are performed on the beach north-east of the bay, as shown in figure 4.5. This specific location is chosen for several reasons:

- Influence of metamorphic rocks surrounding the bay; on the west and south side the bay is surrounded by metamorphic rocks (section 4.1.1). The possibility to find some individual rocks, originating from the rocks surrounding the bay, are higher at the exact bay location. These individual rocks have no significant impact on the overall Rayleigh wave speed in the bay. The measurements however, are possibly influenced by these metamorphic rocks.
- Changing water level during the test; approximately three hours are necessary to perform all three tests correctly.
- Influence of the wind and the hardness of the soil; during the site visit on the 22nd of November 2017 a strong eastern wind blew over the beach. More close to the shoreline the influence of the wind was high and more soft sand was present. Both aspects would influence the geophone measurements and this would result in less accurate results.

Two of the three tests performed include the measurement of Rayleigh waves from a passive source and an active source. The recorded seismic noise is transferred to a Rayleigh wave dispersion curve (via the frequency-wavenumber), which relates the Rayleigh wave velocity to the frequency. Subsequently inversion of this curve is applied, this provides the Rayleigh wave velocity ( $V_s$ ) profile over depth. Based on this curve the structure of the soil can be determined. A more thorough description of this process is given in Appendix C.

During the third test the ratio of the horizontal and vertical component of seismic noise is measured, it only requires passive waves. This test is performed using a triaxial geophone, a three-component seismometer. The result is a H/V spectral ratio (HVSR), which is the ratio between the Fourier amplitude spectra of the horizontal and vertical component of microtremors (Bonnetoy-Claudet et al. 2006). The H/V peak frequency correlates to the fundamental resonance frequency of the specific site under investigation, i.e. the H/V ratio shows a sharp peak around the fundamental Rayleigh wave frequency.

The individual results of the REMI and MASW are shown in Appendix C, in figure C.8 and C.9 respectively. The combined plot of the frequency versus the phase velocity of both tests is shown in figure 4.7. The plot of the measured H/V spectral ratio is shown in figure 4.8a, from the figure it is observed the fundamental frequency of the subsurface,  $f_0$ , is 1.2 Hz. Using this latter result, the fundamental mode can be distinguished in figure 4.7.

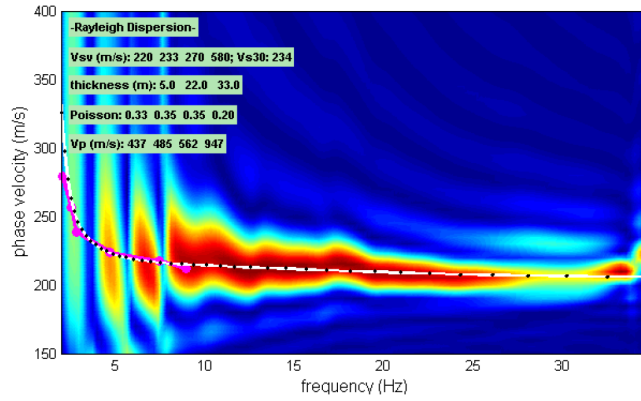


Figure 4.7: Graph of the frequency versus the phase velocity of the combined results of the REMI and MASW test.

Using the graphs from figure 4.7 and figure 4.8a, the depth versus the shear wave velocity is plotted. This graph is obtained via inversion and is shown in figure 4.8b. As can be seen from this plot the shear wave velocity at a depth of 30 m,  $V_{s,30}$ , is 234 m/s. Based on this solution the soil can be classified (section 4.1.3). Another observation from the shear wave velocity profile over depth is the depth of the bedrock. This depth is estimated to be 60 m, at this depth the shear wave velocity shows a sudden increase. This high value corresponds to typical shear wave velocities of a firm rock.

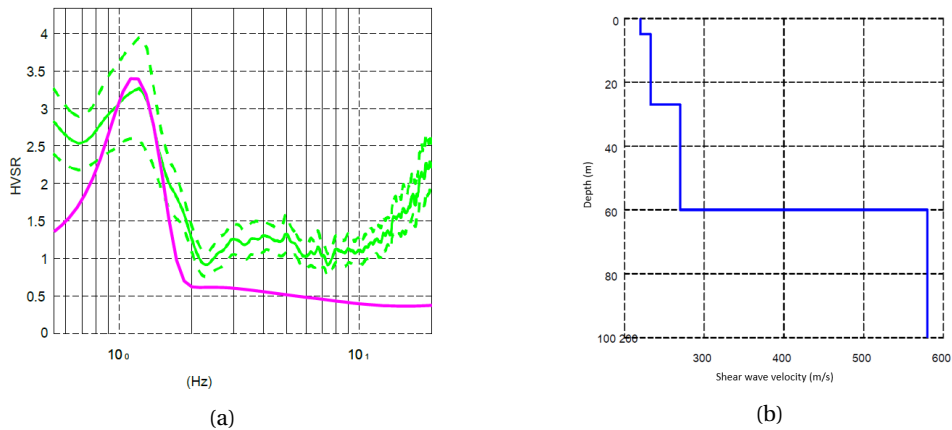
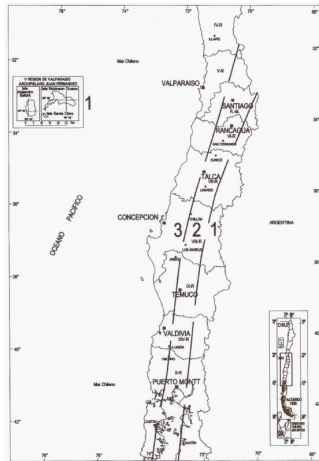


Figure 4.8: (a) Graph of the H/V spectral ratio. (b) Graph of the shear wave velocity profile over depth.

### 4.1.3 Seismic classification

In order to ensure an earthquake resistance design of the onshore facilities and breakwaters within the bay, the first step is to classify the soil in the subsurface. With this classification the parameters to be used regarding the specific soil (e.g. parameters for the design spectrum, several seismic coefficients) are determined. The classification is described in NCh 433-96 (updated in 2012). Besides the soil classification also the location of the project site is of influence on the design peak ground acceleration. Quidico Bay is located in seismic zone 3, as shown in figure 4.9a. This is the zone closest to the shoreline and the region with the highest earthquake intensities. In table 6.2 of NCh 433-1996 the design peak ground acceleration is specified, for Quidico Bay  $A_0 = 0.40 g$ .



(a) Classification zones

Suelo Tipo	$V_{30}$ (m/s)	RQD	$q_u$ (MPa)	(N <sub>60</sub> ) (golpes/pie)	$S_u$ (MPa)
A Roca, suelo cementado	$\geq 900$	$\geq 50\%$	$\geq 10$ ( $f_{cu} \leq 2\%$ )		
B Roca blanda o fracturada, suelo muy denso o muy firme	$\geq 500$		$\geq 0,40$ ( $f_{cu} \leq 2\%$ )	$\geq 50$	
C Suelo denso o firme	$\geq 350$		$\geq 0,30$ ( $f_{cu} \leq 2\%$ )	$\geq 40$	
D Suelo medianamente denso, o firme	$\geq 180$			$\geq 30$	$\geq 0,05$
E Suelo de compacidad, o consistencia mediana	$< 180$			$\geq 20$	$< 0,05$
F Suelos Especiales	*	*	*	*	*

(b) Soil classification table

Figure 4.9: Figure 4.1 and table 4.2 from NCh433-1996.

The main parameter to determine the classification of the soil is the shear (or Rayleigh) wave velocity at a depth of 30 m. As determined by the tests described in section 4.1.2 the value for this parameter is 234 m/s. In order to classify the soil also the number of blows during a SPT and the unconfined compressive strength should be accounted for, see figure 4.9b. Using figure C.3 for the corrected number of hammer blows, it appears that from a depth of 3.14 m the number of hammer blows is  $> 30$ . A correlation to calculate the unconfined compressive strength via the number of hammer blows (Terzaghi and Peck 1948) is used. This correlation is shown in table 4.3. Since the number of blow counts are all above 5 an unconfined compressive strength of at least 0.05 MPa can be guaranteed. Taking into account the above observations the soil can be classified as type D according to figure 4.9b (Table 4.2 from NCh 433-1996).

Table 4.3: Relation between the number of blow counts and the unconfined compressive strength (Terzaghi and Peck 1948)

Blows N (#)	<2	2-4	4-8	8-15	15-30	> 30
$S_u$ (MPa)	0.02	0.025 - 0.05	0.05 - 0.1	0.1 - 0.2	0.2 - 0.4	> 0.4

Every type of soil relates to a certain shape of the acceleration response spectrum. This provides information regarding the frequency content of a certain acceleration, it provides the influence of a certain earthquake on a structure in a descriptive way. The spectrum can therefore serve as basis for the design of the onshore facilities.

#### 4.1.4 Geo-technical hazards

Based on the results of the different tests and by observing the project site and its surrounding, conclusions can be drawn on possible geo-technical hazards in the area.

##### Liquefaction

As described in section 4.1.2 the top sand layer is susceptible to liquefy. From figure C.3 it is seen the FoS for this layer is well below 1.2. Most deformations are caused by liquefaction and thus mitigation of this effect is desired. Liquefaction occurs in a degradation, the extent of liquefaction susceptibility depends on the gradation, shape and size of the sand particles. From the soil samples taken at the beach close to Quidico Bay it was found that the fine sand is poorly graded and contains less than 5 percent fines passing the No. 200 sieve (C.2). This leads to a loose condition of the sand and a low permeability, both these characteristics make the sand layer prone to liquefaction.



Figure 4.10: Vespucio Norte Express bridge, liquefaction was one of the causes for collapse (Maldonado, 2010).

In order to investigate the exact extent of liquefaction over depth, a Standard Penetration Test at the exact position of the project site is necessary. A SPT is a relative simple and cheap geo-technical test but provides the needed soil parameters regarding liquefaction potential prediction. In order to mitigate the liquefaction risk several options can be considered. The most effective method for the current situation is the densification of the soil, a relative simple and cheap solution. This densification is achieved by repeatedly dropping a weight from a certain height on the soil. This could lead to liquefaction of the soil, followed by rearrangement of the particles resulting in a denser configuration. Another possibility is vibro-compaction where vibration of the soil will lead to densification. Despite the execution of this method might be as simple as densification by weights, this method is more expensive and thus not advisable to use in the current case.

Older sediments are likely to be denser than younger sediments. This is due to the fact these sediments have been subjected to ground shaking over a longer time-span. This results in densification or liquefaction after which it densifies. This effect is expected to have partly densified the sandy soils at the position of the breakwater in deeper water. However, due to the strong current and the presence of turbulence close to the shoreline this effect might be negligible at this position. The turbulence intensifies closer to the shoreline due to the shallower depth and increase of breaking waves.

Geo-technical measurements are hard to perform at the position of the breakwater (approximately 50-100 m offshore), therefore liquefaction is hard to predict at this location. In order to validate the liquefaction potential the characteristics of the sand should be determined, mainly the permeability and the extent of contraction are of importance. These characteristics are again influenced by the gradation, shape and size of the sand particles. By performing a SPT (onshore) or CPT (onshore/offshore) at the project site the sand properties of the seabed can be estimated more accurately. In practice it is common to let the soil mass below the breakwater consolidate and provide the possibility for the stresses in the water to diminish. This can however be time-consuming and requires adequate analysis of construction phases. Another option is the use of gravel drain piles, these drain piles are permeable and thus the increase of excess pore pressure can be reduced (Vossenaar 2017).

### **Lateral spreading**

This type of hazard is closely related to liquefaction. The soil liquefies and results in a horizontal movement of gently sloping ground. Especially the small (natural) slopes at the shoreline are prone to lateral spreading, there is a risk of lateral movement of intact soil over shallow liquefied deposits. The combination of loss in soil strength and the cyclic motion due to the earthquake can result in significant ground movement, even on a gentle slope. Different horizontal displacements can result in extra forces within the foundation or the building, possibly leading to cracks and eventually failure. Especially the foundation of the onshore facilities can be prone to lateral spreading. To mitigate the risk for lateral spreading, it is of importance to estimate the depth to which the soil is prone for liquefaction. Reducing the risk of liquefaction will reduce the risk of lateral spreading.

### **Settlement**

The geo-technical hazard regarding settlement is mainly related to the breakwater. In case of significant ground settlement, this settlement can be added to the final construction height in order to fulfill the design requirements. To be able to accurately calculate the final settlement of the breakwater it is of importance

to have accurate information regarding the soil properties. In this case a test to measure these geo-technical properties has to be executed. However, the settlement of the breakwater can be estimated based on the assumptions regarding the structure of the subsurface as described in section 4.1.2. Using these assumptions also the overall stability of the breakwater can be checked. Both the estimation of the settlement and the check of the overall stability of the breakwater are performed in section 5.8.6.

## 4.2 Hydraulic conditions

### 4.2.1 Conventions and definitions

#### Coordinate systems

In this report the WGS-84 reference system is used for Geographic Information Systems applications. All units are specified in meters, therefore the UTM18S projection is applied. It is important to always use the same reference system during modelling. Projection of WGS-84 coordinates into a UTM18S reference is done by the program QGIS, see figure 4.11 (EPSG 2017). The difference between the WGS-84 and the UTM projection is that WGS-84 is a geographic coordinate system and UTM is a projected coordinate system.



Figure 4.11: UTM zone Quidico bay

#### Directions, wave and wind roses

Throughout the report the nautical convention is used, see figure 4.12. In this system the 0 degrees is pointed to the North. The direction of waves and wind is measured clockwise from geographic North. This implies that waves from the East have a direction of 90 degrees. These roses are also used to have a clear view on wave heights, wave periods and wind speeds. The longer the arm of the specific vector, the higher the value. Those various properties are indicated by colours.

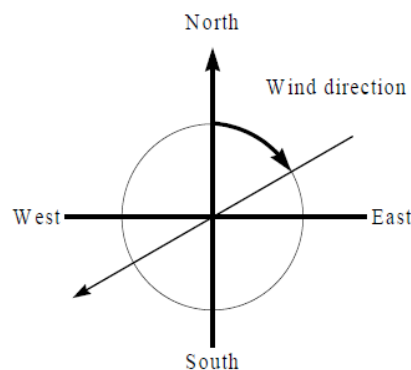


Figure 4.12: Nautical convention (Deltares 2014)

## 4.2.2 Environmental conditions

In this section the environmental and hydraulic conditions are described. The boundary conditions are the necessary input for the modelling phase. These values are also used for designing the breakwater. The wind and wave data are collected from the following two databases:

- ARGOSS (Argoss 2017)
- Atlas de Oleaje de Chile (Oceanica 2017)

ARGOSS has a large database, which contains wind velocities, wave heights and their corresponding directions and periods. Waves are divided into swell and sea waves within this database. The location of the obtained data can be seen in figure 4.13. Also data from a Chilean website is used, named Oleaje Atlas (Oceanica 2017). This database is used by the Department of Ports. Node 11 is used, which is a buoy positioned offshore, just south of Quidico. The location of node 11 is shown in figure 4.14. In this node wave heights, periods and directions are measured. In the database of Atlas de Oleaje only the swell waves are provided. Translation of offshore to near-shore waves is explained in Appendix D.

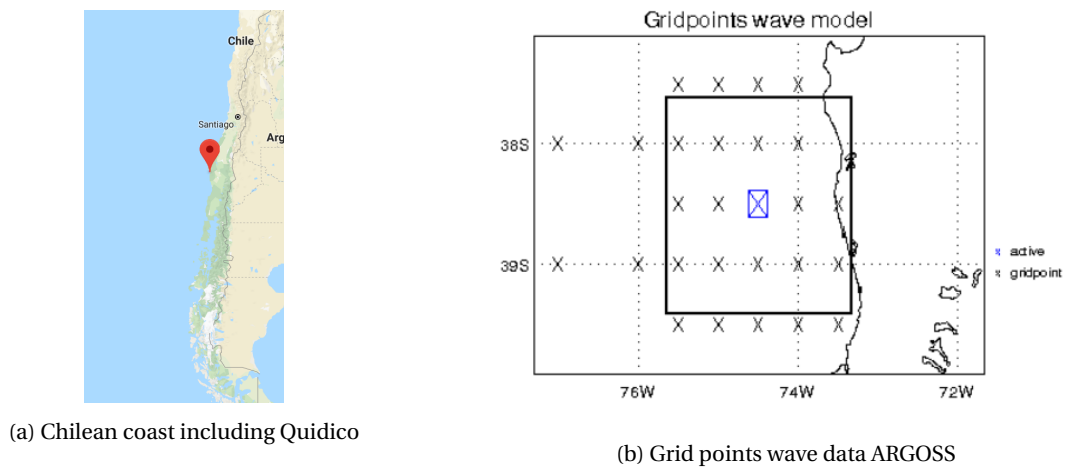


Figure 4.13: Data from ARGOSS

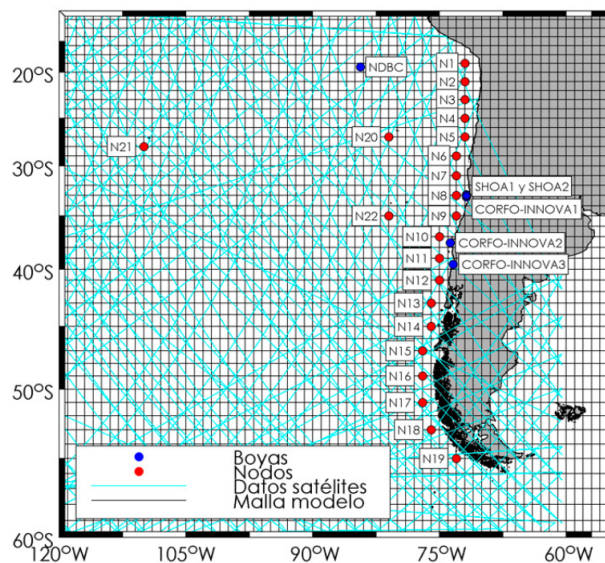


Figure 4.14: Location Atlas

### Wind velocities

Wind data is extracted from ARGOSS. As shown in the wind rose in figure 4.15 the wind is mainly coming from the south. Waves are generated due to these wind velocities. These waves will be discussed in the following section.

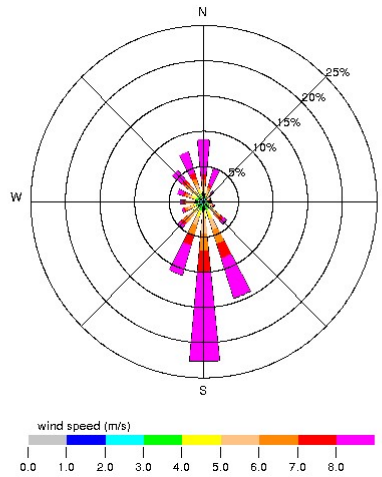


Figure 4.15: Wind rose, from ARGOSS, offshore of Quidico bay

### Wind Waves

Wind waves, also called sea waves, are generated by the wind. Due to the fact that Chile is suited at the South Pacific, winds can be of big influence. The fetch can be large, and therefore large waves could arrive at the coast. The main wind direction is from the south, which is visible in figure 4.15. Due to this wind, waves are generated which have the directions as can be seen in figure 4.16.

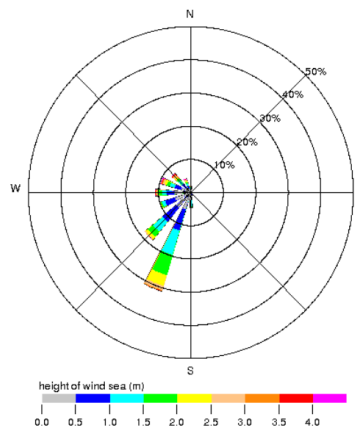


Figure 4.16: Wind waves, from ARGOSS, offshore of Quidico bay

From the wave rose it can be concluded that most wind waves are coming from the south-west and that most waves are relatively small (between 1.0 and 1.5 meters). Furthermore can be seen that the maximum waves are not higher than 5.0 meters. During the wave analysis, the maximum wave heights are shown. From a fast calculation, comparing the mean period and mean wave height, it is almost certain that swell waves will be guiding for this project. Still, swell and wind waves are analysed. The coast of Chile is open and therefore swell waves are able to arrive at the coast. The swell waves are used for designing a breakwater. The height, period and direction of the waves play an important role for the wave-impact at the breakwater.

In tables 4.4 and 4.5 the minimum, mean and maximum values of the wave heights, directions and periods are provided. Tables 4.4 and 4.5 are both obtained from the data of ARGOSS.

Table 4.4: Values for Sea waves from ARGOSS

<b>Sea waves</b>	<b>Mean</b>	<b>Max</b>	<b>Min</b>
$T_m$ (s)	4.79	11.75	2.39
$T_p$ (s)	5.62	17.97	2.43
$H_s$ (m)	1.15	7.32	0
$H_{dir}$ (m)	236.35	359	0

Table 4.5: Values for Swell waves from ARGOSS

<b>Sea waves</b>	<b>Mean</b>	<b>Max</b>	<b>Min</b>
$T_m$ (s)	11.41	24.26	3.70
$T_p$ (s)	12.50	23.92	3.23
$H_s$ (m)	2.47	8.25	0
$H_{dir}$ (m)	235.78	359	0

Table 4.6: Swell numbers from the Chilean data

<b>Sea waves</b>	<b>Mean</b>	<b>Max</b>	<b>Min</b>
$T_m$ (s)	8.968	15.52	4.95
$T_p$ (s)	12.94	23.96	5.21
$H_s$ (m)	2.42	8.543	0.053
$H_{dir}$ (m)	237.65	359.94	0.96

### **Swell Waves**

Both data sets are used to analyse the swell waves. As can be seen from figure 4.17 both data sets measure similar wave data. Also the tables 4.5 and 4.6 show similar data values. The main swell waves come from a south-western direction, with a direction spreading from south to north-west. Swell waves have a larger wave height and longer wave period than wind waves, this results in a higher energy level. Due to this energy level, the influence of the swell waves is larger than of the wind waves.

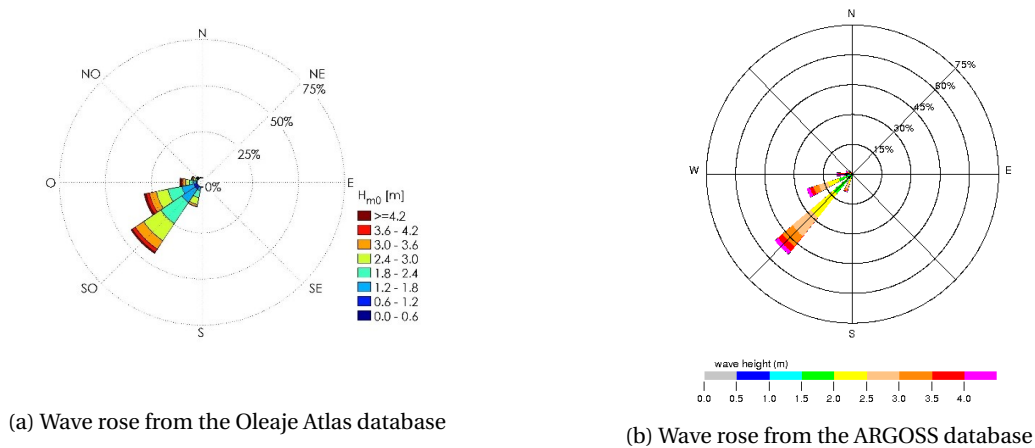


Figure 4.17: Wave roses from both data bases.

### 4.2.3 Water design levels and environmental influences

#### Currents

Looking at a world map including the oceanic currents in figure 4.18, it can be seen the main current in Chile is running from south to north along the Chilean coast. This main current is called the Peru-Humboldt current. The Peru current is mostly a cold current, except at times of the phenomenon known as El Niño. The Peru Current brings fog to the coast, but also helps to keep the coast one of the most intensely arid areas in the world. El Niño usually brings warm ocean conditions along the tropical west coast of South America. Figure 4.18 gives an overview of this main Peru-Current. The Peru-Current extends from 500 to 1000 kilometers offshore.

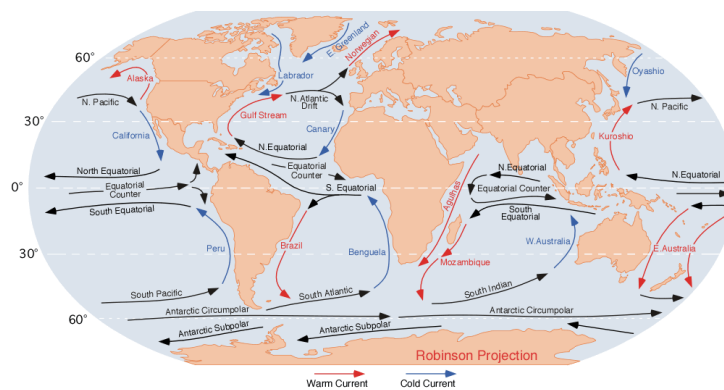


Figure 4.18: Oceanic currents (Wikipedia 2017)

According to the DoP the currents in Quidico and Tirúa are in the order of 0.1 m/s in the coastal sector. Near the coast higher current magnitudes than the tidal current occur. Adjacent projections or abrupt changes in the coastline can cause currents of around 0.15 m/s. Currents can significantly influence the wave propagation. High currents could induce refraction of the waves. According to the currents around Quidico, with a maximum speed of 0.15 m/s, this is not classified as a high current. Probably this current does not have a large influence on the waves.

#### Water levels

In front of the Chilean coast there is a movement around the amphidromical point in the South Pacific. The tidal range is about 2 meters with a micro-tidal regime, see figures 4.19a and 4.19b.

Tidal data is obtained from the Sea Level Station Monitoring Facility (IOC 2017). There was no data available for Quidico, therefore the monitoring station at Lebu is used (70 km North of Quidico). The left figure of figure 4.19 shows the water levels for March 2016 until July 2016 and the right figure shows the water levels during

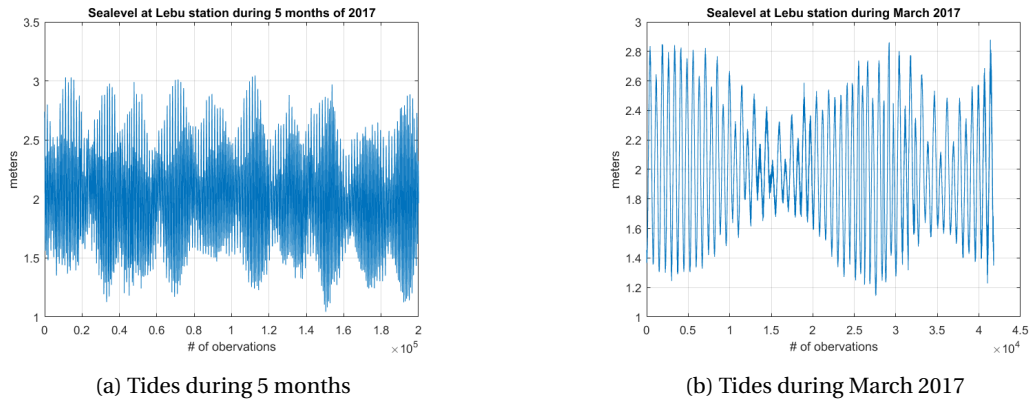


Figure 4.19: Tides

March 2017. The values of the figures must be lowered with a value of 2 m to obtain the correct tidal movements for Quidico. From figure 4.19b it can be concluded that the tidal character is a combination of a semi diurnal and diurnal type, predominantly a semi-diurnal type (Bosboom and Stive 2015). In figure 4.19 it is visible that most of the time a high-high tide and a lower-high tide occur for every 24 hours. In the right figure the high- and low tides and their peaks are visible.

With these data the highest and lowest water level all time is set to (see figure 4.20):

- Lowest water level: -0.98 (m)
- Highest water level: 1.03 (m)

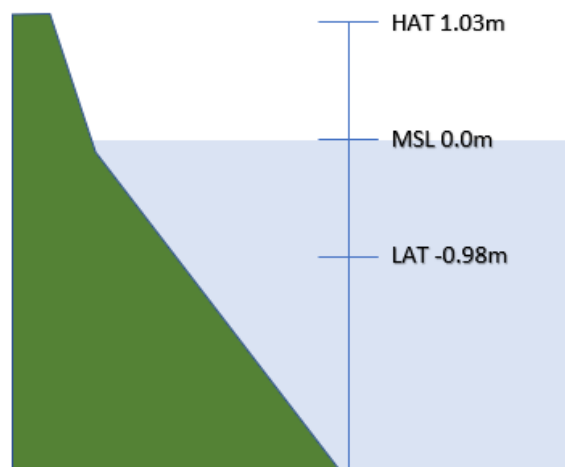


Figure 4.20: Tidal system for the bay of Quidico.

With: HAT = Highest Astronomical Tide, MSL = Mean Sea Level, LAT = Lowest Astronomical Tide

The water levels are also checked for the months November and December, those maximum values are not exceeded. The Department of Ports used a station close to Quidico to obtain their tidal data. It is advised to perform additional (tidal) water level measurements at the site to verify the chosen values. For the design phases of this report a high tide of 0.9m and a low tide of -0.9 m is applied. This is referenced to a mean water level of 0m.

## Salinity

According to CATDS (CATDS 2017), the salinity around Quidico Bay is around 33/34 PSU (Practical Salinity Unit). The salinity level near, for example, Europe is a little higher. The salinity difference over the whole world differs from 31 to around 38 PSU. The water temperature in Quidico is around 14 degrees Celsius with a density of around  $1025 \text{ kg/m}^3$  (Wikiwand 2017).

### 4.2.4 Bathymetry and river influences

#### Bathymetry

In order to make a hydraulic model, water depth measurement are necessary. Most of the time those values are obtained via a bathymetric survey. The bathymetric data of this project is obtained from the DoP. Processes like shoaling, refraction, diffraction and wave breaking are directly related to the water depths. Not all of these processes are correctly included in the used model. Influences of diffraction and wave breaking are based on simple rules of thumb and linear wave approximations. The obtained data offshore is relatively coarse, near the fishing harbour the data is more dense. Still there are some areas where assumptions were necessary. The obtained bathymetric data is shown in figure 4.21.

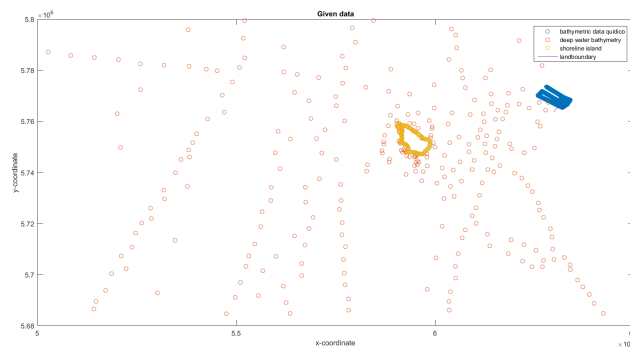


Figure 4.21: Depth points around Quidico bay

Figure 4.22 shows the offshore (left) and near-shore (right) obtained bathymetry for Delft3D. In the right figure, the land boundary of Quidico is plotted as indication. The colours are indicating different water depths. For the right figure a rough estimation gives a water depth of 2m for the yellow areas, the blue areas represent a water depth of 70m. In the near shore data some elevations are given next to the bathymetry points. These elevation-points are mostly skipped when constructing the depth file. Elevations are only given for the headland of Quidico Bay. For the other elevations of the shoreline USGS Earth Explorer is used (USGS 2017). A DEM-file is obtained and processed with QGIS. All the data is geo-referenced to UTM18S. These depth data points are used to create a bathymetry file for the Delft3D-model. Navionics (Navionics 2017) is used for a rough check on the bathymetric data. The whole model set-up and the final depth file is represented in Appendix E.

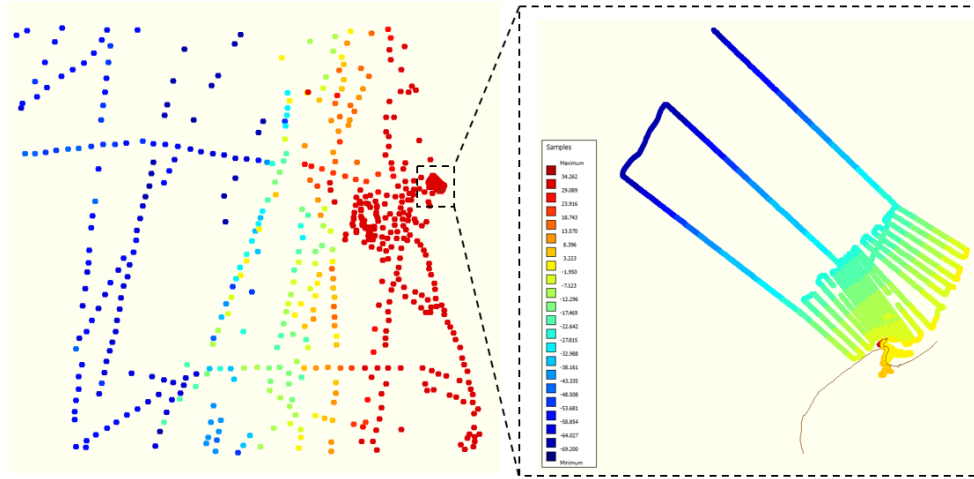


Figure 4.22: Bathymetry offshore and nearshore of Quidico

### River

At the project location a river outflow is entering the bay, see figure G.3 in Appendix G. The river originates in a reservoir upstream, this reservoir is regulated with a dam. There is no exact data available from the outflow from this reservoir. From the site visit and from information of the DoP, the mean discharge is estimated to be  $2 \text{ m}^3/\text{s}$ , with a maximum of  $40 \text{ m}^3/\text{s}$ . Due to the fact that the design rain is quite low and the flow is regulated, the discharge from the river will not fluctuate too much. The sediment in the outflow is very fine sediment. The water from the Andes flows into the reservoir, where the larger sediments will settle. By opening the reservoir most of the suspended sediment will flow towards the bay of Quidico. Because the river is flat, most sediments will sink, the outflow of the river will therefore carry a relatively small amount of sediment. Despite this fact, the river can be of influence on the sediment transport in the bay.

### 4.2.5 Wave analysis

#### Offshore

With the prior mentioned data an extreme value analysis is done, for both the wind waves as the swell waves. The analysis of the swell waves is executed for both the Atlas and ARGOSS data. The Peak over Threshold method is used for this analysis. This method is also used in the report of the consultancy company. The Peak over Threshold method uses the maximum wave heights during a storm. If a wave height is higher than a certain threshold value, this wave height will be considered. The process for the correct threshold value is a bit of trial and error. The aim should be to find around 10 storms a year on average. To avoid using multiple wave heights within one storm, the time between two storms is set to 24 hours. All the extreme wave heights are saved. These maximum values of storms are stored into certain bins, with bin widths of 0.1 meter. These bins are used in the statistical analyses. The statistical calculations can be found in appendix D, the results are given in tables 4.7 and 4.8. The symbol H indicates the wave height and the symbol T indicates the wave period. These symbols are separated in: s = significant, p = peak and m = mean.

Table 4.7: Offshore values for a return period of 50 years (ARGOSS)

Parameter	Exponential	Gumbel	Weibull
$H_s$ (m)	11.32	10.91	10.68
$T_p$ (s)	19.66	19.30	19.10
$T_m$ (s)	17.62	17.30	17.11
$H_s$ (m)	8.79	8.66	8.65
$T_p$ (s)	14.72	14.61	14.60
$T_m$ (s)	12.27	12.17	12.17

Table 4.8: Offshore values for a return period of 50 years (Oleaje Atlas)

Parameter	Exponential	Gumbel	Weibull
$H_s$ (m)	10.95	10.86	10.27
$T_p$ (s)	20.07	19.98	19.43
$T_m$ (s)	14.53	14.76	14.08

The values from tables 4.7 and 4.8 are specific for the offshore waves. In section the next section, wave transformation to near-shore is discussed.

#### Offshore to near shore wave transformation

In the extreme value analyses, the offshore wave data is analysed. The breakwater will be constructed close to the shore, therefore transformation of the waves will be necessary. Through the fact that the bathymetry is quite irregular, it was hard to model the transformation of the guiding wave. The irregularity of the bathymetry is also caused by the Island Isla, which is 35 kilometer south-west-west of Quidico. In the wave roses above it can be seen that many waves are coming from a south-west to western direction. Due to the shadow zone behind the island, the sediment will settle and the depth will decrease. This is visible in the data from the web-app of Navionics (Navionics 2017).

From the offshore data and a meeting with the DoP, it follows that the most unfavourable waves are coming from the North-West (315 degrees). The island is not influencing waves coming from this direction. Therefore, the waves will not lose too much energy. The guiding offshore wave height and corresponding wave period are given in table 4.7. As said, due to the Island, the guiding direction is defined to be 315 degrees and therefore, the values of 4.7 cannot be used. After a meeting with Cristian from the DoP, a new analysis is done for these waves. The database is filtered on waves coming from 270 till 360 degrees. The results of this meeting are stated in table 4.9. The design wave height, period and direction are given.

Table 4.9: The guiding wave height and period found for waves coming from 270 till 360 degrees

$H_s$ (m)	$T_m$ (s)	$T_p$ (s)	Direction (deg)
3.8	17.3	19.3	315

This means that the offshore wave height, coming from the range of 270-360 degrees, will be 7.4 meter. Which is still relatively high.

The values from table 4.9 are obtained by taking the following transformation phenomena into account:

- *Shoaling*: if waves come closer to the coast, the depth becomes less and the waves start to 'feel' the bottom. The wave heights are increasing, which is called shoaling of the waves.
- *Refraction*: waves are trying to arrive perpendicular to the coast. The bathymetry, the initial offshore wave angle and the coastline are influencing how much the wave will bend.
- *Diffraction*: diffraction has to do with obstacles. The waves are curving around the obstacle. Most of the times the waves are diffracting in a sheltered zones.
- *Reflection*: reflection has to do with the energy of a wave. Vertical walls may reflect almost all energy, while on a flat slope the energy will dissipate due to breaking and other energy dissipating phenomena.

The offshore wave height, period and wave direction are known. Therefore the angle of incidence with the breakwater can be calculated if the breakwater orientation is known. Diffraction and reflection are the consequences of building a breakwater. These phenomena are not be taken into account yet, and will be described later this report. Diffraction can be a process that can cause for mooring problems. Refraction and shoaling are important interactions by building the breakwater. To calculate the needed design wave heights, an Excel sheet is used. The results from the Excel sheet are shown in figure D.9.

At the end of the breakwater, the depth will be around 4 meters. With the given offshore values, the guiding onshore wave height is defined to be around 3.8 meters. This can be seen in figure D.9. From this figure it

is also visible that this (extreme) wave is already broken before hitting the breakwater. This should be taken into account by designing the breakwater. In appendix D.2, the calculations and phenomena will be described more elaborately.

#### 4.2.6 Sediment transport

Sediment and the flow of sediment is one of the main issues at Quidico Bay. Therefore, all the relevant hydraulic processes must be investigated. As said in section 4.2.4, the river could be a source for the sedimentation. During the site visit in Quidico Bay, see Appendix B, it was observed that the river barely contains sediment. The sediment transport along the coast, caused by the waves, is the main source. The ratio sediment by the waves and from the river must be investigated. Looking at Google Earth the bay contains black sand, probably coming from the Andes. Sand of the Andes can be characterized as very fine with small diameters. This sand can easily be transported, even with low velocities. In the bay an analysis on the grain sizes is done. The  $d_{n50}$  is estimated from table C.2 and set to 0.2mm. As said, research in the sediment transport is necessary to say something about the water depths in the bay. A certain water depth is necessary for mooring the fishing boats.

#### 4.2.7 Final values for the hydraulic boundary conditions

Table 4.10 summarises the final values used for hydraulic boundary conditions. The values stated below are used for modelling in Delft3D and to design the breakwater with, coming from the north-west. The model will be treated in Appendix E.

Table 4.10: Final values for the hydraulic boundary conditions.

Parameter	Value	Unit
Offshore sea wave height	6.8	m
Sea wave period	14.0	s
Offshore swell wave height	7.4	m
Swell wave period	19.3	s
Near-shore sea wave height	2.2	m
Near-shore swell wave height	3.8	m
Wind velocity	20	m/s
Current velocity	0.2	m/s
Water level	max: + 0.9 min: - 0.9	m
Salinity	33 - 34	PSU
Sediment size	0.2	mm

## 4.3 Structural conditions

### 4.3.1 Current structural elements

The project site currently consists of just a few structural elements. The main structural aspects to consider are the concrete plaza including the cocinerias and the existing access road. The plaza with cocinerias consist of a filling contained by a concrete wall, that protects the area against waves during high tides. A ramp is connected to this plaza. The plaza is connected to the main road by an unpaved road, which also consists of a filling covered by concrete walls. This road continues on the other side of the concourse all the way to the end of the bay. A small concrete mooring location is constructed at the end of this road to unload heavy catches. Opposite to the landing area on the banks of the Quidico river, a basic metal structure is present. This serves as the headquarter for the fishermen unions. The building has a surface area of 27 m<sup>2</sup> and rests on a concrete slab.

### 4.3.2 Traffic

The traffic load has to be estimated, since it will be used as input for the design of the access road and the pavement in the support area. Based on the situation observed in other fishing areas similar to Quidico, information from Sernapesca (the Ministry of Fishing and Agriculture) and the needs expressed by the fishermen, it was estimated that the average traffic load is 5 design trucks per day. For design purposes the DoP requested to consider a design traffic load of 20 trucks per day.

The design truck is defined using the guidelines of the American Association of State Highway and Transportation Officials (AASHTO). The HS 20-44 design truck is selected, based on input given by the DoP. This design truck is slightly adjusted by assuming a front axle with single tires and a rear axle and trailer axle with dual tires. The maximum load of each truck, corresponds to 39 tons for trucks between 13 and 15 meters long. This load is distributed over the axles. The front axle takes 12% of the load and the rear and trailer axles take 44% of the load each.

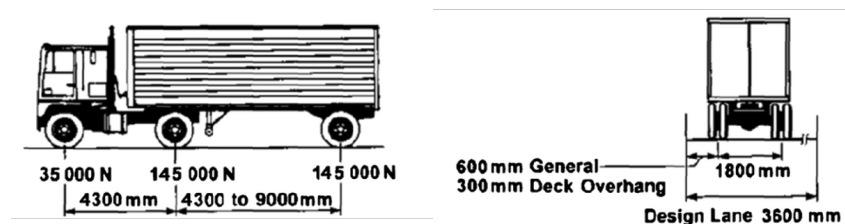


Figure 4.23: HS 20-44 Truck

Based on this distribution, the Equivalent Axle Factor is estimated using AASTHO. Different factors are calculated based on the different materials of the pavement. These factors and the traffic load are shown in table 4.11. The traffic loads are determined for a design lifetime of 20 years.

Table 4.11: Equivalent axle factor and traffic load for a 20 year design lifetime

	Equivalent axle factor (-)	Traffic load (million ESALs)
<b>Asphalt</b>	4.03	0.62
<b>Concrete</b>	7.23	1.1

# PART 2: DESIGNS



# 5 Breakwater Configuration and Design

## 5.1 Design approach

The design process of the breakwater can be divided in several phases. First several alternatives are made by considering the requirements for the breakwater configuration. These requirements are set during the meetings with the Department of Ports (see Appendix N.2.10). Three different breakwater orientations are considered. These alternatives are modelled with Delft3D and discussed with the DoP. The decision for the final breakwater configuration is made by taking into account all relevant processes. The processes which are not covered by the model include diffraction and sediment transport. The next chapter gives a detailed study about the sediment transport around Quidico. After finalizing the breakwater configuration a design is made for the breakwater cross-section. Finally a geo-technical analysis is performed for the subsurface at the position of the breakwater.

## 5.2 Design requirements

The proposal of the DoP for the breakwater configuration was not satisfactory. In cooperation with the DoP new requirements are defined. Based on these requirements and the boundary conditions (as defined in section 4.2) several breakwater alternatives are proposed. A final, satisfactory, design will be build following the project phases as stated below:

1. The breakwater is constructed without use of dredging.
2. Monitor the sediment processes around the bay for a certain period.
3. In case too much sediment enters the bay, the option to construct a contramolò will be considered.
4. Construct the mooring facilities.
5. Finally, construct the onshore facilities.

Dredging is included in the design proposal of the DoP, however in a later stadium dredging was quantified to be too expensive. This new development induced several changes for the design of the port. The main design requirements for the configuration of the breakwater are listed below:

- The stones in front of the bay must be used as foundation for the first part of the breakwater (figure 5.1).
- The end of the breakwater must be out of the breaking zone.
- Protection of the mooring facility against the most unfavorable waves.
- Consider the sediment movement around Quidico.



Figure 5.1: Foundation consisting of stones in front of the headland

### 5.3 Design alternatives

Based on the criteria above three alternatives are obtained. Due to the first criteria stated in the list above, the first section of the breakwater should be in extension of the existing stones (see Figure 5.2a). This first, straight, section however, is not sufficient to protect the bay from high waves. Therefore, a second breakwater section is added. Since this section should also provide protection for the waves coming from the north, the value for the angle between the two sections is proposed to be 45° eastwards. The length of this second section mainly influences diffraction and breaking of the waves. Diffraction is related with the amount of sheltered area behind the breakwater. The amount of sheltered area is depending on the size of the fishing-boats, distance required to reduce their speed and the amount of boats. The most important aspect for the fishers is that they can make a safe movement around the breakwater. It is thereby important to sail oblique on the waves with a relatively large speed towards the breakwater. Behind the breakwater a sheltered zone is created to make a movement into the harbour. Three different lengths for the second part of the breakwater are proposed and investigated: 50 m, 100 m and 150 m, see figure 5.2a.

An important design requirement is to construct the end of the breakwater outside the breaking zone of the waves. This enables the fishermen to safely enter the harbour. The breaking point is estimated by using the ratio of wave height over water depth, see equation 5.1 (Holthuijsen 2007). Since the depth at the end of the breakwater is known, the breaking wave height can be calculated. This procedure is merely a theoretical approach and provides an estimation of the critical breaking depth.

$$\frac{\text{wave height}}{\text{water depth}} > 0.75 \quad (5.1)$$

A rough indication of the initial proposed orientation from the DoP and the new proposed orientation are shown in figure 5.2a. As can be seen from the picture, the new proposed orientation offers protection for waves coming from a south-west till north-west direction. This enables the fishing boats to safely moor and drop off their goods.

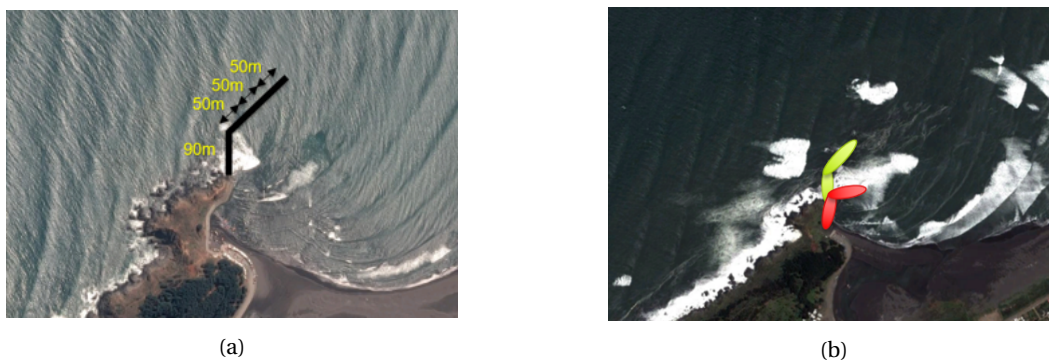


Figure 5.2: (a) The new proposed breakwater orientation. (b) Initial and new proposed breakwater orientation.

The final modelling set-up is given in table 5.1. The wave height and wave period do not change for the different breakwater configurations. The only variables are the length and wave angle. The last column of table 5.1 shows the critical wave height above which the waves break. This is a theoretical value and should be checked using the modelling results.

Table 5.1: Input data for the different models in Delft3D.

Model	Wave height (m)	Wave angle (deg)	Tp (s)	Depth (m)	Critical wave height from which waves start to break
Current situation	2.4	270, 292.5 and 315	12	-	-
50m breakwater	2.4	270, 292.5 and 315	12	4	>3 m
100m breakwater	2.4	270, 292.5 and 315	12	4.5	>3.4 m
150m breakwater	2.4	270, 292.5 and 315	12	4.8	>3.6 m

Since the fishermen are an important stakeholder (see Appendix A), the new proposed breakwater orientation is presented during the meeting on the 11<sup>th</sup> 2017. During this meeting the fishermen agreed on the new proposed orientation. A short summary of this meeting is provided in Appendix N.2.13.

## 5.4 Modelling phase

### 5.4.1 Model set-up

Using the boundary conditions as specified in section 4.2, a Delft3D model is created. Quidico Bay and its surrounding are modelled, this is done via a grid and depth file. These files are based on the obtained bathymetric data from the Department of Ports. Tides and waves are specified at the boundaries of the model. A wave study is performed with SWAN, which is a function implemented in Delft3D. The SWAN model takes into account the following processes: shoaling, refraction, wind growth and wave breaking. Processes as diffraction and reflection of waves are not (fully) included in the model. In Appendix E the entire model set-up is explained in more detail. In figure E.5, the three final breakwater layouts are implemented in the model. The breakwater looks angular due to the grid placement, however this will not effect the main processes too much. Due to the limitation of time for the project, there was not enough time to refine the grid and depth file.

In figure 5.3, a small part of the total depth file is plotted. For a better understanding of the results, a satellite image from Google Earth is plotted over this initial depth file. This figure can be used as reference by analysing the obtained model results. The white arrow is pointing at the bay of Quidico.

The next step in the model set-up is the comparison of the model created and the actual in-situ situation, this validation of the model is discussed in the following section.

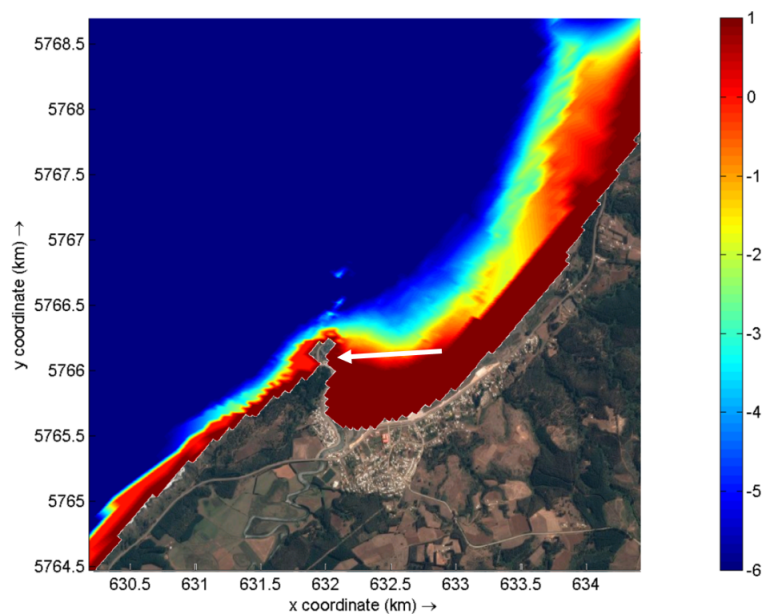


Figure 5.3: Satellite image from Google Earth plotted over the initial bed file from Delft3D. The white arrow is pointing at the bay of Quidico.

### 5.4.2 Model validation

The results of the model (without the breakwater and the contramolo) are compared to the actual situation along the coast of Quidico. In figure 5.4 the model results for the current direction and speed are shown. A circulation of the current is observed north of Quidico Bay. This circulation is also visible in the Google Earth picture (Google-Earth 2017) as shown on the right in figure 5.4. During the meeting with the DoP, December 11<sup>th</sup> 2017 (Appendix N.2.13), the Delft3D model is compared to the model created by the consultancy company (CMS-WAVE). The wave propagation in both models is compared, the models show similar results.

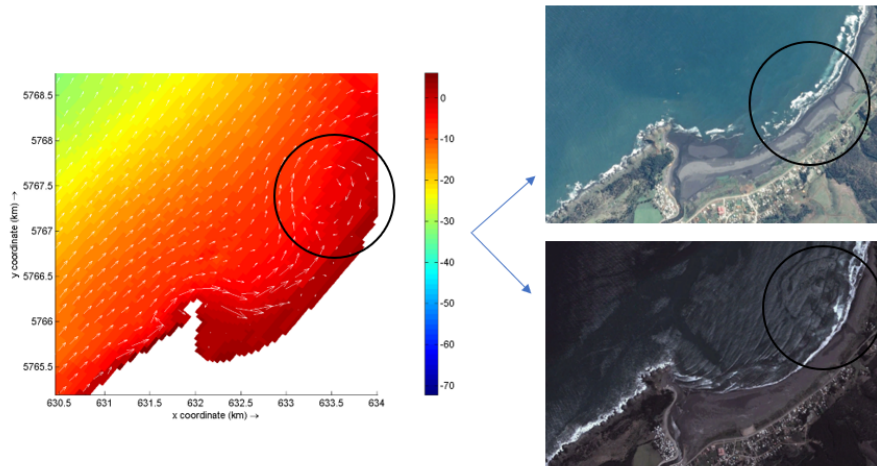


Figure 5.4: Model results compared with Google Earth

As extra validation of the model three random breakwater configurations are implemented, these configurations are shown in figure 5.5. Significant changes in the modelled current directions and wave heights and directions are observed when using these configurations. These results are shown in Appendix F.

Based on the observations as described above, it is concluded that the model works good enough for its specific purpose.



Figure 5.5: Three configurations of the breakwater

### 5.4.3 Modelling results Delft3D

In this section the results of the three final alternatives are discussed. The considered lengths for the second breakwater section (50, 100 and 150 meter) are modelled and the results are shown in the following sections.

### Influence of the different wave angles

The waves are modelled with offshore waves coming from three different directions: 270, 292.5 and 315 degrees. From the results shown in figure E.3 it can be seen that the effect of these different angles on the wave height and currents in the bay is negligible. The waves are refracting towards the coast and approaching the bay in a similar way.

### Wave heights and directions at the breakwater

The wave heights at Quidico Bay and its surrounding with the longest new proposed breakwater orientation (indicated in blue) are shown in figure 5.6. It is observed that the wave height at the end of the breakwater does not exceed 3m. In the same figure also the initial breakwater configuration as proposed by the DoP is also plotted (indicated in black). This is done to compare the wave height at the end of both breakwater configurations. It is observed the wave heights at the end of the breakwater as proposed by the DoP are lower than the wave heights at the end of the new proposed breakwater. These lower wave heights are in all probability caused by the lower water depth. Therefore the waves are expected to break close to the location of the end of the breakwater as proposed by the DoP.

Looking at the wave directions, the waves are refracting towards the coast. For a wave direction of 315 degrees the results for each breakwater length are given in Appendix F (figures E.11 until E.14). It is hard to show the differences in wave heights in this report, however differences are visible for an increasing breakwater length. The influence of the breakwater on the wave height is higher for an increasing breakwater length.

The influence of the waves on the mooring facility are discussed in section 5.5.1, in this section the diffraction of waves is explained in more detail.

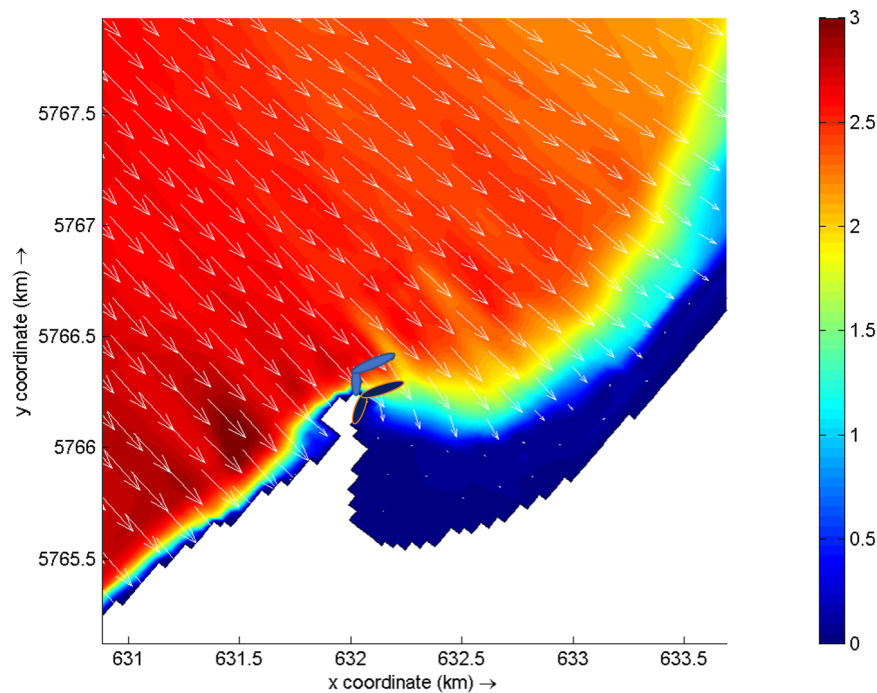


Figure 5.6: Wave height directions plotted with the longest proposed breakwater (indicated in blue) and the initial design from the DoP (indicated in black)

## Currents

By looking at wave induced currents, some differences are visible between the alternatives. In figure 5.7 the direction and size of the wave induced current for the actual situation (white arrows) and the longest new proposed breakwater (black arrows) are presented. A wave angle of 315 degrees is used in this model. In contrast to the modelled wave heights, the differences in wave induced currents for both situations are clearly visible. The black arrows (new proposed breakwater configuration) tend to make a sharper curve into the bay than the white arrows, which is probably caused by an increase of the depth difference between the location at the end of the breakwater and the bay itself. Furthermore, the black arrows are smaller than the white arrows closer to the shore within the bay (as indicated with number 2 in figure 5.7), this is caused by the increase of the sheltered area when a breakwater is present. Further it is observed that the influence of the wave induced current on the most southern point of the bay is negligible. This point is indicated with number 1 in figure 5.7. Based on these observations it can be concluded that a longer breakwater configuration results in a sharper curve of the wave induced current into the bay. Also the speed of the wave induced currents close to the shore within the bay, tend to decrease with an increasing breakwater length.

The modelling results of the wave induced current for each breakwater configuration alternative are shown in Appendix F (figures F4 until F7). In Appendix F also the modelling results of the wave induced current for each of the three wave angles are shown (figures F8 until F10).

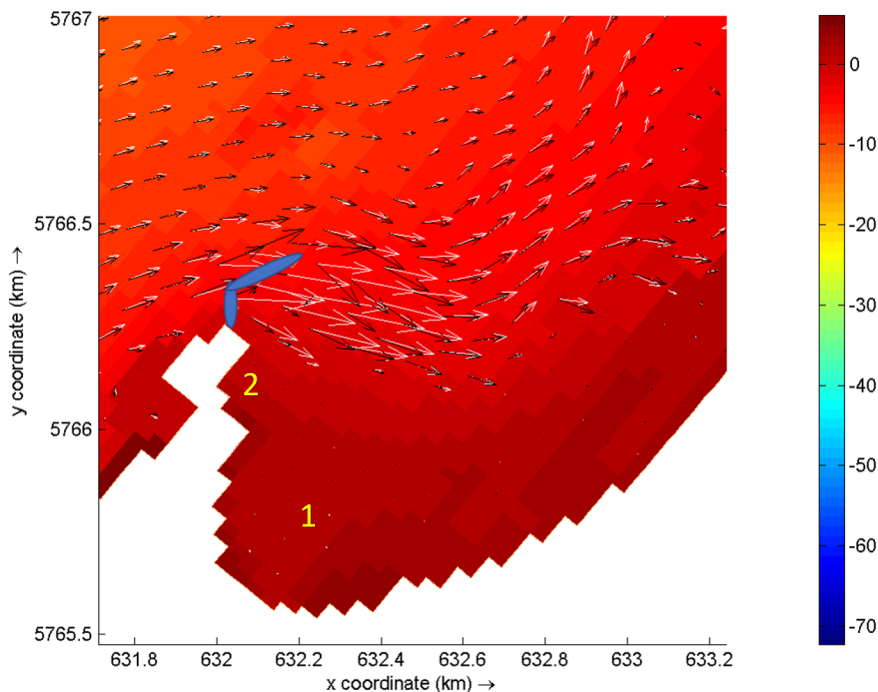


Figure 5.7: Comparison of wave induced currents with the breakwater (black arrows) and without a breakwater (white arrows)

## 5.5 Additional analysis

In the following section some additional analyses are done. Since diffraction and sediment transport are not covered by the Delft3D model, these processes are analysed based on theories. Both processes can be of significant influence and the effects are important for the breakwater configuration.

### 5.5.1 Diffraction around a breakwater

Although a breakwater provides protection from direct wave attack, diffraction around the breakwater end causes wave fronts to bend into the shadow zone. This leads to a leakage of energy into the lee of the breakwater (Briggs et al. 1995). In figure 5.8a this shallow zone is indicated with normal incident waves. In the research of M.J. Briggs a number of laboratory studies are performed whereby wave diffraction around a single breakwater is investigated. In the research of Briggs methods described by Goda and Sommerfeld are discussed. The results of the laboratory test of Briggs have been compared with different computer based programs for regular and irregular waves. During this research different diffraction coefficients were obtained for three different angles: 30, 60 and 90 degrees (see figure 5.8b). For the project site of Quidico an angle of 30 degrees is used to obtain the diffraction coefficient.

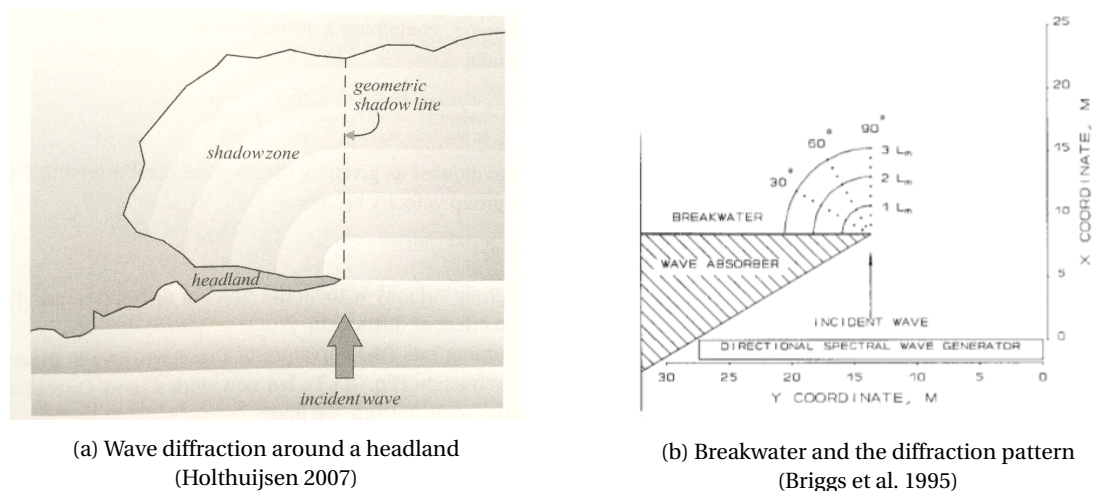


Figure 5.8: Wave diffraction around an object

Regular and irregular waves are tested in the laboratory by Briggs. In the calculations for Quidico, mainly swell waves are investigated since these have the biggest impact. Those waves are relatively regular and can therefore be used and compared with the theoretical tests of Briggs. Furthermore, during the laboratory tests an incident approach of the waves is used, see figure 5.8b. At the project location, most of the swell waves are coming from an angle more to the south-west (looking at figure 5.8b). Assuming an incident wave angle will result in a more conservative approach for the bay of Quidico.

The Sommerfeld solution (Holthuijsen 2007) is used to provide an indication about the wave diffraction in Quidico Bay. A rough estimation for the wave length around the breakwater is used in the calculation since the wave length changes for shallower depths. The water depth is obtained from the bathymetric data. The water depth at the end of the breakwater is to a value of 4 meters and the wave period is calculated to be 12 seconds, this value for the wave period is based on a conservative approach. The wave length is calculated based on these values the wavelength is estimated to be 75 m. According to the table of M.J. Briggs the  $x/L$  ratio is used to determine the diffraction coefficient.  $x$  is the length of the considered breakwater and  $L$  is the wavelength. The water depth at the end of the breakwater is assumed to be equal to 4 m for each of the alternatives. For the 50 m breakwater the  $x/L$  ratio is 0.68, the 100m breakwater this value is 1.33 and for the 150 m breakwater this value is 2.00. From table 4 in Briggs et al. (1995) the diffraction coefficient ( $H/H_{incident}$ ) is obtained. The diffraction coefficient for the three cases respectively have a value of 0.29, 0.22 and 0.17. Based on observations of the fishermen the maximum wave height around Quidico Bay is approximately 4 m. By using the diffraction table the maximum wave heights within the bay due to diffraction are estimated to be 1.18 m for the 50 m breakwater, 0.88 m for the 100 m breakwater and 0.68 m for the 150 m breakwater.

Instead of the tables as provided by Briggs also the Sommerfeld graphs (Holthuijsen 2007) can be used to calculate the diffraction coefficient, as shown in figure 5.9. A  $x/L$ -ratio between 0.68 and 2 corresponds to a value for the diffraction coefficient within the range 0.2 - 0.3. Similar results are obtained for both methods. Due to the wave direction and the assumed wave height of 4 m, the approaches as described above lead to conservative results.

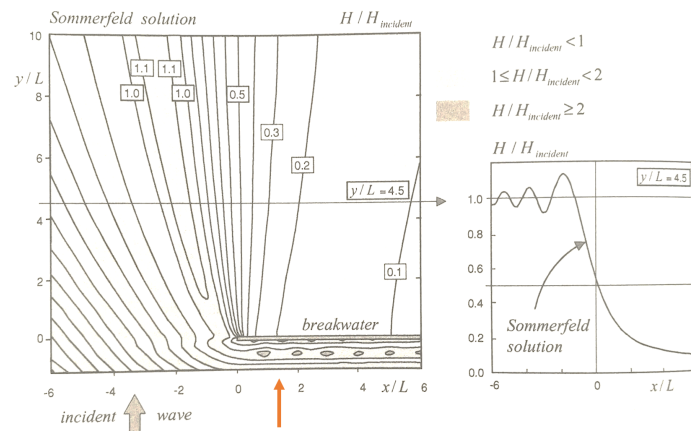


Figure 5.9: Sommerfeld graph for the wave diffraction

### 5.5.2 Breakwater influence on sediment transport

In the current situation the sediment transport around Quidico Bay is practically in equilibrium. The realisation of a breakwater will fluster this equilibrium. An analysis on the sediment transport in the area is performed using relative simple approaches. The greater part of the sediment is moving due to wave breaking and the currents running along the coast. The island Mocha however influences the sediment transport around Quidico. The island reduces the wave heights when the waves come from a west to south-west direction. Those lower wave heights create calmer water, which induces settlement of the sediment.

#### Breakwater influence

Building the breakwater will create accumulation at the updrift side of the breakwater since the sediment cannot pass through the breakwater. At the north-east side of the bay, there will be erosion due to the lack of sediment transport compared to the initial situation. When the accumulated area is reaching the end of the breakwater, the sediment will pass the breakwater again. It is difficult to estimate the time required for this process to occur. The eroded area at the north-east side will accumulate again. Expected areas of accretion after a long time are shown in figure 5.10.

From figure 5.10 it is seen that sediments can be transported in the direction of the bay due to the return current. To prevent the bay from sedimentation, the idea of the Department of Ports is to build a so called 'contramolo'. This contramolo should prevent the sediment to settle in the bay. The solution of the contramolo only is a theoretical solution, because it is not proven yet that this contramolo will solve the wave- and sediment problems. The influence of the return current and the sediments transport should be evaluated. According to the theory particles settle due to gravity if a protected area is created and sediments are present in the water column. If a return current is of significant influence, a contramolo could work. However, the contramolo will only postpone the sediment problem. After a certain period, the area at the north-east side of the contramolo will be full of sediment as well. When this part is accreted, the sediment will start to enter the bay.

It is expected the main breakwater will keep the sediments out of the bay for a certain time. Duration and quantities are however not known and hard to predict. Therefore sediment movement should be monitored after construction. A more detailed study about the sediment movements is given in section 5.7.

#### River influence

As specified in the boundary conditions (section 4.2), the mean river outflow is  $2 \text{ m}^3/\text{s}$  with a maximum of  $40 \text{ m}^3/\text{s}$ . This river is regulated upstream and the outflow therefore mainly depends on the amount of rain. The influence of the river is however not considered to be very large. In section 5.7.7 the river influences are discussed in more detail.

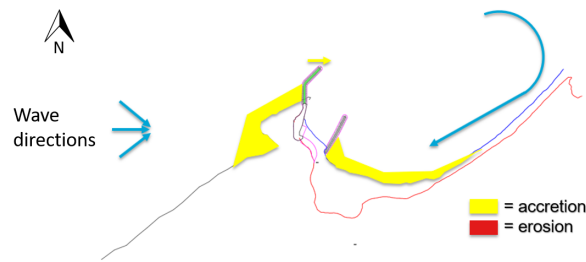


Figure 5.10: The long-term coastal influences of both breakwaters

## 5.6 Final breakwater orientation

During the modelling phase the most unfavorable directions and wave heights are investigated. Based on the wind roses and wave roses three directions with corresponding wave height are modelled. Three breakwater alternatives are modelled for the directions of 270, 292.5 and 315 degrees with a wave height of 2.4m. The decision on the final breakwater orientation, based on these models, is described in this section.

It should be mentioned that the breakwater orientation is based on the results of a model and this model has its flaws. The island 'Isla Mocha' has not been taken into account in the model, however this island is of influence on the results. Also the processes diffraction and reflection are not covered in the model. The results therefore can only be used as a recommendation regarding the final breakwater configuration. It is advised to keep in mind relevant theories about hydrodynamic processes.

### 5.6.1 Contramolo

The main function of the contramolo would be to shelter the bay for sediment transport due to the possible return current. However, this return current was not always visible during the modelling phase and the influence of this current is estimated to be negligible. Therefore it is concluded that sediment problems due to the return current will not occur. Without the sediment problems the contramolo is not required in the design. The contramolo is not constructed in the final design of this report.

### 5.6.2 Main breakwater

The final breakwater orientation is based on the results of the Delft3D model and the sediment analysis as discussed in section 5.5.2. Three different breakwater lengths are evaluated and modelled. Differences in the wave induced current directions are clearly visible for the different breakwater lengths. In theory: the longer the breakwater, the sharper the current is curving into the bay. Also the speed of the wave induced currents close to the shore within the bay, tend to decrease with an increasing breakwater length. Looking at the wave heights, it can be concluded that the waves in the bay for the shortest alternative are too high for sufficient mooring conditions. This option does not provide sufficient protection. The differences between the 100 m and 150 m concerning the wave heights, are small. A simple diffraction method is applied to achieve a better indication of the wave heights concerning these alternatives, however the differences between the two is small. The sediment transport differences between the 100 m and 150 m breakwater are also considered. The length of the breakwater is influencing the time it will take for sediment to pass around the breakwater. A longer breakwater increases the time before the sediment starts to pass the breakwater. How large the influence of the length is, is not known. Following this reasoning, the 150 m is the preferred alternative.

### 5.6.3 Final decision

From the results above it is concluded that the 50 m breakwater does not provide sufficient protection, therefore this alternative is not recommended. The differences concerning the waves within the bay between the 100 m and 150 m breakwater alternative are small. Looking at the sediment transport, the 150 m length is the preferred alternative. Also according to the modelling results the 150 m breakwater is preferred option. However, when looking at the design requirements and costs, which are important aspects, the 100 m breakwater is the recommended length for the breakwater. This decision is mostly based on economical reasons. The costs

of the breakwater greatly increase when the length of the breakwater is increased.

#### 5.6.4 Project planning

As stated before, there are big doubts at the DoP about constructing the contramolo. Based on the Delft3D results the return current is barely visible, therefore the contramolo is assumed to be unnecessary. The main function of the contramolo is to block the sediment from the created return current. It is not proven that this contramolo will solve these wave- and sediment problems. And if the return current is a problem, the contramolo will only delay the sediment problem. Based on the model results from the consultancy company, the DoP is convinced that the return current is present. They are referring to the few moments that the return current is visible in the model results.

Despite the different opinions regarding the return current, the following construction procedure is recommended to be followed for the project. First construct the main breakwater of 100 m and after that, monitor the entire area for a certain time. The movement of sediment quantities should be monitored during this period. Analysing this data could give a better view about the presence of the return current. After analysing the results the decision can be made. If sediment is moving towards the bay, two options are available: construct the contramolo or apply dredging. Dredging is not preferred by the DoP, because it maintenance is not very well applied in Chile. If dredging is chosen, it needs to be applied on a regular basis.

For the mooring places it is recommended to wait some time before constructing them. First analyse the sediment movement in the bay and indicate the accumulated and eroded locations. By doing this, the correct location for the mooring places could be chosen. Placing the mooring places at the breakwater is an option as well. The final orientations of the main breakwater and, if needed, the contramolo are given in figure 5.11.



Figure 5.11: The final orientations of the main breakwater and contramolo

## 5.7 Sediment movement around Quidico

In this chapter a theoretical and qualitative analysis is performed for the sediment transport in and around Quidico Bay. This sediment analysis is done on basis of the final design, presented in section 5.6. First, a short section is included about the sediment characteristics. By using these characteristics the current situation is evaluated. Next, the sediment transport is analysed for the bay including the breakwater configurations. A distinction is made between with and without the contramololo. Finally, a short analysis is done about the mooring facility, river and dredging influences.

### 5.7.1 Sediment characteristics

The sediments in Quidico consists mainly of fine sand. This can be concluded from the three different sediment samples analysed in table C.2. From this analysis, it becomes clear that the sediments in Quidico are poor graded. This means that the diameter range is relatively large. In formula form it can be stated that if  $D_{90}/D_{10}$  is larger than 3.0, the grading is poor. For completeness,  $D_x$  means that x percent of the sediment particles is smaller than this particular size. The grain size is an important parameter in the study of sediment transport. In Quidico Bay, the median grain size ( $D_{50}$ ) is specified to be 0.2 mm, which indicates very fine sand. Other important parameters for sediment transport are:

- density of the grains;
- relative density (density difference between sediment and water);
- characteristics of the fluid, e.g. density and viscosity;
- concentration and the porosity of the sediments;
- fall velocity, which is mainly dependent on the grain size, relative density and viscosity of the fluid.

Some theory about the fall velocity and the threshold of motion is given in Appendix G.

### 5.7.2 Current situation

In the current situation waves are transporting the sediment along the coast. Around the bay of Quidico the mean diameter of the sediment is 0.2 mm, which is relatively small. Due to the main direction of the waves, which is between west and south-west, sediment is mainly moving along the Chilean coast in the northern direction. Due to the natural rock protrusion in front of the headland, Quidico Bay is relatively sheltered. Due to this headland, the bay has to deal with refracting and diffracting waves.

Around Quidico the beach is practically in equilibrium, as can be seen in figure G.3 from Google Earth. The coast is changing over the considered 12 years, but this is not significant. Building a breakwater will change the sediment transport and will create a quiet area behind the breakwater. With the relatively simple sediment approaches mentioned in Appendix G (sections G.1 and G.2), the sediment movement in the current and future situation is analysed. The sediment movement due to the tides will not be guiding. The main causes for sediment transport around Quidico are the currents along the coast and wave breaking. The gradient in the set-up due to breaking waves can create a current as well. Most likely, these processes are responsible for the main sediment transport around Quidico. The ratio between sediment coming from the waves and sediments from the river is difficult to estimate. The expectation is that the river does not contain that much sediment. The discharge of the river is quite low and the characteristic, which are stated in the boundary conditions, 4.2.4, indicate that the river will not be of great influence.

Furthermore, looking at Google Earth, there are a few small beaches visible southward of Quidico. This indicates that the waves carry sediment and that these sediments are able to settle in sheltered areas.

The island Mocha makes the sediment analysis around Quidico more difficult (see figure 4.4 for an impression of the island). As said, southwards of Quidico Bay the sediment is able to settle. The island plays an important role in those accreted areas. The Island significantly reduces wave heights from the west and south-west. The lower wave heights create calmer water, which induces settlement of the sediment. Therefore, the water depths between the island and the coast are significantly smaller compared to the adjacent offshore depths, as clearly visible in figure G.4 and G.5. This is an important conclusion and needs to be taken into account.

As said before, dredging is not an option during the first phase of this project. The main breakwater is constructed first, then the entire area is monitored for a certain period. After studying the monitoring results, more investments can be done. Based on the monitoring results, a decision can be made between dredging or constructing a second breakwater.

Interesting and helpful information was obtained during several discussions with hydraulic engineers from three Dutch companies. This input regarding the sediment problems in and around the bay of Quidico, is included in the following sections. The concerned companies were Royal Haskoning DHV, BAM International and Witteveen+Bos.

### 5.7.3 Main breakwater

After building a breakwater, sediment usually will accumulate at the updrift side of the breakwater (left side in figure 5.12b) and erosion will take place at the downdrift side (right side in figure 5.12b). By constructing the breakwater through the breaking zone, in the littoral zone, the sediment transport is (temporarily) blocked and will therefore accumulate. In figure 5.13 the areas of accretion and erosion are shown for a different project (GeographyPhotos 2017). As previously discussed, areas of accretion just south of Quidico Bay, indicate that sediment in this area is likely to settle. However, in the bay of Quidico, the slope at the left side of the breakwater is relatively steep and the depth remains large. Therefore, it will be harder for the sediment to settle at this location. For these reasons, measurements are required after building the main breakwater, to be able to describe the exact effects of the breakwater on the sediment movement in the bay.

Due to the structure, the sediment transport ( $S_x$ ) along the breakwater will be zero in the beginning. It cannot pass through, and will settle down at the updrift side of the breakwater (figure 5.12a). The accretion will not cause any problems for locals around the bay, since this location is not of great value for the community. Due to the wave direction, depth and the forces of the waves, it is however still questioned if this accretion will occur at all. At the northern side of the bay, there will be erosion due to a reduced amount of sediment supply compared to the initial situation (figure 5.12b). The total sediment discharge will be approximately the same and therefore the coast will erode.

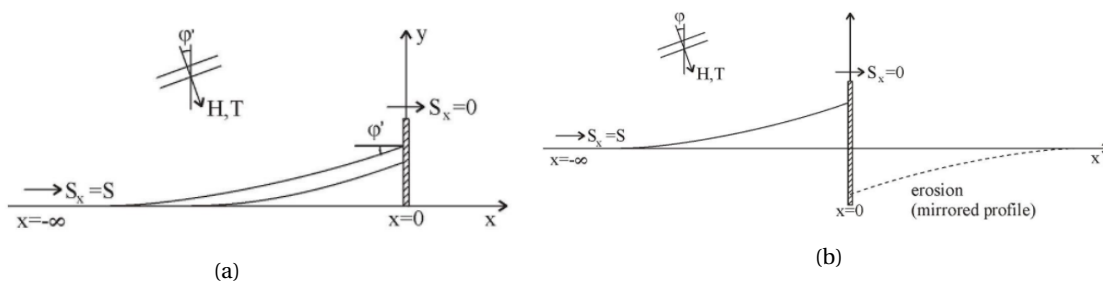


Figure 5.12: (a) Accretion at the left side of a breakwater. (b) Accretion and erosion around a breakwater. (Bosboom and Stive 2015)

The profile in figure 5.12b is quite theoretical. The difference between figures 5.12b and 5.14a is related the profile close to the breakwater, at the downdrift side. Figure 5.14a is more reliable, however only one wave direction is taken into account. Waves do not have too much influence at the part between the breakwater and the dashed-line in figure 5.14a. This causes that the erosion close to the breakwater is less. At Quidico Bay, erosion at the downdrift side will probably not cause problems. The beach is very wide and has no extensive recreational or economical value. To the north of Quidico, there are no other important beaches that should be considered in the sediment study. The general processes around a breakwater are schematized in figure 5.14b.



Figure 5.13: Sedimentation around a large concrete groyne in Newhaven, East Sussex, England

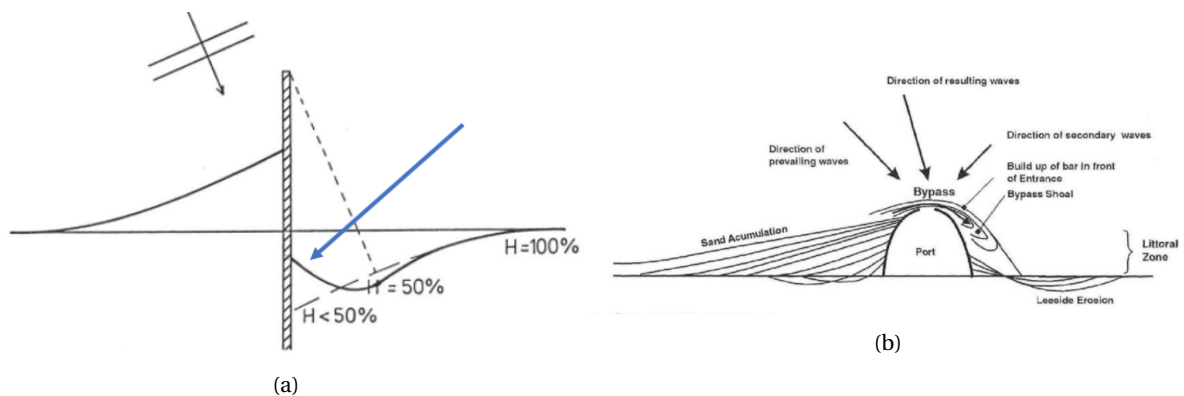


Figure 5.14: (a) Downdrift accretion in reality. (b) General processes around a headland. (Bosboom and Stive 2015)

By constructing the main breakwater the sedimentation in the bay can be even worse than in the current situation without a breakwater. The breakwater will create even calmer water conditions in the bay and therefore sediments are more likely to settle. Due to the small sediment size around Quidico, settling will not happen too fast. Settling of the sediment is unfavorable and the quantity should be monitored.

#### 5.7.4 Contramolo

In figure 5.15 the coastline is plotted in grey on the left side and red at the right side. In this figure both breakwaters and their configuration are shown. The maximum water level during low tide is given with the blue line. Expected areas of sedimentation and erosion after constructing the breakwater are given in figure 5.16a. After some time, the accreted sediment at the updrift side of the bay will reach its maximum and sediment will pass the breakwater (see figure 5.16b). If sediment is passing the breakwater, it is just a matter of time until the bay is full with sediment. Dredging could be the solution or a sediment bypass can be constructed.

If the sediments pass the breakwater, it could turn into the bay or it could move to the beaches more northwards. Sediments can be transported in the direction of the bay due to a return current. In the models of the Department of Ports (and in the Delft3D models) this return current is sometimes visible. To protect the bay from sedimentation due to the return current, the idea of the Department of Ports is to build a so called contramolo (kind of groyne, see figure 5.15). This groyne should avoid entering of sediment into the bay. In figure 5.16b the potential solution of the contramolo is shown.

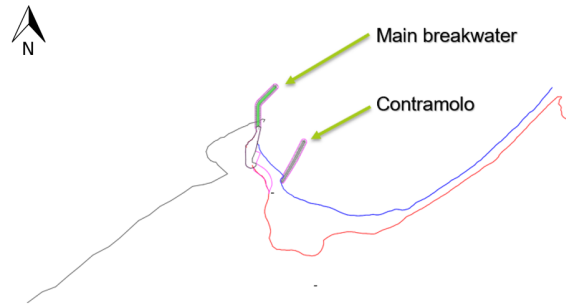


Figure 5.15: The coastline indication the main breakwater and contramolo

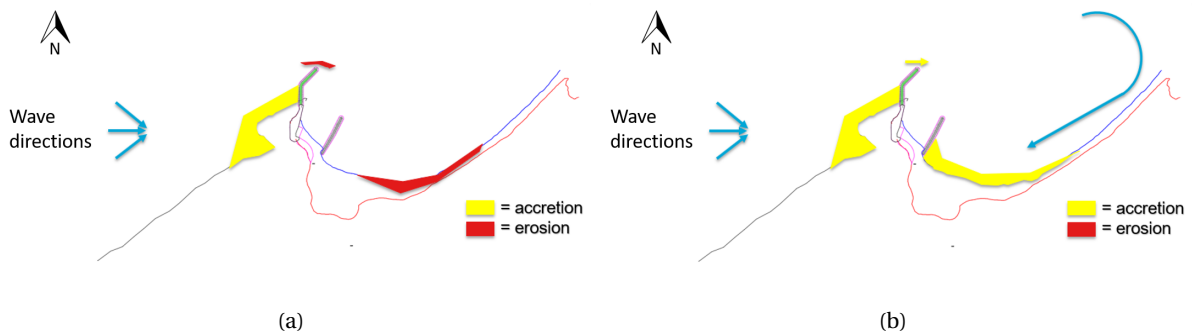


Figure 5.16: (a) Situation directly after building the breakwater. (b) Longterm situation for the bay of Quidico.

As said, first there will be erosion at the downdrift side (red area in figure 5.16a). Therefore, the contramolo is not necessary in the beginning. After building the main breakwater, monitoring of the area is necessary. By studying this data, the decision of building the contramolo can be made. Probably the solution of the contramolo is only a theoretical solution and will not be necessary in reality. It is not proven that this contramolo will solve the wave- and sediment problems. The main theory will always be that if a protected area is created, and there is sediment in the water column, it will settle if conditions are calm. Solving this problem by building the contramolo will only postpone the sediment problem. After a certain period, the area at the right side of the contramolo will be full of sediment as well. When this part is accreted, the sediment will still enter the bay. Biggest doubts are if this return current is actually there and, if so, how strong the influence will be. During the modelling phase the return current was barely visible.

The orientation of the breakwater is proposed in such a way that the bay will be protected from waves in the range coming from the south until the north-west. Waves coming from the north can cause sedimentation in the bay. But through the fact that these waves are quite low and rarely occur, the expectation is that this will not lead to significant problems. Building the contramolo could prevent this problem of sedimentation. Still, further research is required to make a decision about this second breakwater.

### 5.7.5 Mooring places

In the initial design the mooring places are designed at the same place as in the current situation. Through the fact that dredging is not applied in the first stage of the project, the depth may be too low at the mooring location. If the depth is too low, it is an option to move the mooring place further towards the breakwater. The water depth is slightly larger at this location. On the other hand, sedimentation will be a problem at this location, because this is one of the most sheltered locations in the bay. Therefore, the depth may be too low as well after a certain time. It is recommended to wait some time before building the mooring facility, to be able to study the sediment movement in the bay. Afterwards, a better substantiated recommendation can be made concerning the preferred location of the mooring facility.

### 5.7.6 Dredging

As said, building the contramolo will probably only postpone the problem of sedimentation of the bay. Dredging is stated as another option. Problem with dredging is if the water depth becomes deeper  $\Rightarrow$  velocities in the bay will decrease  $\Rightarrow$  sediments will settle more easy and sedimentation will occur again. Therefore, in general, dredging needs to be applied on a regular basis. Problem with regular maintenance is that this is not self-evident in Chile. Furthermore, dredging is relatively expensive and therefore, this solution is not desirable for the Department of Ports.

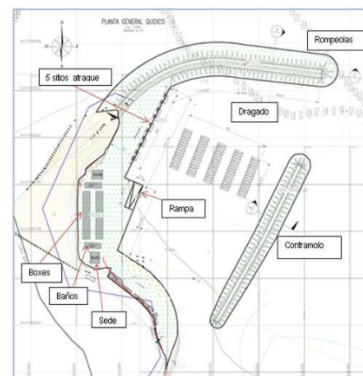
### 5.7.7 River

Finally, the river can cause sediment problems as already mentioned in section 4.2.6. The river is changing and quite braiding, as can be seen in figure G.3. The river is indicated in blue in figure 5.17a. In the initial design of the Department of Ports the main breakwater was made detached from the shore, to be able to enter the river, see figure 5.17b. In the final design of this report it is however recommended to connect the breakwater to the shore, to avoid sediments from entering the bay through a gap. Since, the new contramolo is positioned east of the river, the river will still be accessible for the fishermen.

During a site visit the river outflow was quantified to be almost zero. As already mentioned, the mean river outflow is  $2 \text{ m}^3/\text{s}$  with a maximum of  $40 \text{ m}^3/\text{s}$ . The river is regulated upstream and is therefore mainly a river that depends on the amount of rain. Therefore, the influence of the river is not considered to be very large. This is also discussed and agreed with a river-engineering professor at UdeC. If the river seems to be a problem in the future, a guide bund is recommended (same idea as constructed in Tirúa, see Appendix B). By making a guide bund, the river is smaller and therefore the flow velocity will be larger. Less sediment will settle at larger velocities. If the guide works well, the created velocities can be large enough to create a current out of the bay. This current could counter the wave induced currents, and consequently the wave induced sediment. Problem will be the discharge of the river, which is too low for this. Another option is to guide the river to the right as is indicated in figure 5.17a. By doing this, the sediment will not end up in the bay. This proposal is not worked out because the influence of the river is not known. Estimated is that costs will be too high for this guide bund.



(a)



(b)

Figure 5.17: (a) The proposed guide bund for the river. (b) The initial plan of the Department of Ports.

## 5.8 Breakwater design

The design of the breakwater can be divided into four different aspects:

- Armour layer
- Filter and core layer
- Toe stability
- Crown wall

All possible failure mechanisms are formulated in this section and a further evaluation of the calculations can be found in Appendix H.1. As stated in section 4.2.2, the return period for the waves is set to be 50 years and the lifetime of the structure is determined to be 25 years. Knowing this, the statistical wave heights of section 4.2 are used to compute the breakwater dimensions. The design philosophy used can be found in the the Rock Manual (CIRIA, CUR, and CETMEF 2007). The effect of a tsunami and an earthquake load is elaborated, after which the final design of the breakwater is chosen. A cost estimation can be found in appendix H.1.

### 5.8.1 Armour layer

The armour layer is the most outer layer of the breakwater. These stones should resist the largest wave attack. Concrete prefab blocks or natural can be used for the armour layer, but since a lot of natural stones can be found in the area around Quidico, are natural stones the most cost effective. The stability of these stones is created by their own weight. It is common in Chile to use the Hudson equation for dimensioning the armour layer (see equation 5.2). The nominal stone diameter for the armour layer is calculated to be 1.35 meter with a corresponding weight of 6.5 to.

The armour layer at the seaside must resist bigger wave forces than the lee side. The waves within the bay are lower and contain less energy. Therefore, stones at the inside can be smaller than the stones at the seaside. It is recommended to construct a small stroke of bigger stones at the end of the breakwater at the lee side. Through diffraction and different wave angles the wave attacks can be quite large in this part. The stability and inner slope of the lee side should be checked. The inner slope is checked on transmission, over-topping, direct wave impact and stability. The calculations can be found in Appendix H.1.

$$\frac{H_s}{\Delta D_n} = K_D \cot(\alpha)^{1/3} \quad (5.2)$$

It is common practice to provide a double layer of armour stones, with a thickness equivalent to  $2 \times d_{n50}$  (CIRIA, CUR, and CETMEF 2007).

### 5.8.2 Filter and core layer

The dimensions of the filter and core layer will be calculated based on the weight of the armour layer. These guidelines are given in table 5.2.

Table 5.2: The rules for calculate the dimensions of the filter and core layer

	$W_{\min}$	$W_{n50}$	$W_{\max}$
<b>Armour layer</b>	$0.75 \times W_{n50}$	$W_{n50}$	$1.2 \times W_{n50}$
<b>Filter layer</b>	$0.07 \times W_{n50}$	$0.1 \times W_{n50}$	$0.13 \times W_{n50}$
<b>Core layer</b>	$0.0001 \times W_{n50}$	$0.005 \times W_{n50}$	$0.0075 \times W_{n50}$

Requirements on how to design the core and filter layers of a breakwater are presented in the Rock Manual. Firstly, the core should be permeable. This way no excess pore pressures can build inside the breakwater. These pore pressures could lead to considerable damage to the breakwater. Secondly the gaps should be small enough, to make sure the underlayer can not wash away. Therefore, the size of the stones should be small enough and must be of sufficient mass. To summarise the main filter functions: prevent washing out of finer material, provide drainage, protect sub-layers from erosion and regulate an uneven formation layer.

To avoid the core and filter material to wash through the top layer, geotextile will be placed in between the layers. Another option is to work with multiple filter layers. Due to the fact that the armour layer consist of large stones, many filter layers are necessary. Therefore, a geotextile is chosen in this case. The geotextile is placed between the core and the filter layer Filling in table 5.2, the final dimensions can be found in table 5.3.

Table 5.3: All weights for each breakwater layer

Rock weights per layer				
	$W_{\min}$	$W_{n50}$	$W_{\max}$	Unity
<b>Armour layer</b>	5.25	7	8.4	Ton
<b>Filter layer</b>	0.49	0.7	0.91	Ton
<b>Core layer</b>	17.5	35	52.5	Kg

For the filter and core layer the minimum thickness is also  $2 \times d_{n50}$ . Due to the fact that these stones are smaller than the armour layer, a minimum thickness of 0.5 m is used. Therefore it may be that more than two layers are necessary.

### 5.8.3 Toe stability

The toe is an important part of the breakwater to keep the whole structure stable. The toe is protecting the breakwater from scouring. Scouring can bring the stability of the structure in danger. Another function of the toe is to keep the armour layer stable and retain it from sliding. A general rule for the toe of a breakwater is that the weight is 1/5th of the armour layer (CIRIA, CUR, and CETMEF 2007). From the calculations it follows that a stone weight of 1 ton for the toe could be sufficient. For practical and safety reasons, the DoP suggested to use the same stones as used for the armour layer. Therefore, the stone size for the toe is set to 7 tons. The dimensions of the toe are given in Appendix H.1.

### 5.8.4 Dimensions crown wall

The height of the breakwater and the crown wall are primarily determined by the overtopping limit. The overtopping discharges are calculated with equation 5.3. An elaboration of the calculation can be found in Appendix H.1.

$$Q = g \times H_s \times T_p \times \alpha \times \left( \left( \frac{R_c}{H_s} \right)^2 \times \frac{S_{oms}}{2\pi} \right)^b \quad (5.3)$$

Two geometries are checked for the crown wall design. These two geometries are checked for a different wave angle. A wave approaching the breakwater with a perpendicular direction results in the highest load. To dimension the height of the crown wall the run up must be checked as well. The maximum water level is necessary to calculate the height of the crown wall. By knowing this maximum water level, an extra free-board is included, which is the maximum height of the crown wall minus this maximum water level. It turns out to have a freeboard of 4.52 meter. A general geometric design and the final chosen design for the crown-wall are given in figure 5.18.

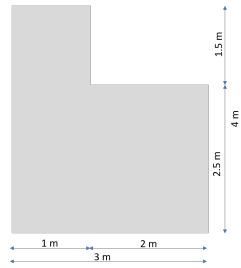


Figure 5.18: Final crown design including dimensions.

### 5.8.5 Final breakwater layout

The final breakwater cross section is presented in 5.19 gives the breakwater cross section with all the dimensions.

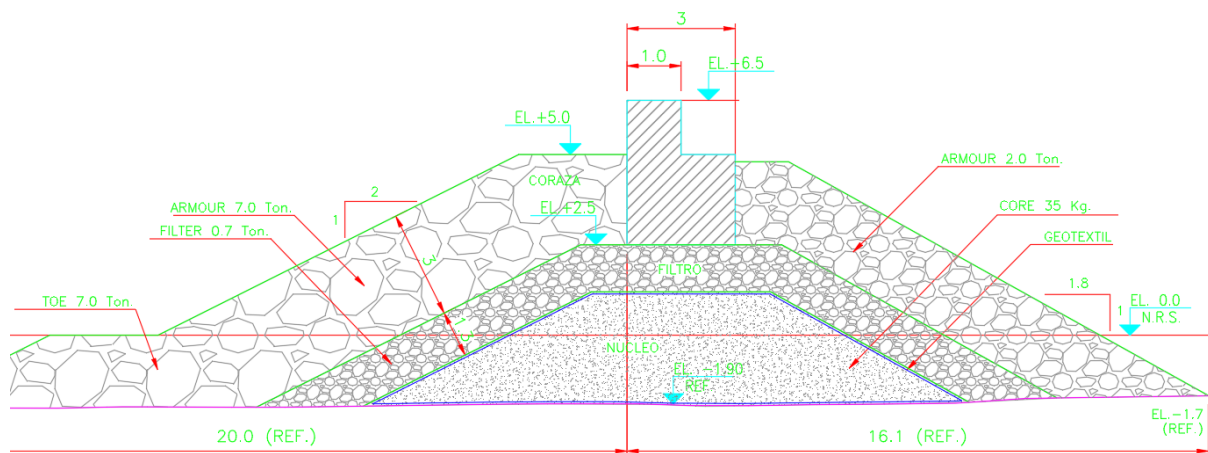


Figure 5.19: Final breakwater cross-section.

### 5.8.6 Geo-technical analysis

As part of the breakwater calculations the settlement of the breakwater is estimated, the overall stability of the breakwater and its subsurface is checked and a short analysis of the earthquake influence on a breakwater is performed. The settlement and the overall stability calculations are performed using the 2D finite element software PLAXIS.

#### Settlement

The settlement of the breakwater is estimated, this settlement can be added to the final construction height in order to fulfill the design requirements. The settlement of the breakwater is calculated based on the assumptions regarding the structure of the subsurface as described in section 4.1.2. Since the geo-technical properties of the sand in Quidico Bay are estimated, an upper and lower settlement limit are calculated. The upper settlement limit is calculated using a softer sand, i.e. the estimated values for the geo-technical parameters are decreased. This softer sand leads to an increase of settlements. The lower settlement limit is calculated using a stronger sand, i.e. the estimated values for the geo-technical parameters are increased. This stronger sand leads to a decrease of settlements. The values for the different types of sand are provided in table H.26. The procedure to construct the PLAXIS model is described in Appendix H.

From the calculations it follows the upper settlement limit is 0.31 m (figure H.10) and the lower settlement limit is 0.18 m (figure H.11).

#### Stability

The overall stability of the breakwater and its subsurface is checked. This analysis is performed using the software PLAXIS, which provides a factor of safety for the governing failure mechanism. The factor of safety is calculated by reducing the shear strength parameters ( $\phi$  and  $c$ ) until failure of the structure occurs. The factor

of safety, in PLAXIS expressed as the total multiplier ( $\sum Msf$ ), is calculated as the input strength divided by the reduced strength. The factor of safety is observed from the graph with the total multiplier on the y-axis and the total displacements on the x-axis. When a constant value for the total multiplier is reached, the graph shows a horizontal plateau and the factor of safety is determined.

The factor of safety for the governing failure mechanism of the breakwater using soft sand is approximately 1.50 (figure H.10), the factor of safety using strong sand is approximately 1.75 (figure H.11).

From the figures it is observed the failure mechanism occurs in the breakwater structure itself, the sliding circle does not cross the subsurface. From this observation it can be concluded the soft and strong sand configurations both have sufficient capacity for the breakwater structure. The governing failure mechanism thus depends on the correct design of the breakwater structure itself. Since the slope angle of the breakwater is the largest at the inside (the 'harbour-side'), the failure mechanism is calculated to occur on this side.

### **Earthquake loading**

Due to the high weight and the low height of the breakwater structure, the influence of an earthquake on the breakwater is relatively small. Cyclic loading possibly results in settlement of the armour and core material, this settlement increases with an increasing base acceleration level (Cihan, Yuksel, et al. 2012). This leads to crest lowering and slumping. Earthquake parameters influencing the breakwaters stability and strength include the duration of the earthquake and the seismic acceleration in vertical and horizontal direction.

The influence of an earthquake on the subsurface however, can be significant. Depending on the type and state of the soil, liquefaction is a possible hazard. Liquefaction could lead to differential settlement and lateral spreading, eventually followed by a possible collapse of the breakwater. Partial mitigation of the liquefaction hazard can be achieved during the construction of the breakwater. The pore water pressures should be able to dissipate in order to enable the soil to regain its original strength. This is achieved by providing enough time for this process to fulfill. A more thorough description of liquefaction as possible hazard is provided in section 4.1.4.

The PLAXIS software could be used to simulate the movement and deformations of a breakwater due to a seismic event. However, substantial knowledge is required to correctly implement the geo-technical properties and the seismic event. Also more information regarding the geo-technical properties of the subsurface and the different breakwater layers (i.e. core, filter and armour) are necessary to accurately simulate movements and deformations of the breakwater.

### **5.8.7 Tsunami attack on breakwater**

A tsunami load is almost never taken into account when designing a breakwater because is economically not viable. The main design philosophy when designing an breakwater in an tsunami prone area is that the damage due to the tsunami should be repairable. This means that the damage to the main core should be prevented, since this is the most expensive layer to repair. The Department of Ports has some experience with tsunamis on breakwaters. They said that if tsunamis approach the breakwater from a parallel direction the damage is at its maximum.

# 6 Mooring Facility Design

Two different types of quay wall are proposed, the sheet pile wall and the concrete mass wall. For both types first a preliminary design is proposed, based on this design the governing load-cases are determined. Subsequently the design is finalized and the construction procedure to follow is proposed.

## 6.1 Sheet pile wall

### 6.1.1 General design

The sheet pile wall is the easiest solution for the design of the quay wall. A sheet pile wall has several advantages, these include the ease of the installation, the costs and the light weight of the structure. A preliminary design of the sheet pile wall is shown in figure 6.1, the values for the soil properties are shown in Appendix I. The embedded depth of the sheet pile wall is set to the same value as the height of the wall above the seabed, which is 5 m. The distance of the sheet pile wall to the rock in the bay has a minimum value of 20 m, in the current situation this distance is approximately 10 m. To create the extra area required behind the sheet pile wall, granular backfill is used. This backfill is deposited on top of the sand fill, on top of this backfill the pavement structure is positioned. To create sufficient capacity of the sheet pile wall every 3 m an anchor is positioned, the length of the anchor is specified in section 6.1.3. To create a sufficient water depth (1.5 m during low tide) the bay is excavated for 1.5 m. Close to the sheet pile wall an extra 0.5 m scouring depth is created.

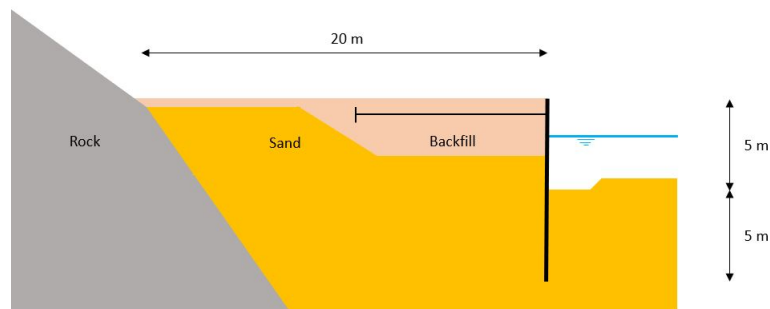


Figure 6.1: Overview of the main dimensions and situation of the sheet pile wall.

The different water tables within the bay are taken from figure 4.20. The different water levels include: low tide, mean sea level and high tide. The pavement is positioned 1.2 m above the high tide level, this value is a summation of 0.5 m storm setup and 0.7 m required minimum freeboard. Taking into account the scouring and the dredged depth, the values for the different water levels are calculated as shown in figure 6.2.

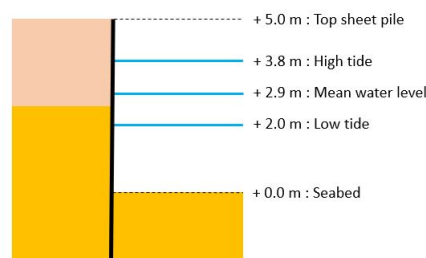


Figure 6.2: The different water levels, measured from the seabed.



mooring facility. According the information in section 4.3.1 the truck can be represented by a load of 6 kN/m. This load is applied on top of the pavement on the first two meters next to the sheet pile wall.

- *Earthquake load*

The earthquake load applied on the structure is caused by an inertia load of the passive soil. It is advised to use a horizontal force equal to 18 - 33% of the weight of the sliding wedge (*Steel Sheet Piling Design Manual* 1984). In the model a value of 20% is used since in practice this value is mostly used in Chile. The weight of the sliding wedge, as shown in figure 6.4, is applied to the sheet pile wall as a horizontal distributed load.

From the loads as described above two different governing load cases can be distinguished. Load-case 1 considers a low tide water level and an earthquake loading applied (1). The low tide water level causes a high freeboard which results in a high moment in the wall. Load-case 2 considers a high tide water level and an earthquake loading applied (2). The high water table results in a saturated soil around a part of the anchor plate. This causes a lower lateral earth pressure and thus a lower capacity of the anchor plate.

The maximum bending moments and shear forces in the sheet pile wall and anchor forces for both load-cases are shown in table 6.3. The maximum bending moment and shear force are calculated per linear meter. The values are the results of the calculations performed in PLAXIS, these calculations and the used soil properties are shown in Appendix I. The anchor spacing is 3 m and the anchor depth is 1.2 m from the top of the pavement. The deformation of the sheet pile wall for both load-cases is negligible.

Table 6.3: The maximum anchor force and maximum bending moment and shear force in the sheet pile wall for the two load-case.

Load case (#)	F <sub>anchor</sub> (kN)	M <sub>max</sub> (kNm/m)	V <sub>max</sub> (kN/m)
1	273	42.2	59.2
2	239	33.8	53.9

### 6.1.3 Design checks

Based on the results from the PLAXIS model, Appendix I, the sheet pile wall, anchor and anchor plate are checked. From the figures I.3 and I.5 it can be concluded that the displacements and deformations of the subsurface and the sheet pile wall are negligible.

#### Sheet pile

The "LARSEN 601" profile is chosen in the preliminary design. This profile is based upon the maximum available anchor capacity for this specific case. For completeness of the design, the profile is checked for the maximum bending moment and maximum shear force. In table 6.4 the results of the unity checks are shown.

Table 6.4: Unity Check results for the maximum bending moment and maximum shear force in the sheet pile wall, calculated for load-case 1 and 2.

Load case (#)	UC M <sub>max</sub> (-)	UC V <sub>max</sub> (-)
1	0.28	0.07
2	0.23	0.07

#### Anchor and anchor plate

The anchor force, as shown in table 6.3, is transferred to the soil via a vertical anchor plate. This anchor plate is located in a zone where the anchor resistance can be fully mobilized. This means the active wedge of the sheet pile wall should not intersect the passive wedge of the anchor plate. When the anchor plate is positioned where both wedges cross, the anchor resistance can only be partially mobilized. The exact shapes of both wedges are calculated based on the soil layers and the corresponding internal friction angles. The safe horizontal position (i.e. fully mobilized anchor resistance) for the anchor tube at a depth of 1.2 m from the top of the pavement, is 11.1 m from the sheet pile wall. This calculation includes an extra safety length of 1.5 m and is shown in figure

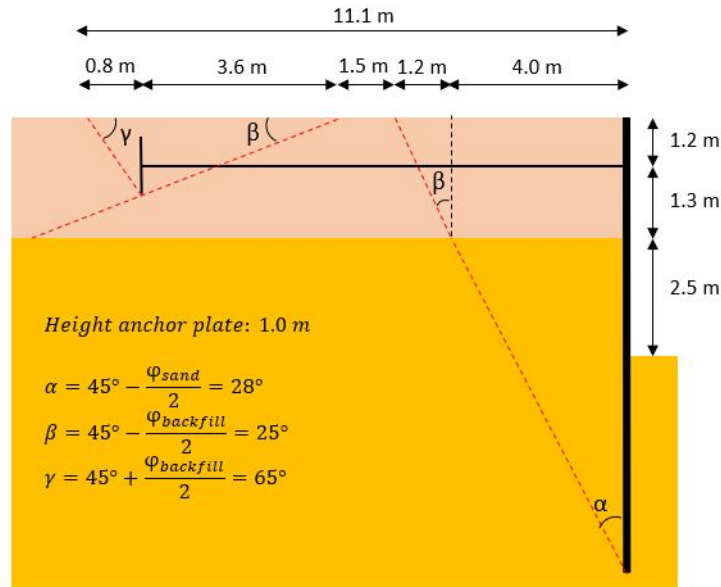


Figure 6.4: The design and position of the anchor, anchor plate and sheet pile wall, including dimensions.

6.4.

The spacing between the anchors is set to a value of 3.0 m. The vertical anchor plate is assumed to be continuous, this means every 3.0 m an anchor tube connects the sheet pile wall to the anchor plate. The resistance of the anchor plate is determined by using the lateral earth pressure coefficients as defined in table 6.2.

The resistance of the anchor plate differs for load-case 1 and load-case 2. The groundwater table in load-case 2 is at the same height as the anchor height. Consequently the lateral earth pressure decreases for the bottom half of the vertical anchor plate, resulting in less anchor capacity. This calculation is performed in Appendix I, from the calculation it followed the height of the anchor plate should be 1.0 m. The capacity of the anchor plate with a height of 1.0 m for load-case 1 and 2 are shown in table 6.5, it is assumed that the capacity of the vertical plate itself is sufficient.

Since the anchor and part of the vertical anchor plate will be below water level during high tide, these elements should be treated with a coating. This coating ensures the material is protected to damage and salt corrosion caused by the salt water.

Table 6.5: Anchor capacity for a plate height of 1.0 m for load-case 1 and 2.

Load-case (#)	$h_{gw-table}$ (m)	$F_{plate-capacity}$ (kN)
1	3.0	316
2	1.2	286

Based upon the results above, the anchor which connects the anchor plate and the sheet pile wall can be chosen. The anchor type, steel yield stress and dimensions can be varied to fulfill the requirements. The specifications of the anchor should be determined in accordance with the contractor. Two possible options are shown in table 6.6.

Table 6.6: Two possible anchor types (*Sheet Piling Handbook* 2010).

	<b>Option 1</b>	<b>Option 2</b>
<b>d<sub>nom.</sub> (mm)</b>	38	50
<b>Anchor type (-)</b>	With upset ends	With upset ends
<b>f<sub>y</sub> (N/mm<sup>2</sup>)</b>	580	355
<b>W (kg/m)</b>	7.6	8.9
<b>F<sub>capacity</sub> (kN)</b>	361	349

### 6.1.4 Construction procedure

During construction of the sheet pile wall, the strength and deformations of the wall have to be checked. A construction procedure is prescribed and is expected to be followed. Following this construction procedure leads to a specific governing configuration of the sheet pile wall in combination with the soil stratigraphy, this configuration is checked using the PLAXIS model as defined in Appendix I.

The following construction procedure will be followed:

#### 1. *Sheet pile driving*

The sheet piles are positioned first. The distance between the sheet pile and the existing sand-structure differs along the length of the quay wall. The sheet pile installation cranes however, should be able to reach to a certain distance from the position of the sheet pile wall. For a part along the quay wall the sheet piles can be installed without first placing the backfill (crushed gravel). However, where this is not possible (i.e. the distance between the existing sand road and the preferred position of the sheet pile wall is too large) first a certain part of the backfill has to be installed in order to be able to install the sheet pile wall. The value of the maximum distance between the installation cranes and the position of the sheet pile wall depends on the machines to be used.

#### 2. *Backfill deposit part I*

After installing the full sheet pile wall, the backfill is deposited up to a height of +3.8 m which is the chosen anchor depth. This is the governing situation during the construction procedure. This configuration is checked using PLAXIS, see Appendix I. The maximum bending moment and shear force in the sheet pile are -8.4 kNm/m and -11.0 kN/m respectively, these values are lower than the values obtained for the final phase and thus the chosen sheet pile section suffices.

#### 3. *Anchor installation*

Next step in the procedure is to install the anchor. The vertical anchor plate should be installed first, subsequently the anchor connecting this plate to the wall is placed. Pre-tensioning of this anchor could decrease the deformations later on in the construction procedure. The need and amount of pre-tension in the anchor is beyond the scope of this report and should be discussed with the contractor.

#### 4. *Backfill deposit part II*

The second and final part of the backfill is deposited. It is of importance to first create full capacity of the anchor plate, therefore the backfill procedure starts more inshore and continuous towards the sheet pile wall. How to reach the desired soil parameter values depends on the backfill procedure and handling, this should again be discussed with the contractor.

#### 5. *Dredging of the bay*

Full capacity of the sheet pile wall and the anchor is reached after the steps above and as final step the bay is dredged to the desired depth.

## 6.2 Concrete mass wall

### 6.2.1 General design

If rocks are present in the soil the concrete mass wall is preferred. The concrete mass wall is relatively large and is a so-called gravity structure. The idea of a gravity structure is that the weight of the structure is creating

enough shear resistance to withstand the horizontal loads. The wall is build up from a numerous of similar concrete elements which can be constructed prefab or in situ. The quay wall is dimensioned like a stairway, as requested by the DoP. The soil above the stairs acts as an extra vertical force on the stair, this results in a higher friction force between the rock and the base of the structure.

The concrete elements have a height of 1.0 meter and a width of 1.1 m. Per step size the height thus increases 1.0 m and the width 1.1 m. These dimensions are chosen such that the structure has sufficient stability against sliding and overturning. Some scouring protection has to be positioned in front of the structure to prevent scouring underneath the structure. This scouring protection could consist of small rocks.

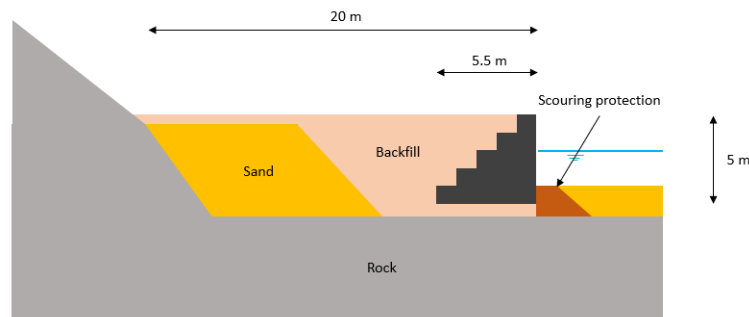


Figure 6.5: Overview of the main dimensions and situation of the concrete mass wall

## 6.2.2 Loads and load-cases

The loads which should be taken into account for the concrete mass wall design include:

- *Dead weight of the structure*

The dead weight of the structure is equal to the weight of the concrete plus the weight of the soil above the stairs. The density of the concrete is  $24 \text{ kN/m}^3$  and the density of the sand is  $18.5 \text{ kN/m}^3$ , as defined in table C.1. The dead weight of the structure is required to determine the friction force and resistance against overturning.

- *Buoyancy*

The buoyancy force is an upward force exerted by the water. The higher the buoyancy, the lower the effective weight of the structure which results in a smaller friction force. Due to different water levels on both sides of the structure, the buoyancy has a different value at both sides. This is not taken into account, the conservative situation with a buoyancy force using the highest water level on both sides is used.

- *Friction force*

The friction force is equal to the normal force of the structure multiplied with the friction coefficient. The normal force is equal to the dead weight of the structure minus the buoyancy. The friction coefficient between concrete and a semi coarse soil is equal to 0.6. This friction coefficient is prescribed by the DoP manual.

- *Active soil pressure*

The active soil pressure is calculated using Rankine's theory. A further evaluation of this pressure can be found in section 6.1.2.

- *Horizontal water pressure*

The horizontal water pressure depends on the ground water table and the water depth. This pressure increases linearly with the water depth and acts on both sides of the structure. For the static case it is assumed that the water level on the pavement is at +5.00 and on the sea side at +2.00. For the dynamic low tide case is assumed that the water level is at high tide (+3.80).

- *Seismic load on both sides*

The earthquake load acting on the structure can be divided in two different loads: an inertia load of the

structure and an inertia load of the active soil. The inertia load of the structure is equal to the weight of the structure times an acceleration. The DoP manual prescribes a horizontal acceleration of 0.2g. This load acts on the structure in the center of gravity. The inertia load of the soil on the right hand side is equal to the weight of the sliding wedge of the active soil times the same acceleration of 0.2g.

Two different load-cases are taken into account for the design of the structure. First a static load-case and second a dynamic load case. In the static load-case it is assumed that the ground water table is at the top of the pavement (+5.00) and that the sea water level is at low tide (+2.00). For the dynamic load case it is assumed that the ground water table and the sea water level are at the same level. This is allowed because it would be too conservative to assume that a different water level on both sides of the structure and an event earthquake would happen at the same time. A summary of the loads acting on the concrete mass wall is shown in table 6.7.

Table 6.7: Summary loads concrete mass wall

	<b>Static (kN)</b>	<b>Dynamic (kN)</b>
<b>Dead Weight</b>	616	616
<b>Buoyancy</b>	250	190
<b>Friction Force</b>	220	256
<b>Active soil pressure</b>	42	42
<b>Water left hand side</b>	125	72
<b>Water right hand side</b>	20	72
<b>Seismic load inertia structure</b>	0	67
<b>Seismic load active soil</b>	0	123

### 6.2.3 Design checks

The design of the structure is sufficient if the structure does not slide away and does not turn over. Different safety factors are prescribed by the DoP for these cases. The safety factor for sliding is higher than the safety factor for rotation, since failure due to overturning of the structure leads to more un-repairable damage.

Table 6.8: Safety factors concrete mass wall

	<b>Static</b>	<b>Dynamic</b>
<b>Safety factor sliding</b>	1.2	1.2
<b>Safety factor rotation</b>	1.0	1.1

The applied loads should be smaller than the resistance of the structure. The sliding capacity is equal to the friction force. The rotation capacity is equal to the weight of the structure multiplied with the distance between the centre of gravity of the structure and the rotation point of the structure. Dividing the applied loads by the capacity of the structure results in the unity checks presented in table 6.9.

Table 6.9: Unity checks concrete mass wall

	<b>Static</b>	<b>Dynamic</b>
<b>Unity check sliding</b>	0.91	0.99
<b>Unity check rotation</b>	0.34	0.57

### 6.2.4 Construction procedure

As mentioned before the concrete mass wall will be applied in case of a shallow rock bed or the appearance of a substantial amount of rock within the subsurface. The construction procedure requires some critical aspects to ensure a safe design.

The following construction procedure will be followed:

1. *In-situ or prefab construction*

The concrete mass wall is a build-up of concrete blocks, in this specific case these blocks have a width of 1.1 m and a height of 1.0 m. The concrete blocks can be constructed in-situ or can be prefabricated. The latter option is a big advantage and eases the construction at the project site. The next steps in the construction procedure are based on prefabricated concrete blocks.

2. *Excavation*

The subsurface at the desired position of the concrete mass wall should be excavated. The excavation depth depends on the depth of the bedrock and the presence of the soil above this bedrock.

3. *Creation of sublayer*

An important aspect of the concrete mass wall construction is the creation of the sublayer. This sublayer, positioned between the bedrock and the concrete mass wall, mobilizes the desired friction coefficient.

4. *Positioning of wall*

The concrete blocks are subsequently positioned to create the wall. The blocks are connected via shear connectors to ensure the separate blocks behave as a whole.

5. *Backfill deposit*

Next step in the procedure is the deposit of backfill on top of the blocks.

6. *Positioning of scouring protection*

In the case of the concrete mass wall it is common to create protection against scouring at the bottom of the wall. This prevents the sand to be eroded which could lead to instability of the mass wall.

# 7 Steel Building Design

A preliminary steel building design is developed, to accommodate all supporting facilities required for the fishermen of Quidico. The design process of this steel building is performed in phases, starting with the functional design. Next, the global structural design is defined, followed by the structural analysis and finally the structural design on an element level. In Appendix J an elaboration of the structural analysis is provided.

## 7.1 Design approach

The design process of the steel building structure can be divided in several phases. First a functional design is made by considering the requirements for supporting facilities as discussed in the first meeting (Appendix N.2.3) with the Department of Ports. After finishing the preliminary functional design an optimal structural configuration is determined, within the boundaries set by the functional requirements. During the process, different configurations were studied. The final configuration is considered to be optimal in terms of structural performance.

After finalizing the configuration and the global structural design of the building, all load cases and load combinations are defined using the Chilean building standards. Next, hand calculations and rules of thumb were used to dimension all structural elements. To verify the conceptual structural design a computational model is created in ETABS. With this model a more detailed structural calculation is performed. The structural model is also used to determine the natural frequency and the self weight of the structure, both are needed to determine the seismic load acting on the building.

After defining all the necessary input and applying multiple iterations, the final design is obtained satisfying all design criteria set by the Chilean building standards. The resulting types and dimensions of the structural elements are additionally checked by quick hand calculations to validate the computational model. For several structural elements it was not possible to perform a complete structural analysis in ETABS. Therefore, additional (hand)calculations are performed for these elements.

## 7.2 Functional design

A functional design for the steel building is made by considering the requirements for supporting facilities as discussed in the first meeting with the Department of Ports, presented in Appendix N.2.3 and section 3.2. By taking into account the wish of the DoP to include all supporting facilities in one building, a relatively simple and symmetric steel frame design is generated that consists of three stories. This design is shown in 7.1.

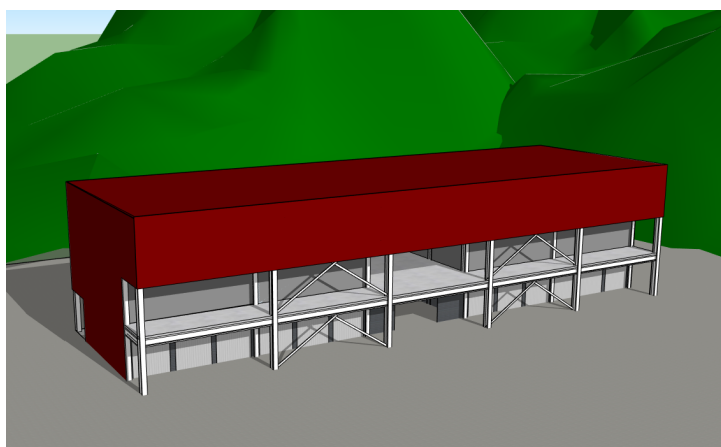


Figure 7.1: 3D view steel building design (without windows)

The first floor of the building consist of storage boxes and bathrooms. All the storage boxes will be accessible from the outside. The storage boxes will be divided by masonry walls since the Department of Ports requested for solid, strong walls. Due to the movement of rather big equipment, considerable lateral loads could act on the dividing walls and therefore thin steel walls would not suffice. The second floor is designed for the cocenerias (small basic restaurants), these are currently in front of the bay in small wooden buildings. The entire floor can be divided in different areas by non-structural dividing walls. A balcony is accessible on the second floor, where visitors can enjoy the food with a nice view over the bay. The third floor will be used as office place by the two fishermen unions. Just like the second floor, it is possible to adjust the layout of the top floor to the preference of the client since all walls are non-load bearing.

## 7.3 Global structural design

### 7.3.1 Conceptual structural design

To acquire optimal structural performance of the steel building a good structural design is of great importance. Within the boundaries, set by the functional requirements, a well thought out configuration of columns, braces, floors, beams and walls is developed. In this process rules of thumb and guiding principles governing seismic design are considered. Important principles to take into account for a conceptual design with good seismic performance are: simplicity, symmetry, bi-direction resistance and stiffness, torsional resistance and stiffness and diaphragmatic behaviour at storey level.

The vertical forces acting on the floors and roof will be transferred by steel beams to the columns. By axial stresses the columns will transfer the load to the foundation. An important aspect to consider in determining a suitable column spacing of the building, is the choice of the dimensions of the storage boxes. Furthermore, the span of the steel beams and floors should be taken into account. By using rules of thumb, final column spacing of 6.0 meters is assumed to be optimal in the longitudinal direction of the building and 5.0 meters in the transverse direction.

In the horizontal direction of the building, the strength, stiffness and stability of the structure are provided by interaction of beams, braces and columns. The braces will be applied along the vertical building facades (inverse V-shape) as well as in the roof (X-shape). These roof braces ensure diaphragmatic action of the top storey, which is of great importance for the seismic performance of the building. The joints between beams and columns can be executed as pinned connections because the bracing will provide sufficient stability. Also the connection of the columns to the foundation will be moment free.

The design requirements prescribe that the storage boxes need to be accessible from the outside of the building. However, the bracing at the longitudinal side of the building will impede this. To solve this problem, there will be a 2.0 meter distance between the entrance of the storage boxes and the outermost building facade that includes the bracing.

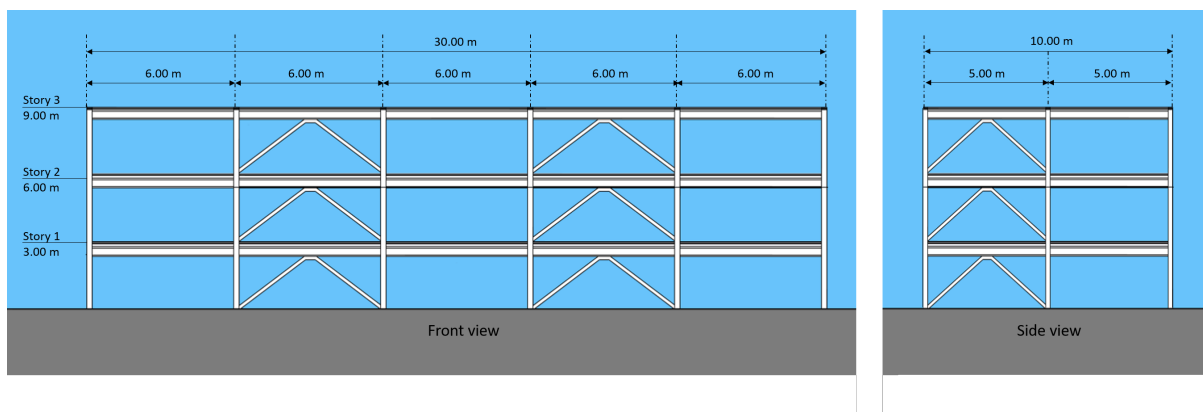


Figure 7.2: Structural design steel building

### 7.3.2 Construction materials

The steel building design consists of a steel frame structure, supported by a reinforced concrete strip foundation. The floors of the second and third storey of the building will be performed as composite deck floors. The materials used in the building design are therefore: steel, concrete and steel reinforcement.

#### Steel

The typically used steel grade in Chile is A36. It is a commonly used steel in the United States, since the most Chilean codes are based on the American codes it is frequently used in Chile. The properties of the steel are comparable with the S235 that is commonly used in the Netherlands and the rest of Europe. The material properties of the A36 type of steel are:

- Density:  $7800 \text{ kg/m}^3$
- Young's Modulus:  $200.000 \text{ N/mm}^2$
- Shear Modulus:  $77.000 \text{ N/mm}^2$
- Poisson's ratio: 0.3
- Yield stress:  $250 \text{ N/mm}^2$
- Tensile strength:  $400 \text{ N/mm}^2$

#### Concrete

The standard concrete type used in Chile is H25. This type will be used for the composite floor slabs and the foundation of the building. The properties of the H25 type of concrete are:

- Density:  $2450 \text{ kg/m}^3$
- Young's Modulus:  $30.000 \text{ N/mm}^2$
- Shear Modulus:  $12.500 \text{ N/mm}^2$
- Poisson's ratio: 0.2
- Compressive strength:  $25 \text{ N/mm}^2$
- Tensile strength:  $3.2 \text{ N/mm}^2$

#### Rebar

The rebar used in the deck is made of A630H420 steel. The material properties of the A630H420 type of reinforcement steel are:

- Density:  $7800 \text{ kg/m}^3$
- Young's Modulus:  $195000 \text{ N/mm}^2$
- Shear Modulus:  $77.000 \text{ N/mm}^2$
- Poisson's ratio: 0.2
- Yield strength:  $420 \text{ N/mm}^2$
- Tensile strength:  $630 \text{ N/mm}^2$

### 7.3.3 Loads

The loads that have to be taken into account are prescribed in NCh3171. The following loads have to be taken into consideration according to this code: permanent load, live load, wind load, snow load, rain load, ceiling load and seismic load.

- *Dead load*

The dead load consists of the self-weight of all structural elements, including non-structural elements like dividing walls. This load always acts in the vertical downwards direction. The self-weight of the structure is determined by making use of the model in ETABS. The self-weight is also used as input for determining the seismic load.

- *Live load*

The imposed live loads on the building structure includes floor loads due to the use of the building structure. NCh1537 prescribes an imposed load of  $5.0 \text{ kN/m}^2$  for public areas, like the restaurant area on the second floor. Since the third floor is an office area, only a load of  $2.5 \text{ kN/m}^2$  has to be considered.

- *Wind load*

The horizontal wind loads acting on the structure will have compression on the windward side, while it will result in a tensile load on the leeward side. NCh432 combines these loads in a single area load, that should be applied to each side of the building. The magnitude of this linearly increasing load is  $70 \text{ kg/m}^2$  at ground level and  $102 \text{ kg/m}^2$  at the top of the building.

- *Snow load*

The snow loads that should be taken into account are prescribed in NCh431. The snow load that has to be taken into consideration depends on the altitude and the geographical latitude of the building site. The code prescribes a snow load of 25 centimetres, the DoP however requested not to take this load into account since the possibility of snow this close to the beach is small.

- *Rain load*

Rain loads that should be taken into account are defined in ASCE Section 8.0. This code states that each part of the roof should be designed to sustain the load of all the water that will accumulate when the primary drainage system is blocked. Since the roof has a small angle of inclination it is not possible for water to accumulate on the roof. Therefore rain load is not considered in the structural calculations.

- *Ceiling load*

A ceiling load only has to be taken into account if the roof is used as a terrace. Since this is not the case this load can be neglected.

- *Tsunami load*

Although the building structure will be constructed at a location near the ocean, with risk of future tsunami impact, a tsunami load will not be considered. Dimensioning a building structure on this load is not feasible and no guidelines are prescribed by the building standards. Therefore, the DoP requested to not consider this impact load.

- *Seismic load*

The seismic load is prescribed in NCh433. Only a horizontal load due to an earthquake has to be taken into account. The effect of the vertical seismic accelerations can be neglected since the building does not contain any cantilevered parts. The Chilean building code describes non-linear and linear calculation methods, the non-linear method should only be applied in special cases. Two possible linear methods are described in the code: the lateral force method and the modal response analysis.

In the design calculation the lateral force method will be used, since this is advised by NCh433 (Seismic design of buildings), for simple low-rise building structures. In this method, the seismic action is taken into account as a system of lateral forces applied to the centre of mass of each of the floors. To determine the horizontal forces, first the seismic base shear force needs to be determined. The base shear is determined by multiplying the mass of the structure with a seismic coefficient and an importance factor. This seismic coefficient depends on the natural period of the structure, the natural period of the soil and the ground peak acceleration. This ground peak acceleration is determined in section 4.1.2. For the design of the earthquake resistant structures it is not necessary to combine the effects due to the two horizontal components of the seismic event. The formula 7.1 and 7.2 are applied to determine the base shear and to determine the seismic load on each floor.

$$Q_0 = CIP \quad (7.1)$$

$$F_k = \frac{A_k P_k}{\sum_{j=1}^N A_j P_j} Q_0 \quad (7.2)$$

in which:

$$A_k = \sqrt{1 - \frac{Z_{k-1}}{H}} - \sqrt{1 - \frac{Z_k}{H}} \quad (7.3)$$

Where:

- $Q_0$  = Base shear (N)
- $C$  = Seismic coefficient based on natural period and peak ground acceleration (-)
- $I$  = Importance factor related to the type of building(-)
- $P$  = Total weight of the structure (N)
- $F_k$  = Seismic load on each floor (N)
- $Z_k$  = Height of each floor (m)
- $H$  = Total height of structure (m)

The resulting static forces applied in each of the lateral directions need to be combined with effect of accidental twisting. To account for this effect, a torque must be applied at each floor level. This torque can be calculated as the product of the static forces acting at a level and an accidental eccentricity. The accidental eccentricity is calculated using formula 7.4. The torque should be applied with equal signs for every floor level of the building.

$$e_{x,y} = \pm 0.10 b_{kx,y} \frac{Z_k}{H} \quad (7.4)$$

In formula 7.4  $b_{kx,y}$  is the width of the structure perpendicular to the direction of the earthquake. Meaning, for an earthquake acting in the x-direction the width in the y-direction is used to determine the accidental eccentricity.

### Overview loads

A summary of all the applied loads can be found in table 7.1. It should be noted that the loads in this table have not been multiplied by the load factors.

Table 7.1: Overview loads steel building

Load type	Description	Storey	$F_x$ (kN)	$F_y$ (kN)	$F_z$ (kN)	$M_{xy}$ (kNm)
Dead load	Self-weight storey	Storey 1			1240	
	Self-weight storey	Storey 2			1240	
	Self-weight storey	Storey 3			107	
Live load	Variable load public area	Storey 1			1500	
	Variable load office	Storey 2			750	
Wind load	Wind lateral force	Storey 1+2	85	257		
Seismic load	Seismic force and torque	Storey 1	331	331		330
	Seismic force and torque	Storey 2	431	431		858

### 7.3.4 Load combinations

The load combinations that should be applied are prescribed in NCh3171. The design strength of the structure must be higher than or equal to the effect of the factored loads in the combinations as shown in table 7.2. It should be noted that the snow, rain and ceiling loads have not been included in the load combinations, due to the reasons mentioned above. In the load combinations prescribed by NCh3171, the wind load and seismic load do not have to be considered at the same time.

Table 7.2: LRDF Load Combinations

	1	2	3x	3y	4x	4y	5x	5y	6x	6y	7x	7y
<b>Permanent</b>	1.4	1.2	1.2	1.2	1.2	1.2	1.2	1.2	0.9	0.9	0.9	0.9
<b>Live</b>		1.6			1	1	1	1				
<b>Wind transverse</b>			0.8		1.6				1.6			
<b>Wind longitudinal</b>				0.8		1.6				1.6		
<b>Seismic transverse</b>							1.4				1.4	
<b>Seismic longitudinal</b>								1.4				1.4

## 7.4 Structural analysis

To ensure that the global structure and the structural members have sufficient structural capacity, a structural analysis is performed by making use of the engineering software ETABS. ETABS is an engineering software product that can be used to design and analyze multi-storey buildings. Additional hand calculations are performed to validate the model. All calculations are performed according to Chilean and American building standards. Not all structural elements and connections can be analyzed by ETABS. For this reason other calculation methods are used as well. These methods are elaborated in section 7.5 where all structural members are discussed independently.

### 7.4.1 Modeling input

The following steps as defined below are taken to create a structural model in ETABS. The model input consist of the geometry of the structure, support conditions, material properties, section properties and structural loads.

#### Define overall geometry

The first step of creating the model is defining the overall geometry. This is done by first defining a useful grid system. This grid should correspond to the positions of the columns and floor levels. By using the grid system the overall geometry of the building and the structural elements can be defined. Three different types of structural elements are used in the building design: columns, beams and composite decks.

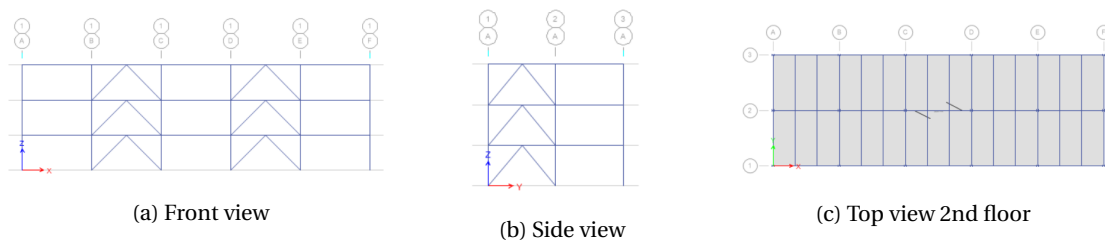


Figure 7.3: Overview geometry in ETABS

#### Define and assign properties

First the material properties are defined. The concrete and steel strength classes applied in this model are respectively H25 and A36, as described in section 7.3.2. Furthermore, section properties are defined for all the different structural components. The sections used in the first iteration are dimensioned by making use of simple rules of thumb. Finally, the support conditions are defined, as discussed in the global structural design (section 7.3).

### Define load cases and combinations

After defining these properties, the load cases need to be specified. The magnitude, direction and location of the loads are described in Section 7.3.3. The self weight of the structure is determined by ETABS and is automatically included as dead load. The live load is applied as a shell load at all floors. A linearly increasing line load on the columns is included to take into account the wind load. The seismic load is applied as a point load in the center of mass of all the floors and an extra torsional moment is considered to take into account the accidental twisting. The load combinations are defined as presented in table 7.2.

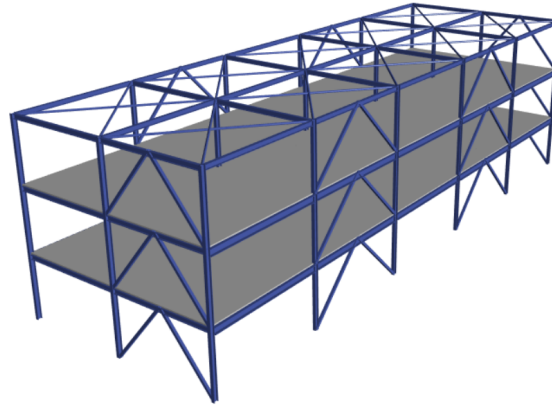


Figure 7.4: 3D view of structural model

## 7.4.2 Model validation and output

A static linear analysis is run after all the input is defined. Static means that dynamic effects are not taken into account, linear means that material and geometrical non-linearity are not considered. The output of the model first has to be validated by some checks to make sure the input given input is correct. The first method to validate the model is to check the model shapes and natural frequencies of the structure. From the modal shapes it can be concluded that the structure behaves in a realistic way. The highest natural period of the structure is 0.22 seconds, a value that can be expected from a three-storey steel building. The second validation of the model is to check if the structures behaves in a realistic way under the application of the different loads. For example, does the structure displace in the positive x-direction if a lateral wind load is applied in this same direction. The last check is to compare the sum of the reaction forces with the applied loads. For all load cases the reaction force should be equal to the applied loads.

After the model is validated, the effects of loads on the structure and their components can be analyzed. The results of the structural model include support reactions, stresses, displacement and dynamic behaviour. This information is compared to design criteria that indicate the conditions of failure. In this structural analysis in ETABS the criteria prescribed in the American building standards are used. The structural checks of all the members are presented by means of a unity check, describing the ratio between the actual and allowable force/stress/displacement. By making use of the unity check values presented by ETABS, the structural members of the steel building structure are dimensioned in an iterative way. The resulting dimension are presented in section 7.5.

## 7.5 Structural design on an element level

### 7.5.1 Columns

A column is a structural element which transmits the weight of the structure above to the foundation, via compression. In general the axial capacity of the column is governing but the bending stresses due to lateral wind and seismic loads should also be considered. For the building design the steel section H200x150x47.9 is selected. This section is depicted in figure 7.5. The governing design check of the columns is the axial capacity, with a unity check of 0.95.

## 7.5.2 Beams

A beam is a structural element that primarily resists loads applied laterally to its axis. The beams used in the building design are connected to the columns or to other beams. All connections between beams and other structural elements are pinned connections. This implies that only axial and shear forces can be transferred at the outer ends of the beams. The two major failure mechanisms of simply supported beams are failure due to bending in the center of the beam span and shear failure at the outer edges.

The beams used in the design can be divided in two different categories: transverse and longitudinal beams. This separation between the beams has been made, because the load that will be transferred by the longitudinal beams is larger than the load transferred by the transverse beams. The longitudinal beams are the main supporting beams in the structure. Their primary function is to transfer the load from the slabs to the columns. The length of these beams is 6.0 meter. For the design, H300x250x80.1 steel beams are selected. The second beam type is the transverse beam. The main function of this type of beam is to transfer the load from the slabs to the longitudinal beams. For the final building design a steel beam profile named H200x150x47.9 is chosen. The governing unity check for both beams is bending in the center of the beams. An overview of the unity checks of the beams can be found in figure J.2.

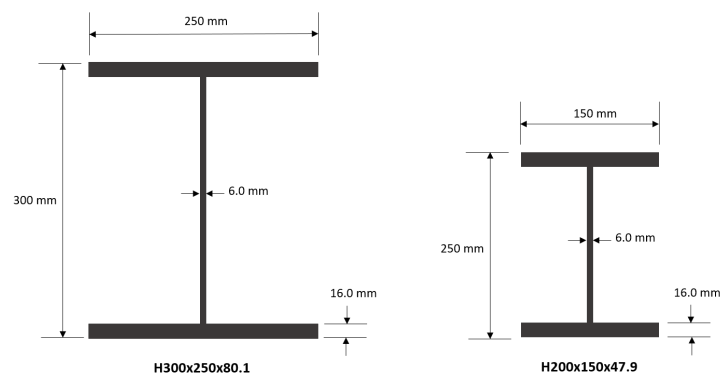


Figure 7.5: Steel section: column/longitudinal beam (left) and transverse beam (right)

## 7.5.3 Bracing

The vertical bracing will be performed as an inverse V-shape (chevron bracing). The main function of the bracing is to improve the stability of the structure. The braces will be attached with a moment-free connection to the columns and beams. The main failure mechanism of the braces is axial failure. The vertical braces in the design will be performed as 120x120x8 square braces.

The roof will also be executed with bracing to further improve the stability, strength and stiffness of the building structure. The bracing type used for the roof will be X-bracing. In the final design the roof braces will be performed as O 96-6.3 steel profiles. An overview of the unity checks of the braces can be found in figure J.1.

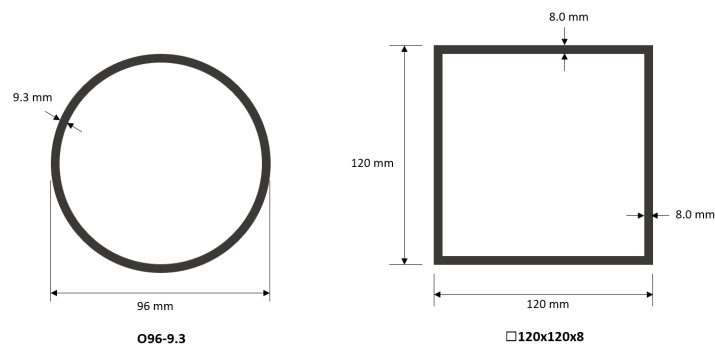


Figure 7.6: Steel section: vertical bracing (left) and roof bracing (right)

## 7.5.4 Joints

Designs for the connections of the steel structure are proposed. In practice, these designs will be adjusted by the steel manufacturer according to the specific preferences of the manufacturing company. For this reason the design of the joints will be performed in a conceptual stage and quick, efficient design methods will be used. The connections present in this steel frame structure can be roughly divided into two categories: beam-to-beam joints and beam-to-column joints.

First a conventional joint type is selected for each connection. Not only the strength requirements are relevant in the conceptual design, but it is also important to consider the feasibility and practicality of the joint type. During construction welding is generally not desirable on site, thus bolted connections are preferred. For this reason, the welded components will be limited to elements that can be welded in the workshop.

Next, the relevant structural checks are performed by using ETABS, to determine the dimensions and properties of the joints. This is done according to the Manual of the American Institute of Steel Construction (AISC 360-10) and taking into account the forces resulting from the structural analysis. Three different joint designs are required: column to transverse beam, column to longitudinal beam and transverse beam to longitudinal beam. Different structural checks have to be performed for the two different beam-to-column joints since in one case the beam is connected to the web of the column and in the other case it is connected to the flange. In figure 7.7 the final joint designs including dimensions are presented. The structural calculations are clearly presented in Appendix J.1.3, including dimensions, properties and unity checks.

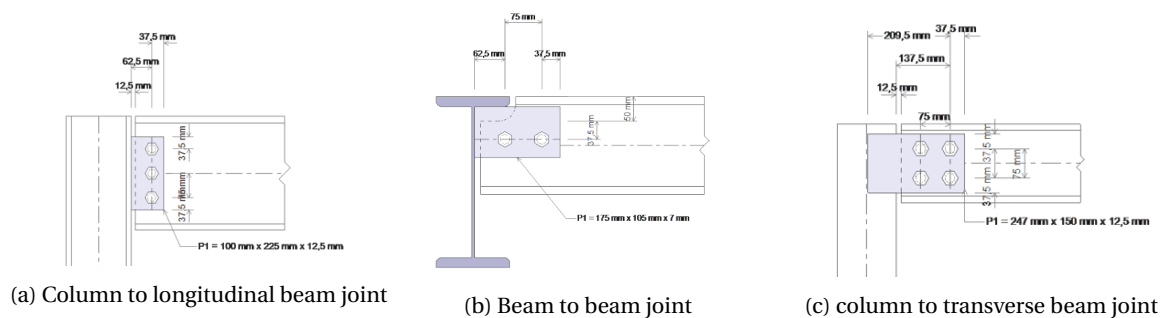


Figure 7.7: Overview of the final joint designs, including dimensions

## 7.5.5 Composite deck

A composite slab consisting of a sheet of structural steel and reinforced concrete, will be used for the floors of the second and third storey. The steel plate is shaped with stiffening ribs in the form of trapezoids to create a large resistant of the element. Since the full span of 6.0 meters between the main beams is too large, two intermediate beams will be applied to reduce the distance between the supports.

The capacity of the composite deck depends primarily on the use of shear connectors, the type and thickness of concrete and the characteristics of the steel plate. The type and number of shear connectors will be determined by the structural calculation performed by ETABS. The composite slab itself will be dimensioned by making use of an Excel sheet that is based on the Chilean building standards and prescriptions from the Steel Deck Institute. This Excel sheet performs the required structural calculations and presents clear unity checks. The complete calculation including strength and deformation checks is presented in Appendix J.

In the final design of the composite deck a steel sheet with a thickness of 0.8 mm will be used. The rib height will be 63.5 mm and a concrete height of 50 mm will be applied, creating a total deck thickness of 113.5mm. Steel type A36, concrete type H25 and reinforcement steel type A630H420 will be used. A reinforcement mesh of  $\phi 8$ -150 mm will be applied in the top of the slab. The final design is shown in figure 7.8.

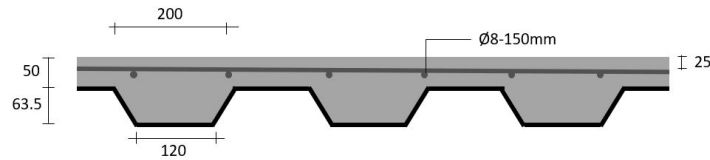


Figure 7.8: Composite deck section

### 7.5.6 Walls

The walls of the steel building structure will be performed as simple aluminum sheets with a relatively small thickness. The walls do not have a structural or load-bearing function and its properties are therefore mostly determined by practical considerations. For this reason no strength calculation is performed and a section is determined just by using rules of thumb, to be able to include the mass in the structural model.

### 7.5.7 Foundation

The ground floor slab will be constructed from a 100 mm thick in situ concrete slab. Important to consider is that cuts (contraction joints) should be made each 1.5/2.0 meters to enable expansion and shrinkage of the slab. The top of the base slab should be positioned about 0.20 m above the ground level, to prevent ground-water to enter the building.

The actual foundation of the building that will transmit the force from the columns to the soil, will be performed as continuous strip-foundations. The dimensions of this strip will be larger directly underneath the columns, to enable connection of the steel base plate to the concrete foundation.

A quick design of the foundation is presented in figure 7.9. This design is not based on structural calculations, but is dimensioned by making use of rules of thumb and engineering experience. Therefore it just serves as a preliminary design and further analysis should be performed. The width of the footing is dependent on the type of soil present below the foundation. For sand type soils, like the one present in Quidico bay, a width of 90-100 cm is typically applied. Since the bearing capacity of the surface soil is good and the settlement characteristics are suitable, a very shallow foundation can be applied. The typical total depth of the foundation, assumed to be sufficient to overcome soil movement is around 70 cm.

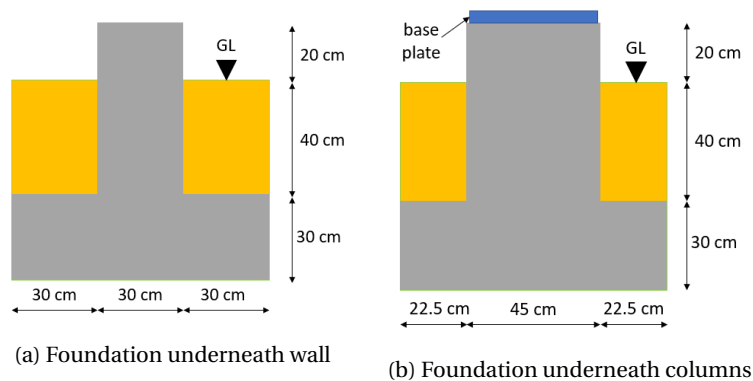


Figure 7.9: Foundation for steel building

The column is welded to a base plate and this base plate is attached to the concrete foundation using bolts. Four bolts are required with a diameter of 38 millimeter. The design checks performed can be found in the appendix J.1.5. The governing unity check is the welded connection between the base plate and the column.

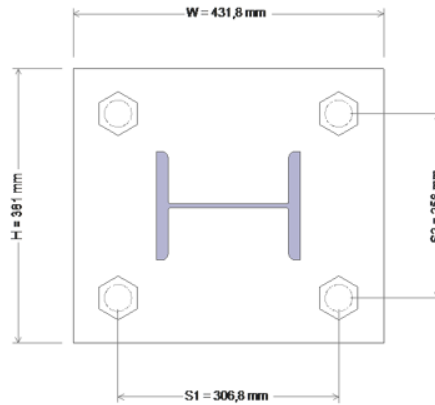


Figure 7.10: Connection column to foundation

## 7.6 Summary structural checks

The governing failure mechanism and corresponding unity check of each of the structural members are shown in table 7.3. Reference is also made to the appendices where additional information and the used formulas can be found.

Table 7.3: Summary unity checks

Structural Element	Governing failure mechanism	Unity Check	Appendix
Column	Axial and bending failure	0.76	J.1.2.2
Longitudinal Beams	Bending failure	0.87	J.1.2.2
Transverse Beams	Bending failure	0.78	J.1.2.2
Vertical bracing	Axial failure	0.97	J.1.2.1
Roof Bracing	Axial failure	0.95	J.1.2.1
Beam to beam joint	Shear rupture of web plate	0.82	J.1.3.5
Trans beam to column joint	Strength of column web at weld	0.89	J.1.3.7
Long beam to column joint	Bolt bearing on beam web	0.41	J.1.3.3
Foundation	Base plate thickness	0.93	J.1.5.3
Composite deck	Bending failure	0.63	J.1.4

# 8 Concrete Building Design

Besides the design for a steel building, a reinforced concrete building design is developed. The design process of this concrete building is performed in phases, starting with the functional design. Next, the global structural design is defined, followed by the structural analysis and finally the structural design on an element level. In Appendix J an elaboration of the structural analysis is provided.

## 8.1 Design approach

The design process of the concrete building can be divided in several steps. An important aspect of the building design is the functional design. This functional design is developed in close cooperation with the engineers and architects of the DoP, to ensure that all the functional requirements are fulfilled and the client is satisfied with the design. After finishing the preliminary functional design, an optimal structural configuration is determined, within the boundaries set by the functional requirements. During this process several different structural configurations were studied, with a final result that is considered to be optimal in terms of structural performance.

After finalizing the configuration and the global structural design of the building, all load cases and load combinations are defined using the Chilean building standards. Next, hand calculations and rules of thumb were used to dimension all structural elements. To verify the conceptual structural design a computational model is created in ETABS. With this model a more detailed structural analysis is performed. All structural members are checked and the required reinforcement is determined. In contrary to the steel building design, the final dimensions of the concrete members are mostly governed by practical considerations and are not dimensioned by an iterative procedure based on strength criteria.

Since the adjustment of the design requirements set by the DoP came up for discussion relatively late in the process of the project, there was limited time left and only a preliminary design is developed for the concrete building. A detailed, final design will require a more thorough structural analysis, further detailing of reinforcement and a more in depth study of the foundation.



Figure 8.1: Concrete building 3d view

## 8.2 Functional design

A functional design is developed in close cooperation with the engineers and architects of the DoP that meets all of the design requirements set by the Ministry of Public Works. The final design is based on a reference harbour building in the fishermen bay of Coliumo. This building consists of similar supporting facilities as the ones required in Quidico Bay. More information about the design process and the reference project can be found in Appendix N.

In the resulting functional design, shown in figure 8.1, the first floor of the building will consist of storage boxes and bathrooms. The 24 storage boxes will be all accessible from the outside of the building and will be divided by masonry and concrete walls. The masonry walls are indicated with the color red in the floor plans of figure 8.3 and will not have a structural purpose. A small area of about 6.6 by 7.0 meters is designed to facilitate three different bathrooms. One for women, one for men and one accessible for disabled people. The bathrooms will be divided by non-structural walls. These walls are not included in the ground plans.

The second floor will mainly function as an office area and will additionally accommodate several bathrooms. The floor area is kept as open as possible to enable the user and client to determine a layout according to their preferences. This can be done by adding non-structural dividing walls. These are not included in the floor plan in figure 8.3. Entrances on both sides of the building will be constructed, to enable entering the two office areas separately. One of the entrances is designed with a large ramp, to give disabled people the opportunity to reach the second floor. The design of the ramp is based on the ramp of the Coliumo harbour building.

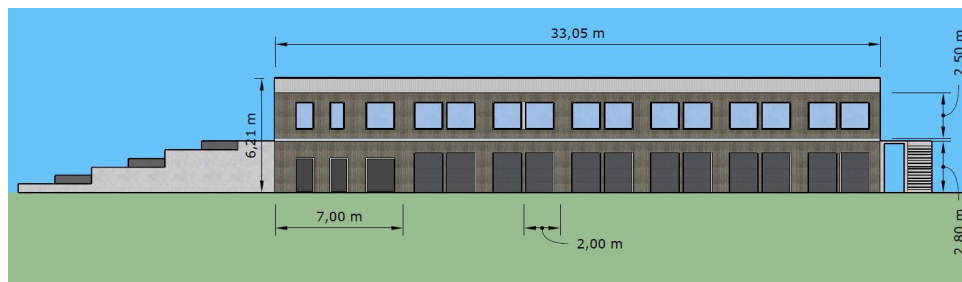


Figure 8.2: Concrete building front view



Figure 8.3: Concrete building floor plans

## 8.3 Global structural design

In this section the global structural design is presented, starting with the conceptual structural design phase. Next, the construction materials, load cases and load combinations are defined, all needed as input for the structural analysis.

### 8.3.1 Conceptual structural design

To acquire optimal structural performance of the concrete building a good structural configuration is of great importance. Within the boundaries set by the functional requirements a well thought out configuration of columns, walls, beams and slabs is developed. In this process engineering experience, building codes, rules of thumb and guiding principles governing seismic design are considered.

In seismic design of building structures it is of great importance to equally distribute strength and stiffness throughout the building, to create a structure with low eccentricity. High eccentricity would lead to significant torsional modes, that can create large stresses and can possibly lead to failure of the structure during an earthquake event. For this reason a constant shear wall spacing of 6.5 to 7.0 meters is applied in the longitudinal direction of the building. In the other direction, equally spaced smaller wall elements on the outside of the building provide strength and stiffness. To further ensure a good distribution of stiffness, it is important to structurally decouple the stiff ramp structure from the building by creating a small gap.

Between the entrances of the storage boxes, reinforced concrete columns will be constructed to transfer the forces from the floors to the foundation. Furthermore, eight reinforced concrete columns will be applied in the middle of the building to divide the masonry wall elements. This is done to meet the requirements set by the Chilean building code, prescribing a maximum masonry wall area of  $12.0 \text{ m}^2$ . The columns will be connected to transverse concrete beams. These beams will transfer the forces from the slabs to the columns. In figure 8.4 the structural design of the concrete building is depicted. In Appendix K additional building drawings are presented, to further illustrate the structural design and its components.

To create a continuous structural design and a good distribution of forces, the openings in the outer walls of the first and second floor are exactly aligned. Furthermore, the same wall spacing of the inner walls is applied for the second floor as for the first floor. In contrast to the inner concrete walls of the first floor, the walls of the second floor consist of large openings to create the open office area. To still ensure sufficient support for the roof, two transverse beams are designed. The roof as well as the first floor will be constructed from a simple reinforced concrete slab.

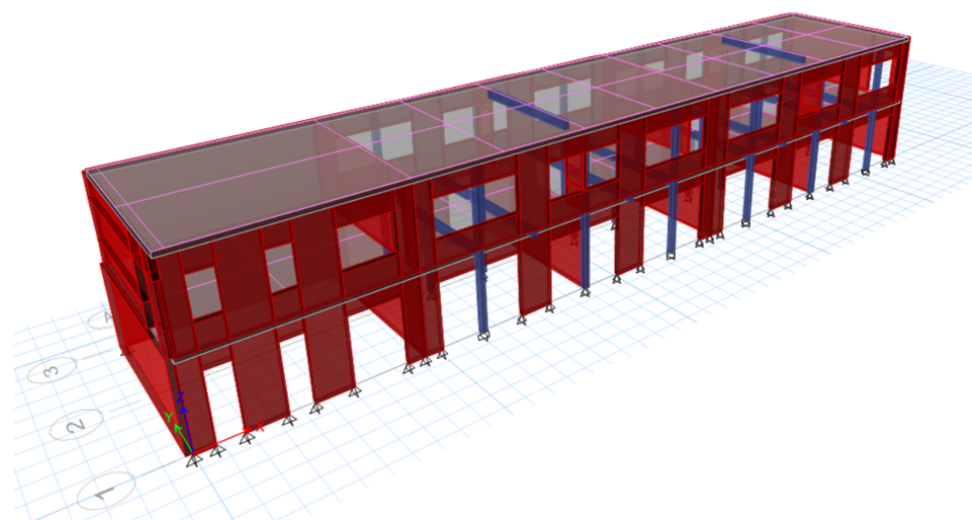


Figure 8.4: Structural model of concrete building

### 8.3.2 Construction materials

Concrete type H25 will be used for all reinforced concrete elements used in the building design. The rebar used in the reinforced concrete will be A630H420 steel. The material properties of H25 and A630H420 are elaborated in section 7.3.2

### 8.3.3 Load cases

The load cases that have to be taken into account are prescribed in NCh431, NCh432, NCh433 and NCh1537. The following loads are considered: permanent load, live load, wind load, rain load, ceiling load and seismic load. The loads are determined in the same way as for the steel building. A summary of all the applied loads can be found in table 8.1. It should be noted that the loads in these table have not been multiplied by the load factors.

- *Dead load*  
The dead load consists of the self-weight of all structural elements, including non-structural elements like dividing walls. The self-weight of the building structure is determined by making use of the model in ETABS
- *live load*  
The imposed live loads on the building structure includes floor loads due to the use of the building structure. NCh1537 prescribes an imposed load of  $2.5 \text{ kN/m}^2$  for office floors.
- *Wind load*  
The horizontal wind loads acting on the structure will have compression on the windward side, while it will results in a tensile load on the leeward side. NCh432 combines these loads in a single area load, that should be applied to each side of the building. The magnitude of this linearly increasing load is  $70 \text{ kg/m}^2$  at ground level and  $95 \text{ kg/m}^2$  at the top of the building
- *Snow load*  
The code prescribes a snow load of 25 centimetres, but the DoP requested not to take this load into account, so it is not included in the structural analysis..
- *Rain load*  
Since the roof has a small angle of inclination it is not possible for water to accumulate on the roof. Therefore rain load will not be considered in the structural calculations.
- *Ceiling load*  
A ceiling load only has to be taken into account if the roof is used as a terrace. Since this is not the case this load can be neglected.
- *Tsunami impact load*  
As described for the steel building, a tsunami impact load will not be considered in the structural analysis of the concrete building structure.
- *Seismic load*  
The seismic load is applied in the same way as for the steel building and therefore no extensive explanation will be presented here. The horizontal load due to an earthquake event is again considered by making use of the lateral force method. The fundamental period of the structure, in both the longitudinal and transverse direction, is about 0.05 seconds. By using this value and the ground peak acceleration determined in Chapter 4.1.2, the seismic loads are determined. The two lateral loads as well as the torque are presented in table 8.1.

Table 8.1: Overview of load cases for the concrete building design

Load type	Description	storey	F <sub>x</sub> (kN)	F <sub>y</sub> (kN)	F <sub>z</sub> (kN)	M <sub>xy</sub> (kNm)
Dead load	Self-weight storey	Storey 1			1929	
	Self-weight storey	Storey 2			2011	
	Self-weight timber truss	Storey 2			33	
Live load	Variable load office	Storey 1			545	
Wind load	Wind lateral force	Storey 1+2	34	174		
Seismic load	Seismic force and torque	Storey 1	323	323		533
	Seismic force and torque	Storey 2	800	800		2640

### 8.3.4 Load combinations

The load combinations that should be applied are prescribed in NCh3171 and are the same as for the steel building design. The design strength of the structure must be higher than or equal to the effect of the factored loads in the combinations as shown in table 7.2.

## 8.4 Structural analysis

To ensure that the global structural design and the structural members have sufficient structural integrity, a structural analysis is performed by making use of the engineering software ETABS. Additional hand calculations are performed to validate the model. All calculations are performed according to the Chilean and American building standards. The steps performed to create a structural model in ETABS are elaborated in section 7.4. These steps are the same for the concrete building. An elaboration of the performed design checks per structural member can be found in Appendix K.

## 8.5 Structural design on an element level

The structural members of the concrete building design are dimensioned by making use of rules of thumb and by taking into account practical considerations. The assumed dimensions are verified by making use of the structural model in ETABS. Design checks are performed according to ACI-318, to verify the structural integrity of the structure and its members. Finally, a proposed amount of reinforcement is determined for the different structural elements. This proposed rebar is merely based on the output from the structural model, by following the relevant building standards, detailing of the reinforcement is still required. This is however beyond the scope of the project. For every type of structural component, only the governing member is considered. By performing a more extensive structural analysis a more economical rebar design can be obtained. An elaboration of the performed design checks and results from the structural analysis is presented in Appendix K, for all different structural components.

### 8.5.1 Walls

The outermost structural walls will be performed as reinforced concrete walls with a thickness of 200 mm. Since the concrete is exposed to a wet environment, with risk of corrosion induced by chlorides from the sea water, a concrete cover of 50 mm is required. Because of the large concrete cover, the thickness of the wall is not governed by strength criteria, but by practical considerations relating to rebar detailing. A longitudinal reinforcement ratio of 0.25 percent is proposed for all outer wall elements. This value is based on the minimum rebar ratio prescribed by ACI-318-14 (Shear Wall Design). Applying this ratio results in a basic longitudinal rebar of  $\phi 8$ -200mm. For practical reasons, the same reinforcement is advised for the horizontal direction. An elaboration of the performed design checks can be found in Appendix K.

The structural walls inside the building will have a thickness of 150mm. These walls require a smaller concrete cover of 30mm due to the lower exposure class and can therefore be executed thinner than the outer walls. For the inner walls also a reinforcement of  $\phi 8$ -200 mm is proposed in both directions. Additional masonry walls will be used as dividing walls between the storage boxes. These walls will not have a structural function and are not considered in structural calculations and modelling.



Figure 8.5: Concrete cross-sections: Outer walls (left), Inner walls (right). Units in mm

### 8.5.2 Columns

The dimensions of all column elements will be  $200 \times 200$  mm. These dimensions are determined by practical considerations, taking into account the thickness of the connecting walls. The columns are checked according to the ACI-318-14 (Column Section Design) by making use of the structural model in ETABS. A longitudinal reinforcement ratio of 1.0% will be applied for all columns, corresponding to a rebar of  $4\phi 12$  mm.

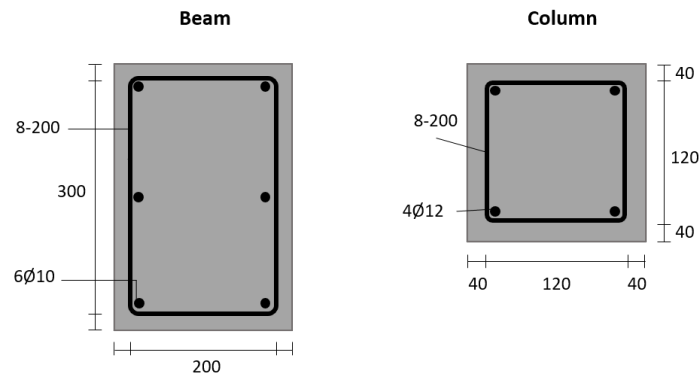


Figure 8.6: Concrete cross-sections: Beam (left), Column (right). Units in mm

### 8.5.3 Beams

Two beams are designed at the top floor of the building to transfer the loads from the roof to the wall elements. Furthermore, eight transverse beams will be constructed at the first storey of the building to confine the masonry walls. Both types of beams will have a width of 200 mm and a depth of 300 mm. Flexural, axial and shear design checks are performed to check the dimensions of the beam and to determine the required steel reinforcement. For the governing beam the results of the structural analysis are presented in Appendix K.1.2. The final design includes longitudinal reinforcement of  $6\phi 10$  mm and shear reinforcement of  $\phi 8-200$  mm. This reinforcement is advised for all beam members of the concrete building structure.

### 8.5.4 Floor slab

The second floor will be performed as a reinforced concrete slab of 180 mm thickness, supported by the beams and walls of the first storey. The slab is continuous and has a maximum span of 7.00 meters. The required longitudinal and transverse reinforcement is determined by following the code ACI-318-08, using the output provided by software ETABS as presented in Appendix K.

The maximum positive bending moment in the longitudinal direction of the slab is 32 kNm and the maximum negative bending moment is 62 kNm. Following the approach prescribed in ACI-318-08 and by assuming a concrete cover of 30 mm, a required reinforcement of  $1123 \text{ mm}^2/\text{m}$  in the top of the slab is determined. This corresponds to a reinforcement grid of  $\phi 12-100$  mm. Even though the positive bending moment is lower, the same amount of reinforcement is proposed for the bottom side of the concrete slab for practical reasons. In the transverse direction the bending moments are in the same order of magnitude, as shown in Appendix K. Therefore, the same reinforcement will be applied in this direction, both in the top and bottom of the slab. The final design is presented in figure 8.7.

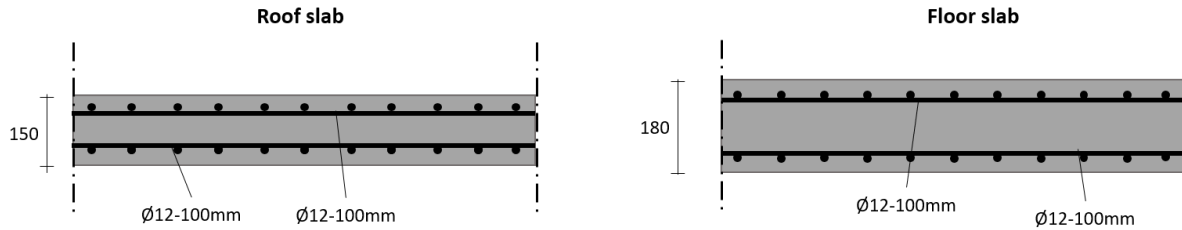


Figure 8.7: Concrete cross-sections: Roof slab (left), Floor slab (right), Units in mm

### 8.5.5 Roof

Two different options for the roof structure can be distinguished. The first option is a concrete slab and the second one is a steel truss structure. The concrete slab is heavier and requires more material than a truss roof. However, the structural performance of the reinforced concrete slab is better since it creates diaphragmatic action at storey level. A diaphragm is a plane member that rigidly transfers lateral loads to the supporting vertical elements. Diaphragmatic behaviour is of great importance in the design of seismic resistant structures. For this reason, the concrete slab roof will be applied in this design. On top of this slab a slender timber frame will be constructed, to create a small inclination of the roof for good drainage. This frame has no extensive structural purpose and therefore no structural calculation is performed for this element. A quick design by making use of rules of thumb is generated to be able to include the dead load of this timber frame in the structural analysis.

The reinforced concrete slab will be constructed as a continuous slab with a thickness of 150 mm. Supports are created at the beams and walls of the second storey. The required amount of reinforcement is determined in the same way as for the floor slab, by making use of ETABS. In the longitudinal direction of the slab 1400 mm<sup>2</sup>/m rebar is required and 1191 mm<sup>2</sup>/m in the transfers direction. This corresponds to a basic reinforcement grid of  $\phi 12-100$  mm, in both directions. In the longitudinal direction, four additional reinforcement bars of  $\phi 12$  mm should be applied in the design strip RS1. An elaboration of the structural calculations and the results is presented in the Appendix K.

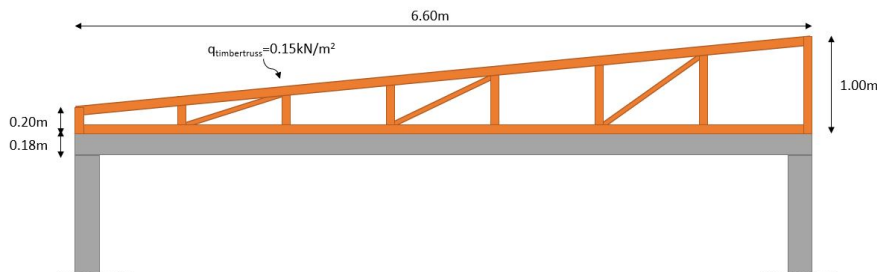


Figure 8.8: Concrete slab roof with timber frame

### 8.5.6 Foundation

The design of the ground floor slab of the concrete building will be similar to the one of the steel building design, because of the comparable design conditions. The slab will be constructed from a 100 mm thick layer of in-situ concrete. Important to consider is that the top of the base slab should be positioned about 0.20 m above the ground level, to prevent groundwater to enter the building.

The actual foundation of the building that will transmit the force from the walls and columns to the soil, will be performed as continuous strip-foundations. Since the masonry dividing walls will transfer significantly lower loads to the foundation than the reinforced concrete walls, the strip foundation below those masonry walls will be performed more slender than the strips below the concrete walls. A quick design of the foundation is presented in figure 8.9. This design is not based on structural calculations, but is dimensioned by making use of rules of thumb and engineering experience. Therefore it just serves as a preliminary design and further analysis should be performed.

The width of the foundation is dependent on the type of soil present below the footing. For sand type soils, like the one present in Quidico bay, a width of 90-100 cm is typically applied. For the footing below the masonry walls a slightly lower width of 80 cm is assumed to be sufficient. Since the bearing capacity of the surface soil is good and the settlement characteristics are suitable, a very shallow foundation can be applied. The typical depth assumed to be sufficient to overcome soil movement is around 70 cm. The width of the top part of the strip footing is governed by the width of the connecting walls and columns. For reasons of rebar detailing, the width of the top strip part should be slightly larger than the external wall thickness. The final top dimension of the strip foundation is therefore determined to be 30 cm below the concrete wall and 20 cm below the masonry dividing walls.

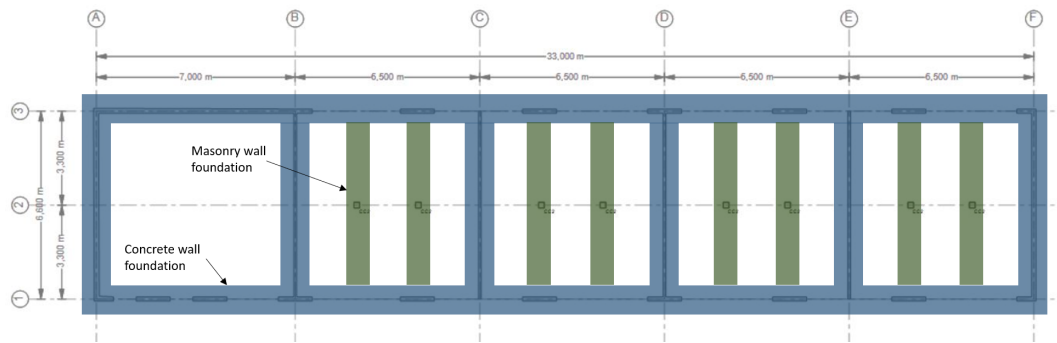


Figure 8.9: Strip foundation plan for concrete building

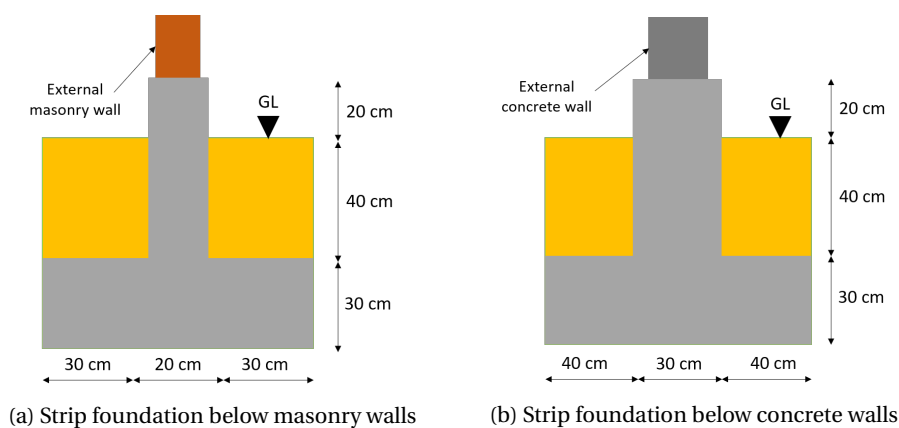


Figure 8.10: Foundation for concrete building

### 8.5.7 Summary reinforced concrete structural elements

Below a summarizing table is presented, including final dimensions, proposed basic reinforcement and the corresponding Appendices.

Table 8.2: Summary structural components

Structural element	Dimensions	Proposed basic reinforcement	Appendix
Outer walls	200 mm	$\phi 8-200$ mm	K.1.3
Inner walls	150 mm	$\phi 8-200$ mm	K.1.3
Columns	200 x 200 mm	4 $\phi 12$ mm.	K.1.1
Beams	200 x 300 mm	6 $\phi 10$ mm	K.1.2
Floor slab	180 mm	$\phi 12-100$ mm	K.1.4
Roof slab	150 mm	$\phi 12-100$ mm	K.1.5

# 9 Pavement Design

A pavement design is required for both the access road and the support area, that fulfills the structural and serviceability requirements defined by the Department of Ports. The DoP requested to evaluate different alternatives for both the access road and the support area. These alternatives are worked out by following the relevant Chilean standards for pavement design and by considering the input from the DoP. First the design alternatives for the paved support area are discussed (section 9.1) and next the pavement designs for the access road are studied in section 9.2.

## 9.1 Support area

Two different concrete slab designs are proposed for the support area. In the first design traditional concrete slabs are proposed and in the second design slabs with optimized geometry (short slabs). The short slabs method is based on a new technology that is still under development and has great advantages in terms of costs and structural performance. First, a design is made for the traditional slabs and the minimum required slab thickness is determined for this pavement design. Next, a short slab design is worked out to determine if this alternative is applicable as well. A great advantage of the short slabs is that the reduced slab size lowers the load and curling-induced tensile stresses and therefore a thinner concrete slab can be constructed. However, the DoP requested to consider the same thickness as taken into account for the traditional slab, since short slab pavement is a new technology and they are cautious about innovation. Only designs without dowel bars are considered, since dowel bars are not commonly applied in Chile.

### 9.1.1 Traditional concrete slabs

Traditional concrete slabs are square slabs with a width of 3.5 meter. The design of the traditional concrete slabs is based on the AASHTO design method modified by the Ministry of Public Works proposed in the Highway Manual Volume 3 (MCV3). Even though this manual is typically used for the regular roads, it is allowed to use it for the support area. The loads on this support area is in the same order of magnitude as the regular road. The design procedure is based on a theoretical-empirical method. The main design equations are shown below. In table 9.1 the relevant parameters are given. A further elaboration of each of the parameters can be found in Appendix L.1.1. The only unknown parameter is the slab thickness. This thickness can be determined through an iterative process.

$$\log EE = \log R + \frac{G}{F} + \left(5.07 - 3.30 \times 10^{-2} p_f^{2.5}\right) \left[ \log \left( \frac{S'_c}{\sigma'_t} \right) - \log \left( \frac{4.75}{\sigma_t} \right) \right] + Z_R S_0 \quad (9.1)$$

$$\log R = 5.85 + 7.35 \log \left[ \left( \frac{D}{25.4} \right) + 1 \right] - 4.62 \log \left[ \left( \frac{L_1}{4.45} \right) + L_2 \right] + 3.25 \log L_2 \quad (9.2)$$

$$G = \log \left( \frac{p_i - p_f}{p_i - 1.5} \right) \quad (9.3)$$

$$F = 1.00 + \frac{3.63 \left[ \left( \frac{L_1}{4.45} \right) L_2 \right]^{5.2}}{\left[ \left( \frac{D}{25.4} \right) + 1 \right]^{8.46} L_2^{3.52}} \quad (9.4)$$

Table 9.1: Overview parameters used for traditional slab design equations

Description	Symbol	Value	Unit
Traffic load	$EE$	$1.1 \times 10^6$	ESALs
Reliability parameter	$Z_r$	-0.84	-
Reliability parameter	$S_0$	0.36	-
Flexural strength concrete	$S'_c$	4.8	MPa
Single axis load	$L_1$	80	kN
Single axis factor	$L_2$	1	-
Initial serviceability index	$P_i$	4.5	-
Final serviceability index	$P_f$	2	-
Max tensile stress for edge load	$\sigma'_t$	2.05	MPa
Maximum tensile stress edge load (AASHTO conditions)	$\sigma_t$	2.61	MPa
Slab thickness (to be determined)	$D$		mm

Table 9.2: Calculated slab thickness for traditional slabs

Alternative	Base thickness (mm)	Calculated slab thickness (mm)
1	300	110
2	200	115
3	150	120

Based on the design parameters, a minimum slab thickness is determined to support the traffic loads, corresponding to the design lifetime of 20 years. A minimum slab thickness is calculated for a base thickness of 300, 200 and 150 millimeter. A base with a CBR of 60% is considered in all cases. The calculated slab thicknesses for the different alternatives is shown in table 9.2.

A slab thickness of 120 mm and a base layer thickness of 150 mm, is recommended for the traditional pavement design. This is assumed to be the most optimal design since the required slab thickness hardly decreases for a thicker base layer. It should be noted that the minimum slab thickness that is prescribed by the DoP is 180mm, which is higher than all the slab thicknesses that followed from the design procedure. This is mainly because the traffic loads in Quidico are significantly lower than most harbors designed by the DoP. To validate the calculated thickness, a reference calculation is made, based on a method from the Ministry of Housing and Urban Development. This method determines the capacity of the pavement, using different equations. The full calculation is shown in chapter L.1.2. The allowable traffic load that is calculated using this method is 2.6 million ESALs, which is more than 2 times the design traffic load. Therefore, it can be concluded that the previously determined thicknesses of 120mm by the AASHTO method is sufficient.

### 9.1.2 Short concrete slabs for the support area

Short concrete slabs are slabs with a optimized geometry that is significantly smaller the traditional slab pavement designs. It is an interesting type of concrete pavement, since their installation and maintenance costs are significantly lower compared to the traditional slabs. Furthermore, the smaller panel sizes decreases the load and curling induced tensile stresses in the slab. A slab thickness of 120 mm is recommended for the traditional slabs. This thickness is also assumed for the short slabs, since this was requested by the Department of Ports. However, by optimizing the geometry of the pavement and consequently reducing stresses it might be possible to apply an even smaller thickness. The design of square slabs with a width of 1.75 meters is considered. Design checks are performed using the program OptiPave2, from the company TCPavements. This program calculates the required slab thickness to support the loads throughout the design life time, based on three different design criteria: percentage of cracked slabs, average amount of faulting and the international roughness index (IRI). The design parameters used in the design procedure are given in table 9.3.

Table 9.3: Design parameters short slab pavement support area

Description	Value
Design life	20 years
Joint Spacing	1.75 m
Slab thickness	120 mm
Initial IRI	1.8 m/km
Maximum IRI	3.5 m/km
Maximum percentage of cracked slabs	30%
Maximum mean faulting	5 mm
Reliability	80%
Traffic load	$1,1 \times 10^6$ ESALs
CBR base	60%
CBR subgrade	40%

A summary of results from the program OptiPave 2 is shown in table 9.4. Graphs and a further evaluation of the design checks can be found in appendix L.2.2. All the unity checks are smaller than 1.00, thus can be concluded that a short slab design of 120 mm is sufficient.

Table 9.4: Design verification short slabs support area

	Allowed	Calculated	UC
<b>Cracked Slabs</b>	30%	27%	0.90
<b>Mean faulting</b>	5 mm	0.61 mm	0.12
<b>Final IRI</b>	3.5 m/km	2.39 m/km	0.68

### 9.1.3 Conclusion pavement support area

In case of the traditional slabs, the third alternative (see table 9.2) with a slab thickness of 120 millimeter is recommended. This is mainly due to economical reasons, since only a base of 150 millimeter is required in this case. If the pavement would be executed by making use of short slabs with the same thickness of 120 mm, the structural capacity of the pavement would still be sufficient. Since the structural performance of this short slab is better, the maintenance costs will be lower and the serviceability requirements are easily met throughout the design life of the structure, this alternative is recommended. However, further analysis is required to consider the possibility of performing the short slab with even smaller thickness. It must be noted that an estimation of costs is beyond the scope of this project and therefore a more thorough study should be performed to formulate the final recommendation.

## 9.2 Access road

For the access road that connects Quidico Bay to the main road, three different types of pavement are evaluated. These are: surface treatment, asphalt and concrete slabs of optimized geometry (short slabs). A daily traffic of 20 design trucks and a design life time of 20 years is considered. The corresponding equivalent single axle load (ESALs) is determined and presented in section 4.3.2.

### 9.2.1 Surface treatment

For the design of the surface treatment, the Morin Todor method is used, valid for low-traffic roads according to Chile's Road Manual Volume 3 (MCV3). The Morin Todor method provides a structure with a certain structural capacity, based on the amount of equivalent axles (ESALs) that it must withstand. This method is based on the relation between the structural behaviour of the structure and the capacity of the different layers that it consist of. A structural coefficient is associated to each layer of the structure. This coefficient does not only depends on the properties of the material, but also on its relative position within the structure. The method makes a difference in the structural contribution of layers between 0-250 mm, 250-500 mm and 500-900 mm. Layers below 900 mm are not considered. The structural coefficients for the base, sub-base and subgrade types are

presented in tables M.1, M.2 and M.3 in Appendix M.1. The final results of the design procedure include the required thickness and structural properties of the different layers, forming the pavement of the access road. The structural properties of the layers are represented by the California Bearing Ratio (CBR), describing the mechanical strength of the soil type.

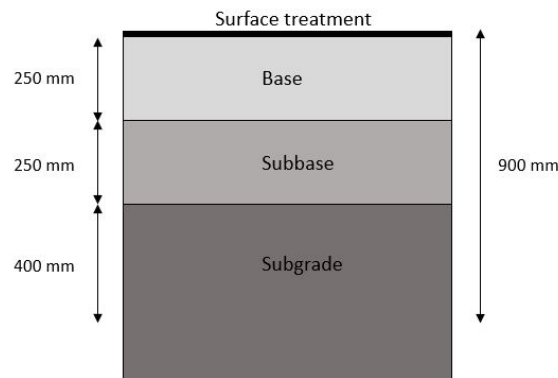


Figure 9.1: Surface treatment layers

### Design procedure

The basic design procedure to determine the thickness of the different layers, consists of three steps. First a required structural index (IEr) is determined. Next, the minimum thickness of the base plus sub-base layer is determined and finally the required thickness for all the separate layers is calculated. The input and formulas used in this design procedure are presented in Appendix M.1.

### Design results

Applying the described formulas for the three steps and by using an iterative procedure, a final pavement design is made for the relevant design conditions. The final result includes only treatment of the top base layer, no sub-base is required. The results are presented in table 9.5.

Table 9.5: Final surface treatment design for access road

Layer	Depth	CBR
Base	0-200	90%
Subgrade	220-500	18%
Subgrade	500-900	18%

## 9.2.2 Asphalt

In Chile the method used for the design of flexible pavements (layers of asphalt mixture) is based on the American method AASHTO version 1993, discussed in MCV3 of Chile. An adaptation of this method is made to be able to apply the method to different climates, designs, materials and soils in order to suit the Chilean circumstances.

### Design procedure

To create a pavement design in asphalt, several design formulas are used. The results of the design procedure using these equations, are the required thicknesses and structural properties of the different layers. The two main design formulas are presented in equation 9.5 and 9.6. The parameters used as input for the design procedure are listed in table 9.6. A more thorough explanation per parameter is presented in Appendix M.2.

$$EE = (NE_{tmin} + 25.4)^{9.36} 10^{(-16.4 + Z_R S_o)} Mr^{2.32} \left( \frac{P_i - P_f}{P_i - 1.5} \right)^{1/\beta} \quad (9.5)$$

$$NE_{tmin} \leq a_1 h_1 + a_2 m_2 h_2 + a_3 m_3 h_3 \quad (9.6)$$

Table 9.6: List of design parameters asphalt pavement

Description	Symbol	Value	Unit
Equivalent axles during design life time	$EE$	$0.62 \times 10^6$	ESALs
Total required structural coefficient	$NE_{tmin}$	23.9	mm
Asphalt layer structural characterization	$a_1$	0.43	-
Base layer structural characterization	$a_2$	0.13	-
Subbase layer structural characterization	$a_3$	-	-
Base layer coefficient of drainage	$m_2$	1.15	-
Subbase layer coefficient of drainage	$m_3$	-	-
Reliability parameter	$Z_r$	-0.84	-
Reliability parameter	$S_0$	0.36	-
Resilient modulus subgrade	$M_r$	108.3	MPa
Initial serviceability index	$P_i$	4.2	-
Final serviceability index	$P_f$	2.0	-
Asphalt layer thickness (to be determined)	$h_1$		mm
Base layer thickness (to be determined)	$h_2$		mm
Subbase layer thickness	$h_3$	0	mm

### Design results

The asphalt pavement design will consist of just a single asphalt layer supported by a base layer, no subbase layer will be constructed. A design with just these two components is assumed to be sufficient to fulfill the design requirements, taking into account the relatively low traffic load conditions. It is proposed to use a base layer of granular material with a CBR no less than 80%. This granular layer is associated with a structural coefficient of 0.13. The coefficient of drainage of the granular layer must be considered as well. By making use of the tables provided in MCV3, a required drainage coefficient of 1.15 is determined. An elaboration of the assumptions is presented in Appendix M.2. Considering the defined characteristics of the layers, the thickness of the base and asphalt layer is determined for the relevant design conditions. The results are presented in table 9.7.

Table 9.7: Final design: layer thickness and characteristics

Layer	Structural coefficient (a)	Drainage coefficient (m)	Thickness
Asphalt	0.43	-	90 mm
Base	0.13	1.15	170 mm

### 9.2.3 Short concrete slabs for the access road

As previously described in the section about the pavement of the support area, short concrete slabs are an interesting type of pavement because their costs are significantly lower compared to traditional slabs and their structural performance is better. For this reason, a pavement design is generated for the access road using these slabs of optimized geometry.

#### Design procedure

For dimensioning of the concrete short slabs, the software program OptiPave 2 TCPavements is used. This program is based on a series of input values and calculates the slab thickness required to support the applied loads throughout the design life of the project. Three design criteria are considered: percentage of cracked slabs, average faulting and the international roughness index (IRI). The design parameters required as input, are given in table 9.8 and further explained in Appendix M.3.

Table 9.8: Design parameters short slab pavement access road

Description	Value
Design life	20 years
Joint Spacing	2.00 m
Slab thickness	Variable
Initial IRI	2.0 m/km
Maximum IRI	3.5 m/km
Maximum percentage of cracked slabs	30%
Maximum mean faulting	2.5 mm
Reliability	80%
Traffic load	$1.1 \times 10^6$ ESALs
CBR base	60%
CBR subgrade	40%

### Design results

The length and width of the short slab may vary between 1.4 and 2.3 m. For the access road, a standard dimension of 1.75 m is assumed, since this corresponds to half the track width. The thickness of the final short slab design is 110 mm. The unity checks for the three different design criteria are presented in table 9.9, for the final design of 110 mm thick. The governing failure mechanism is the percentage of cracking of the slabs at the end of the design life time.

Table 9.9: Design verification short slabs access road

	Allowed	Calculated	UC
<b>Cracked Slabs</b>	30%	30%	1.00
<b>Mean faulting</b>	2.5 mm	0.70 mm	0.28
<b>Final IRI</b>	3.5 m/km	1.71 m/km	0.49

### 9.2.4 Conclusion pavement access road

Among the three technologies analyzed, surface treatment, asphalt concrete and short concrete slabs, the less recommended is the surface treatment. This is because this is a non-permanent solution, which will require a lot of maintenance. Furthermore, the surface treatment pavement will not provide the necessary conditions for surface regularity and comfort. Asphalt concrete may turn out to be the least expensive option in terms of construction. However, it requires a lot of maintenance and constant monitoring of the conditions. If the maintenance is not sufficient, rapid deterioration of the pavement will occur, especially in regions with high precipitation. It is for these reasons that the use of the short slabs is recommended, despite the fact that it might be a slightly more expensive option. The short slab design is ideal for roads with relatively low traffic loads and locations with high precipitation. Furthermore, it will provide good surface regularity and can be performed relatively thin. Based on cracking, the final thickness that must be provided is 110 mm, with a base layer of 150 mm thickness and CBR 60%. It must however be noted that an estimation of costs is beyond the scope of this project and therefore a more thorough analysis should be performed to formulate the final recommendation.

# 10 Conclusion and Recommendations

## 10.1 Conclusion

The analysis and designs presented in this report can be combined into a final conclusion, on which this chapter will elaborate. An integral design is developed that includes all required facilities and structures to improve the effectiveness of Quidico Bay as a fishing harbour. The new design offers the possibility for fishermen to berth safely, unload their goods, achieve smooth transshipment, maintain their equipment and accommodate their offices.

Several important aspects have been improved with respect to the current situation. First, due to the breakwater, a sheltered area in the bay is created where fisherman can moor their boats safely. This situation was already realised in the design proposal by the DoP. However, this design had the disadvantage that entering the harbour could lead to unsafe circumstances due to breaking of waves, at the end of the breakwater. This problem is solved by changing the breakwater orientation in such a way, that the entrance of the harbour located in an area where waves do not break during design conditions. When a breakwater is build, sediment transport will be blocked. This will result in accretion at the sea side and erosion at the lee side. In the models of the DoP, a return current is visible which could counteract the erosion at the lee side. Therefore the contramolo is designed. In new models, the return current was not visible most of the time. Due to the absence of a return current, building a contramolo is discouraged.



Figure 10.1: Overview of design proposal for Quidico Bay, including contramolo

Subsequently a design is made for the quay wall, which is an important aspect for the mooring facility. Two different quay wall designs are worked out, a sheet pile wall and a concrete mass wall. The preferences of which quay wall must be built, mainly depends on the soil conditions and the available construction space. The sheet pile wall is the preferred solution in case of a sandy subsurface and little construction space and the concrete mass wall is preferred in case of a shallow rock basement and enough construction space.

From the geo-technical boundary conditions (section 4.1.2) it is concluded the subsurface in Quidico Bay mainly consists of sand. The results of the seismic vibration test indicate that the bedrock is found at an approximate depth of 60 m. Based on these observations the sheet pile wall is the preferred type of mooring facility.

The design of an onshore building is developed, that includes all supporting facilities that are proposed in the initial design of the DoP. The main reason for combining the buildings into one multi-story design, is to reduce the surface of the support area. A design is proposed in two different building materials, a steel and a concrete building structure. The two designs are based on slightly different requirements, since the exact criteria were still under discussion during the design phase. Due to these differences, the designs are not directly comparable. While not comparable, what can be concluded is that the concrete building suits the wishes of the DoP best. This, because it fulfills all the final design requirements, possible corrosion problems are less likely to occur and the total costs of the building are lower, compared to the steel building.

A pavement design is required for both the access road and the supporting area of the harbour. The DoP requested to evaluate different alternatives for both paved areas. For the pavement in the supporting area, two different concrete slab designs are developed, varying in geometry and thickness. For the access road three technologies are analysed: surface treatment, asphalt concrete and concrete slabs. Alternatives for all pavement options are worked out and the conclusion for both the access road and supporting area is that short concrete slabs are the preferred solution. Short concrete slabs is an upcoming technology which has an advantage compared to traditional slab sizes, in terms of structural performance and construction and maintenance costs.

## 10.2 Recommendation

In the coming sections design recommendations are given for the breakwater, mooring facility, onshore buildings and the pavement designs. For each design the specific parts of improvement are presented.

### Breakwater design

In order to give a more reliable recommendation, more advanced models should be used. Especially the near-shore processes and influences of the breakwater should be considered. Some assumptions are made during the modelling phase, mainly through lack of time or knowledge.

The main recommendation related to hydraulic modelling is to create a more detailed model, as stated before. A Boussinesq model like MIKE21 is preferred. Multiple processes are implemented using a more advanced model. Especially wave breaking, diffraction and a sediment model will add value to this project.

Further, the directional grid placement was not in line with the direction of the breakwater configurations. If this would have been the case, the breakwater could have been implemented in the depth file in the right orientation. This would have made the modelling results more trustworthy. Another part which could have been done different in this model, is the density of the grid. If the grid at points of interest would have been more dense, more specific information could have been extracted from the models. Disadvantage of a denser grid, however, will be the calculation time.

Another improvement for the modelling results would be a more detailed hydrological survey around Quidico. This survey should include:

- Current measurements for validation of the model
- Obtain near-shore wave measurements (spectral if possible). This data can be used to calibrate and improve the model.
- More bathymetric measurements near-shore, for a better bathymetry file. By having more detailed bathymetric data the predictive capabilities will improve. Enough offshore data is available, however there is lack of near-shore bathymetric data. This part is probably of great value to obtain better results
- Water-level measurements at the bay of Quidico, this will lead to more accurate data.

In the end, this will help to validate the model and to have better insights in some processes.

### Mooring facility

It is advised that the construction procedure as proposed in section 6.1.4 is followed since a different procedure could lead to new governing load-cases. The distance between the sheet pile wall and the rock on the mainland varies along the coast. Since this distance influences the horizontal anchor length and the construction procedure, it is advisable to perform a more thorough analysis of this exact distance.

In the calculations the earthquake load acting on the mooring facility is taken into account via an inertia load applied on the structure. The horizontal inertia force is equal to 20% of the weight of the sliding wedge, for the concrete mass wall an extra inertia load is caused by the weight of the structure itself. This method is a simplified and conservative approach. A more advanced and less conservative method, as the Mononobe-Okabe method, could however lead to more accurate results. Based on these results the design of the sheet pile wall can be optimized.

### **Onshore building designs**

The two building designs created, serve as a preliminary design proposal for the Department of Ports. The steel building is worked out in depth, a well-thought-out structural design is developed with good structural performance and a thorough structural analysis is performed, validated with adequate hand calculations. Full comprehending of the global structural mechanism and the structural performance of the members is obtained. Additional studies are mainly required for the foundation and for the details of the steel structure, including connections between the different components and non-structural elements like the different walls.

For the concrete building a structural design is created, by considering basic structural and seismic design principles. By taking practical considerations into account and by using rules of thumb, the structural members of the concrete building structure are dimensioned. A basic structural analysis is performed, but a more extensive study is required to fully ensure structural integrity. Furthermore, additional analyses and calculations are required to design a good foundation and to determine an optimal distribution of reinforcement. The proposed rebar for the structural components, is merely based on the output from the structural model, by following the relevant building standards, detailing of the reinforcement is still required.

For both buildings structures merely the structure is considered, building services and installations are not included. A detailed description of the required construction processes and an estimation of costs is beyond the scope of this project and should therefore be performed in the next phase of the project.

From the geo-technical boundary conditions it is concluded the sand layer present in Quidico Bay is prone to liquefaction. Liquefaction results in significant soil deformation and movement, causing extra forces in the foundation and structure of the onshore facilities. To mitigate the risk for liquefaction, it is of importance to estimate the exact extent of liquefaction over depth. It is advised to perform a Standard Penetration Test to obtain the required soil parameters to predict the liquefaction potential over depth.

### **Pavement**

For both the access road and pavement in the support area is concluded that short concrete slabs are the preferred solution, mostly based on economical reasons. However, a thorough analysis of the construction and maintenance costs has not been made for the different alternatives. It is recommended to make such an analysis, to further convince the DoP of this new technology. Furthermore, an advantage of the short slabs is that the thickness could be thinner, with respect to traditional slabs, while in the design phase was assumed that these thicknesses are the same. Additional studies are required to optimize the short slab thickness.

# PART 3: APPENDICES



# A. Stakeholder Analysis

In order to ensure the final design proposal and solution results in a successful way, a good stakeholder analysis is of great importance. The different project goals include all demands and requirements of the different individuals and organizations involved in the project. The stakeholder analysis contains the determination of the project stakeholders, the demands and requirements and translating these to practical project goals.

The stakeholder analysis can graphically represented by the so-called stakeholder matrix, this is presented after a more thorough description of the different stakeholders and their needs. In the description of the different stakeholders also the 'area of influence' and 'the impact on- and benefits from the project' are defined. The area of influence can be categorized in local, communal and regional. The impact on- and benefits from the project are divided into three levels: low, medium and high.

## Executive actors (primary stakeholders)

The executive actors are the organizations and individuals within the project who have an interest in the final design. The financing and executing phases of the project are accounted to this group. The executive actors can also be identified as primary stakeholders. See table A.1

Table A.1: Primary Stakeholders

Stakeholder	Description	Area of influence	Impact on/ benefits from
Bio Bio Regional Government	The Bio Bio Regional Government determines the development of the region Bio Bio. It also finances most of the projects executed in the region.	Regional	Medium
Tirúa municipality	The Tirúa municipality determines the policies and projects which should be followed and executed, in order to ensure the community's economic development.	Communal	High
Ministry of Public Works - Department of Ports	The Department of Ports is in charge of the planning, study, execution and maintenance of the project.	Regional	Medium
UdeC	The University of Concepción (UdeC) is connected to the Ministry of Public Works via a student project. Within this project students are contributing to certain parts of the work performed by the DoP, with the aim of learning and gaining experience from real projects.	Local	Low

## Using actors (secondary stakeholders)

Using actors are the organizations and individuals from outside of the project, this group makes use of the final design. The using actors can also be identified as secondary stakeholders. See table A.2.

Table A.2: Secondary stakeholders

Stakeholder	Description	Area of influence	Impact on/ benefits from
Fisherman unions	The fishermen are divided into four different unions, each of these is represented by a president and chairman.	Local	High
Neighborhood and indigenous organizations	The local population is divided in several so called "neighbourhood organizations". Part of the local population is from the Mapuche ethnic group, this group is represented by several presidents.	Local	High

**Control actors (interface stakeholders)**

Control actors are organizations or individuals which can influence the project via laws and regulations. The group includes certain institutions which mainly act on the regional level. The control actors can also be identified as interface stakeholders. See table A.3.

Table A.3: Interface stakeholders

Stakeholder	Description	Area of influence	Impact on/ benefits from
DIRECTEMAR	DIRECTEMAR is the general Chilean institution of maritime territory and marine workers, the institution also includes the maritime authority of Talcahuano and harbour master of Lebu . It supervises the activities executed in the region.	Regional	Medium
Sernatur	Sernatur is the National Tourism Service which has as mission to promote the region for tourism purposes. It also encourages the participation of the private sector in the region.	Regional	Low
Sernapesca	Sernapesca is the National Fisheries Service and supervises the compliance with fishery and aquaculture standards.	Regional	Medium

## B. Site Visit Quidico

### Quidico

At Tuesday 22-11-2017 a group, consisting of students and employees of UdeC and DoP, visited the project site: Quidico Bay. Aim of the visit was to explore the bay and its surroundings. This visit can be used to highlight certain parts and photos and videos can be used as reference material. During the field visit the following Geo-physical tests were done: REMI, MASW and H/V ratio test. After the visit to Quidico, another project was visited. The reference project in Tirúa, which is located 10 km south of Quidico Bay and which is quite similar to the project in Quidico.

The following attendees joined the group to the side visit:

- Cristian Figueroa de La Hoz (DoP)
- Mauricio Predena Miquel (UdeC)
- Alfonso Neumann (UdeC)

In figures B.1, B.2, B.3 and B.4 the bay of Quidico is visible. A few photos are made in seaward direction and some are showing the specific bay. From figure B.4 the global wave propagation around the tip can be obtained.



Figure B.1: Quidico Bay, photo taken in northern direction



Figure B.2: Quidico Bay, photo taken in northern direction



Figure B.3: Quidico Bay, photo taken in eastern direction



Figure B.4: Quidico Bay, panorama of the whole bay

Figure B.5a shows a photo from the other side of the bay. The existing (rocky) coast protection along the bay is clearly visible. Figure B.5b shows a photo of the river entering the bay.



(a) Quidico bay



(b) River ending in Quidico Bay

Figures B.6a and B.6b are indicating the river. These photos are more from upstream. The boats from the fishermen are visible. They currently more their boats in the river.



(a) The river entering the bay



(b) The specific fishing boats

During the site visit a surface wave analysis is performed. Geo-phones were installed in a linear pattern and are able to measure the natural and/or manually induced vibrations. Based on the measurements the velocity of shear waves can be determined. These data can characterize the soil specifications and its layers. See figure B.7 for an indication of the measurements.

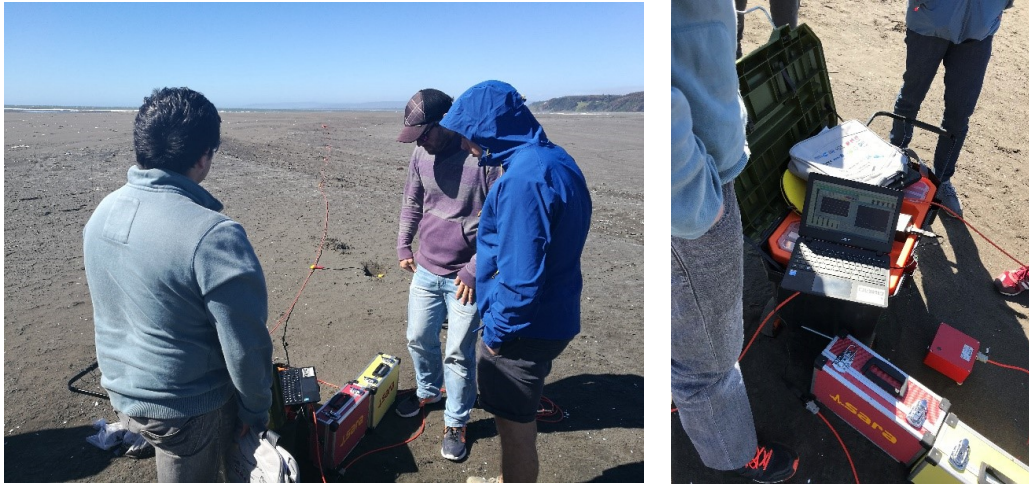


Figure B.7: Seismic wave analysis performed at the beach next to Quidico Bay

### **Tirúa**

Tirúa is located 10 km southwards of the bay of Quidico. The bay in Tirúa also had some navigational problems. These problems are fixed by making a large guide bund in the river (see figure B.8). This idea can also be used in Quidico if the river will cause for any problems. After constructing this guide bund in Tirúa, there were still some problems. The fishermen had trouble with entering the bay. Therefore they made an extension to the breakwater (see figure B.8). This extra part created a sheltered zone in a direction in which the waves are sheltered and the boats were able to enter the river. This solved the entering problems. The orientation of the entrance of Tirúa is a little different as in Quidico. Still the bay of Tirúa and its solutions are quite similar and can serve as reference project for Quidico Bay.



Figure B.8: Reference bay and harbour at Tirua, 10km south of Quidico

# C. Geo-Technical Conditions

## C.1 Standard Penetration Test

### C.1.1 Geo-technical soil properties

The Chilean standard NCh1508 (2014) advises to use different international standards (i.e. (ASTM-International 2004) and ASTM D 1586) to perform a SPT and to analyse its results. The standard describes the way different phenomena which influence the number of hammer blows should be taken into account. The borehole diameter, rod length, sampling method, the energy adjustment, the overburden pressure and the fines content should be considered and the correction factors of these phenomena contribute to the final use-able number of hammer blows,  $(N_1)_{60}$ . This value subsequently is used to calculate the different material parameters.

#### (a) Borehole diameter, rod length and sampling method

When a borehole diameter of 65-115 mm is used, no correction to the SPT results is applied. The same accounts for a rod length of 10-30 meters and a standard sampler as sampling method. For the SPT data used in this report no correction has to be applied for the borehole diameter, rod length and sampling method.

#### (b) Energy adjustment

The correction factor for the hammer blow energy input is applied for shallow measurements. At shallow depths the energy input is cancelled due to the occurrence of a reflected tensile wave, this results in a higher value of the hammer blows close to the ground surface. When the energy input for the hammer blows is not obtained during the experiment, an assumed correction factor of 1.0 is used. This factor takes into account a value of 60 percent for the hammer energy ratio. The following applies to the used data:  $N = N_{60}$ .

#### (c) Overburden pressure

The penetration resistance is influenced by the overburden pressure executed on the soil sample. A higher value of overburden pressure results in a higher value of the penetration resistance. According to international standard ASTM D6066:96 (2004) the correction factor,  $C_N$ , is a function of many variables such as particle size, density, stress history and aging. The standard provides a graph which represents several methods of correction, it however describes the use of the correction factor (Liao and Whitman 1986):

$$C_N = \left( \frac{P_a}{\sigma'_v} \right)^{0.5} \quad (C.1)$$

The correction factor  $C_N$  normalizes the number of hammer blows to an effective overburden pressure of 100 kPa (1 kg/cm<sup>2</sup>). The maximum value for  $C_N$  is 1.7, defined by the workshop participants in a follow-up of the National Center for Earthquake Engineering Research (NCEER) workshop (Youd and Idriss 1997). For an overburden pressure higher than 300 kPa (3 kg/cm<sup>3</sup>) the correction factor as defined above should not be applied due to the uncertainties occurring at these high pressures. The classification of the different soil layers is based on the soil samples taken during the SPT.

The densities of the different soil types are estimated, the values are shown in table C.1. This data is used for the determination of the correction factor regarding over-consolidation.

Table C.1: Densities of the soil types.

Soil type	$\gamma_{unsat}$ [kg/m <sup>3</sup> ]	$\gamma_{sat}$ [kg/m <sup>3</sup> ]
Clay	1500	1800
Fine sand	1850	2000

#### (d) Soil classification and fines content

Three soil samples were taken, the location of these samples is indicated in figure 4.5. These soil samples

are analysed at the University of Concepción (UdeC). The results of these analyses are shown in C.2. The granulometric analysis is performed according guideline number 105 developed by the National Laboratory of Railways (Laboratoria Nacional de Validad), LNV 105. A summary of the results are shown in table C.2, the number indicates the percentage passing the sieve.

Table C.2: Granulometric analysis of the soil samples.

Sieve number (degree)	Sieve size (mm)	Sample #1 (percent)	Sample #2 (percent)	Sample #3 (percent)
4	4.750			
10	2.000			
20	0.850			100
40	0.425	100	100	99
60	0.250	59	75	69
200	0.075	2	2	1

With the results of the granulometric analysis the Atterberg limits (plastic limit, liquid limit) of the soil samples can be determined. Using the Chilean National codes NCh 1517/1 and NCh1517/2, respectively the liquid limit and the plastic limit are determined. All three soil samples are classified as non-plastic (NP).

With the information calculated in step (a), (b), (c) and (d) the profile of the number of corrected blow counts is determined. The correction factors and the corrected values for the number of blow counts is shown in figure C.3. With this the profile of the number of corrected blow counts over the height of the soil column is determined, as shown in figure 4.6.

### C.1.2 USCS classification

The Unified Soil Classification System (USCS) is also used to classify the different samples, using table 1 from ASTM D2487 (ASTM-International 2006) this classification is performed. This table is presented in figure C.1. More than 50 percent of the fraction passes sieve no. 4 and less than 5 percent fines (percentage retained on sieve no. 200) are present in all three soil samples. This results in a soil classification indicated by SP: poorly graded sand containing less than 15% of gravel.

Criteria for Assigning Group Symbols and Group Names Using Laboratory Tests <sup>A</sup>				Soil Classification		
				Group Symbol	Group Name <sup>B</sup>	
COARSE-GRAINED SOILS	Gravels	Clean Gravels	$Cu \geq 4$ and $1 \leq Cc \leq 3^C$	GW	Well-graded gravel <sup>D</sup>	
	More than 50% retained on No. 200 sieve	More than 50% of coarse fraction retained on No. 4 sieve	$Cu < 4$ and/or $1 > Cc > 3^C$	GP	Poorly graded gravel <sup>D</sup>	
		Gravels with Fines	Fines classify as ML or MH	GM	Silty gravel <sup>D, F, G</sup>	
		More than 12% fines <sup>E</sup>	Fines classify as CL or CH	GC	Clayey gravel <sup>D, F, G</sup>	
		Sands	Clean Sands	SW	Well-graded sand <sup>F</sup>	
		50% or more of coarse fraction passes No. 4 sieve	Less than 5% fines <sup>F</sup>	SP	Poorly graded sand <sup>F</sup>	
			Sands with Fines	SM	Silty sand <sup>F, G, H</sup>	
			More than 12% fines <sup>F</sup>	SC	Clayey sand <sup>F, G, H</sup>	
			Fines classify as ML or MH			
			Fines classify as CL or CH			
FINE-GRAINED SOILS	Silts and Clays	inorganic	$PI > 7$ and plots on or above "A" line <sup>J</sup>	CL	Lean clay <sup>K, L, M</sup>	
	50% or more passes the No. 200 sieve	Liquid limit less than 50	$PI < 4$ or plots below "A" line <sup>J</sup>	ML	Silt <sup>K, L, M</sup>	
			Liquid limit – oven dried <sup>K</sup> $> < 0.75$	OL	Organic clay <sup>K, L, M, N</sup>	
			Liquid limit – not dried	OL	Organic silt <sup>K, L, M, O</sup>	
		Silts and Clays	inorganic	PI plots on or above "A" line	CH	Fat clay <sup>K, L, M</sup>
		Liquid limit 50 or more	organic	PI plots below "A" line	MH	Elastic silt <sup>K, L, M</sup>
				Liquid limit – oven dried $< 0.75$	OH	Organic clay <sup>K, L, M, P</sup>
				Liquid limit – not dried		Organic silt <sup>K, L, M, Q</sup>
	HIGHLY ORGANIC SOILS	Primarily organic matter, dark in color, and organic odor		PT	Peat	

Figure C.1: Soil Classification chart from ASTM-International 2006.

### C.1.3 Liquefaction Potential

The Chilean standard (mainly based on Youd, Idriss, and Andrus 2001) prescribes a method to evaluate liquefaction resistance based on the corrected SPT data.

The value fines content (FC) influences the liquefaction potential, hence an increase in the fines content results in an increase of the liquefaction resistance. In the soil analysis performed above the fines content for all three soil samples is determined to be less than 5%. These values determine the values for the coefficients as used in the following formula to calculate the corrected number of hammer blows (Youd, Member, et al. 2011):

$$(N_1)_{60} = \alpha + \beta(N_1)_{60} \quad (C.2)$$

Since for a fines content of less than 5% the value for coefficient  $\alpha$  is equal to 0 and the value for coefficient  $\beta$  is equal to 1, meaning that no correction has to be made for the number of hammer blows.

According the Chilean standard Nch1508 2014 the liquefaction potential is analysed with a specific methodology using the cyclic stress ratio and the cyclic resistance ratio (Seed and Idriss 1971). The cyclic stress ratio ( $CSR$ ) and the cyclic resistance ratio ( $CRR$ ) are used for evaluation of liquefaction resistance of soils. The cyclic stress ratio is calculated as:

$$CSR = \frac{\tau_{av}}{\sigma'_{vo}} = 0.65 * \left( \frac{a_{max}}{g} \right) \left( \frac{\sigma_{vo}}{\sigma'_{vo}} \right) r_d \quad (C.3)$$

With  $a_{max}$  as the peak horizontal acceleration at the ground surface generated by the earthquake and  $r_d$  as the stress reduction coefficient which accounts for the flexibility of the soil profile.  $r_d$  is calculated as follows (Blake 1996):

$$r_d = \frac{1.0 - 0.4113 * z^{0.5} + 0.04052 * z + 0.001753 * z^{1.5}}{1.0 - 0.4177 * z^{0.5} + 0.05729 * z - 0.006205 * z^{1.5} + 0.001210 * z^2} \quad (C.4)$$

With  $z$  as the depth below ground surface. The liquefaction resistance can be calculated with the following formula (Rauch 1998):

$$CRR_{7.5} = \frac{1}{34 - (N_1)_{60}} + \frac{(N_1)_{60}}{135} + \frac{50}{[10 * (N_1)_{60} + 45]^2} - \frac{1}{200} \quad (C.5)$$

This equation only is valid for  $(N_1)_{60} < 30$ , for higher values the soil is too dense to liquefy and is classified as non-liquefiable. Since the formula of  $CRR_{7.5}$  only applies to magnitude 7.5 earthquakes, the magnitude scaling factor  $MSF$  can be used to adjust to smaller or higher magnitude earthquakes (Kaznbach, Clauss, and Rochee 2013). This liquefaction potential (or factor of safety for liquefaction) is calculated as:

$$FoS = \left( \frac{CRR_{7.5}}{CSR} \right) * MSF \quad (C.6)$$

Various investigators defined magnitude scaling factors. The workshop participants of the National Center for Earthquake Engineering Research (NCEER) workshop proceedings (Youd and Idriss 1997) proposed a lower and upper bound to define a range of  $MSF$ 's. For a magnitude lower than 7.5 the lower bound consists of the values defined by Idriss (1995), the upper bound consists of the values defined by Andrus and Stokoe (1997). For a magnitude higher than 7.5 the values defined by Idriss 1995 should be used. The following formula is proposed for the calculation of  $MSF$  (Idriss 1995), (Andrus and Stokoe 1997):

$$MSF = 6.9 * e^{-\frac{M}{4}} - 0.058 \leq 1.8 \quad (C.7)$$

To examine the soil to the earthquake of February 2010 in Chile, the magnitude scaling factor for an earthquake magnitude of 8.8 is calculated. This value is used to calculate the factor of safety regarding liquefaction for the subsurface.

$$MSF = 6.9 * e^{-\frac{8.8}{4}} - 0.058 = 0.71 \leq 1.8 \quad (C.8)$$

No exact value for the factor of safety is defined. In general practice a value of 1.2 is used, a soil with a plasticity index value below 1.2 is classified as susceptible to liquefy. The values for the liquefaction potential are obtained for a magnitude 7.5 earthquake and a magnitude 8.8 earthquake over a depth of 21.2 m, this is shown in figure C.3. As said earlier in this section soil with values of  $(N_1)_{60}$  higher than 30 are too dense to liquefy and is classed as non-liquefiable. From the results it is obtained the first 1.5 m of the thick sand layer is susceptible to

liquefy. Also some deeper thin sand layers are susceptible for liquefaction according the test results, however these layers are assumed to have no impact on the liquefaction intensity.

The above calculations apply only to sand-like soils and do not count for clay-like soils (Idriss and Boulanger 2004). Boulanger and Idriss (2004) advice to use the term 'liquefaction' for sand and sand-like fine-grained soils and the term 'cyclic failure' for clay and clay-like fine-grained soils. Several procedures are proposed to determine the potential of cyclic failure of clay-like fine-grained soils. A relative simple way includes the determination of the plasticity index, however the limited geo-technical data (SPT) is not sufficient to determine the needed Atterberg limits. The SPT number is not affected by the Atterberg limits of the soil layers (Mahmoud 2013). In order to be able to classify the cyclic failure of the top clay layer the undrained shear strength should be determined. Boulanger and Idriss (2004) describe several tests to determine this parameter for clay-like fine-grained soil deposit.

The shear wave velocity could also be used for the determination of this potential. Some papers (e.g. (Idriss and Boulanger 2010)) show some accurate results using the shear wave velocity, however the relationship is more complicated due to an increase of data with time and use of new parameters. The derivations between the method using SPT data and the method using shear wave velocity data indicate the necessity of further investigation of the latter method (Kaznabach, Clauss, and Rochee 2013).

### C.1.4 Raw SPT data and final results

Below the following items are presented:

- Analysed soil sample data, the analysis is performed at UdeC (figure C.2)
- Corrected number of blow counts and the corresponding liquefaction potential (figure C.3).
- Raw SPT data (figure C.4)

LABORATORIO MECANICA DE SUELOS UNIVERSIDAD DE CONCEPCION

1-ENSAYOS CLASIFICACION MUESTRAS

Muestra	1	2	3
Profundidad (m)	0,00	0,00	0,00
Análisis Granulométrico LNV 105 (% en peso que pasa)			
Tamiz n°	4		
	10		
	20		10
	40	100	99
	60	59	69
	200	2	1
Límites de Consistencia NCh 1517/I, NCh 1517/II			
Límite líquido (%)	--	--	--
Límite plástico (%)	--	--	--
Índice de plasticidad	NP	NP	NP
Clasificación USCS	SP	SP	SP
Propiedades índices NCh 1532, NCh 1515			
Peso Específico Gs	2,743	2,762	2,688
Humedad (%)	29,8	25,9	29,3

Figure C.2: Analysed soil samples from Quidico Bay, the analysis is performed at UdeC.

Layer number (#)	Meters (m)			Corrected blows (#)	Soil type	FoS (M = 7.5)	FoS (M = 8.0)
	From	To	Diff.				
1	0.00	0.65	0.65	-	Clay	-	-
1	0.65	1.10	0.45	9		-	-
1	1.10	1.55	0.45	7		-	-
2	1.55	2.00	0.45	15	Stratifications of fine sand	0.64	0.56
2	2.00	2.69	0.69	19		0.66	0.58
2	2.69	3.14	0.45	23		0.78	0.68
2	3.14	3.59	0.45	39		>1.2	>1.2
2	3.59	4.04	0.45	70		>1.2	>1.2
2	4.04	4.49	0.45	92		>1.2	>1.2
2	4.49	5.19	0.70	99		>1.2	>1.2
2	5.19	5.90	0.71	80		>1.2	>1.2
2	5.90	6.35	0.45	81		>1.2	>1.2
2	6.35	6.80	0.45	78		>1.2	>1.2
2	6.80	7.25	0.45	94		>1.2	>1.2
2	7.25	7.70	0.45	72		>1.2	>1.2
2	7.70	8.15	0.45	84		>1.2	>1.2
2	8.15	8.60	0.45	73		>1.2	>1.2
2	8.60	9.05	0.45	67		>1.2	>1.2
2	9.05	9.50	0.45	64		>1.2	>1.2
2	9.50	9.95	0.45	62		>1.2	>1.2
3	9.95	10.40	0.45	4	Clay	-	-
3	10.40	10.85	0.45	8		-	-
4	10.85	11.3	0.45	51	Stratifications of fine sand	>1.2	>1.2
4	11.30	11.75	0.45	54		>1.2	>1.2
4	11.75	12.2	0.45	62		>1.2	>1.2
4	12.20	12.65	0.45	56		>1.2	>1.2
4	12.65	13.1	0.45	17		>1.2	>1.2
4	13.10	13.55	0.45	51		>1.2	>1.2
4	13.55	14	0.45	44		>1.2	>1.2
4	14.00	14.45	0.45	52		>1.2	>1.2
4	14.45	14.9	0.45	44		>1.2	>1.2
4	14.90	15.35	0.45	47		>1.2	>1.2
4	15.35	15.8	0.45	55		>1.2	>1.2
4	15.80	16.25	0.45	35		>1.2	>1.2
4	16.25	16.7	0.45	33		>1.2	>1.2
4	16.70	17.15	0.45	32		>1.2	>1.2
4	17.15	17.6	0.45	37		>1.2	>1.2
4	17.60	18.05	0.45	31		>1.2	>1.2
4	18.05	18.5	0.45	25		0.95	0.83
4	18.50	18.95	0.45	34	>1.2	>1.2	
4	18.95	19.4	0.45	39	>1.2	>1.2	
4	19.40	19.85	0.45	42	>1.2	>1.2	
4	19.85	20.3	0.45	41	>1.2	>1.2	
4	20.30	20.75	0.45	34	>1.2	>1.2	
4	20.75	21.2	0.45	28	1.25	1.09	

Figure C.3: The corrected blow counts and the corresponding liquefaction potential over the depth.

MINISTERIO DE OBRAS PÚBLICAS  
DIRECCIÓN DE VIALIDAD  
SUBDIRECCIÓN DE OBRAS  
DEPARTAMENTO DE PUENTES  
SUBDEPARTAMENTO DE  
MAQUINARIAS, EQUIPOS Y  
PUENTES DE EMERGENCIA

# FICHA DE SONDADJE

PUENTE: PASARELA GUÍDICO  
CAMINO: ...  
REGION: VII PROVINCIA: ARBUCO  
SONDAJE: I UBICACION: LAGO SUR  
COTA CERO: 0,65 +2M

MTR	LMT	PENETRACION CON C.N.						HTAS. PERFORACION				TIPO DE SUELO	
		PROFUNDIDAD		ENSAYES S.P.T.				ENTUBACION		PER TRICOR		DESCRIPCION GENERAL DE LA MUESTRA	
Nº	m	DE	A	N1	N2	N3	N4	DE	A	DE	A		
1	0,65	1,0	2	2	3	5						LIMO ARCILLA COLOR CAFE	
2	1,0	1,55	2	2	2	4						" " " " " "	
3	1,55	2,00	2	3	6	9						" " " " " "	
4	2,00	2,65										ARENA FINA LIMO	
5	2,65	3,14	4	7	7	14						ARENA FINA	
6	3,14	3,69	7	11	14	25						" " " " " "	
7	3,69	4,04	16	20	27	47						" " " " " "	
8	4,04	4,49	16	26	39	65						" " " " " "	
9	4,49	5,19	18	30	43	72						" " " " " "	
10	5,19	5,90	17	27	37	64						" " " " " "	
11	5,90	6,25	19	28	34	61						" " " " " "	
12	6,25	6,80	16	26	31	57						" " " " " "	
13	6,80	7,25	19	30	37	63						ARENA FINA ALGO DE CONCHUELA	
14	7,25	7,70	16	28	38	66						" " " " " "	
15	7,70	8,14	14	30	34	59						" " " " " "	
16	8,14	8,60	19	32	42	70						" " " " " "	
17	8,60	9,05	13	26	40	66						" " " " " "	
18	9,05	9,50	12	26	34	61						" " " " " "	
19	9,50	9,95	15	32	38	64						" " " " " "	
20	9,95	10,40	2	2	2	4						ARCILLA LINDA COLOR GRIS HUMEDA PATE	
21	10,40	10,85	3	3	6	8						" " " " " "	
22	10,85	11,30	15	25	31	56						ARENA FINA COLOR GRIS	
23	11,30	11,75	16	26	34	60						" " " " " "	

OBSERVACIONES: X con 2 Cos Hojas de la OLA OLA OLA

EQUIPO: ...  
OPERADOR: Hugo BELTRAN R  
FECHA INICIO: 16.12.09  
FECHA TERMINO: 21.12.09

MINISTERIO DE OBRAS PÚBLICAS  
DIRECCIÓN DE VIALIDAD  
SUBDIRECCIÓN DE OBRAS  
DEPARTAMENTO DE PUENTES  
SUBDEPARTAMENTO DE  
MAQUINARIAS, EQUIPOS Y  
PUENTES DE EMERGENCIA

# FICHA DE SONDADJE

PUENTE: PASARELA GUÍDICO  
CAMINO: ...  
REGION: VII PROVINCIA: ARBUCO  
SONDAJE: I UBICACION: LAGO SUR  
COTA CERO: 0,65 +2M

MTR	LMT	PENETRACION CON C.N.						HTAS. PERFORACION				TIPO DE SUELO	
		PROFUNDIDAD		ENSAYES S.P.T.				ENTUBACION		PER TRICOR		DESCRIPCION GENERAL DE LA MUESTRA	
Nº	m	DE	A	N1	N2	N3	N4	DE	A	DE	A		
24	11,75	12,20	20	24	31	50						ARENA FINA COLOR GRIS	
25	12,20	12,66	19	26	32	54						" " " " " "	
26	12,66	13,10	8	10	10	20						" " " " " "	
27	13,10	13,55	27	24	24	61						ARENA FINA ALGO DE CONCHUELA	
28	13,55	14,00	14	23	30	53						" " " " " "	
29	14,00	14,45	20	28	36	64						" " " " " "	
30	14,45	14,90	18	24	31	55						" " " " " "	
31	14,90	15,35	19	26	34	60						" " " " " "	
32	15,35	15,80	21	32	38	70						ARENA FINA GRUESA CON ALGO DE CUARZO	
33	15,80	16,25	14	19	26	43						" " " " " "	
34	16,25	16,70	12	17	23	34						" " " " " "	
35	16,70	17,15	12	19	24	43						ARENA FINA COLOR GRIS OSCURA	
36	17,15	17,60	14	22	28	50						" " " " " "	
37	17,60	18,05	15	17	23	34						" " " " " "	
38	18,05	18,50	10	12	19	35						" " " " " "	
39	18,50	18,95	21	27	26	47						" " " " " "	
40	18,95	19,40	22	24	37	55						" " " " " "	
41	19,40	19,85	20	26	32	60						" " " " " "	
42	19,85	20,30	22	27	33	60						" " " " " "	
43	20,30	20,75	19	22	28	50						" " " " " "	
44	20,75	21,20	16	19	22	41						" " " " " "	

OBSERVACIONES: X con 2 Cos Hojas de la OLA OLA OLA

EQUIPO: ...  
OPERADOR: Hugo BELTRAN R  
FECHA INICIO: 16.12.09  
FECHA TERMINO: 21.12.09

MINISTERIO DE OBRAS PÚBLICAS  
DIRECCIÓN DE VIALIDAD  
DEPARTAMENTO DE PUENTES  
SUBDEPARTAMENTO DE MAQUINARIAS,  
EQUIPOS Y PUENTES DE EMERGENCIA

SONDAJE Nº: I  
PUENTE: PASARELA GUÍDICO  
REGION: VII PROVINCIA: ARBUCO

MINISTERIO DE OBRAS PÚBLICAS  
DIRECCIÓN DE VIALIDAD  
DEPARTAMENTO DE PUENTES  
SUBDEPARTAMENTO DE MAQUINARIAS,  
EQUIPOS Y PUENTES DE EMERGENCIA

SONDAJE Nº: I  
PUENTE: PASARELA GUÍDICO  
REGION: VII PROVINCIA: ARBUCO  
FECHA: 16.12.09

## MEDICIONES DEL NIVEL FREÁTICO

FECHA	HORA	COTA REVES (m)	COTA SONDADJE (m)	COTA NAPTA (m)
16-12-09	17:30	6,83	6,80	2,00
17-12-09	08:10	6,83	6,80	1,90
	17:35	10,76	10,40	2,10
18-12-09	08:10	10,76	10,40	2,65
	17:15	18,36	18,95	2,40
21-12-09	08:10	18,36	18,95	2,06
	17:15	21,90	21,20	

OBSERVACIONES:

OPERADOR: Hugo BELTRAN R  
FECHA: 21.12.09

## MUESTRAS DE PROSPECCIONES PARA ANÁLISIS DE LABORATORIO

PROFUNDIDAD (m)	DESCRIPCION VISUAL	HORIZTE	Nº	FECHA	OBSERVACION
0,00	LIMO ARCILLA COLOR CAFE		1		
2,00	" " " " " "				
3,14	ARENA FINA LIMO		1		
	ARENA FINA		2		
6,80	ARENA FINA ALGO DE CONCHUELA		3		
9,95	ARCILLA LINDA COLOR GRIS HUMEDA PATE		7		
10,85	ARENA FINA COLOR GRIS		8		
13,10	ARENA FINA ALGO DE CONCHUELA		9		
14,90	ARENA FINA GRUESA CON ALGO DE CUARZO		8		
16,70	ARENA FINA COLOR GRIS OSCURA		9		
21,20					

DE: OPERADOR DE MAQUINA DE SONDADJE  
A: JEFE LABORATORIO REGIONAL

Ajuste remitido a UAI, muestras provenientes del SONDADJE para determinar su Analisis Granulométrico, Constantes Hídricas, Materia Orgánica, Humedad natural, Punto específico, Punto urbano, y Clasificación de suelos.

ATENTAMENTE  
OPERADOR: Hugo BELTRAN R  
FECHA: 21.12.09

RECIBI CONFORME:

Figure C.4: The raw SPT data used for defining the geo-technical boundary conditions.

## C.2 Seismic vibration tests

### C.2.1 Performed tests

The velocity of the Rayleigh waves are mainly influenced by the material properties to a depth of approximately 1 to 2 wavelengths. Longer wavelengths will propagate deeper and thus these wave velocities are mainly influenced by the layers at higher depths. For a subsurface consisting of only one type of soil, the different wavelengths have the same phase velocity. When the subsurface is layered, each wavelength has a different phase-velocity as shown in figure C.5a.

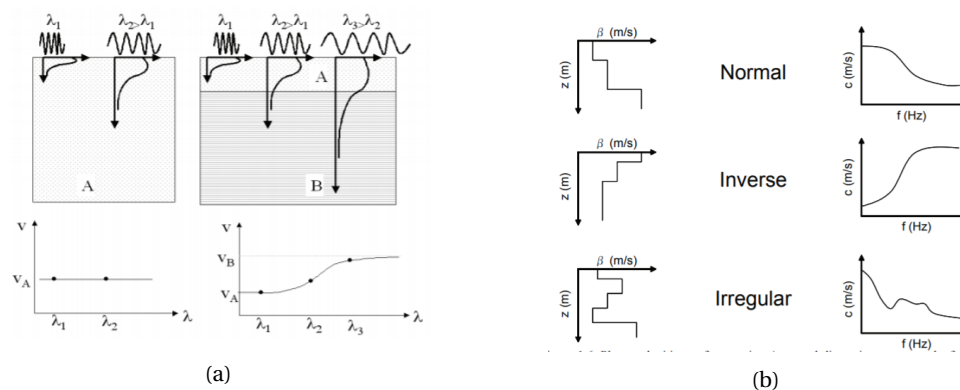


Figure C.5: (a) Surface wave dispersion in a homogeneous and heterogeneous subsurface. (b) Different shapes of dispersion curves. (Pei 2007)

The latter will be the basis of the dispersion curve. The seismic record is transformed to the Rayleigh wave dispersion curve, which is the plot of the Rayleigh wave phase velocity ( $V_\phi$ ) with the frequency, via the frequency-wavenumber. A normal dispersion curve corresponds to a subsurface where the Rayleigh wave velocity increases with depth. In most cases the Rayleigh wave velocities increase with depth, thus showing a normal dispersion curve. A reverse dispersion curve corresponds to a subsurface where the Rayleigh wave velocity decrease with depth. These phenomena are shown in figure C.5b.

The Rayleigh wave propagation in a layered subsurface contains multiple modes. Different wavelengths can exist at different phase velocities, as shown in figure C.6a and figure C.6b. This means each mode of propagation corresponds to a certain phase velocities at each frequency. The different modes only exist above their cut-off frequency, this is the lowest frequency at which the mode occurs. With an increasing frequency the number of modes thus can increase, multiple modes can occur at the same time.

After inversion of this curve the Rayleigh wave velocity ( $V_s$ ) at a certain depth can be determined from the Rayleigh wave velocity profile over depth. This Rayleigh wave velocity profile can be used to determine the structure of the soil.

A schematic representation of the inverse analysis is shown in figure C.7.

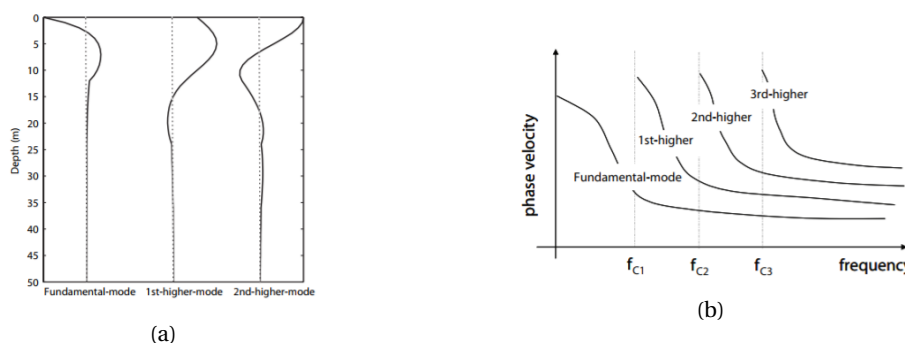


Figure C.6: (a) Modes of surface waves. (b) Dispersion curves of different modes of surface waves. (Pei 2007)

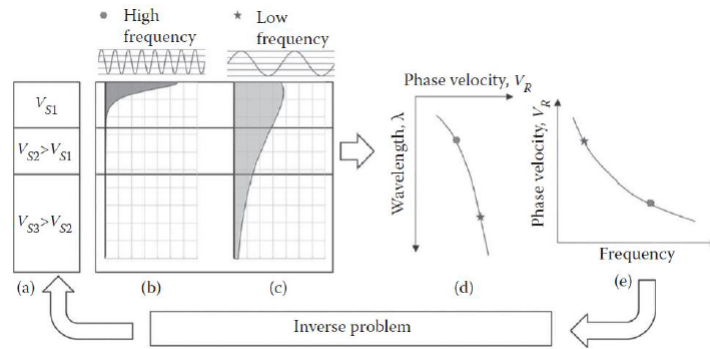


Figure C.7: Schematic representation of the inverse analysis followed during the seismic data analysis. (Pei 2007)

## C.2.2 Results of the tests

For the passive test the refraction microtremor (REMI) method is used, for the active test the multi-channel array surface wave (MASW) method is used. These tests are performed using geophones which are positioned in a linear array. During the site test the interval-distance is set to 6 m, in total 16 geophones are used. Each of the geophones is connected to a multi-channel seismograph which measures the seismic record.

During the passive test the geophones record the surface waves (noise) originating from microtremors. Microtremors are low amplitude vibrations of the ground caused by environmental sources (e.g. ocean wave activity, wind) or man-made disturbances (e.g. traffic, factories). These waves mainly contain relatively low frequencies, corresponding to depths higher than approximately 30 m. During the active test an active source, in this case a hammer blow, produces the surface waves. The hammer blow is offset at a distance of 10 m from the last geophone in the linear array. The active source creates surface waves with relatively high frequencies, which mainly correspond to depths till 30 m.

The results of the REMI and MASW tests are shown in figure C.8 and figure C.9 respectively. In the left graph of the figures the time versus the amplitude of each of the geophones is shown. With these data the Rayleigh wave dispersion curve is constructed via the frequency-wavenumber. This graph is shown on the right part of the figures and shows the Rayleigh wave phase velocity versus the frequency. As can be seen from the dispersion curve of the passive test (REMI) the frequency numbers are relatively low, corresponding to depths higher than 30 m. From the dispersion curve of the active test (MASW) the phase velocity speed corresponding higher frequencies are obtained, corresponding to depths up to 30 m.

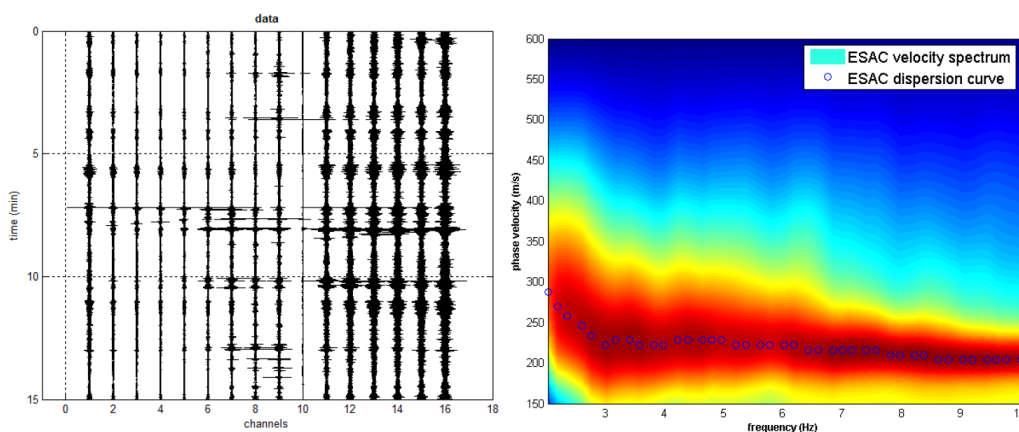


Figure C.8: Results of the REMI test, with on the left the time versus the amplitude of each of the geophones and on the right the Rayleigh wave dispersion curve.

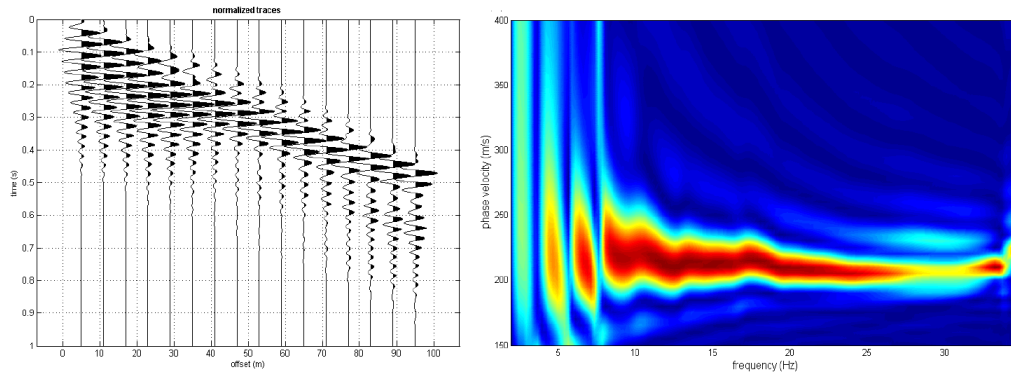


Figure C.9: Results of the MASW test, with on the left the time versus the amplitude of each of the geophones and on the right the Rayleigh wave dispersion curve.

The results of the HVSR test are shown in figure C.10. The results consist of a graph the Fourier amplitude versus the time of the three principal directions (the two horizontal directions and the vertical direction) and a graph of the Fourier amplitude versus the time of the three directions individually. The three principal directions are defined as North-South, East-West and Up-Down. In total the test took 22 minutes. Using the results from the four graphs the H/V spectral ratio can be constructed, this graph is shown on the right side of figure C.10.

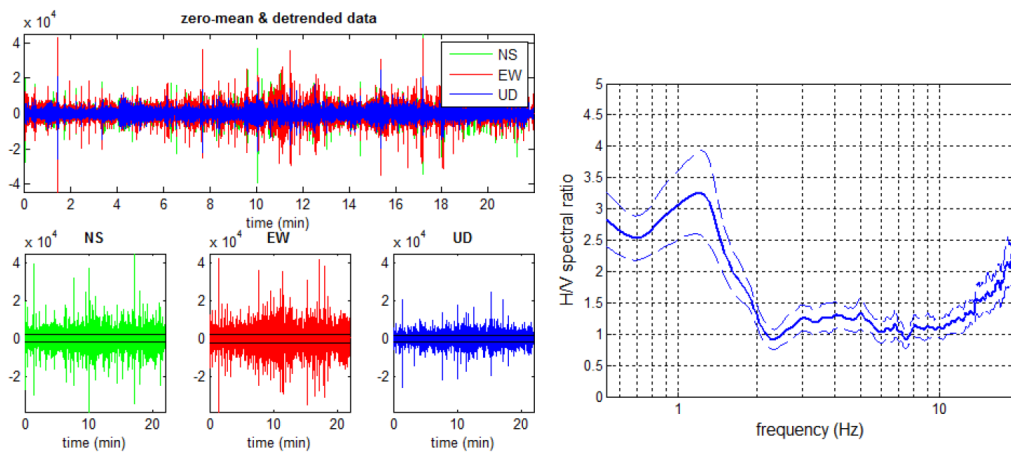


Figure C.10: Results of the HVSR test, with on the left the Fourier amplitude versus the time of the three principal directions individually and combined and on the right the H/V spectral ratio.

# D. Statistical Wave Analysis

## D.1 Offshore statistics

The maximum height, period and direction of the waves should be determined for the breakwater design. To determine these parameters, wave data is used from ARGOSS (Argoss 2017) and from Atlas de Oleaje (Oceanica 2017). The data from Atlas de Oleaje is online available. For ARGOSS it is necessary to have a licence. A threshold analysis is done with these two data sets. A design life time of 25 years is used for this breakwater. For the wave height a return period of 50 years is used, which is relatively low compared to Dutch standards.

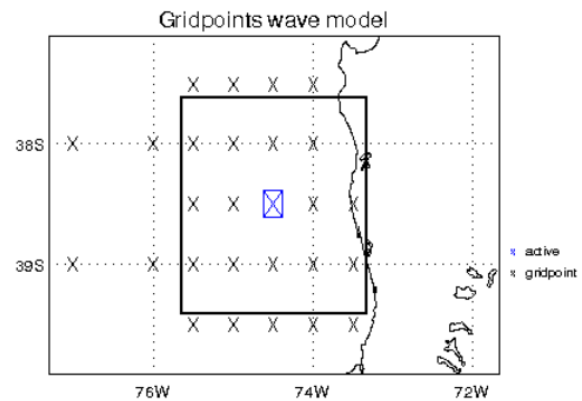
### D.1.1 Obtained wave data

#### ARGOSS

Data is extracted from ARGOSS in a square area of 200 by 200 kilometers in from of the Chilean coast (see figures D.1a and D.1b).



(a) Chilean coast indicating the location of Quidico



(b) Grid points of the wave data from ARGOSS

Figure D.1: Data obtained from ARGOSS

### Data from Atlas de Oleaje

The Department of Ports of Chile is using wave data from Atlas de Oleaje. After discussion with DoP, this data is used as well for comparison. With the data of Atlas de Oleaje the same analysis is done. The data sets seems to be quite similar. One of the differences is that ARGOSS has 25 years of data and Atlas de Oleaje has 35 years of data. The data from Atlas de Oleaje is obtained from node N11. Node N11 is situated at 39 degrees South and 75 degrees West as can be seen in figure D.2.

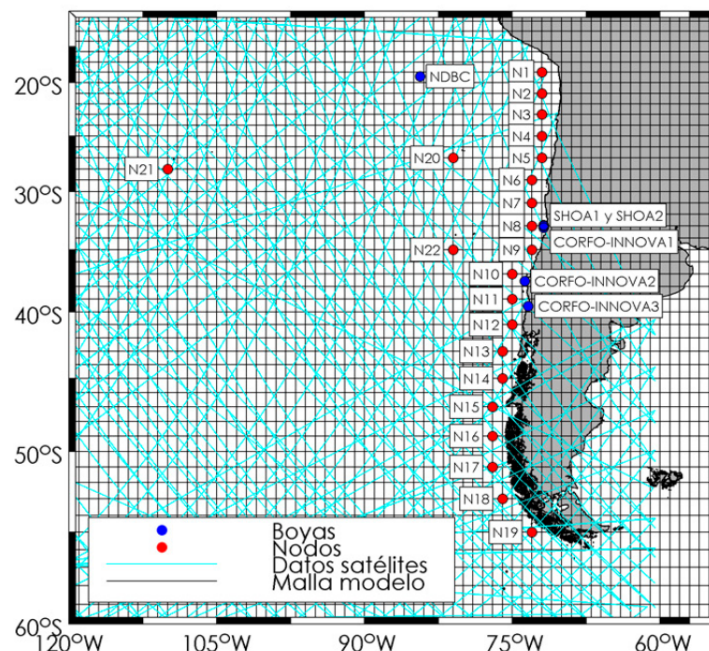


Figure D.2: Location of measurement from Atlas de Oleaje

### D.1.2 Peak over Threshold

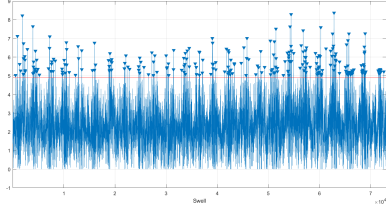
As said, two data sets are used to calculate the maximum wave height. This is done with the peak over threshold method. Using the peak over threshold method it is recommended to aim for around 10 storms per year. In the peak over threshold method, it is important not to take into account two wave heights of one storm. Therefore, in this calculation the time between two storms is set to be at least 24 hours. This is done, to prevent blurred data. To have reliable outcomes of this analysis, the data base should be large. On the other hand it should be relevant data. As already mentioned, the ARGOSS data base contains measurements of the last 25 years and Atlas de Oleaje contains 35 years of data. From these data sets, waves are separated in swell and wind waves. Homogeneous events should be evaluated independently to obtain reliable statistical values for the deep water wave height.

For analysing both data sets, for the peak over threshold method a horizontal line is drawn, which is the threshold level. All maximum values of peaks which are larger than the line, are stored in an array. The number of storms should be, as mentioned, the years of data times 10, which comes down to 250 and 350 storms in total, see equation D.2. The number of storms is, of course, not known on beforehand. Therefore this part is a little trial and error. In figure D.3 the storms are indicated and the red line shows the threshold level.

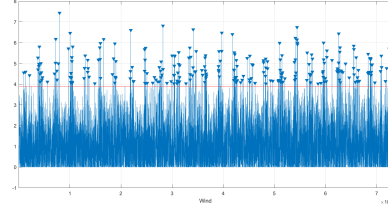
Finally, an array with all data about the storms is used further. This array is stored into different bins. These bins are ordered by wave height with a width of 0.1 meter. A histogram is made with these bins, which can be seen in figure D.4. These bins contain only storm waves and will further be used. With Excel three different statistical analyses are carried out. These methods will be explained in section D.1.3.

Before going to the probabilistic calculations, the corresponding  $T_{m,p}$  needs to be found. This is done by using equation D.1.

$$T_{m,p} = a \cdot \sqrt{H_s} \quad (D.1)$$

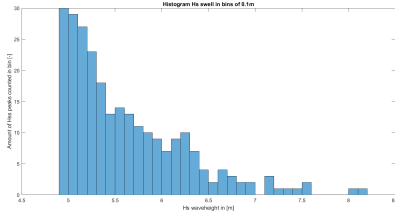


(a) Peak over Threshold executed for the Swell waves

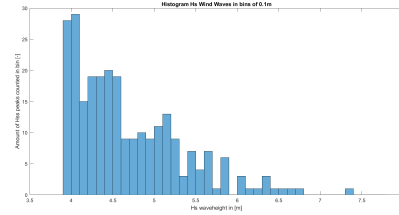


(b) Peak over threshold executed for the wind waves

Figure D.3: Peak over Threshold analysis for the ARGOSS database



(a) Storms for swell waves stored in bins



(b) Storms for wind waves stored in bins

Figure D.4: Storing of the storms in bins with a bin-width of 0.1 meter

The value of  $a$  is calculated for all waves from both data sets. By taking the mean of all these values,  $a_m$  is calculated. With this  $a_m$  and  $H_m$ , the  $T_m$  is obtained. The same is done for  $a_p$  and, therefore the corresponding  $T_p$ .

### D.1.3 Probabilistic calculations

In the next few sections the three statistical methods are explained. Those statistical methods are the Gumbell, Weibull and Exponential distribution. For all three calculations an Excel sheet is used. In this section the used statistic methods will be given and the parameters will be explained. The wind, swell and all waves are calculated separately, but the approach stays the same. Finally, a table with all the final values will be given. These values are used to dimension the breakwater.

Before starting the probabilistic calculations, a few numbers are expressed and calculated. Those values are used in all statistical methods. The following numbers are needed:

$$N_s = \frac{\text{Total amount of storms}}{\text{Number of years of data}} \quad (\text{D.2})$$

$$P_i = \frac{\text{Cumulative number of } storms_i}{\text{Total number of storms per year } (N_s)} \quad (\text{D.3})$$

$$Q_i = 1 - P_i \quad (\text{D.4})$$

$$Q_s = \frac{1}{N_s \cdot R} \quad (\text{D.5})$$

$$G = -\ln - \ln P \quad (\text{D.6})$$

Whereby:

- $N_s$  = is the average total amount of storms per year for the chosen threshold value.
- $P_i$  = chance that this storm, plus the lower storms occur, with  $i$  the number of the bin.
- $Q_i$  = chance that this storm, excluding all lower storms, that this storm will not occur.
- $Q_s$  = total chance of the probability of exceedance of a storm in a year
- $R$  = return period, chosen as 50 years, as stated in the Chilean guidelines and recommended by the Department of Ports.

### D.1.4 Gumbel

For the Gumbel distribution, the Gumbel reduced variable  $G$  is plotted against the mean wave height of the bins (see equation D.7 for the Gumbel reduced value =  $G$ ). Through this data points a line is plotted and a trend line is added. The coefficient of the trend line and the point of intersection are calculated. With these values, named  $A$  and  $B$ , a line in the form of  $y = Ax + B$  is obtained. From this trend line, the wave height corresponding to the return period is calculated. In equation D.7 the storm wave height will be calculated with the numbers  $A$  and  $B$  and the chosen return period. The results are shown for the ARGOSS dataset in figure D.5.

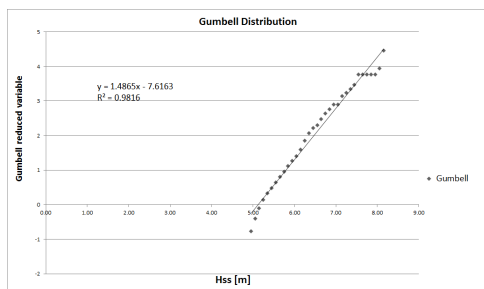
$$\gamma = -\frac{B}{A} \quad (D.7)$$

$$\beta = \frac{1}{A} \quad (D.8)$$

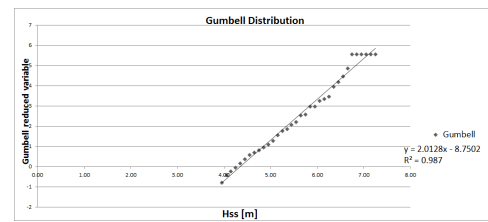
$$-\ln(-\ln(P)) = \frac{H_s - \gamma}{\beta} = \frac{1}{\beta} \cdot \quad (D.9)$$

$$H_s - \frac{\gamma}{\beta} = A \cdot H_s + B \quad (D.10)$$

$$H_s = \gamma - \beta \cdot \ln \ln \frac{N_s}{N_s - Q_s} \quad (D.11)$$



(a) Swell wave heights



(b) Wind wave heights

Figure D.5: Wave height versus the reduced Gumbel variable

### D.1.5 Weibull

For the Weibull distribution the values for  $\gamma$  and  $\beta$  are needed. These values are calculated in the same way as in equation D.7. Almost the same approach as in the Gumbel equation is used. All the data is plotted, here the reduced variable  $W$ , which is stated in equation D.12 is plotted against the mean wave height of a bin. Through these data points a trend line is added, which again is extrapolated till the given return period of 50 years.

The Weibull distribution is given by equation D.12.

$$W = -\ln(Q)^{1/\alpha} \tag{D.12}$$

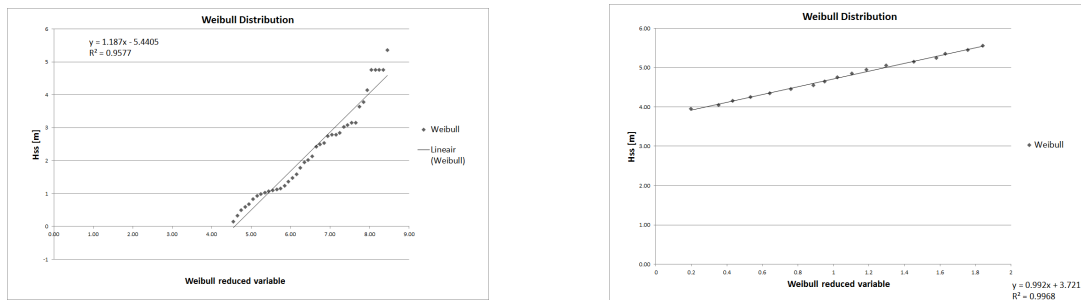
$$P = \exp \left[ \frac{H_{ss} - \gamma}{\beta} \right]^\alpha \tag{D.13}$$

$$H_s = \gamma + \beta * (W) \tag{D.14}$$

As can be seen in the formula above, the Weibull distribution needs to be reduced too. The reduced Weibull variate is calculated in the second part of the equation.

In the Weibull formula also the value of  $\alpha$  is visible. To get the best curve, the  $R^2$  value should be as close to 1.0 as possible. Therefore  $\alpha$  should be adjusted by trial and error.

The results are shown for the ARGOSS data set in figure D.6.



(a) Swell wave heights

(b) Wind wave heights

Figure D.6: Wave height versus the reduced Weibull variable

### D.1.6 Exponential distribution

Also the exponential distribution is used.

The general exponential formula and the wave height are calculated from the general equations given in equation D.15.

$$f_H = B^{-1} \cdot \exp\left(\frac{-(h-A)}{B}\right) \quad (D.15)$$

$$H_s = A \cdot \ln(Q_s) + B \quad (D.16)$$

Again the values A and B from the trend line are used as can be seen above. In this equation the log-normal function is used to describe the trendline. This trendline is used to calculate the  $H_s$ , which corresponds to the 50 year return period.

The results are shown for the ARGOSS data set in figure D.7.

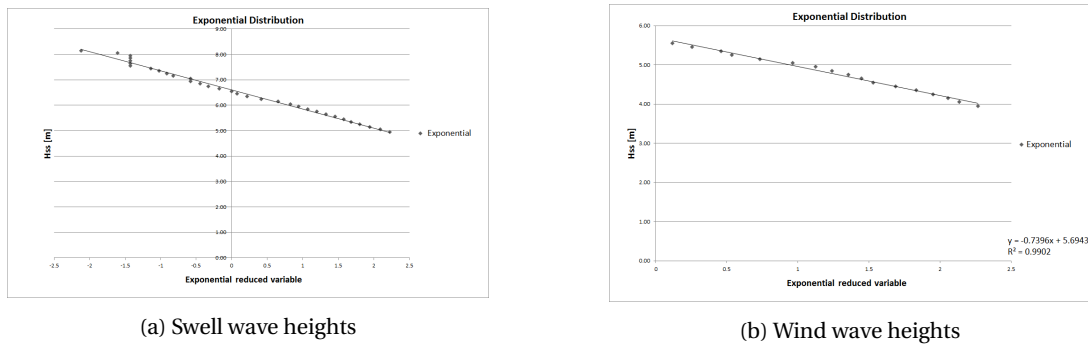


Figure D.7: Wave height versus the reduced Exponential variable

### D.1.7 Final offshore conditions

The Weibull and Gumbell distributions are extreme value distributions. The swell waves and wind waves are analyzed separately from the data from ARGOSS.

Different threshold values are chosen for the swell and wind waves. For the wind waves a threshold value of 3.9 meter is used. This gives a  $N_s$  value of 10.83 storms per year. For the swell waves a threshold value of 4.9 is used. This gives a  $N_s$  value of 10.44 storms per year. The design wave height can be determined after computation in a near shore wave model.

For the waves of the Atlas of Chile, the waves were not split into wind waves and swell waves, only one wave variable was given. With this  $H_{m0}$  the analyses is done. For this data, the value for the threshold is set to 4.5 meter. With this threshold, there will be 9.71 storms per year.

Now the wave heights can be calculated, the corresponding wave periods should be found as well. This is done with the following formula:

$$T_{m,p} = a \cdot \sqrt{H_s} \quad (D.17)$$

From all wave heights in the storm, the  $a$  value is calculated. This is done for  $a_m$  and  $a_p$ . With those two values, the corresponding wave periods are calculated. The  $\alpha$ -values are given in table D.1. The corresponding wave heights and wave periods are given in table D.2.

Table D.1: Obtained a-values to calculate the wave periods

Parameter	Value	Database
$a_{\text{mean,wind}}$	4.14	ARGOSS
$a_{\text{peak,wind}}$	4.96	ARGOSS
$a_{\text{mean,swell}}$	5.24	ARGOSS
$a_{\text{peak,wind}}$	5.84	ARGOSS
$a_{\text{mean}}$	4.39	Atlas de Oleaje
$a_{\text{peak}}$	6.06	Atlas de Oleaje

Table D.2: Offshore values for a return period of 50 years, ARGOSS

Parameter	Exponential	Gumbel	Weibull
$H_{s,\text{swell}}$ (m)	11.32	10.91	10.68
$T_{p,\text{swell}}$ (s)	19.66	19.31	19.10
$T_{m,\text{swell}}$ (s)	17.62	17.29	17.10
$H_{s,\text{wind}}$ (m)	8.79	8.66	8.65
$T_{p,\text{wind}}$ (s)	14.72	14.61	14.60
$T_{m,\text{wind}}$ (s)	12.27	12.17	12.17

Table D.3: Offshore values for a return period of 50 years, Oleaje

Parameter	Exponential	Gumbel	Weibull
$H_s$ (m)	10.95	19.86	10.27
$T_p$ (s)	20.07	19.98	19.43
$T_m$ (s)	14.54	14.48	14.08

### Comparison data sets

As can be seen in the results above, the data sets have similar outcomes. Both data sets contain enough data to be reliable. Because the Chilean data set does not contain wind waves, the values of ARGOSS are used for designing the breakwater. Also, the location of the ARGOSS measurements is more specific for the bay of Quidico.

## D.2 Offshore to near shore

In this section the processes shoaling and refraction will be described. Diffraction and reflection are not treated in this section. Diffraction is described in section 5.5.1 and the reflection parameter will be described in section 5.8. The offshore values need to be translated to near-shore values. This process is described in this section. To make this translation the following parameters are needed from offshore:

- $H_0$  = Wave height offshore
- $T_0$  = Wave period offshore
- $L_0$  = Wave length offshore
- $c_{g0}$  = Group Wave speed offshore
- $c$  = Wave speed
- $\alpha$  = angle between offshore wave crest and shoreline

The following parameters are needed from near-shore:

- $d$  = Depth near shore
- $T$  = Wave period near shore
- $L$  = Wave length near shore
- $c_g$  = Group wave speed near shore
- $c$  = Wave speed
- $\alpha$  = angle between near shore wave crest and shoreline

With the parameters from above the following formulas can be filled in:

$$\begin{aligned}
 c &= \sqrt{\frac{g}{k} \tanh(kd)} \\
 c_g &= nc \\
 n &= \frac{1}{2} \left( 1 + \frac{2kd}{\sinh(2kd)} \right) \\
 k &= \frac{2\pi}{L}
 \end{aligned} \tag{D.18}$$

Because the near-shore wave length is not known, and  $k$  is dependent on  $L$ , an iterative calculation is done to obtain the values for  $k$  and  $L$ .

Shoaling is of big importance in Quidico Bay, Chile, through the fact that the slope at this coast is gentle. This means that depth decreases slowly towards the coast. Waves come from offshore, where depths are large. If waves approach the beaches, the depth decreases. Therefore, the waves start to 'feel' the bottom. This causes friction, which on its turn slows down the waves, and creates energy bunching. Depending on the bottom specifications, sediment can start to move through shoaling waves. The shoaling parameter is a parameter which describes the ratio of wave height offshore and near-shore. This parameter can be calculated with equation D.19.

$$K_{sh} = \sqrt{\frac{c_{g,offshore}}{c_{g,onshore}}} \tag{D.19}$$

Because the group velocity at the shore goes to zero, in theory the shoaling factor can go to infinity. Therefore the near-shore wave height goes, in theory, to infinity as well. Due to other processes, like breaking and refraction, this will not happen in reality.

Refraction is a parameter that has influence on the direction of the waves. Waves want to arrive perpendicular to the shore. If waves come under an angle, they will turn in shallow water towards the coast. This is called refraction and can be seen in figure D.8.

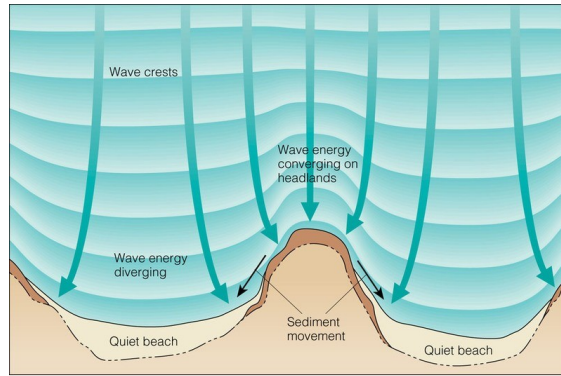


Figure D.8: Refraction at a coast

The refraction coefficient is described by equation D.20.

$$K_r = \sqrt{\frac{b_{offshore}}{b_{nearshore}}} \quad (D.20)$$

The combination of shoaling and refraction is given in equation D.21.

$$K = \sqrt{\frac{c_{g,offshore}}{c_{g,nearshore}}} \sqrt{\frac{b_{offshore}}{b_{nearshore}}} \quad (D.21)$$

All these equations are derived by using an energy balance. All these formula are filled in by using a spreadsheet. With this spreadsheet the wave height around the breakwater is calculated. As said, some values are obtained via iteration. The values in the table can be seen in figure D.9.

59	d	L	C	alfa	Ks*Kr	H		WAVE BROKEN OR NOT
95	8.5	180.032	9.002	16.2	0.694	7.421	H increases	YES - H/d > 0.75
96	8	174.806	8.740	15.7	0.702	7.516	H increases	YES - H/d > 0.75
97	7.5	169.400	8.470	15.2	0.712	7.619	H increases	YES - H/d > 0.75
98	7	163.797	8.190	14.7	0.723	7.733	H increases	YES - H/d > 0.75
99	6.5	157.973	7.899	14.1	0.734	7.858	H increases	YES - H/d > 0.75
100	6	151.907	7.595	13.6	0.747	7.997	H increases	YES - H/d > 0.75
101	5.5	145.564	7.278	13.0	0.762	8.153	H increases	YES - H/d > 0.75
102	5	138.910	6.945	12.4	0.778	8.329	H increases	YES - H/d > 0.75
103	4.5	131.896	6.595	11.8	0.797	8.530	H increases	YES - H/d > 0.75
104	4	124.477	6.224	11.1	0.819	8.765	H increases	YES - H/d > 0.75
105	3.5	116.575	5.829	10.4	0.845	9.041	H increases	YES - H/d > 0.75
106	3	108.103	5.405	9.6	0.876	9.377	H increases	YES - H/d > 0.75
107	2.5	98.947	4.947	8.8	0.916	9.800	H increases	YES - H/d > 0.75
108	2	88.973	4.449	7.9	0.968	10.360	H increases	YES - H/d > 0.75
109	1.5	78.022	3.901	6.9	1.044	11.170	H increases	YES - H/d > 0.75 AND H/L > 1/7
110	1	65.964	3.298	5.9	1.172	12.542	H increases	YES - H/d > 0.75 AND H/L > 1/7
111	0.5	52.947	2.647	4.7	1.481	15.847	H increases	YES - H/d > 0.75 AND H/L > 1/7
112	0.1	41.213	2.061	3.7	2.917	31.208	H increases	YES - H/d > 0.75 AND H/L > 1/7

Figure D.9: Part of the calculation sheet called WAVESHOREF

This is just a small part of the calculation sheet, but it shows at which depth the maximum wave height will break.

Used for further calculation are the values which correspond to the depth of 4 meters. Which is the depth which is in line with the depth at the end of the breakwater.

# E. Model Set-Up Delft3D

In this chapter the set-up of the Delft3D model will be explained. The necessary input is given to run the Delft3D models.

## E.1 General

To model the waves in Quidico, Delft3D is used. The main question before making the model is how and where to place the breakwater. The angle of the breakwater must be placed in a way that it breaks the most unfavourable waves from the north, but also in a way that the the circulation in the bay will be favorable.

Modelling of near-shore wave conditions will allow for answering the objectives stated in chapter 3. In this section the method is described for making the near-shore model. Based on the stated environmental conditions in section 4.2.2, a model is made and prepared. First the model set-up is explained, then the used grid and depth file are presented. Finally, the used parameters and boundary conditions are given.

In the model the operational waves are treated only. The extreme values from the statistical analysis are used for dimensioning the breakwater. Those extreme values are transformed to near shore values by using an Excel sheet. Those statistics are treated in section D. The main waves of influence for the bay of Quidico are the swell waves. Wind waves are not threatened in the model. Still different models are created to see the influence of the different directions. Also, different wave heights are investigated. The used wave heights are obtained from the reports of the Department of Ports. The important swell wave direction is 292.5 degrees, which is equal to a NNW direction. The main question during modelling is to find the existence of the so called 'return current'. And, if present, if this return current is important or not. Another part is to see if it is possible to say something about the location of wave breaking. Also the evaluation of waves will be investigated. Those three phenomena are investigated during the modelling phase.

## E.2 Model Set-up

The used model is Delft3D, in this program a wave study is done by SWAN (Simulating WAVes Near shore). This third-generation wave model is developed at the Delft University of Technology. The difference with first- and second-generation models is that first generation models do not account for physical processes and second-generation models try to fix those processes by using certain parameters. In third generation models, most of these phenomena are included. This SWAN model is implemented in Delft3D as a FLOW module. In Delft3D the FLOW-module is combined with a WAVE-module. Therefore, it is possible to combine the flow and wave effects of the area.

The SWAN model takes several interactions into account like shoaling, refraction, wind growth and wave breaking. Processes like diffraction and reflection of waves are interactions that are not fully included in the model. This can be an issue, because diffraction can be of importance by investigating the hydraulics in Quidico Bay. For depth-induced breaking, bottom friction and non-linear triad interactions the default settings of Delft3D are used.

It is advised that detailed modelling of the waves in the harbour (behind the breakwater) should be done by using other models like a boussinesq-model or MIKE 21 . The impact of structures on wave propagation is not very well implemented in SWAN. But probably a good recommendation to the DoP can be given after investigating the model results.

Different models were made and investigated. Different wave heights and directions were implemented. The wave heights are obtained from the reports of Department of Ports and validated with the data obtained from ARGOS (Argoss 2017).

### E.3 Grid

The grid that is used in the models is the core of the model study. The coarser the grid, the less detailed the results. But the coarser the grid, less computing time is needed. The quality and speed of the model are determined by the computational grid. A good balance should be obtained. It is possible to make the grid finer at interesting areas. The grid is finer at the bay and coarser outside the bay. The modelled area is given in figure E.1b. The area is indicated with the black square. The grid is made with RGFGRID, which is a function in Delft3D. The used grid consists of 136 by 122 grid cells, see figure E.2a.

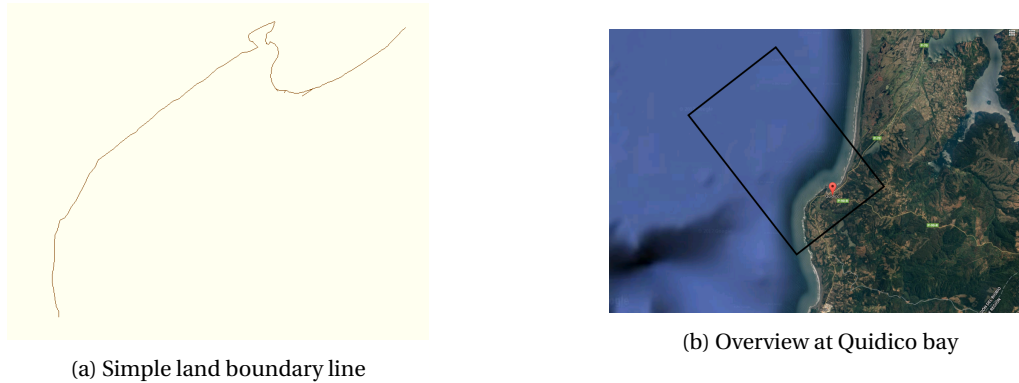


Figure E.1: Landboundary

In figure E.2a it is visible that the size of the grid cells in the bay of Quidico are smaller than in the area around it. The grid is referenced by using a landboundary file. This land boundary file (.ldb extension) is made by using AutoCAD, see figure E.1a.

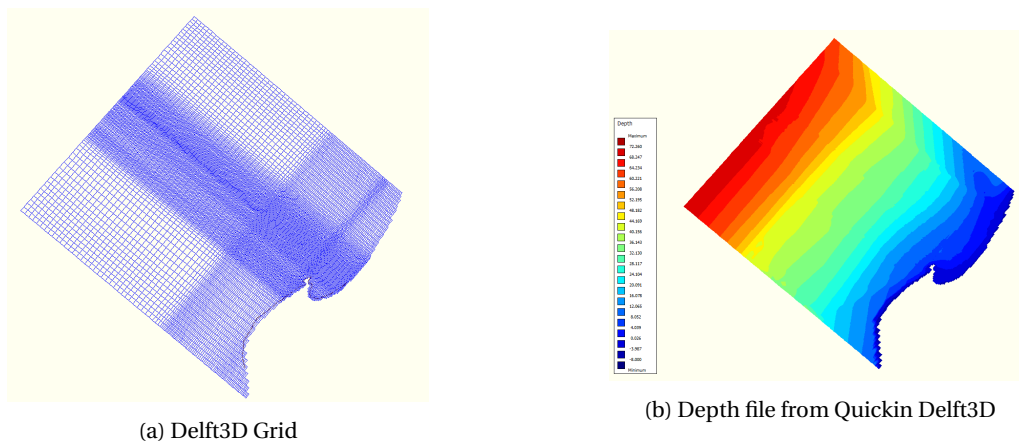


Figure E.2: Model input

The bathymetry data is obtained from the Department of Ports, see section 4.2.4. In figure E.2b the depth data is given. The deepest point is around 80 meters and indicated in red. To achieve this final depth file, data processing was necessary. Some data points are manually added or changed. By using the functions grid cell averaging, grid cell interpolation and internal diffusion, the depth file is made in the module QUICKIN. Figure E.3 summarizes the modelling input necessary to model with Delft3D.

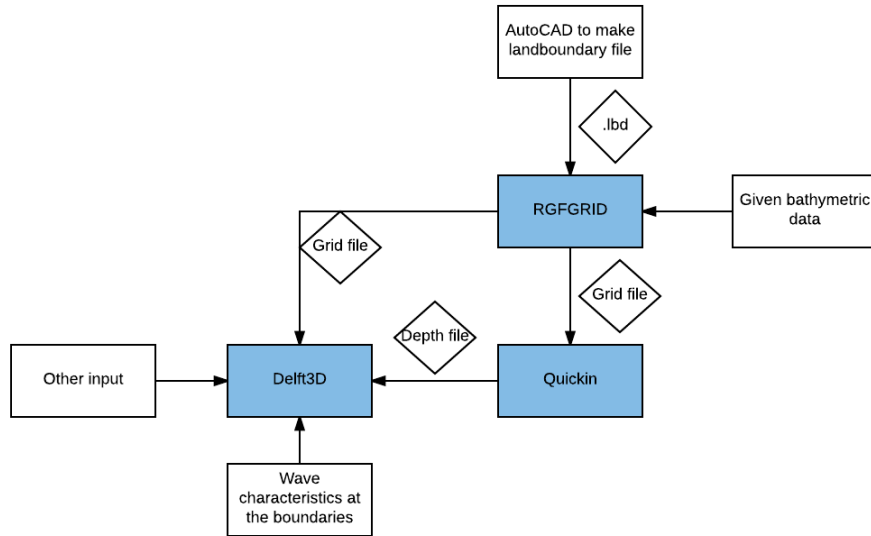


Figure E.3: Scheme of all steps during modelling.

There was lack of data for some areas around Quidico. For those areas assumptions were necessary. It is advised to improve the bathymetry for these near-shore areas to obtain better modelling results. Most likely the bathymetry is one of the main sources of inaccuracies. Therefore, the model output should be validated and common sense must be used.

## E.4 Boundary Conditions

At each boundary, the conditions are specified in the Delft3D model. Those boundary conditions can be seen as the input for the model. For all boundaries the tides are included as an open water level boundary with an astronomic forcing type. The other input is kept as default. The input values for the tides are given in section 4.2. The waves are implemented in the WAVE module. First a wave direction of 292.5 degrees is used in the models, as discussed with the Department of Ports. The model has three offshore-boundaries and one closed boundary, which is the shore.

## E.5 Different models

Different computational models are modelled with Delft3D. First, the present situation is modelled to validate the model. The model can be calibrated by comparing the model results with the model results from the report of the Department of Ports. Another validation is to check the model results with the theory and reality. The main functions of the breakwater are to break the incoming waves and create a calm zone behind this breakwater, to moor the ships. Another problem which should be solved, is that fishermen have some issues, under certain circumstances, entering the harbour. They cannot make their movement into the harbour due to the breaking waves. Firstly two different options are modelled. The breakwater placement is obtained through different discussions with the Department of Ports and other professors of UdeC. Different layouts are tested and validated.

The breakwater orientations for the validation models are as follows:

- Current situation without a breakwater
- Large breakwater to break the waves without contramolo, see figure E.4a
- Large breakwater to break the waves with contramolo, see figure E.4b
- Some other alternatives for indication of the currents, see for example figure E.4c



Figure E.4: Three configurations of the breakwater

The main idea of the contramolo is to block the sediment which comes from the return current. The Department of Ports thinks that this contramolo will keep the sediment, that comes from the return current, out of the bay. This is a first thought and research is necessary. It is not yet proven that building this contramolo will solve the wave- and sediment problems. The sediment transport is treated in section 5.7. By placing the contramolo it is important to look at the entrance area of the harbour. During the discussions with the fishermen, they were still a bit anxious about the angle of the initial conceptual design by the Department of Ports. The breakwater and contramolo were close to each other, which made steering into the bay a problem. The fishermen proposed a more straight breakwater in extension with the headland, so the entrance will be larger. Also the direction of waves were a problem is what the fishermen said. The doubts of the fishermen has also the do with another project in Tirúa (see Appendix B). During this project the first design was not sufficient and therefore an extension is made. After making the extension the breakwater works well.

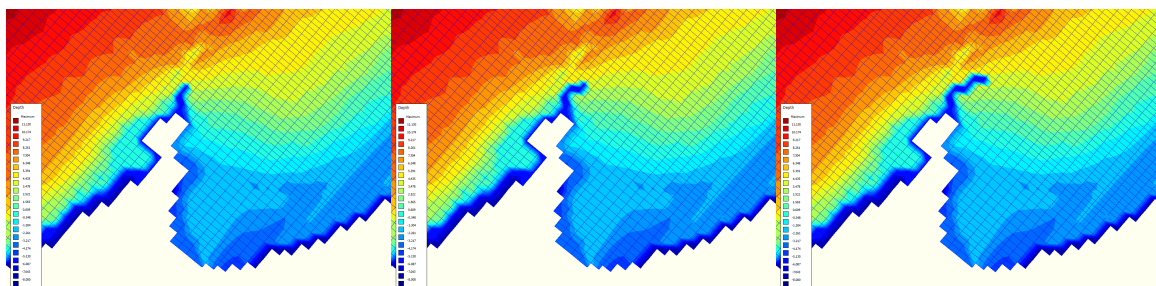
See table E.1 for the specific input values for each breakwater layout. Other input conditions are explained in section 4.2.2. Those values were used in the first models. The input during the other modelling phases is explained in section 5.4.1.

Table E.1: Delft3D input for the first models

Input Variable	Value	Unit
$H_s$	2	m
$T_p$	10	s
$H_{dir}$	292.5	deg
$W_w$	15	m/s
$U_{dir}$	270	deg

## E.6 Three final Breakwater models

For the final modelling phase, three breakwater lengths are considered. In the following figure, figure E.5, the final breakwater models are shown. What must be said is that, due to the grid placement, the direction of the breakwater is not modelled the exact way as proposed. The breakwaters look a bit angular in the figures below.



(a) Second breakwater section of 50 m (b) Second breakwater section of 100 m (c) Second breakwater section of 150 m

Figure E.5: Three configurations of the breakwater

## F. Delft3D Model Results

In the coming sections the model results are given. Figure F.1 is given for indication. In this figure a satellite image from Google Maps is plotted over a part of the initial depth file. The white arrow is indicating the considered bay of Quidico.

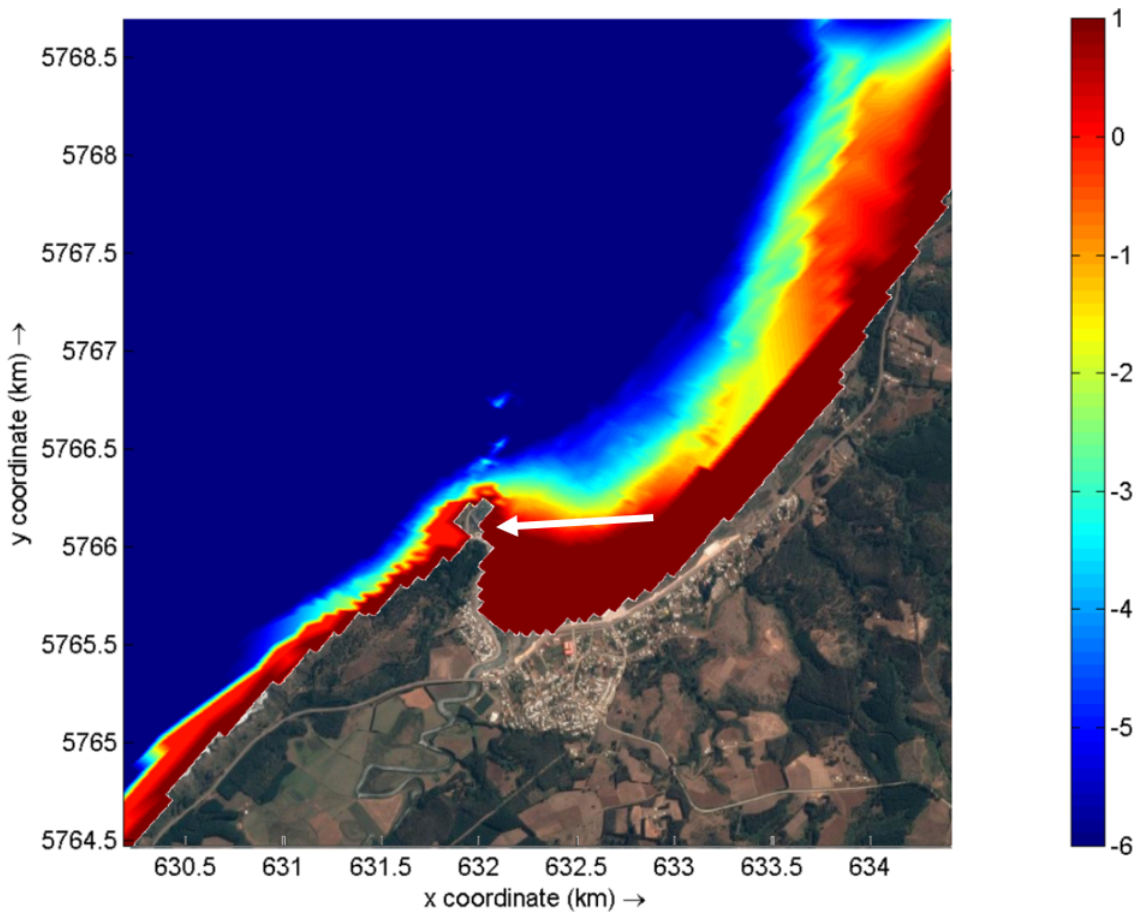


Figure F.1: Satellite image from Google Earth plotted over the initial bed file from Delft3D

## E.1 Result validation models

In figure E2 the upper two figures are representing the wave induced current directions for different breakwater configurations. The configurations of the breakwater are shown in blue. The lower figure represent the wave height and directions for the drawn breakwater configuration. The figures are used to validate the created model and analyse the processes in the bay.

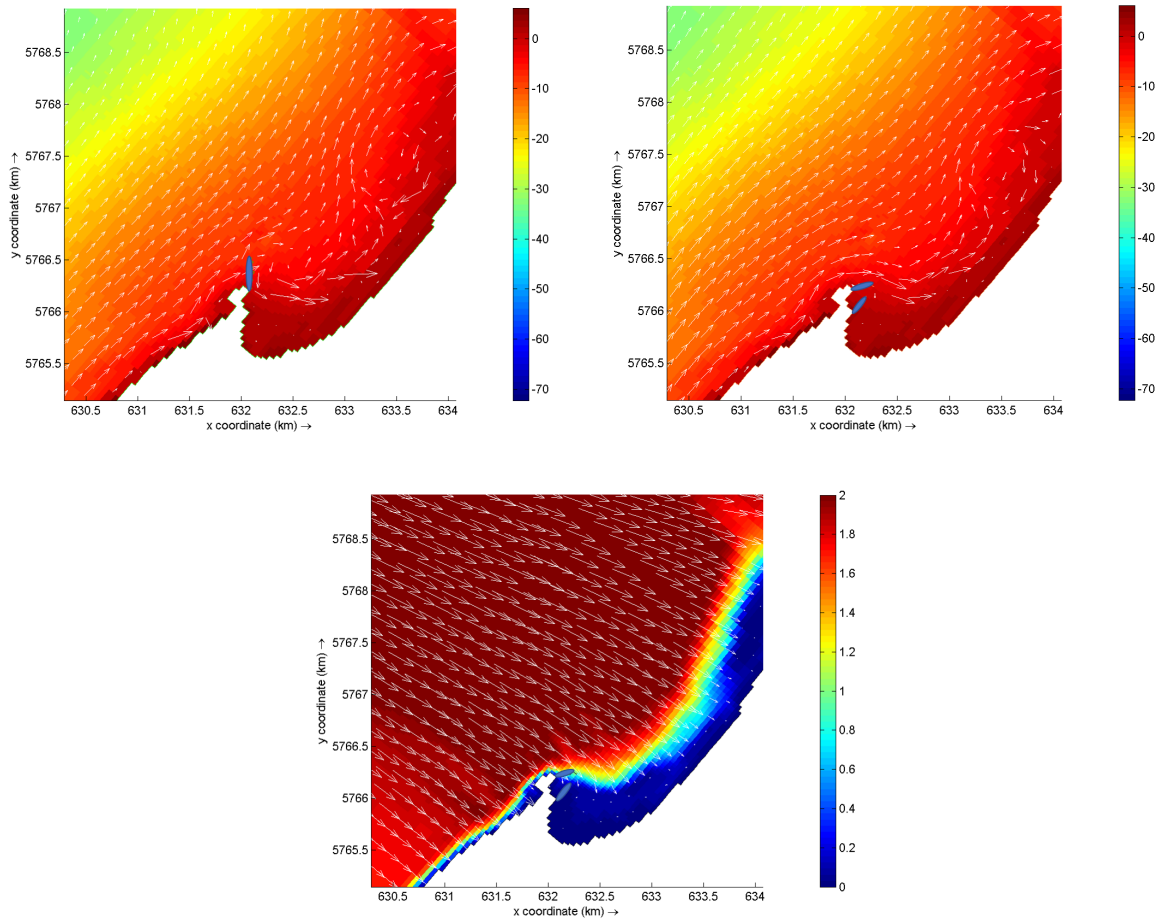


Figure E2: Figures to validate the model and to analyse the processes in Quidico

## E.2 Result final proposed model

In figure E3 the wave directions are plotted for all considered wave directions (270, 292.5 and 315 degrees). The figure is for the initial situation, that means without the breakwater. The arrows are indicating the following directions:

- White = 315 degrees
- Yellow = 292.5 degrees
- Black = 270 degrees

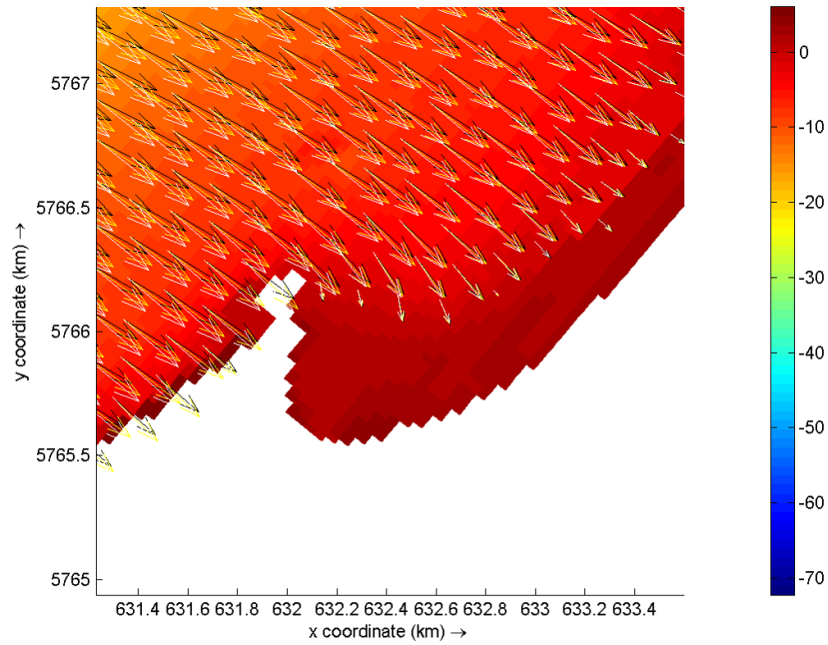


Figure E3: Three wave directions plotted in one figure

In figures F4 until F7, the wave induced current directions are given for each breakwater length. At all figures the waves are coming from a direction of 315 degrees.

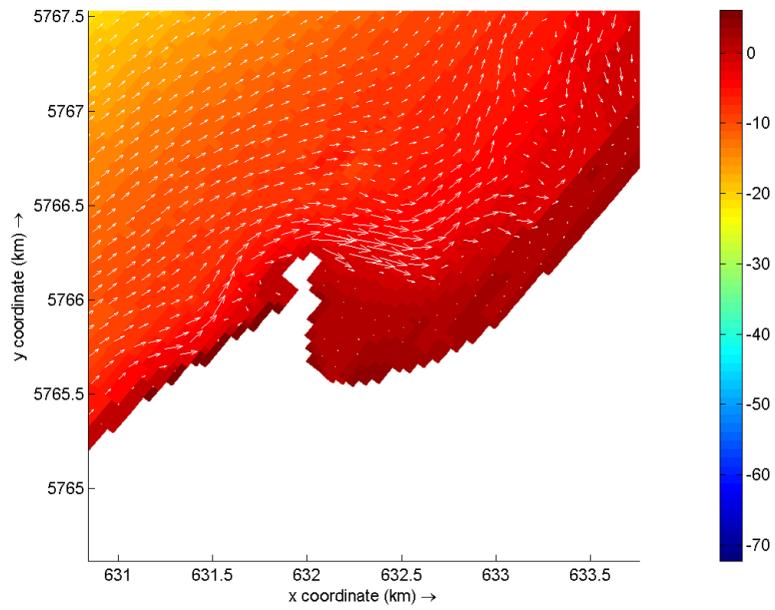


Figure F4: The current directions without any breakwater

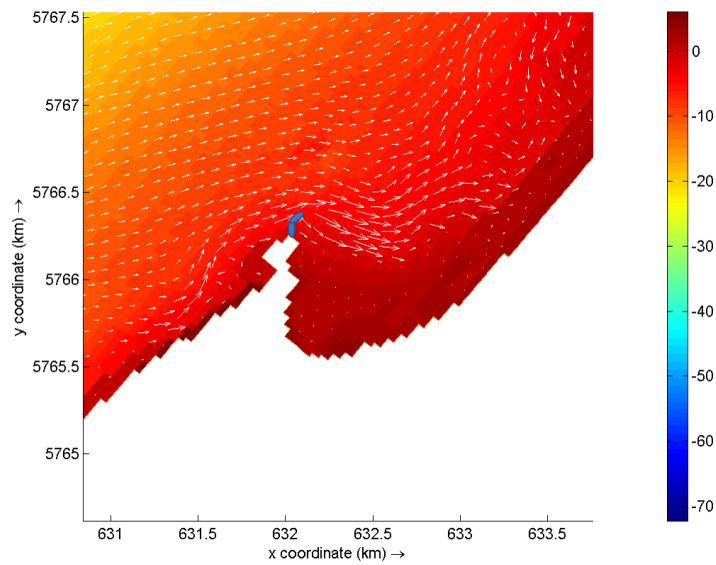


Figure E5: The current directions with the 50 m breakwater

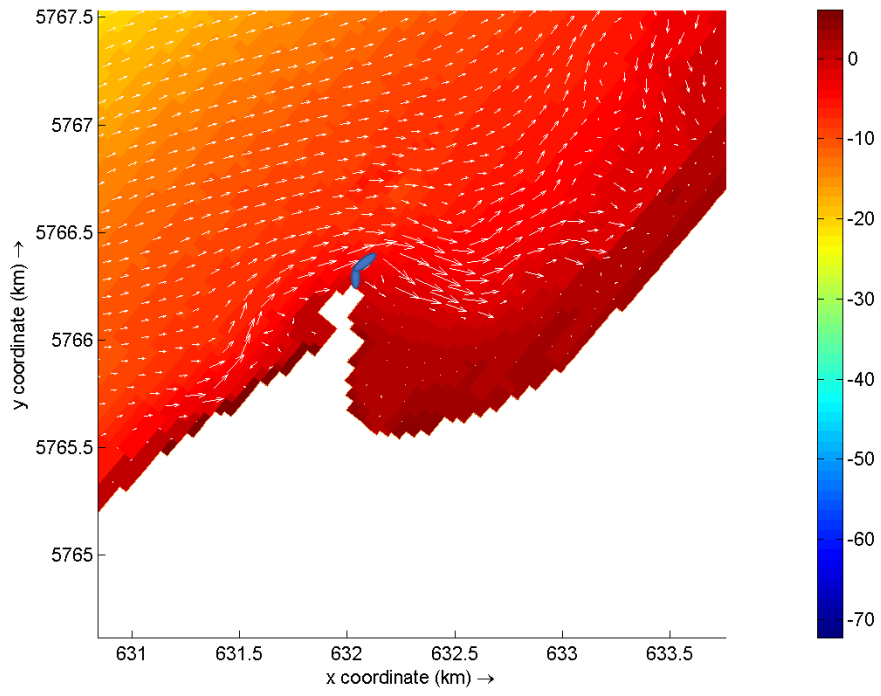


Figure F6: The current directions with the 100 m breakwater

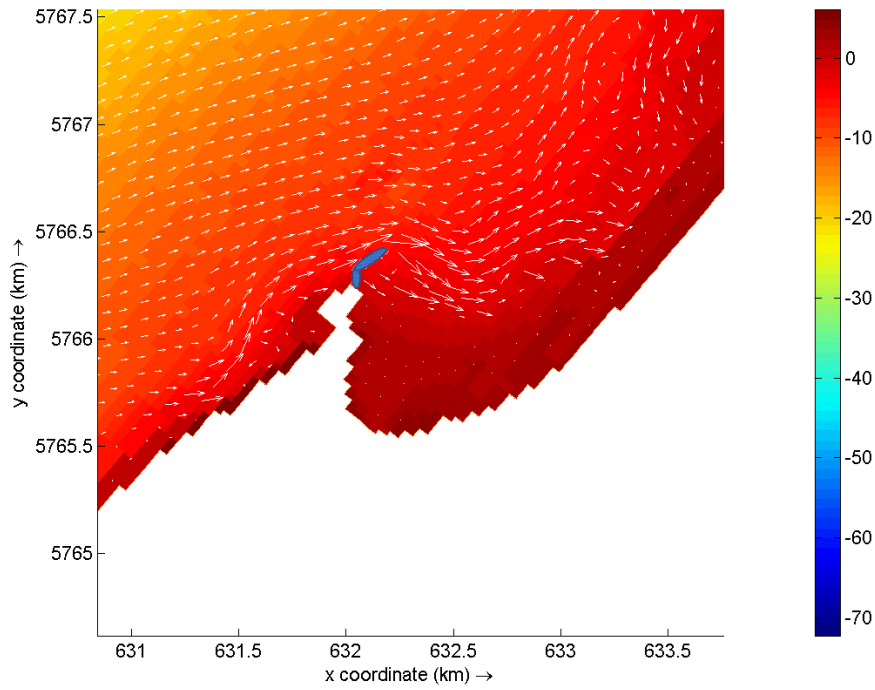


Figure F7: The current directions with the 150 m breakwater

In figure E8 the current directions are given for each breakwater length. In this figure the waves are coming from an angle of 270 degrees. For simplicity the longest breakwater is also plotted. The arrows are indicating the following breakwater lengths:

- White is the initial situation without breakwater
- Yellow is the shortest breakwater (50m)
- Blue is the middle breakwater (100m)
- Black is the longest breakwater (150m)

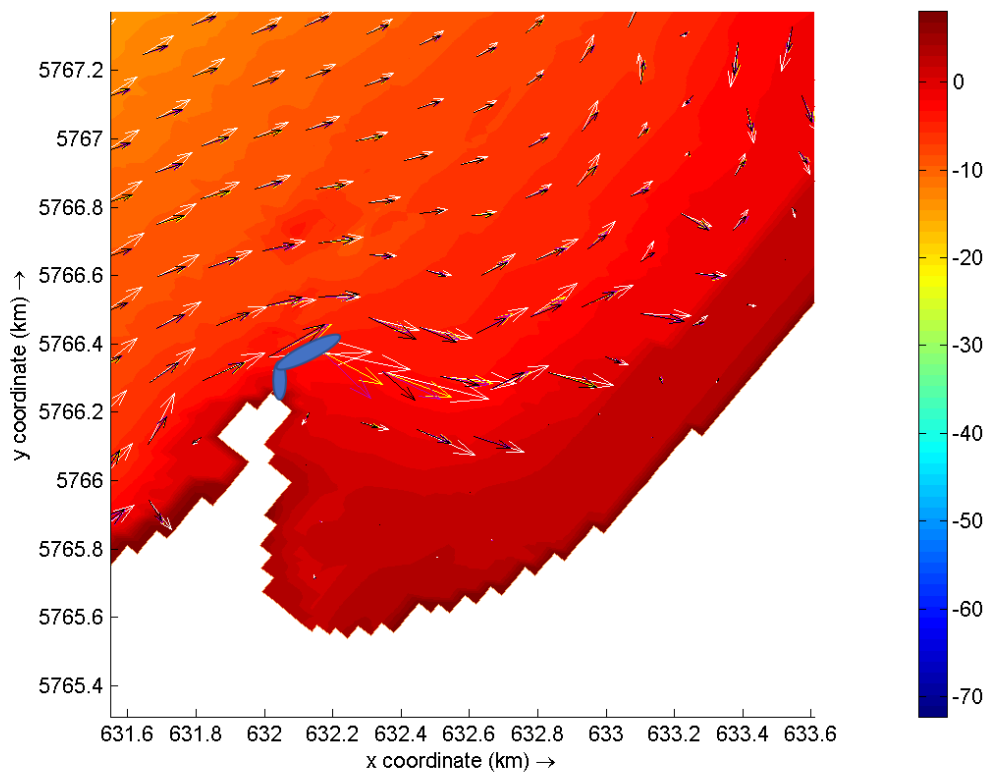


Figure E8: Currents due to waves which come from 270 degrees, for all lengths of breakwaters

In figure E9 the wave induced current directions are presented for each breakwater length. In this figure the waves are coming from an angle of 292.5 degrees. For simplicity the longest breakwater is also plotted. The arrows are indicating the following breakwater lengths:

- White is the initial situation without breakwater
- Yellow is the shortest breakwater (50m)
- Blue is the middle breakwater (100m)
- Black is the longest breakwater (150m)

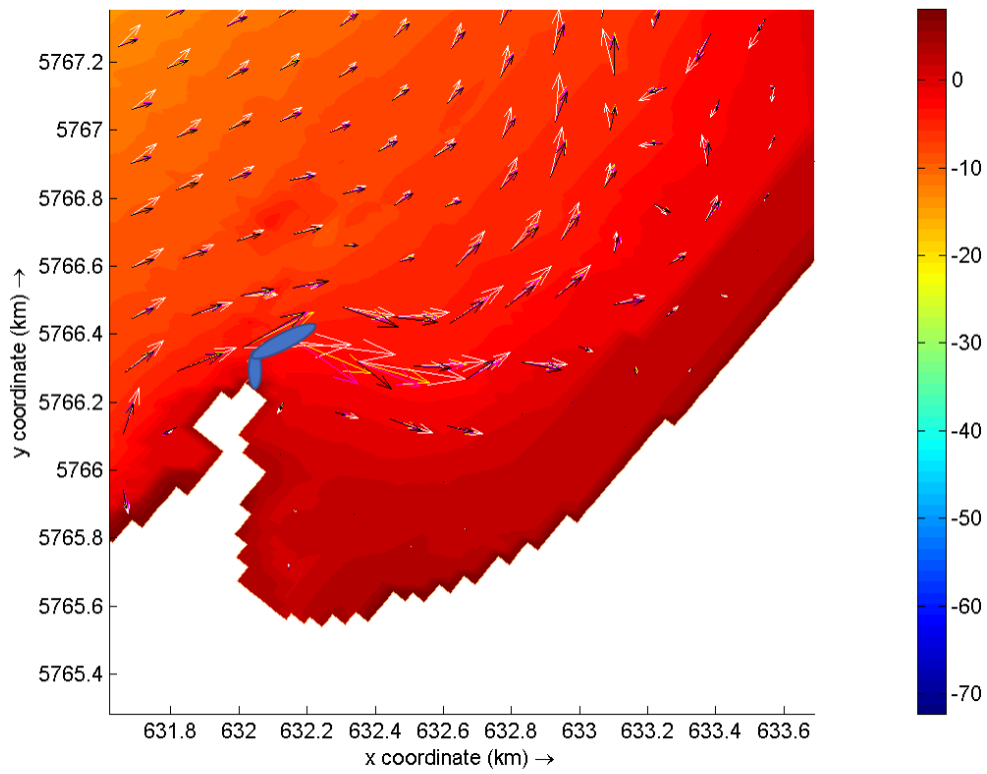


Figure E9: Currents due to waves which come from 292.5 degrees, for all lengths of breakwaters

In figure E10 the wave induced current directions are given for each breakwater length. In this figure the waves are coming from an angle of 315 degrees. For simplicity the longest breakwater is also plotted. The arrows are indicating the following breakwater lengths:

- White is the initial situation without breakwater
- Yellow is the shortest breakwater (50 m)
- Blue is the middle breakwater (100 m)
- Black is the longest breakwater (150 m)

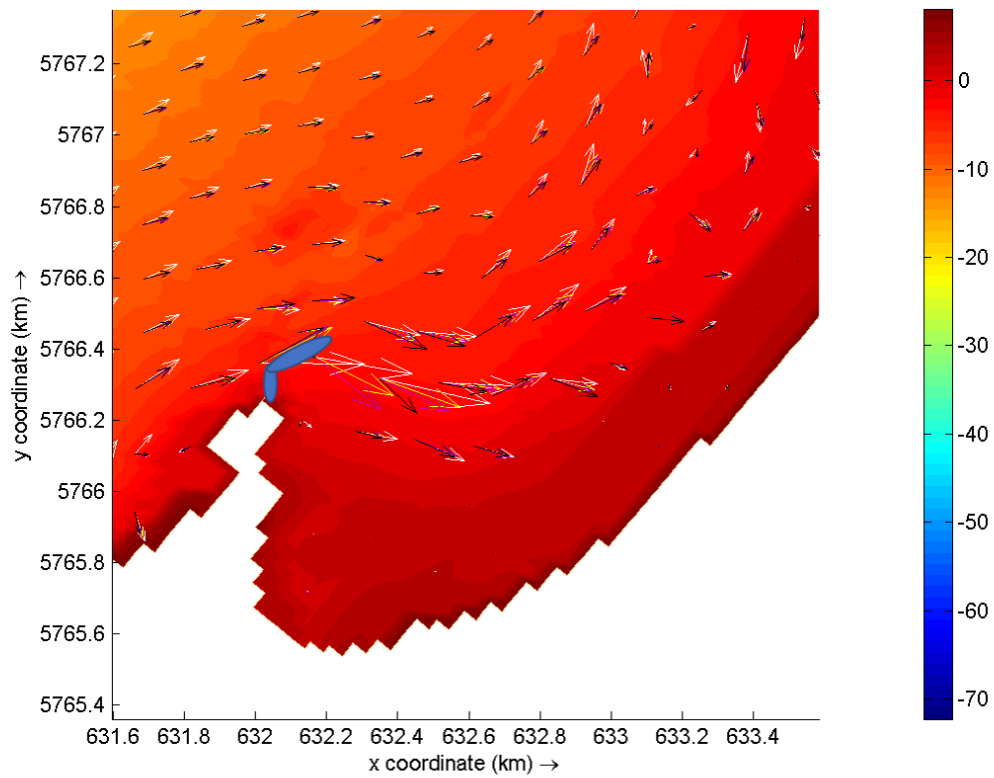


Figure E10: Currents due to waves which come from 315 degrees, for all lengths of breakwaters

In figures E11 until E14 the wave induced wave directions and wave heights are plotted for each breakwater length. The waves are coming from a direction of 315 degrees.

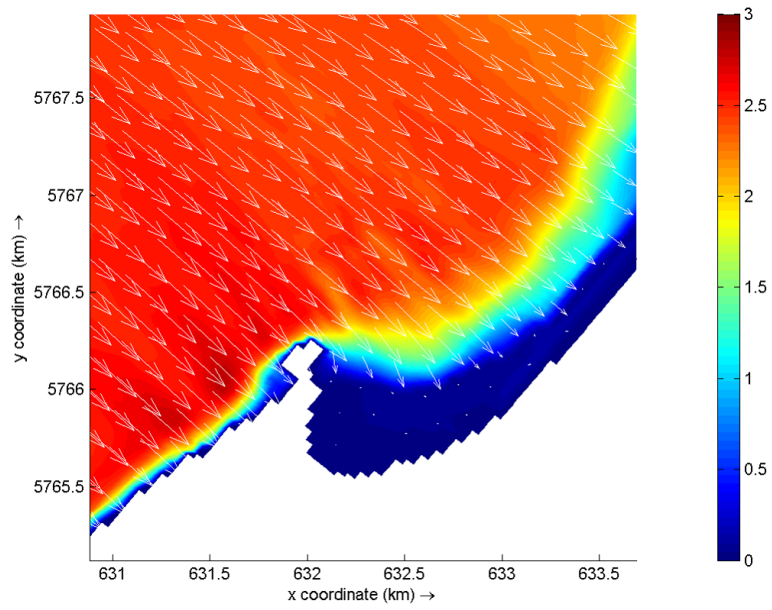


Figure E11: The wave directions without any breakwater

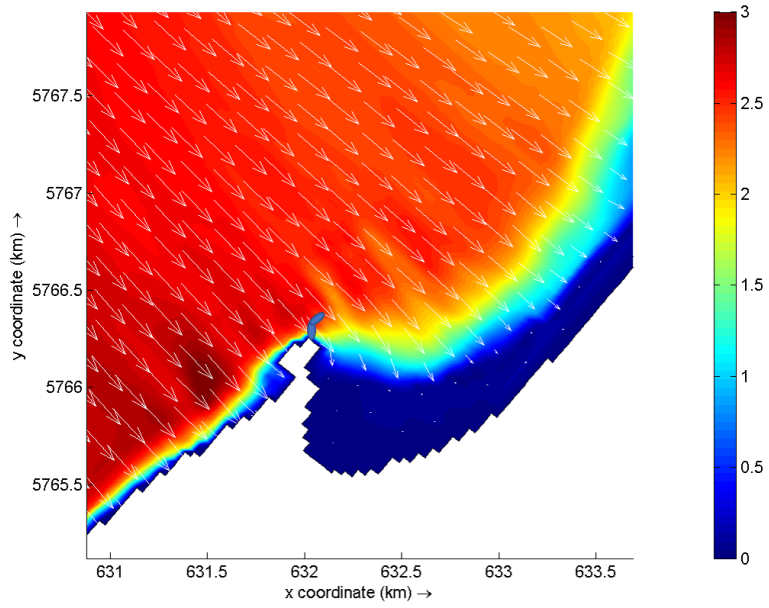


Figure F.12: The wave directions with the 50 m breakwater

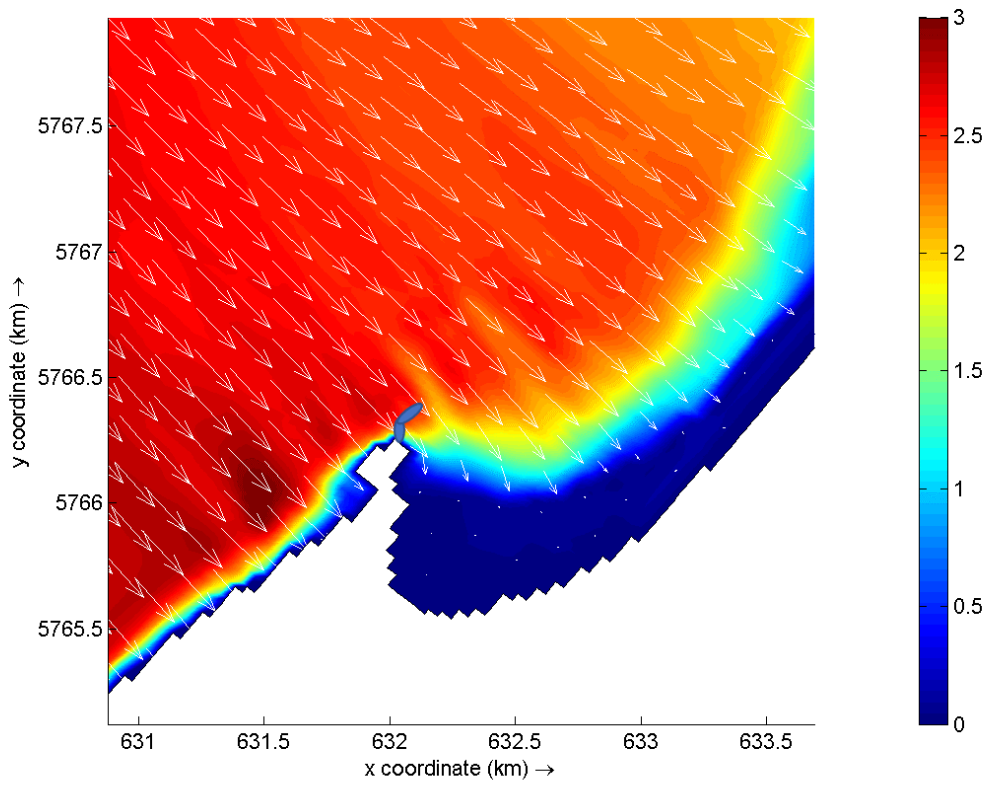


Figure F.13: The wave directions with the 100 m breakwater

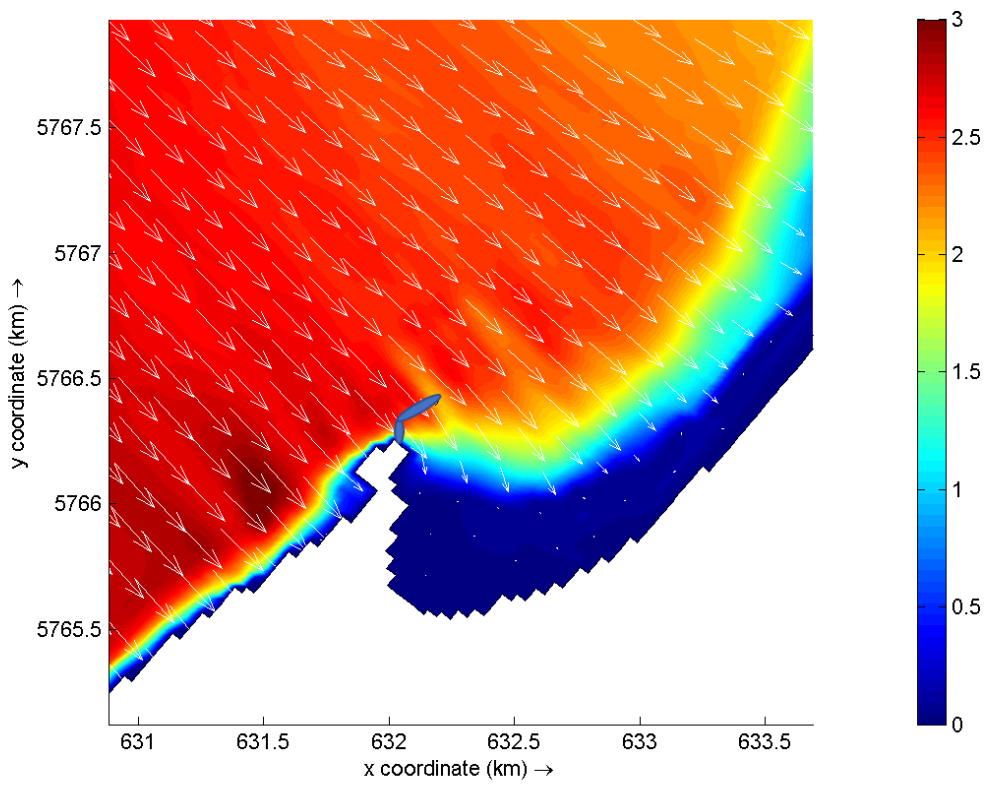


Figure E.14: The wave directions with the 150 m breakwater

# G. Sediments

In the following sections some basic theories about the sediment transport is given.

## G.1 Fall velocity

The fall velocity of particles can be estimated by using a force balance. In case of a single grain, this means that the gravitational force acts downwards, and the drag force is acting upwards. A single grain approach does not consider interaction between particles and the influence of other particles in the water column. For this approach, the water is assumed to be still. Assuming this, the fall velocity can be calculated with equation G.1 (Bosboom and Stive 2015).

$$w_s = 1.6 \times \sqrt{gD(s-1)} \quad (\text{G.1})$$

This equation comes from the force balance, by using a value of 0.5 for the drag coefficient. The drag coefficient is valid if the Reynolds number is between the 400 and 200,000. If there is hindered settling, equation reduces to equation G.2 (Bosboom and Stive 2015).

$$w_e = (1 - c)^\alpha \times w_s \quad (\text{G.2})$$

Whereby:

- D is the sand grain diameter
- s is the relative density
- g is the acceleration of gravity = 9.81 ( $m/s^2$ )
- $w_e$  is the effective fall velocity (m/s)
- $w_s$  is fall velocity of one grain in clear water (m/s)
- c is the sediment concentration (-), estimated to be 0.05.
- $\alpha$  is a coefficient (ranging from 2.3 to 4.6 (-)), estimated to be 3.

From this, it became clear that the hindred fall velocity in still water,  $w_e$  would be around 0.05 m/s, which is low. Therefore, sediment of this range will not settle too fast in the bay.

## G.2 Threshold of motion

Sediments resting at the bottom will start to move if the shear stress acting on the particle is larger than the threshold value. Again, all forces on the grain should be considered. These forces are the drag force and gravity force. The drag force can be divided into skin friction on the grain and pressure differences around the grain. Pressure differences are happening due to flow separation. Shields came up with a diagram for sediment movement (Schierck and Verhagen 2016). From this diagram, sediment movement can be interpreted, quite easily. However applying Shields is not always valid. Using Shields, it can be concluded that a very low velocity near the bottom is needed to bring the fine sediments in movement in Quidico Bay. The shields diagram is not valid if the bed is not flat and if the flow is not uniform. Also, all influences due to irregular patterns, like oscillatory flow and unidirectional flow, are not considered.

Through the fact that the bed is changing all the time, some particles may be closed in by larger particles. Keeping the small particles closed in between the larger particles is called bed armouring. This is mostly the

case in poorly graded beds. In Quidico Bay, the bed consists of poorly graded material. Bed armouring should be included in investigating the sediment movement.

The sediment transport can be categorized in three types of transport. The types of transport are depending on the type of flow and the stresses that will act on the particles. The considered types in Quidico are the bed load transport and suspended load transport. The third type is wash load transport. This consists of very fine particles, which will only settle if the water is completely still. The water is never completely still in the bay of Quidico, therefore wash load transport will not contribute to the total amount of sediment transport. The velocity profile, concentration and therefore the sediment transport can be schematized as in figure G.1. By multiplying the velocity and concentration profiles, the profile of the sediment transport can be obtained.

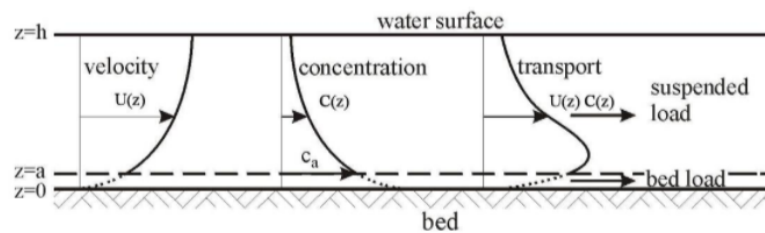


Figure G.1: Velocity, concentration and sediment transport profiles (Bosboom and Stive 2015)

The sediment movement in deep oceans can be assumed to be almost zero. In figure G.2 it is visible that the waves do not influence the bottom velocity and, therefore the waves cannot bring the sediment into movement.

If looking closer to shore. Waves will break at certain depths. Wave breaking creates lots of turbulence in the water column. This turbulence creates extra stresses, through these extra stresses the threshold is exceeded and, therefore more sediment is moving.

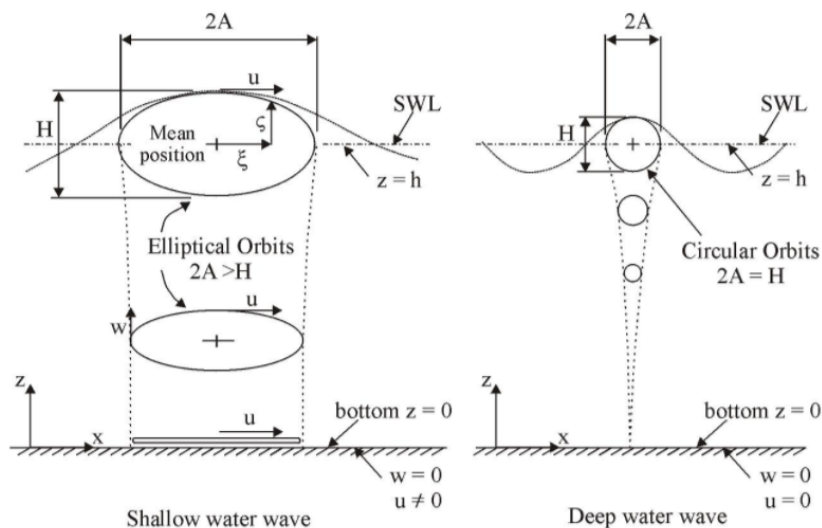


Figure G.2: Influence of waves on the bottom (Bosboom and Stive 2015)

## G.2.1 Evolution of the coastline in Quidico



(a) Coastal situation at 14-04-2004 (left) and 05-08-2004 (right)



(b) Coastal situation at 03-07-2011 (left) and 25-11-2011 (right)



(c) Coastal situation at 12-09-2013 (left) and 01-07-2015 (right)



(d) Coastal situation at 27-02-2016

Figure G.3: Evolution of the coast around the bay of Quidico obtained from Google Earth

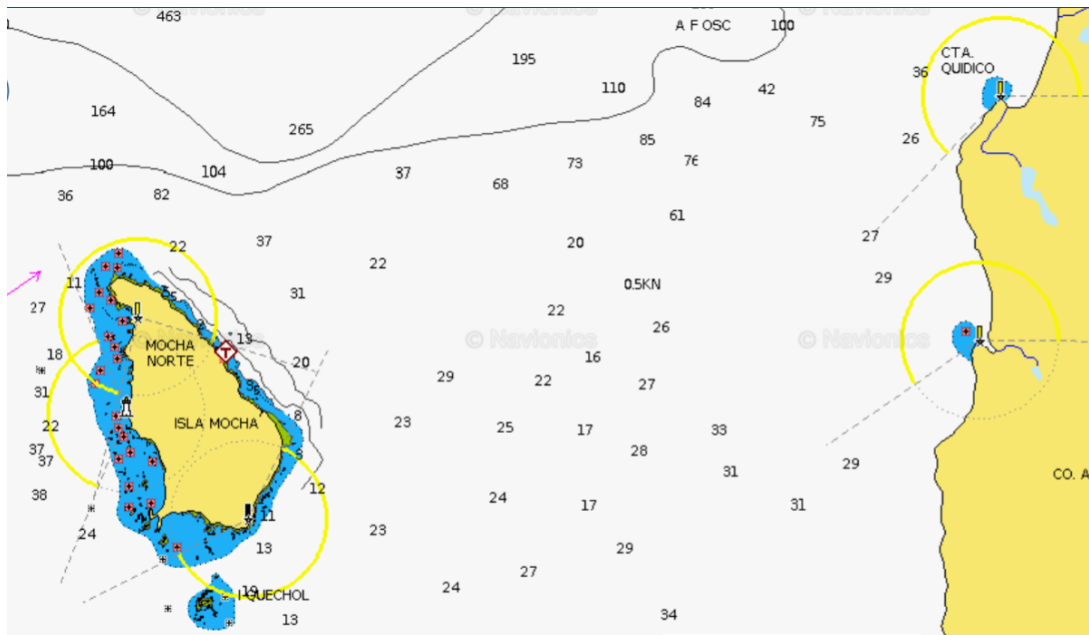


Figure G.4: Influence of the island on the water depths (Navionics 2017)

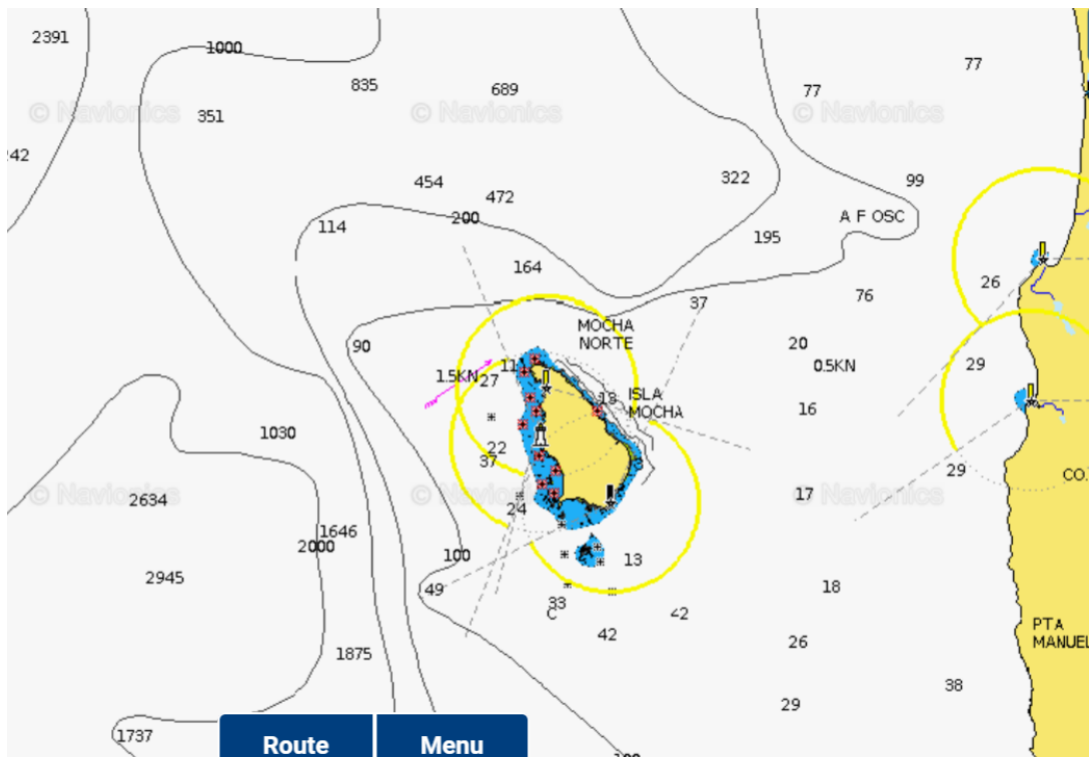


Figure G.5: Water depths in front of Quidico due to the island (Navionics 2017)

# H. Breakwater

## H.1 Breakwater design

First the outer layer of the breakwater is designed. This layer is the most important and must resist the highest wave forces. This layer is known as the armour layer of the breakwater. The standard transformation formulas of the Shore Protection Manual are used (CIRIA, CUR, and CETMEF 2007). With these transformation formulas the dimensions and weights of the core and filter layers can be calculated. After that, the stability of the breakwater and the stone size of the toe is calculated. Later on, the superstructure on top of the breakwater, known as the crown wall, is designed. Data about the waves, tides and water heights are used to design the breakwater. Also the overtopping criteria and run-up are taken into account. Finally, a cost indication of both breakwaters is given.

Later in this chapter the stability and settlement of the breakwater are analysed by using the model PLAXIS.

### H.1.1 Rock Stability

#### Breakwater

First, the used parameters for the rock stability calculations are given in table H.1.

Table H.1: List of used symbols

Definition	Symbol
Wave Height	$H_{m0}$
Wave Period	$T_p$
Depth NRS	$h_0$
Sea level	NM
Slope angle	$\tan \alpha$
Stability Coefficient	KD

With these parameters, the Hudson formula is used (see equation H.1).

$$\frac{H_s}{\Delta D_{n50}} = \frac{K_d \cdot \cot(\alpha)^{1/3}}{1.27} \quad (\text{H.1})$$

With the following numbers for the symbols:

- $H_s$  is the design wave height = 3.8 (m).
- $K_D$  is the stability coefficient, = 2.5 (-).
- $\rho_r$  is the density of the rock = 2650 (kg/m<sup>3</sup>).
- $\Delta$  is the relative density between stone and water = 1.65 (-).
- $\alpha$  slope angle of the breakwater = 26.6 (deg).

From equation H.1 the  $D_{n50}$  is the unknown parameter. The Hudson relation is in the current state dependent on the nominal diameter ( $D_{n50}$ ) of the armour stone. Equation H.1 is rewritten to equation H.2 to obtain the  $D_{n50}$ .

$$D_{n50} = \frac{H_s \cdot 1.27}{\Delta (K_d \cdot \alpha)^{1/3}} \quad (\text{H.2})$$

In table H.2 the final values for the armour layer are given. The stones for the armour layer will have a diameter of 1.35 meter.

Table H.2: Nominal diameter and weight for the armour layer

	Value	Unit
<b>D<sub>n50</sub></b>	1.35	m
<b>W<sub>n50</sub></b>	6.47	ton

The dimensions of the other breakwater layers are depended on the results of the armour layer. Table H.3 gives the specific factors for the other layers. The maximum and minimum weights are given as well.

Table H.3: Design rules to calculate the dimensions of the filter and core layer

	<b>W<sub>min</sub></b>	<b>W<sub>n50</sub></b>	<b>W<sub>max</sub></b>
<b>Armour layer</b>	$0.75 \times W_{n50}$	$W_{n50}$	$1.2 \times W_{n50}$
<b>Filter layer</b>	$0.07 \times W_{n50}$	$0.1 \times W_{n50}$	$0.13 \times W_{n50}$
<b>Core layer</b>	$0.0001 \times W_{n50}$	$0.005 \times W_{n50}$	$0.0075 \times W_{n50}$

For the the breakwater design a  $W_{n50}$ -value of 7 ton is chosen for the armour layer. Filling in that value in table H.3, the final weights for each layer are obtained. Those results are given in table H.4. Several filter rules exist to prevent sediment from flushing out. Applying these rules for the used armour stones, gives a breakwater of many layers. Therefore, a geotextile is recommended between the filter layer and core layer. Water is able to pass through this geotextile. Small sediments are blocked by the small gaps.

Table H.4: Stone sizes for all layers of the breakwater

	<b>W<sub>min</sub></b>	<b>W<sub>n50</sub></b>	<b>W<sub>max</sub></b>	<b>Unity</b>
<b>Armour layer</b>	5.25	7.0	8.4	ton
<b>Filter layer</b>	0.49	0.7	0.91	ton
<b>Core layer</b>	17.5	35	52.5	kg

### Contramolo

The same procedure as for the main breakwater is followed for the smaller breakwater (named contramolo). The same formulas are used to calculate the different stone weights for the different layers. All design values for the contramolo are given in table H.5.

Table H.5: Parameters to calculate the stone sizes of the contramolo

<b>Definition</b>	<b>Symbol</b>	<b>Magnitud</b>	<b>Unity</b>
Wave Height	$H_{m0}$	0.88	m
Wave Period	$T_p$	8	s
Objective depth NRS	$h_0$	1.5	m
Sea level	NM	1.98	m
Slope	$\alpha$	2:1	-
Stability Coefficient	KD	2.5	-

With the Hudson equation the values for the armour layer are obtained and given in table H.6. The needed stone diameter is set to 0.29 meter.

Table H.6: Stone size and weight for armour layer

<b>Definition</b>	<b>Symbol</b>	<b>Magnitud</b>	<b>Unity</b>
Armour's Nominal Diameter	$D_{n50}$	0.29	m
Armour's Nominal Weight	$W_{n50}$	0.065	ton

Table H.7 gives the stone weights for the filter and core layer. Those values depends on the weights of the armour layer. The maximum and minimum values for the filter and core layer are specified as well. To obtain these values table H.3 is used.

Table H.7: Stone sizes for the contramololo

Layer	$W_{min}$	$W_{n50}$	$W_{max}$	Unity
Armour	562.50	750.00	900.00	kg
Filter	52.50	75.00	97.50	kg
Core	18.75	37.50	56.25	kg

### H.1.2 Toe Stability

The stone sizes of the armour layer are known. The next step for the breakwater design is to calculate the toe stability. The given parameters from table H.8 are used to determine the toe design.

Table H.8: Parameters used for calculating the toe

Definition	Unit
Wave Height	m
Wave Period	s
Objective depth NRS	m
Sea level	m
Slope	2:1
Depth over the toe	m
Significant Height	m

The rock manual is used to calculate the stability for the toe (CIRIA, CUR, and CETMEF 2007). Equation H.3 is used to calculate this stability. In figure H.1 this equation is plotted. The curve visible in figure H.1 is not completely satisfactory. The equation is based on experiments with depth limited conditions. And the possible influences from the wave period or wave steepness has not been investigated.

$$\frac{H_s}{\Delta D_{n50}} = 8.7 \left( \frac{h_t}{h_m} \right)^{1.4} \quad (H.3)$$

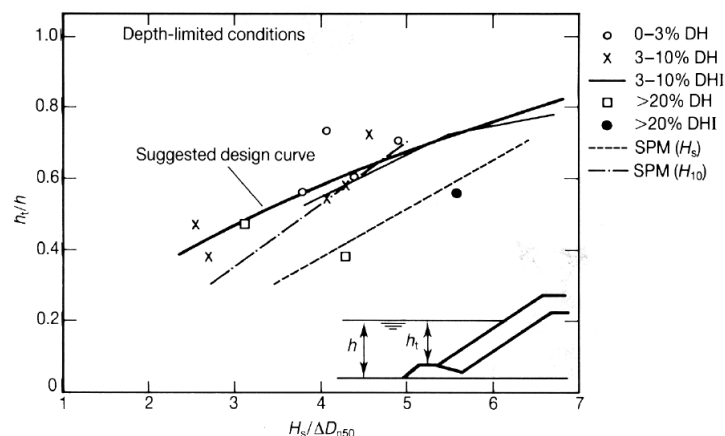


figure 5.73 Toe stability as a function of the relative toe depth,  $h_t/h$

Figure H.1: Toe stability formula

The stability of the toe is also checked with the van der Meer equation (CIRIA, CUR, and CETMEF 2007). This equation is mainly used in The Netherlands for breakwater designs. In Chile it is more common to use the

Hudson equation for the toe stability. Therefore the calculations of van der Meer are not presented in this report. The Hudson equation is chosen to be guiding. The design values of table H.9 are used to derive the dimensions of the toe.

Table H.9: Values used for the toe

Definition	Values	Unit
Wave Height	3.8	m
Wave Period	17.3	s
Objective depth NRS	2	m
Sea level	1.98	m
Slope	2:1	-
Depth over the toe	1.98	m
Significant height	2.46	m

After these calculations it is concluded that the minimum required diameter for the toe is 0.7m. The corresponding weight is given in table H.10.

Table H.10: Dimensions of the toe

Definition	Values	Unit
Minimum required diameter	0.7	m
Minimum required weight	1	ton

The minimum weight for the rocks of the toe is calculated to be around 1 ton. After discussion with the DoP, this value is set to the same value as the armour layer. This is due to practical reasons. Using the same value for the toe as for the armour layers will make the construction easier. This is done quite often in Chile.

### H.1.3 Crown-Wall stability

The next element is the crown-wall. This element reduces the amount of overtopping over the breakwater. The design parameters for the crown wall stability are given in table H.11.

Table H.11: Crown wall stability parameters

Data Entry	Symbol	Data 1	Data 2	Unity
Wave height	$H_{m0}$	3.8	3.8	m
Wave period	$T_m$	17.3	17.3	s
Objective depth NRS	$h_0$	2.2	2.2	m
Sea level	NM	1.98	1.98	m
Slope	m	0.016	0.016	-
Incidence angle	b	15	5	deg

Two different geometries of the crown-wall are determined. The general geometry is given in figure H.2. This should be the general layout of a crown-wall. All the lengths are indicated with a certain symbol. The two chosen geometries are given in figure H.3.

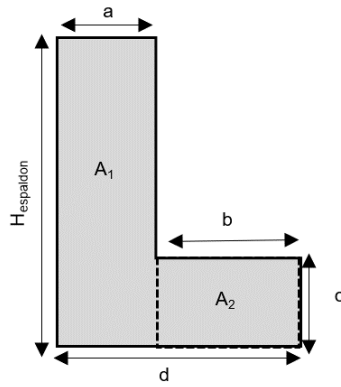


Figure H.2: General crown wall geometry



Figure H.3: Two different crown wall geometries

The characteristics of both crown-walls is given in table H.12.

Table H.12: Geometry for the crown wall

Data Entry	Calculated value	Data 1	Data 2
Crown wall height	$H_{\text{espaldon}}$	4.00 (m)	2.50 (m)
Crown wall width	a	1.00 (m)	0.50 (m)
Base width	d	3.00 (m)	3.00 (m)
Base height	c	2.50 (m)	2.00 (m)
Foundation level	CSF	2.00 (m)	2.00 (m)
Crown wall level	CB	5.00 (m)	5.00 (m)

To decide which layout is guiding for our design, the wave impact is determined. The wave impact is calculated with the Iribarren number. Using this number, the impact and wave run-up can be evaluated. With equation H.4 the Iribarren number is used.

$$I_{r0} = \frac{\tan \beta}{\sqrt{\frac{H_0}{L_0}}} \quad (\text{H.4})$$

The values for this equation are given in table H.13.

Table H.13: Values used to fill in the Iribarren formula

Parameter	Value
$\beta$	26.56 (deg)
$H_0$	6.0 (m)
$L_0$	624 (m)

Using this numbers, the Iribarren number is determined to be 4.4. This means that the type of waves are between a surging or collapsing type. To calculate the force on the crown-wall the run-up is necessary as well. The run-up is calculated with equation H.5.

$$Y = \frac{(R_u - A_c) \cdot \sin(\beta)}{\sin(\arctan(0.5)) \cdot \cos(\arctan(0.5 - \beta))} \quad (\text{H.5})$$

The values for equation H.5 are given in table H.14.

Table H.14: Calculated values for the run-up and crown-wall heights

<b>Freeboard crown wall</b>	$A_c$	3.02	3.02
<b>Height till shoulder</b>	S	3	3
<b>Iribarren number</b>	$\xi$	5.1	5.1
<b>Expected run-up</b>	$R_u$	4.9	4.9
<b>Run-up</b>	Y	1.11	0.39

In the following calculations a different wave attack is used for both geometric designs. From figure H.3 it is visible that the left geometry is thicker and higher. The wave on this geometry is approaching the breakwater in a perpendicular direction. This gives a higher wave attack. The wave coming at the right geometry is approaching with an angle of 15 degrees (seen from the a perpendicular approach). This induces lower wave forces. If the right figure can hold this forces, the left figure can have those forces as well.

Using the values of table H.14, the hydrodynamic forces acting on the crown-wall are calculated with equation H.6.

$$\begin{aligned}
 P_m &= \frac{1025Y}{2} \\
 P_h &= 1025Y + S \\
 P_s &= P_h + \frac{P_m}{2}
 \end{aligned} \quad (\text{H.6})$$

Equation H.6 uses the following parameters:

- With  $P_m$  the dynamic pressure
- with  $P_h$  the hydrostatic pressure
- with  $P_s$  Total pressure acting

Filling in of those parameters gives the results stated in table H.15.

Table H.15: Pressures

<b>Dynamic pressure</b>	$P_m$	5.6	2.0	kPa
<b>Hydrostatic pressure</b>	$P_h$	41.3	34.1	kPa
<b>Sub pressure</b>	$P_s$	44.1	36.0	kPa

The next step is to check the stability of the crown-wall. For this, the dead weight of the concrete is necessary. The dead weight is determined by the volume times the density. This is given in table H.16.

Table H.16: Areas and their corresponding weight of the crown wall

Definition	Symbol	Max	Min	Unit
Area 1	A1	4	1.25	m
Area 2	A2	5	5	m <sup>2</sup>
Weight area 1	W1	10000	3125	kg/m
Weight area 2	W2	12500	12500	kg/m

A common value for the density of concrete is a value between the 2400 and 2600 kg/m<sup>3</sup>. For this design a value is used of 2500 kg/m<sup>3</sup>.

Safety factors are used as stated in the Rock Manual (CIRIA, CUR, and CETMEF 2007). These values are given in table H.17.

Table H.17: Safety coefficients used for the crown wall

Safety factor for sliding	CSD	1.2
Safety factor for overturning	CSV	1.2
Friction coefficient	$\mu$	0.7

All forces acting on the crown wall are given in equation H.7. All the equations come from the Protection Manual volume 2.

$$\begin{aligned}
 F_v &= 0.5 \cdot P_s \\
 N &= W_1 + W_2 - F_v \\
 F_r &= N \cdot \mu \\
 F_h &= 0.5 \cdot P_h(Y + S) \\
 F_1 &= P_h(S - H_{\text{espaldon}}) \\
 F_2 &= 0.5 \cdot P_m \cdot 0.5 \cdot S \\
 F_3 &= 0.5 \cdot P_m \cdot S
 \end{aligned}
 \tag{H.7}$$

All symbols used in equation H.7 are explained in table H.18.

Table H.18: Explanation of the forces and their calculated values

Name	Abbreviation	Data 1	Data 2	Unity
Hydrodynamic force	$F_v$	66.1	52.6	kN
Normal force	N	154.4	100.5	kN
Friction force	$F_r$	108.1	70.4	kN
Hydrostatic force	$F_h$	84.8	57.8	kN
Dynamic force 1	$F_1$	5.6	-1.0	kN
Dynamic force 2	$F_2$	4.2	1.5	kN
Dynamic force 3	$F_3$	8.4	3.0	kN

Using table H.18 and equation H.7, the sliding force can be calculated. The total force included for sliding is the sum of the three dynamic forces. A unity check will be done, by dividing the sliding force by the resistant force. All forces are stated in table H.19.

Table H.19: Unity check for sliding of the Crown Wall

	Abbreviation	Data 1	Data 2	Unity
Sliding force	SF	18.1	3.46	kN
Resistant force	RF	108	70.4	kN
Sliding coefficient	UC	5.97	20.4	-

From table H.17, it can be seen that the unity check should be larger than 1.2. From table H.19 it can be observed that all unity checks are higher than 1.2, and therefore quantified as stable.

In the following part, the overturning moment of the crown-wall is checked. All moments acting on the crown wall will be considered. All equations stated in H.8 are used. Calculated values and abbreviations of these moments are stated in table H.20.

$$\begin{aligned}
 M_{w1} &= 0.5 \cdot W_1 \cdot a \\
 M_{w2} &= W_2(d + 0.5(a - d)) \\
 M_{Fv} &= \frac{1}{3} \cdot F_v \cdot d \\
 M_{Fh} &= \frac{1}{3} \cdot F_h \cdot (Y + S) \\
 M_{F1} &= F_h \cdot (S + 0.5(H_{espaldon} - S)) \\
 M_{F2} &= \frac{2}{3} \cdot F_2 \cdot S \\
 M_{F3} &= \frac{1}{2} \cdot F_3 \cdot S
 \end{aligned}
 \tag{H.8}$$

Table H.20: Moments acting on the crown wall to calculate the overturning moment

Name	Abbreviation	Data 1	Data 2	Unity
Moment of area 1	$M_{W1}$	49.0	7.66	kNm
Moment of area 2	$M_{W2}$	245	214	kNm
Moment due to hydrodynamic lift	$M_{Fv}$	66.1	52.6	kNm
Moment due to hydrostatic force	$M_{Fh}$	116	65.4	kNm
Dynamic moment part 1	$M_{F1}$	19.5	-2.72	kNm
Dynamic moment part 2	$M_{F2}$	8.35	2.96	kNm
Dynamic moment part 3	$M_{F3}$	12.5	4.44	kNm

For the overturning moment a unity check is done as well. The moments given in table H.20 are added up depending on their direction as stated in table H.21. All unity checks are again higher than 1.2, and therefore the overturning moment is stable for the crown-wall.

Table H.21: Unity check for the overturning moment

	Symbol	Data 1	Data 2	Unity
Resistant moment	$M_r$	294	222	kNm/m
Overturning Moment	$M_v$	223	123	kNm/m
Unity check	$U_c$	1.32	1.81	kNm/m

Looking at the prior results of both crown-walls, it is decided to use the left geometry of figure H.3. The left geometry can hold the forces of the larger wave attacks. Therefore, the left design is quiding for the crown-wall design.

### H.1.4 Overtopping

In this section, the overtopping limit of the crown wall is checked. In table H.22 all the necessary parameters are described.

Table H.22: Overtopping values used

Definition	Symbol	All Swell	Unity
Mean wave height	$H_m$	2.46	m
Maximum height	$H_{max}$	3.9	m
Wave period	$T_p$	17.3	s
Objective depth NRS	$h_0$	3.57	m
Sea level	NM	1.98	m
Crown wall height	CE	6.5	m
Shoulder width	G	2	m
Admissible flow	$Q_{adm}$	20	l/s/m

With the given parameters of table H.22, the height of the crown wall is checked. This height should be high enough to meet the overtopping requirement. The values stated in table H.23 are used for equation H.9.

$$Q = g \cdot H_{max} \cdot T_p \cdot a \cdot \left( \frac{R_c}{H_s} \right)^2 \cdot \left( \sqrt{\frac{S_{oms}}{2\pi}} \right)^b \quad (H.9)$$

Table H.23: Values used to calculate the overtopping limits

<b>Free board</b>	$R_c$	4.52	m
<b>Significant swell</b>	$S_{oms}$	0.01	m
<b>Maximum swell height</b>	$S_{om}$	0.01	m
<b>Coefficient 1</b>	a	1.60E-09	-
<b>Coefficient 2</b>	b	3.2	-

The results of equation H.9 are shown in table H.24.

Table H.24: Overtopping results

Overtopping determination	Abbreviation	Swell	Unity
Mean flow	q	1.5E-03	l/s/m
Maximum flow	q	1.64E-02	l/s/m

Looking at the results of table H.24, it can be concluded that the amount of overtopping will not exceed the overtopping limit of 20 l/s/m. Therefore, the chosen design of the crown wall will be fine.

### H.1.5 Summary breakwater

In this section all prior calculations for the breakwater design are summarised. In figure H.4 the total design of the breakwater is given. The layer thicknesses and stone sizes are indicated in this figure.

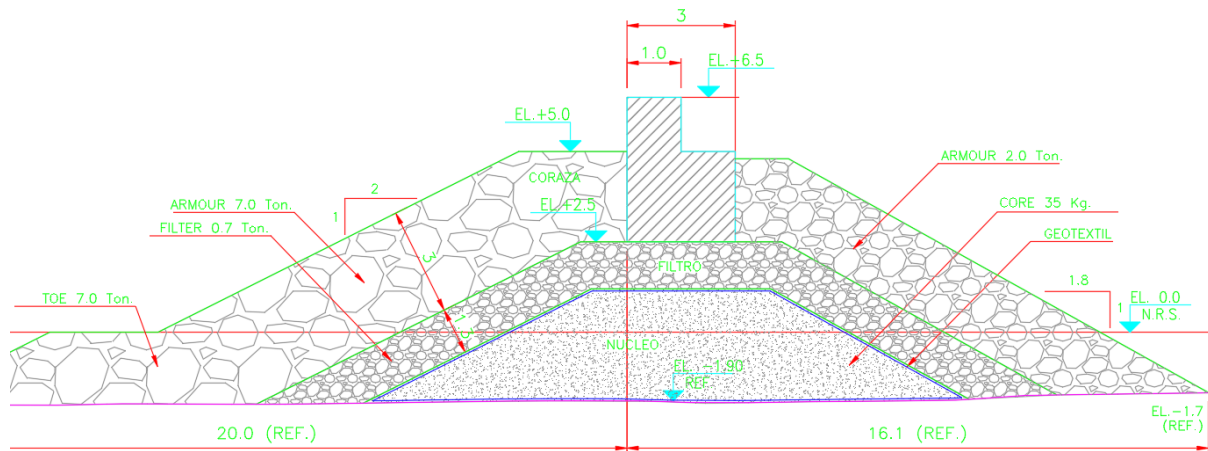


Figure H.4: Total design of the breakwater including toe and crown wall

Table H.25 gives a summary about the used stone classes for both the main breakwater as the contramolo.

Table H.25: Summary of the used stone sizes

Summary of $W_{n50}$	Molo		Contramolo	
Armour, sea side	7.00	ton	750.00	kg
Filter	0.70	ton	75.00	kg
Core	35.00	kg	37.50	kg
Toe	7.00	ton	750.00	kg
Armour, bay side	2.00	ton		

Figure H.5 gives the crown-wall on top of the breakwater. This crown-wall is partly included in the armour layer. This is visible in figure H.4.

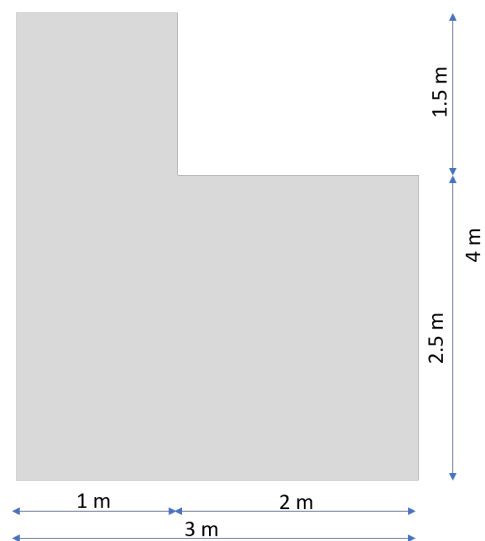


Figure H.5: Chosen dimensions for the Crown Wall

### H.1.6 Cost estimation

After the total breakwater design is finished, a cost estimation can be made. The Department of Ports provided a sheet to quickly calculate the costs of both breakwaters. Figure H.6 shows all considered costs. Within this figure a distinction is made between the main breakwater and the contramololo. The given costs are an estimation and, for example, due to problems during installation or other factors costs may deviate from the estimated numbers.

<b>1</b>	<b>Maritime Works</b>					
<b>1.1</b>	<b>Breakwater</b>	<b>Unit</b>	<b>Quantity</b>	<b>Unit price</b>	<b>Total per unit</b>	
1.1.1	Supply and instalation of the armour rock 4500 to 8000 Kg	m <sup>3</sup>	10648	\$ 100.000	1.064.820.680	\$
1.1.2	Supply and instalation of the filter rock 450 to 800 Kg	m <sup>3</sup>	5896	\$ 70.000	\$ 412.687.310	
1.1.3	Supply and instalation of the core rock 40 Kg	m <sup>3</sup>	7252	\$ 50.000	\$ 362.580.610	
1.1.4	Supply and instalation of the core rock 2.0 Ton	m <sup>3</sup>	5606	\$ 80.000	\$ 448.444.304	
1.1.5	Reinforced concrete blocks H-30	m <sup>3</sup>	2079	\$ 400.000	\$ 831.558.000	
1.1.6	Supply and instalation of the geotextile	m <sup>2</sup>	7279	\$ 7.000	\$ 50.955.316	
<b>1.2</b>	<b>Contramololo</b>					
1.2.1	Supply and instalation of the armour rock 750 Kg	m <sup>3</sup>	4877	\$ 70.000	\$ 341.423.320	
1.2.2	Supply and instalation of the filter rock 75 Kg	m <sup>3</sup>	1042	\$ 60.000	\$ 62.542.950	
1.2.3	Supply and instalation of the core rock 40 Kg	m <sup>3</sup>	3882	\$ 50.000	\$ 194.119.055	
1.2.4	Supply and instalation of the geotextile	m <sup>2</sup>	3151	\$ 7.000	\$ 22.054.995	
					Total CLP	\$ 3.791.186.539
					Total USD	\$ 6.215.060

Figure H.6: Costs for the Breakwater and contramololo

## H.2 Geo-technical analysis PLAXIS

The geo-technical calculations for the breakwater design are performed using the 2D finite element software PLAXIS. The following steps are followed to generate the PLAXIS model:

### 1. General settings

The first task in creating the PLAXIS model is defining the model dimensions. For the sheet pile wall the following dimensions are used:  $x_{\min} = -40.0$ ,  $x_{\max} = 40.0$ ,  $y_{\min} = -10.0$  and  $y_{\max} = 10.0$ .

### 2. Soil stratigraphy

Within the defined model dimensions, as defined above, the soil stratigraphy can be created. This is done by creating different boreholes along the x-axis. Soil layers are created on specific depths, the soil properties and water table are defined accordingly. In this specific case the subsurface consists of sand. The properties of the different types of sand are specified in table H.26.

A low water table (i.e. 2 m water depth) is used to calculate the upper and lower settlement limit.

Table H.26: Geo-technical properties of different types of sand.

	Soft sand	Quidico Bay sand (as from figure 4.2)	Strong sand
<b>Material model (-)</b>	Hardening soil	Hardening soil	Hardening soil
<b>Drainage type (-)</b>	Drained	Drained	Drained
<b><math>y_{\text{unsat}}</math> (kN/m<sup>3</sup>)</b>	1850	1850	1850
<b><math>y_{\text{sat}}</math> (kN/m<sup>3</sup>)</b>	2000	2000	2100
<b><math>E_{50}</math> (kN/m<sup>2</sup>)</b>	25000	42000	42000
<b><math>E_{\text{oed}}</math> (kN/m<sup>2</sup>)</b>	25000	42000	42000
<b><math>E_{\text{ur}}</math> (kN/m<sup>2</sup>)</b>	75000	120000	126000
<b><math>c_{\text{ref}}</math> (kN/m<sup>2</sup>)</b>	0	10	10
<b><math>\phi</math> (°)</b>	32	36	40
<b><math>\psi</math> (°)</b>	1	6	10
<b>Groundwater data set (-)</b>	Standard	Standard	Standard
<b>Groundwater soil type (-)</b>	Coarse	Coarse	Coarse

### 3. Structural elements

Next step in defining the PLAXIS model is adding the structural elements to the soil stratigraphy, also the loads are specified in this phase. The structure of the different layers of the breakwater are implemented in this phase. The design is taken from section 5.8.

The breakwater structure is as shown in figure H.7. The geo-technical properties of the core, filter and armour are based on several papers ((Cihan, Yuksel, et al. 2012) and (Cihan and Yuksel 2013)) and are shown in table H.27. For the settlement calculations especially the weight of the breakwater is of importance. These weights are based upon the individual weight of the layer-rocks, as defined in section 5.8.

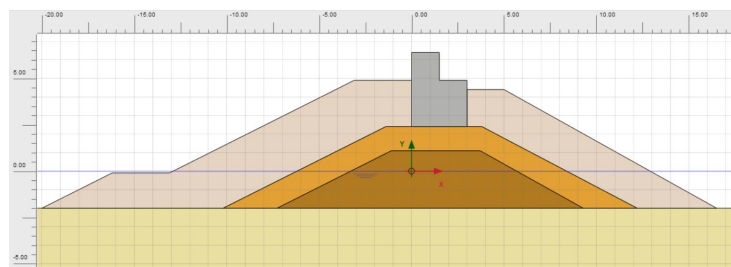


Figure H.7: PLAXIS model of the breakwater.

### 4. Mesh generation

Within the "Mesh mode" the geometry model is discretized and transformed to a finite element model.

Table H.27: Geo-technical properties of the core, filter and armour.

	<b>Core</b>	<b>Filter</b>	<b>Armour</b>
<b>Material model (-)</b>	Hardening soil	Hardening soil	Hardening soil
<b>Drainage type (-)</b>	Drained	Drained	Drained
<b><math>\gamma_{unsat}</math> (kN/m<sup>3</sup>)</b>	20	20	26
<b><math>\gamma_{sat}</math> (kN/m<sup>3</sup>)</b>	21	21	26
<b><math>E_{50}</math> (kN/m<sup>2</sup>)</b>	70000	110000	110000
<b><math>E_{oed}</math> (kN/m<sup>2</sup>)</b>	70000	110000	110000
<b><math>E_{ur}</math> (kN/m<sup>2</sup>)</b>	150000	230000	230000
<b><math>c_{ref}</math> (kN/m<sup>2</sup>)</b>	0	0	0
<b><math>\phi</math> (°)</b>	45	50	45
<b><math>\psi</math> (°)</b>	5	10	5
<b><math>K_0</math> (-)</b>	0.35	0.35	0.35
<b>Groundwater data set (-)</b>	Standard	Standard	Standard
<b>Groundwater soil type (-)</b>	Coarse	Coarse	Coarse

For this particular case a "Fine mesh" is chosen. 15-Node triangular elements are used within the model, this is specified in the "Project properties".

#### 5. Calculations

Two types of calculations are performed using PLAXIS. These include the upper and lower settlement limit and the overall stability of the breakwater.

For the settlement limits two models are generated, one model containing the geo-technical properties of the soft sand and one model of the strong sand. As defined at item *Soil stratigraphy* the water table is assumed to be at low-tide level. For this type of calculation only gravity loading is applied to the breakwater.

Also for the overall stability calculation low tide and only gravity loading are assumed.

#### 6. Results

The results of the settlement (1) and overall stability (2) calculations are presented below.

##### 1 - Settlement

The upper limit of the breakwater settlement is shown in figure H.8, the estimated maximum settlement is 0.32 m.

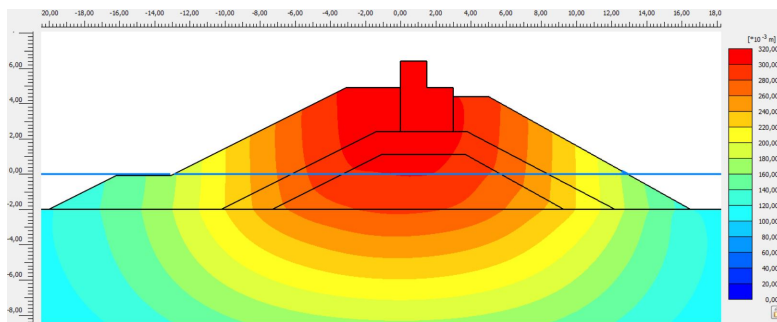


Figure H.8: Upper settlement limit PLAXIS model.

The lower limit of the breakwater settlement is shown in figure H.9, the estimated minimum settlement is 0.18 m.

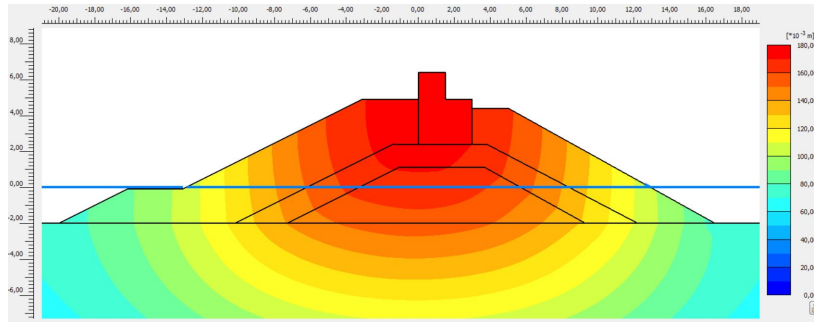


Figure H.9: Lower settlement limit PLAXIS model.

## 2 - Overall stability

The overall stability of the breakwater using the soft sand conditions is sufficient, the governing failure mechanism is shown in figure H.10a. Since the slope angle of the breakwater is the largest at the inside, the failure mechanism occurs at this side first. The failure mechanism occurs in the breakwater structure itself, the sliding circle does not cross the subsurface. From this observation it can be concluded the soft sand has sufficient strength for the construction of the breakwater. The governing failure mechanism depends on the correct design of the breakwater itself.

The factor of safety is calculated by reducing the shear strength parameters ( $\phi$  and  $c$ ) until failure of the structure occurs. The factor of safety, in PLAXIS expressed as  $\sum Msf$ , is calculated as the input strength divided by the reduced strength. From the graph in figure H.10b it can be seen that the factor of safety for the governing failure mechanism is approximately 1.50.

The overall stability of the breakwater using the strong sand conditions is sufficient as well. Again the governing failure mechanism is at the inside of the breakwater, as shown in figure H.11a. From the graph in figure H.11b it can be seen that the factor of safety for the governing failure mechanism is approximately 1.75. This factor of safety is higher than for the model using soft sand.

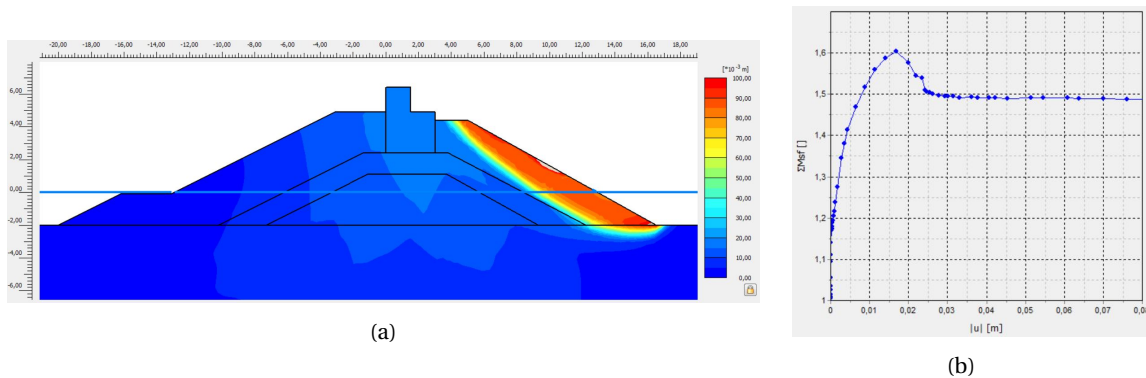
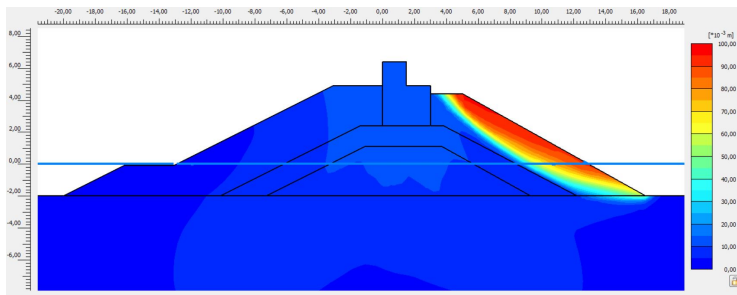
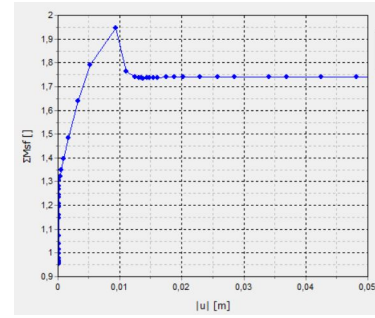


Figure H.10: (a) Governing failure mechanism and (b) factor of safety calculation for the breakwater using the soft sand conditions.



(a)



(b)

Figure H.11: (a) Governing failure mechanism and (b) factor of safety calculation for the breakwater using the strong sand conditions.

# I. Mooring Facility

The calculations for the sheet pile wall variant for the mooring facility are performed using the 2D finite element software PLAXIS. The following steps are followed for the PLAXIS input:

## 1. General settings

The first task to create the PLAXIS model is to define the model dimensions. For the sheet pile wall the following dimensions are used:  $x_{\min} = -30.0$ ,  $x_{\max} = 30.0$ ,  $y_{\min} = -15.0$  and  $y_{\max} = 10.0$ .

## 2. Soil stratigraphy

Within the defined model dimensions, as defined above, the soil stratigraphy can be created. This is done by creating different boreholes along the x-axis. Soil layers are created on specific depths, the soil properties and water table are defined accordingly. In this specific case the subsurface mainly consists of sand, to create the extra required pavement area within the harbour crushed gravel is used as backfill. The properties of the different soil types are specified in table I.1.

Table I.1: Soil properties for definition of the soil stratigraphy at the mooring facility.

	<b>Pavement</b>	<b>Foundation</b>	<b>Crushed gravel</b>	<b>Sand</b>
<b>Material model (-)</b>	Linear elastic	Mohr-Coulomb	Mohr-Coulomb	Mohr-Coulomb
<b>Type of material behaviour (-)</b>	Non-porous	Drained	Drained	Drained
<b><math>y_{\text{unsat}}</math> (kN/m<sup>3</sup>)</b>	20	20	19.5	18.5
<b><math>y_{\text{sat}}</math> (kN/m<sup>3</sup>)</b>	20	22	20.0	20.0
<b><math>e_{\text{int}}</math> (-)</b>	-	0.5	0.5	0.5
<b>E (kN/m<sup>2</sup>)</b>	$340 \cdot 10^3$	$100 \cdot 10^3$	$50.0 \cdot 10^3$	$42.0 \cdot 10^3$
<b><math>\nu</math> (-)</b>	0.30	0.30	0.35	0.30
<b>G (kN/m<sup>2</sup>)</b>	$130.8 \cdot 10^3$	$37.0 \cdot 10^3$	$18.5 \cdot 10^3$	$16.2 \cdot 10^3$
<b><math>E_{\text{oed}}</math> (kN/m<sup>2</sup>)</b>	$457.7 \cdot 10^3$	$160.5 \cdot 10^3$	$80.3 \cdot 10^3$	$56.5 \cdot 10^3$
<b><math>c'_{\text{ref}}</math> (kN/m<sup>2</sup>)</b>	-	10	10	10
<b><math>\phi</math> (°)</b>	-	40	40	36
<b><math>\psi</math> (°)</b>	-	10	10	6

## 3. Structural elements

Next step in defining the PLAXIS model is to add the structural elements to the soil stratigraphy, also the loads are specified in this phase. The two main elements for the sheet pile wall include the sheet pile wall itself and the anchor.

The sheet pile wall is modelled as a plate passing through (0.0 5.0) - (0.0 -5.0). The anchor is added as a fixed-end anchor, the 'Equivalent length' of the anchor is set to a safe value of 12.0 m (considering the active and passive wedges of the construction). The material of the sheet pile wall and the anchor are specified in the 'Material' function, the properties are shown in table I.2.

Table I.2: Material properties of the sheet pile wall and the anchor.

<b>Sheet pile wall</b>	
Material type (-)	Elastic
EA <sub>1</sub> (kN/m)	2.9*10 <sup>6</sup>
EI (kNm <sup>2</sup> /m)	56.3*10 <sup>3</sup>
w (kN/m/m)	1.1
v (-)	0.15
<b>Anchor</b>	
Material type (-)	Elastic
EA (kN)	500*10 <sup>3</sup>
L <sub>spacing</sub> (m)	3.0

Subsequently the loads are defined and assigned to a position at the soil stratigraphy or the structural elements. Two loads work on the sheet pile wall: a distributed line load induced by the presence of trucks (1) and a distributed line load induced by an earthquake (2).

(1) The load induced by the presence of a truck has a value of 6 kN/m<sup>2</sup> and works on the line which starts at (-2.0 5.0) and ends at (0.0 5.0).

(2) The load induced by an earthquake is defined as 20% of the weight of the sliding wedge. Using the internal friction angle and unsaturated/saturated weight of sand and crushed gravel (as defined in table I.1) this load is calculated. Since the earthquake load is based on a rule-of-thumb a conservative approach is used. The earthquake force is calculated under the assumption of low tide and the friction angle of sand, both assumptions lead to the largest sliding wedge and thus to the highest possible load. The calculations performed include:

$$W_{\text{wedge}} = 20 * (0.5 * 10 * (\text{TAN}(27) * 7)) = 510 \text{ kN/m}$$

$$W_{\text{wedge}, 20\%} = 0.2 * 510 = 102 \text{ kN/m}$$

$$q_{\text{wedge}}(y) = 2.04 * y + 10.2 \text{ for } -5 \leq y \leq 5$$

The final values for the distributed line load are:

$$q_{\text{wedge}}(-5) = 0 \text{ kN/m}^2 \text{ and } q_{\text{wedge}}(5) = 20.4 \text{ kN/m}^2$$

#### 4. Mesh generation

Within the "Mesh mode" the geometry model is discretized and transformed to a finite element model. For this particular case a "Fine mesh" is chosen. 15-Node triangular elements are used within the model, this is specified in the "Project properties".

#### 5. Calculations

The calculation of this project consists of three phases. The initial phase (Phase 0) is used to generate the initial stresses. In Phase 1 the sheet pile wall is added and the granular backfill (crushed gravel) up till the position of the anchor is added. In Phase 2, the final stage, the anchor is added to the construction, the final layer of granular backfill is added, the pavement structure is positioned on top of the backfill and the sand which is planned to be excavated is removed.

The forces and stresses in Phase 2 are of interest, since this will be the final design situation. However it is of importance that during construction the sheet pile wall has sufficient capacity, this is checked during Phase 1.

#### 6. Results

The two governing stages in the construction procedure are Phase 1 and Phase 2, as described above. The results for both phases are shown below.

### 1 - Construction stage

The governing situation in the construction stage is shown in the figure I.1, the backfill is deposited up to the height of the anchor position. The maximum bending moment and maximum shear force are shown in table I.3.

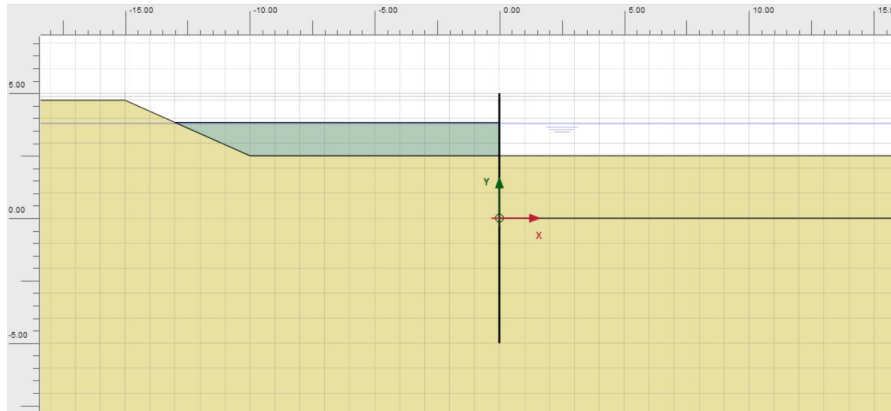


Figure I.1: Overview of the governing situation during construction of the sheet pile wall.

Table I.3: The maximum bending moment and shear force in the sheet pile wall during construction phase.

$M_{\max}$ (kNm/m)	- 8.4
$V_{\max}$ (kN/m)	-11.0

### 2 - Final stage

In the final stage, Phase 2, the situation of the sheet pile wall under service is simulated. First different anchor depths and its influence on the forces in the anchor and the sheet pile wall are examined. Based on these results a choice for the anchor depth is made. Subsequently the results for load-case 1 and 2, considering the chosen anchor depth, are presented.

#### 2a - Different anchor depths

Different depths (1.0 m, 1.2 m, 1.5 m and 2.0 m) of the anchor are examined for both load-cases. The results for the anchor force and maximum bending moment and shear force in the sheet pile wall are shown in table I.4.

Table I.4: The values for wall bending moment, wall shear force and anchor force for different anchor depths.

Load-case (#)	Anchor height (m)	Anchor force (kN)	$M_{\max}$ (kNm/m)	$V_{\max}$ (kN/m)
1	1.0	263	48.6	62.4
2	1.0	232	42.5	57.0
1	1.2	273	42.2	59.2
2	1.2	239	33.8	53.9
1	1.5	285	29.0	54.9
2	1.5	250	-23.3	49.3
1	2.0	298	-45.5	50.8
2	2.0	264	-41.6	44.5

As can be seen from the results, the anchor forces increase with an increasing depth. As the distance between the position the anchor force and the rotation centre decreases with an increasing anchor depth, this force increases. From the results it can be seen that the positive bending moment decreases with an increasing depth, the governing maximum bending moment becomes negative from a depth of 1.5 m. The maximum shear force varies between a value of 44.5 kN/m and 62.4 kN/m.

As expected the highest anchor forces occur for load-case 1. However, due to the high water table in load-case 2 the anchor plate has less capacity in this load-case. Therefore the anchor force in both load-cases need to be checked.

*2b - Load-case 1*

The results from load-case 1 are shown in figure I.2 and I.3.

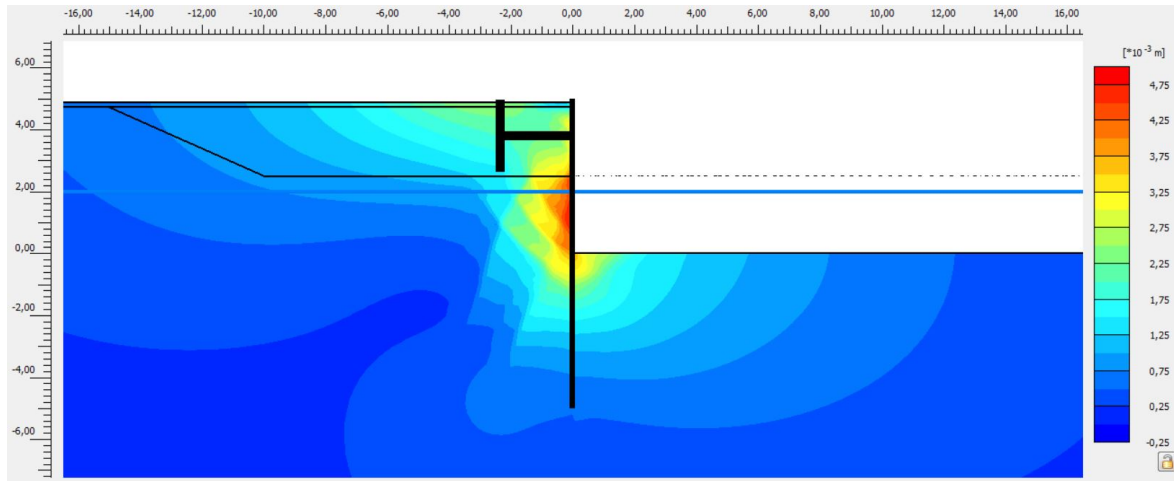


Figure I.2: The displacements for sheet pile wall load-case 1.

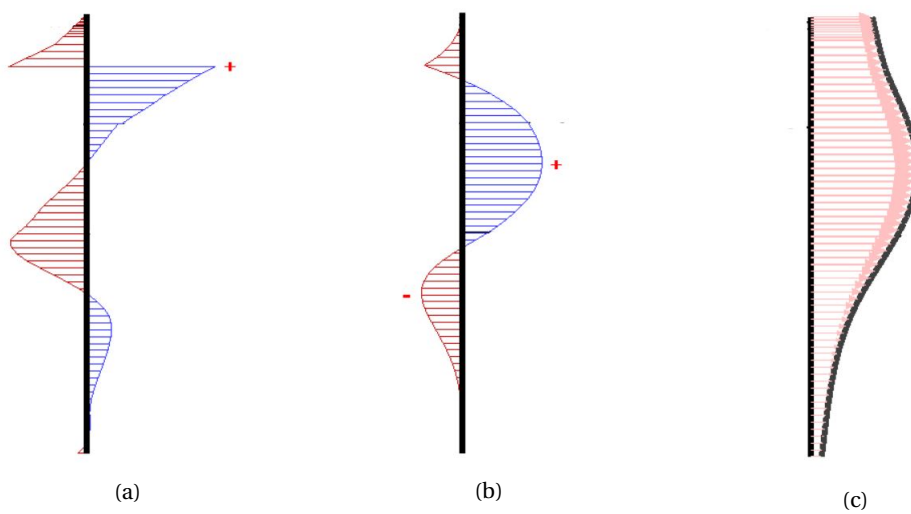


Figure I.3: The shear force (a) and bending moment (b) distribution in and the horizontal displacement (c) of the sheet pile wall for load-case 1. The maximum bending moment is 42.2 kNm/m, the maximum shear force is 59.2 kN/m and the maximum horizontal displacement is 5 mm.

2c - Load-case 2

The results from load-case 2 are shown in figure I.4 and I.5.

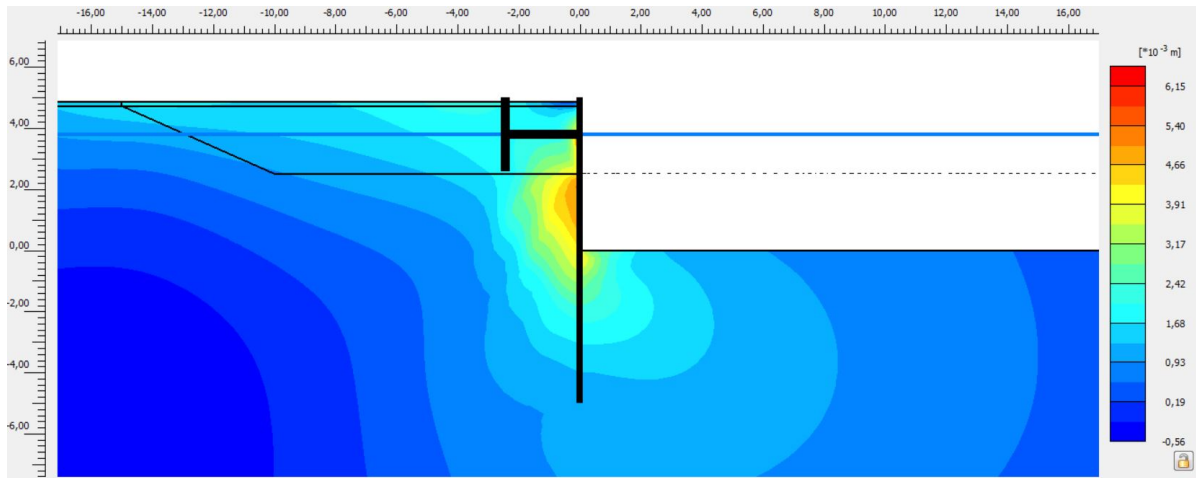


Figure I.4: The deformations for sheet pile wall load-case 2 (scaled up 100 times).

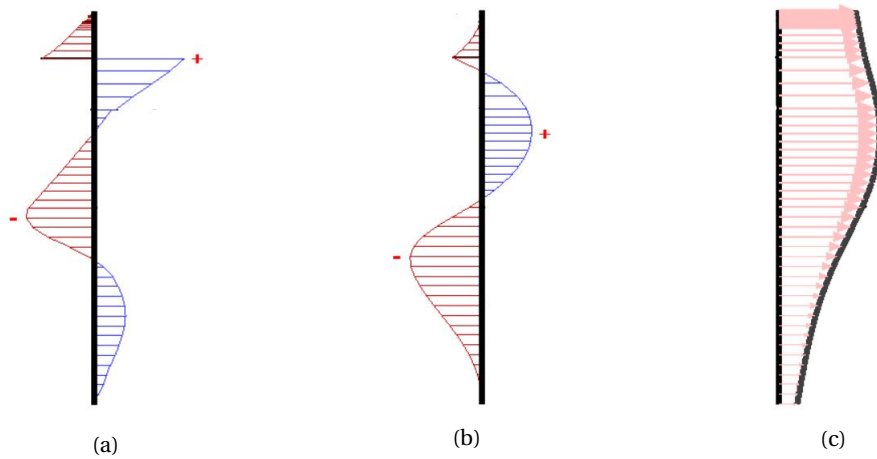


Figure I.5: The shear force (a) and bending moment (b) distribution in and the horizontal displacement (c) of the sheet pile wall for load-case 1. The maximum bending moment is 33.8 kNm/m, the maximum shear force is 53.9 kN/m and the maximum horizontal displacement is 4 mm.

## 7. Checks

The anchor plate capacity should be checked for both load-case 1 and 2. Despite the anchor force for load-case 2 is lower, the anchor capacity is less due to a higher water table. Due to the presence of water at the bottom half of the anchor plate the effective lateral earth pressure is lower, compared to the dry situation. This phenomenon is shown in figure I.6, the left figure corresponds to load-case 1 and the right figure to load-case 2.

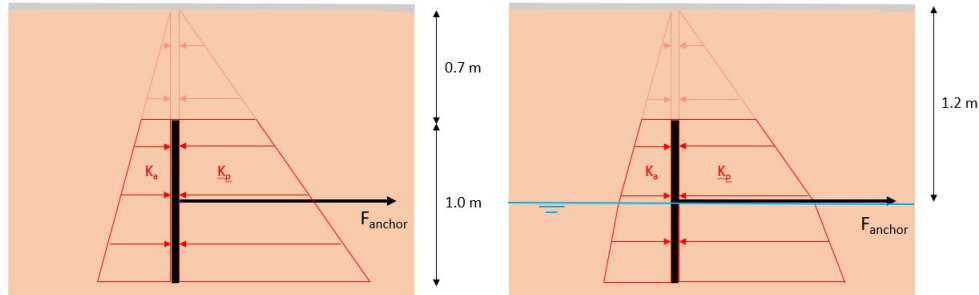


Figure I.6: The active and passive lateral earth pressure working on the anchor plate.

In table I.5 the anchor plate capacity is determined for an anchor plate height of 1.0 m. As can be seen from the results the capacity of the anchor plate is 30 kN less for load-case 2, compared to load-case 1.

Table I.5: Capacity of the anchor plate for load-case 1 and load-case 2.

Load-case 1			Load-case 2		
Parameter	Value	Unit	Parameter	Value	Unit
Dist. anchor - pavement	1.2	m	Dist. anchor - pavement	1.2	m
Height anchor plate	1.0	m	Height anchor plate	1.0	m
Length anchor plate	Continuous	m	Length anchor plate	Continuous	m
Top anchor plate	0.7	m	Top anchor plate	0.7	m
Bottom anchor plate	1.7	m	Bottom anchor plate	1.7	m
$K_a$	0.22	-	$K_a$	0.22	-
$K_p$	4.60	-	$K_p$	4.60	-
$y_{sat}$	21	kN/m <sup>3</sup>	$y_{sat}$	21	kN/m <sup>3</sup>
$y_{unsat}$	20	kN/m <sup>3</sup>	$y_{unsat}$	20	kN/m <sup>3</sup>
Pressure top anchor	61	kN/m <sup>2</sup>	Pressure top anchor	61	kN/m <sup>2</sup>
Pressure bottom anchor	149	kN/m <sup>2</sup>	Pressure bottom anchor	129	kN/m <sup>2</sup>
Anchor capacity per 3 m	316	kN	Anchor capacity per 3 m	286	kN/m

# J. Steel Building

## J.1 Structural Calculations

In this section, the structural analysis performed for the steel building building is elaborated. Design checks are performed for all structural members, the connections between these members, the composite deck and the foundation. Furtjermore, some output from ETABS is presented.

### J.1.1 Design philosophy

The Chilean building codes defines two different methods for strength calculations, load resistance and factor design (LRFD) and allowable stress design (ASD). LRFD and ASD loads are not directly comparable because they are used differently by the design codes. LRFD loads are generally compared to member or component strength whereas ASD loads are compared to member or component allowable values that are less than the full strength of the member or component.

The second major difference between the two methods is the difference in effective factors of safety. The LRFD method accounts separately for the predictability of applied loads through the use of load factors side and for material and construction variability through resistance factors. The ASD specification combines the two factors into a single factor of safety. For both concrete and steel members it is common to use the load and resistance factor design method from AISC 2010 to perform a structural calculation. Therefore, this LRFD method is applied in this design report.

All performed design checks are in accordance with the following formula:

$$R_u = \phi R_n \quad (J.1)$$

Where:

- $R_u$  = required strength using LRFD load combinations
- $R_n$  = nominal strength
- $\phi$  = resistance factor
- $\phi R_u$  = design strength

### J.1.2 Structural member checks

Structural design checks that should be performed to verify the structural integrity of members in compression, tension and bending are elaborated in this section. These checks concern the columns, beams and braces. The final design of these members is presented in Chapter 7.5.

#### J.1.2.1 Design for tension and compression members

Two different checks are performed for tensile members. First it is checked if yielding of the cross section can occur, taking into account the gross area of the cross section. Secondly it is checked if tensile rupture can occur in net area of the member. The difference between the gross and net area is that for the gross area, the entire cross-sectional area has to be taken into account, while for the net area the cross sectional area of each element individually has to be taken into account. For example the flanges and web of a cross section have to be checked separately on tensile rupture. The following formulas are applied:

For tensile yielding in the gross section:

$$P_n = F_n A_g \quad (J.2)$$

For tensile rupture in the net section:

$$P_n = F_u A_e \quad (J.3)$$

Where:

- $A_e$  = effective net area (mm<sup>2</sup>)
- $A_g$  = gross area of member (mm<sup>2</sup>)
- $F_y$  = specified minimum yield stress (MPa)
- $F_u$  = specified tensile strength (MPa)

For members in compression the same structural checks are performed as for members in tension, plus an additional buckling check. First is determined for each element if it is a slender or a non-slender element. A member can be considered as slender if its width-to-thickness ratio of its compression elements is lower than the specified value in AISC 2010. The members used in the design do not have any slender elements, therefore only the non-slender element check is performed. The nominal compressive strength of a member can be determined using the following formulas:

$$P_n = F_{cr} A_g \quad (J.4)$$

The critical stress  $F_{cr}$  is determined as follows:

When  $\frac{KL}{r} \leq 4.71 \sqrt{\frac{E}{F_y}}$  or  $\frac{F_y}{F_e} \leq 2.25$

$$F_{cr} = \left(0.658 \frac{F_y}{F_e}\right) F_y \quad (J.5)$$

When  $\frac{KL}{r} \geq 4.71 \sqrt{\frac{E}{F_y}}$  or  $\frac{F_y}{F_e} > 2.25$

$$F_{cr} = 0.877 F_e \quad (J.6)$$

Where:

- $F_e$  = elastic buckling stress determined according eq. or through an elastic buckling analysis.

$$F_e = \frac{\pi^2 E}{\left(\frac{KL}{r}\right)^2} \quad (J.7)$$

### J.1.2.2 Design of members for flexure

The design checks as explained in this chapter are only applicable to members subject to a bending moment about one axis. The design flexural strength of a member depends on the type of cross section. Sections are classified as compact, non-compact or as slender-element sections. A section is classified as compact if the flanges are continuously connected to the web and the width-to-thickness ratio of its compression elements does not exceed a certain ratio as specified in AISC 2010. All cross sections used in the design can be classified as compact. The design capacity of a member is the lower value of the plastic moment capacity and the lateral torsional buckling capacity. The lateral torsional buckling moment of the composite beams can be neglected, due to the extra rotational stiffness the deck provides. The following formulas are applied to determine the flexural strength:

#### Yielding

$$M_n = M_p = F_y Z_x \quad (J.8)$$

Where:

- $M_n$  = flexural strength (KNm)

- $M_p$  = plastic moment capacity (MPa)
- $F_y$  = specified minimum yield stress (MPa)
- $Z_x$  = plastic section modulus (mm<sup>3</sup>)

### Lateral-Torsional Buckling

When  $L_b \leq L_p$ , the limit state of lateral torsional buckling does not apply When  $L_p \leq L_b \leq L_r$

$$M_n = C_b \left[ M_p - \left( M_p - 0.7F_y S_x \left( \frac{L_b - L_p}{L_r - L_p} \right) \right) \right] \leq M_p \quad (J.9)$$

When  $L_b \geq L_r$

$$M_n = F_{cr} S_x \leq M_p \quad (J.10)$$

$$F_{cr} = \frac{C_b \pi^2 E}{\left( \frac{L_b}{r_{st}} \right)^2} \sqrt{1 + 0.078 \frac{J_c}{S_x H_o} \left( \frac{L_b}{r_{st}} \right)^2} \quad (J.11)$$

Where:

- $L_b$  = length between points that are either braced against lateral displacement (mm)
- $J$  = torsional moment of inertia (mm<sup>4</sup>)
- $J_x$  = torsional constant (mm<sup>3</sup>)
- $h_0$  = distance between flange centroids (mm)

The limiting lengths  $L_p$  and  $L_r$  are determined as follows:

$$L_p = 1.76 r_y \sqrt{\frac{E}{F_y}} \quad (J.12)$$

$$L_r = 1.95 r_{ts} \frac{E}{0.7F_y} \sqrt{\frac{J_c}{S_x h_o} + \sqrt{\left( \frac{J_c}{S_x h_o} \right)^2 + 6.76 \left( \frac{0.7F_y}{E} \right)^2}} \quad (J.13)$$

For some members it is possible that they are loaded by an axial force and a bending moment. For those members an interaction formula is be ued.

When  $\frac{P_r}{P_c} \geq 0.2$

$$\frac{P_r}{P_c} + \frac{8}{9} \frac{M_r}{M_c} \leq 1.0 \quad (J.14)$$

When  $\frac{P_r}{P_c} \leq 0.2$

$$\frac{P_r}{2P_c} + \frac{M_r}{M_c} \leq 1.0 \quad (J.15)$$

Where:

- $P_r$  = required axial strength using LRFD combinations (N)
- $P_c$  = available axial strength (N)
- $M_r$  = required flexural strength using LRFD combinations (Nm)
- $M_c$  = flexural axial strength (Nm)

### J.1.3 Joint checks

#### J.1.3.1 Overview performed checks

Three different types of joints are used in the design. Different design checks are performed for each joint. A summary of all the performed checks is shown below, with a reference to a further elaboration of the check. The final joint designs including dimension are presented in Chapter 7.

Table J.1: Design checks beam to beam joint

Design Check Type	UC	Reference
Bolt strength in single shear	0.36	J.1.3.2
Bolt bearing on web plate	0.37	J.1.3.3
Shear yielding of web plate	0.57	J.1.3.4
Shear rupture of web plate	0.82	J.1.3.5
Block shear rupture strength of web plate	0.44	J.1.3.6
Design strength of weld	0.31	J.1.3.7
Bolt bearing on beam web	0.38	J.1.3.3
Block shear rupture strength of beam web	0.36	J.1.3.6
Flexural yielding of the coped section	0.52	J.1.3.10
Local web buckling on coped section	0.13	J.1.3.11
Shear rupture of girder web	0.79	J.1.3.5

Table J.2: Design checks column to transverse beam joint

Design Check Type	UC	Reference
Strength of bolt group	0.21	J.1.3.8
Maximum plate thickness for plate yielding	0.27	J.1.3.9
Shear yielding of web plate	0.09	J.1.3.4
Critical flexural stress	0.09	J.1.3.10
Shear rupture of web plate	0.12	J.1.3.5
Block shear rupture strength of web plate	0.09	J.1.3.6
Flexure rupture of plate	0.26	J.1.3.10
Local buckling of plate	0.33	J.1.3.11
Strength of column web at weld	0.89	J.1.3.7

Table J.3: Design checks column to longitudinal beam joint

Design Check Type	UC	Reference
Bolt strength in single shear	0.31	J.1.3.2
Bolt bearing on web plate	0.24	J.1.3.3
Shear yielding of web plate	0.30	J.1.3.4
Shear rupture of web plate	0.41	J.1.3.5
Block shear rupture strength of web plate	0.37	J.1.3.6
Design strength of weld	0.30	J.1.3.7
Bolt bearing on beam web	0.41	J.1.3.3

### J.1.3.2 Bolt strength in single shear

Shear failure of the bolt means that the bolt fails due to the shear force between the two connected plates. The shear capacity of the bolts is checked using the following formulas:

$$A_b = \frac{\pi d_b^2}{4} \quad (J.16)$$

$$\phi R_n = \phi F_{nv} A_b n \quad (J.17)$$

Where:

- $A_b$  = bolt surface area (mm<sup>2</sup>)
- $d_b$  = bolt diameter (mm)
- $n$  = amount of bolts (-)
- $F_{nv}$  = shear stress capacity (-)

### J.1.3.3 Bolt bearing on web plate or web

Bolt bearing is the failure of the plate material around the hole, due to the load that the bolt acts on the plates. The bearing capacity is checked using the following formulas:

$$L_{c1} = L_{ev} \frac{d_h}{2} \quad (J.18)$$

$$L_c = s d_h \quad (J.19)$$

$$\phi r_{n1} = \phi 1.2 l_{c1} t F_u \quad (J.20)$$

$$\phi r_{n2} = \phi 1.2 l_c t F_u \quad (J.21)$$

$$\phi r_{nmax} = \phi 2.4 d t F_u \quad (J.22)$$

$$\phi R_n = \min(\phi r_{n1}, \phi r_{nmax}) + (n - 1) \min(\phi r_{n2}, \phi r_{nmax}) \quad (J.23)$$

Where:

- $s$  = bolt spacing (mm)
- $d_h$  = bolt diameter (mm)
- $L_c$  = distance between bolts (mm)

### J.1.3.4 Shear yielding of the web plate

Shear yielding means that the yield stress in the plate is reached due to the shear force that is transferred through the bolt. The shear yielding capacity is checked using the following formulas:

$$A_{gv} = L t \quad (J.24)$$

$$\phi R_n = \phi 0.6 F_y A_g \quad (J.25)$$

Where:

- $L$  = width of plate (mm)
- $t$  = plate thickness (mm)

### J.1.3.5 Shear rupture of web plate

Shear rupture means that the tensile strength in the plate is reached due to the shear force that is transferred through the bolt. The difference with the shear yielding calculation is that a smaller surface area is taken into account. The shear capacity is checked using the following formulas:

$$A_{nv} = \left[ L - n \left( d_h + \frac{1}{16} \right) \right] t \quad (J.26)$$

$$\phi R_n = \phi 0.6 F_u A_{nv} \quad (J.27)$$

Where:

- $d_h$  = bolt diameter (mm)
- $t$  = plate thickness (mm)

### J.1.3.6 Block shear rupture strength of web plate or beam web

Block shear rupture is a type of shear failure along a block like pattern between the bolts. The shear force is divided over the net area between the bolts. The capacity is checked using the following formulas:

$$A_{nt} = \left( L - n \left( d_h + \frac{1}{16} \right) \right) t \quad (J.28)$$

$$A_{nv} = \left[ ((n-1)s + L_{ev}) \left( \frac{2n-1}{2} \left( d_h + \frac{1}{16} \right) \right) \right] t \quad (J.29)$$

$$A_{gv} = [(n-1)s + L_{ev}] t \quad (J.30)$$

$$\phi R_n = \phi (F_u A_{nt} + \min(0.6 F_y A_{gv}, 0.6 F_u A)) \quad (J.31)$$

### J.1.3.7 Design strength of the welds

The design capacity of all welds should always be higher than the capacity of the elements that it is connecting. For the calculation of the design strength it is assumed that the full plastic capacity of the weld is available. The following formula is used to determine the capacity of the welds:

$$\phi R_n = \frac{\phi 1.2 D L F_{exx}}{22.627} \quad (J.32)$$

Where:

- $F_{exx}$  = allowable stress in weld (MPa)
- $D$  = weld leg size (mm)
- $L$  = weld length (mm)

### J.1.3.8 Strength of bolt group

It can be assumed that a group of bolts transfers the load as a group. The capacity of each individual bolt is first determined and afterwards the capacity of the entire group can be determined, making use of a capacity reduction factor.

$$L_{c1} = L_{ev} \frac{d_h}{2} \quad (J.33)$$

$$L_c = sd_h \quad (J.34)$$

$$\phi r_{n1} = \min(\phi 1.2l_{c1}tF_u, 1.2l_{c2}tF_u) \quad (J.35)$$

$$\phi r_{nmax} = \phi 2.4dtF_u \quad (J.36)$$

$$A_b = \frac{\pi d_b^2}{4} \quad (J.37)$$

$$\phi r_{n2} = \phi F_{nv} A_b \quad (J.38)$$

$$\phi R_n = C \min(\phi R_{n1}, R_{n2}) \quad (J.39)$$

Where:

- $L_c$  = distance between bolts (mm)
- $C$  = bolt group reduction factor (-)
- $F_u$  = tensile rupture strength of bolt (MPa)

### J.1.3.9 Maximum plate thickness

A maximum capacity of all plates is specified by by AISC 2010. The reason of this rule is that the plate material should first yield before the bolt fails due to shearing. Failure due to plate yielding is preferred because it is a ductile failure mechanism and bolt shearing is a brittle failure mechanism. Brittle failure mechanism should always be avoided where possible. The following formulas are used to determine the maximum thickness of the plates.

$$A_b = \frac{\pi d_b^2}{4} \quad (J.40)$$

$$M_{max} = \frac{F_{nv}}{0.9} A_b C \quad (J.41)$$

$$M_{max} = \frac{F_{nv}}{0.9} A_b C \quad (J.42)$$

$$t_{max} = \frac{6M_{max}}{F_y L^2} \quad (J.43)$$

### J.1.3.10 Critical flexural stress

The bending capacity in the joint also has been taken into account. For this check the flexural and shear capacity are combined with an interaction formula. The following formulas are used:

$$\phi V_n = \phi 0.6 F_y A_{gv} \quad (J.44)$$

$$e = \frac{b_f t_w}{2} + a_1 + \frac{g}{2} \quad (J.45)$$

$$a = \frac{b_f t_w}{2} + a_1 \quad (J.46)$$

$$Z = \frac{tL^2}{4} \quad (J.47)$$

$$M_u = V_u e \quad (J.48)$$

$$M_u = V_u e \quad (J.49)$$

$$\phi_b M_n = \phi F_y Z \quad (J.50)$$

$$UC = \left( \frac{V_u}{\phi V_n} \right)^2 + \left( \frac{M_u}{\phi M_n} \right)^2 \quad (J.51)$$

Where:

- $b_f$  = flange width (mm)
- $t_w$  = web thickness (mm)
- $t$  = plate thickness (mm)
- $M_u$  = flexural capacity
- $V_n$  = shear capacity

### J.1.3.11 Local buckling of plate

An axial load has to be transferred through the plates. Due to this, buckling could occur in the plates. To determine the buckling capacity of the plate, the slenderness has to be determined first. The following formulas are used to determine the buckling capacity:

$$\lambda = \frac{L\sqrt{F_y}}{10t\sqrt{475 + 280\left(\frac{l}{s}\right)^2}} \quad (J.52)$$

$$F_{cr} = F_y Q \quad (J.53)$$

$$S_{net} = \frac{tL^2}{6} \quad (J.54)$$

$$\phi M_n = \phi F_{cr} S_{net} \quad (J.55)$$

Where:

- $b_f$  = flange width (mm)
- $t_w$  = web thickness (mm)
- $\lambda$  = slenderness (-)

## J.1.4 Composite deck

The structural calculation for the composite slab is performed by making use of an Excel sheet that is based on the Chilean building standards and prescriptions from the Steel Deck Institute. In the Excel sheet checks are performed for the construction phase as well as the use phase. All structural checks are explained below. The bending moments are calculated by 'vergeet-mij-nietjes' for multiple span beams/slabs.

### J.1.4.1 Deflection non-composite system

The calculated deflections of the deck in a non-composite system, is based on the load of the concrete and the self weight of the steel deck. The deflection shall be limited to the lesser of  $L/180$  or 19 mm.

$$\delta = \frac{0.0069W_d L^2}{EIb} < \frac{L}{180} \quad (J.56)$$

Where:

- $W_d$  = distributed design load (kN/m<sup>2</sup>)
- $L$  = effective span (m)
- $E$  = Youngs Modulus (MPa)
- $I$  = Moment of inertia (m<sup>4</sup>)
- $\delta$  = deflection (mm)

### J.1.4.2 Bending non-composite system

The flexural capacity of the steel deck is checked for the non-composite system. The load of the concrete and the self weight of the steel deck is considered and additionally a point and distributed construction load should be taken into account.

$$M_1^+ = 0.2P_{sd}L + 0.094W_dL^2 \quad (J.57)$$

$$M_2^+ = 0.094(W_{sd} + W_d)L^2 \quad (J.58)$$

$$M_3^- = 0.117(W_{sd} + W_d)L^2 \quad (J.59)$$

$$f^+ = \frac{M_1^+}{S^+} < 0.6f_y \quad (J.60)$$

$$f^+ = \frac{M_2^+}{S^+} < 0.6f_y \quad (J.61)$$

$$f^- = \frac{M_3^-}{S^-} < 0.6f_y \quad (J.62)$$

Where:

- $W_d$  = distributed design load (kN/m<sup>2</sup>)
- $W_d$  = distributed construction load (kN/m<sup>2</sup>)
- $P_{sd}$  = design point load (kN)
- $L$  = effective span (m)
- $E$  = Youngs Modulus (MPa)
- $I$  = Moment of inertia (m<sup>4</sup>)
- $M_i^+$  = positive design moment (kNm)
- $M_i^-$  = negative design moment (kNm)
- $f^+$  = positive flexural stress (MPa)
- $f^-$  = negative flexural stress (MPa)
- $f^y$  = steel yield stress (MPa)

### J.1.4.3 Bending composite system

The positive and negative bending capacity of the composite system is also be checked. The load of the concrete and the self weight of the steel deck should be considered and additionally the live load acting on the floor should be taken into account.

$$M_n = A_s f_y \left( d - \frac{a}{2} \right) \quad (J.63)$$

$$Q_u = 1.2W_d + 1.6W_l \quad (J.64)$$

$$M_u^+ = 0.094Q_uL^2 \quad (J.65)$$

$$M_u^- = 0.117Q_uL^2 \quad (J.66)$$

$$M_u^+ < 0.9M_n \quad (J.67)$$

$$M_u^- < 0.9M_n \quad (J.68)$$

#### J.1.4.4 Deflection composite system

The instantaneous deflection for the composite system should be checked, as well as the deflection after considering time dependent behaviour. The deflection shall be limited to the lesser of  $L/360$ .

$$\delta_{ins} = \frac{0.0069(W_d + W_L)L^2}{EIb} \quad (J.69)$$

$$\delta_{ins} < \frac{L}{360} \quad (J.70)$$

$$\lambda_{\Delta} = \frac{\xi}{1 + 50p'} \quad (J.71)$$

$$\delta_{long-term} = \delta_{ins}\lambda_{\Delta} \quad (J.72)$$

$$\delta_{long-term} < \frac{L}{360} \quad (J.73)$$

### J.1.5 Foundation

#### J.1.5.1 Overview foundation checks

The foundation of the building will consist of a continuous concrete strip underneath the building. The dimensions of this strip will be larger directly underneath the columns, because a larger load needs to be transferred by the columns than by the walls. The columns are attached to the foundation, using a base plate and bolts. A summary of all the performed checks is shown in table J.4, with a reference to a further elaboration of the checks.

Table J.4: Design checks column to foundation connection

Design Check Type	UC	Reference
Anchor rod strength	0.61	J.1.5.2
Base plate thickness	0.93	J.1.5.3
Weld strength	0.29	J.1.3.7
Column web stress	0.92	J.1.3.4
Concrete pullout strength	0.34	J.1.5.4
Concrete breakout strength	0.31	J.1.5.5
Side-face blowout strength	0.04	J.1.5.6

#### J.1.5.2 Anchor rod strength

The axial capacity of each individual rod is checked. This is done by distributing the load over the load over each rod equally and then dividing it by the capacity of each rod. The following formulas are used to check the anchor rod strength:

$$P_r = \frac{F_u}{n} \quad (J.74)$$

$$A_r = \frac{\pi d_r^2}{n} \quad (J.75)$$

$$R_n = 0.75F_u A_r \quad (J.76)$$

Where:

- $d_r$  = rod diameter (mm)
- $n$  = amount of rods (-)
- $F_u$  = rupture strength (MPa)

### J.1.5.3 Base plate thickness

The thickness of the base base should have sufficient capacity to transfer the bending moment caused by the anchor rods. This is checked by determining a minimum section modulus of the plate. This minimum section modulus than results in a minimum thickness of the base plate. The following formulas are used to determine the minimum base plate thickness:

$$P_r = \frac{F_u}{n} \quad (J.77)$$

$$M_u = P_r \frac{S_2 - t_w}{2} \quad (J.78)$$

$$b_{eff} = S_2 - t_w \quad (J.79)$$

$$t_{req} = \sqrt{\frac{4Z}{b_{eff}}} \quad (J.80)$$

Where:

- $S_2$  = distance between rods (mm)
- $t_w$  = web thickness (mm)
- $t_{req}$  = required plate thickness (mm)

### J.1.5.4 Concrete pullout strength

The concrete surrounding the rods should have sufficient capacity to to transfer the load of the rods to the foundation block. This capacity is determined using the following formula:

$$\phi N_p = \phi \Psi_4 A_{brg} 8 f'_c \quad (J.81)$$

Where:

- $A_{brg}$  = pullout surface area (mm<sup>2</sup>)
- $f'_c$  = concrete compressive strength (MPa)

### J.1.5.5 Concrete breakout strength

The capacity of the concrete entire foundation should be sufficient to to transfer the axial load that is transferred by the column. This check is done by first determining the minimum effective area over which the axial load can be transferred. The following formulas are used to determine the concrete breakout strength:

$$ca_1 = L_{eh} + b \quad (J.82)$$

$$ca_2 = L_{ev} + a \quad (J.83)$$

$$A_{N0} = 9h_{ef}^2 \quad (J.84)$$

$$A_N = (\text{Min}[2C_{a1}, 3h_{ef}] + \text{Min}(S_1, 3h_{ef})) [\text{Min}(2C_{a2}, 3h_{ef}) + \text{Min}(S_2, 3h_{ef})] \quad (J.85)$$

$$\phi N_{cbg} = \phi \Psi_3 16 \sqrt{f'_c} h_{ef}^{\frac{5}{3}} \left( \frac{A_N}{A_{N0}} \right) \quad (J.86)$$

Where:

- $h_{ef}$  = effective height (mm)
- $A_n$  = breakout surface area (mm)

### J.1.5.6 Side-face blowout strength

The side-face blowout strength of a foundation is the capacity of the foundation against failure due to a shear force. This check is especially for the foundations where the columns and the braces meet each other, because the due to the load transfer of the brace to the column, the shear force will be at its highest. The following formulas are used to check the side-face blowout strength:

$$ca_1 = \min((L_{eh} + b), (L_{ev} + a)) \quad (J.87)$$

$$ca_2 = \max((L_{eh} + b), (L_{ev} + a)) \quad (J.88)$$

$$h_{ef} \geq 2.5C_{a1} \quad (J.89)$$

$$N_{sb} \phi 160 c_{a1} \lambda_a \sqrt{A_{brg} f'_c} \quad (J.90)$$

$$N_{sb} = \frac{1}{4} \left( 1 + \frac{ca_2}{ca_1} \right) N_{sb} \quad (J.91)$$

Where:

- $L_{ef}$  = Effective height
- $h_{ef}$  = effective height (mm)
- $A_n$  = breakout surface area (mm)

## J.2 Output ETABS

### J.2.1 Overview unity checks

An overview of all the unity checks of the steel members is shown in this chapter. The unity checks of the regular steel members and steel member attached to the composite deck are shown in a different figure. This is automatically done by ETABS, because different checks are performed on regular steel members and composite members.

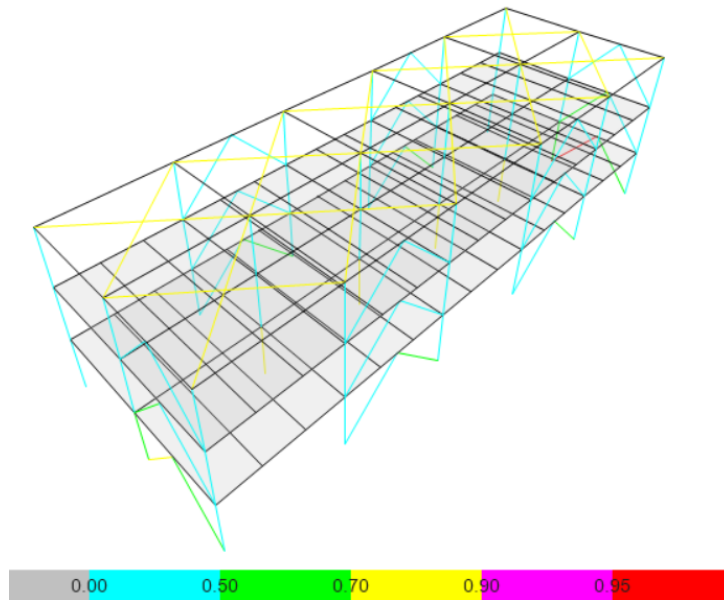


Figure J.1: Unity checks steel structural members

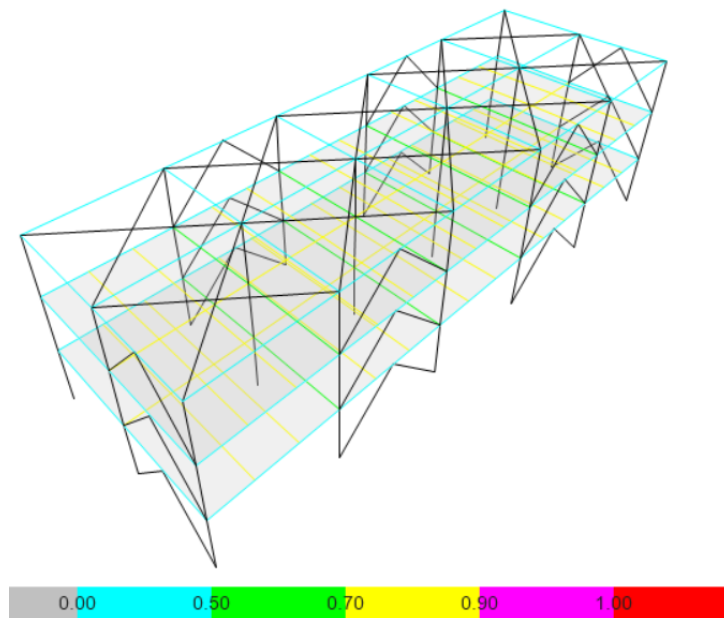


Figure J.2: Unity checks composite members

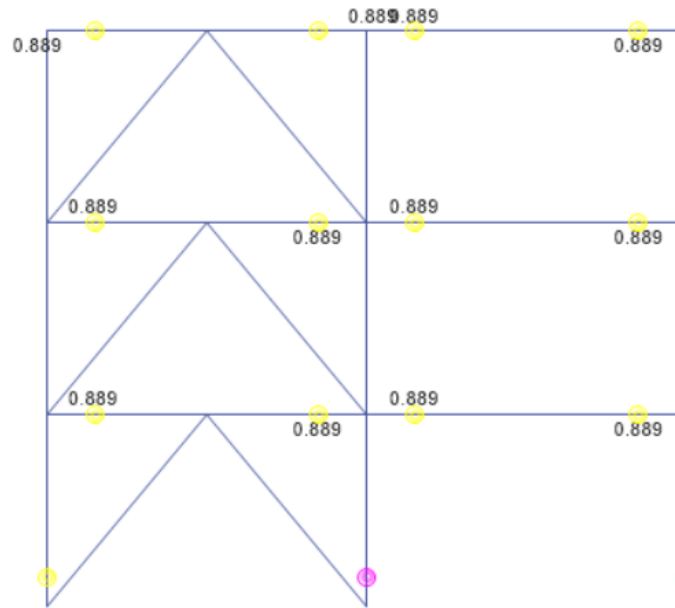


Figure J.3: Unity checks joints side view

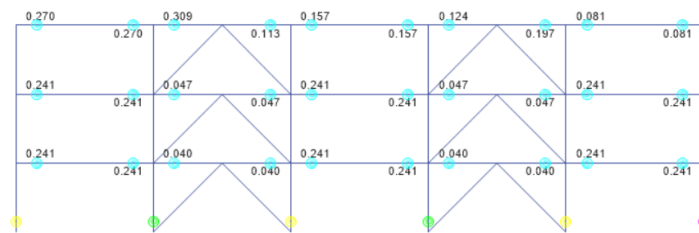


Figure J.4: Unity checks joints front view

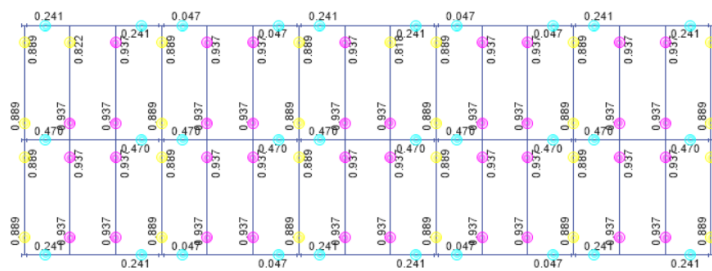


Figure J.5: Unity checks joints top view second floor

# K. Concrete Building

In this section, the structural analysis of the concrete building structure design and its structural components is elaborated.

## K.1 Structural Member Calculations

In this section, the procedure and the results of the structural analysis performed for the concrete building are presented. These calculations are made according to ACI 318-14, by making use of the software ETABS and are checked by means of hand calculations. The purpose of the calculations performed in this section is to verify the dimensions assumed for the structural elements of the reinforced concrete building. The output will be presented in tables, showing the different forces and stresses active in the specific structural component. Furthermore, the required amount of reinforcement to meet all the strength requirements is given. If necessary an explanation is given about the results in the tables.

It is important to comprehend that assumptions are made in this calculation procedure that enable a quick preliminary design process. For this reason, the results of this structural calculation can not be considered as impeccable values, without performing a more thorough analysis. The assumptions made for each structural member, are elaborated in the relevant subsections.

Below an elaboration of the structural analysis for the following structural components is presented: columns, beams, walls and slabs.

### K.1.1 Columns

An overview of the columns of the concrete building structure is presented in Figure K.1. All columns have the same cross-sectional dimensions and will be performed with the same amount of longitudinal and shear reinforcement. The detailing will be different for the inner columns (C2) compared to the outer columns (C1), since the outer columns continue over two stories.

Strength calculations are performed according to ACI 318-14 (Column Section Design). By making use of ETABS, axial forces, bi-axial moments and shear forces are checked and the required amount of reinforcement is determined. A summary of the checks and results can be found in tables K.1, K.2 and K.3. Only one governing column is considered. The governing load combination for the axial force and biaxial moment interaction check is LRFD7Y. For the shear force the leading load combination LRFD5X and LRFD5Y.

The resulting reinforcement in the longitudinal direction of the columns is  $400\text{mm}^2$ . The applied longitudinal reinforcement will therefore be  $4\phi 12\text{mm}$ . An amount of  $125\text{mm}^2/\text{m}$  shear reinforcement is required. Braces of  $\phi 8\text{mm}$  with a spacing of  $200\text{mm}$  will therefore be easily sufficient.

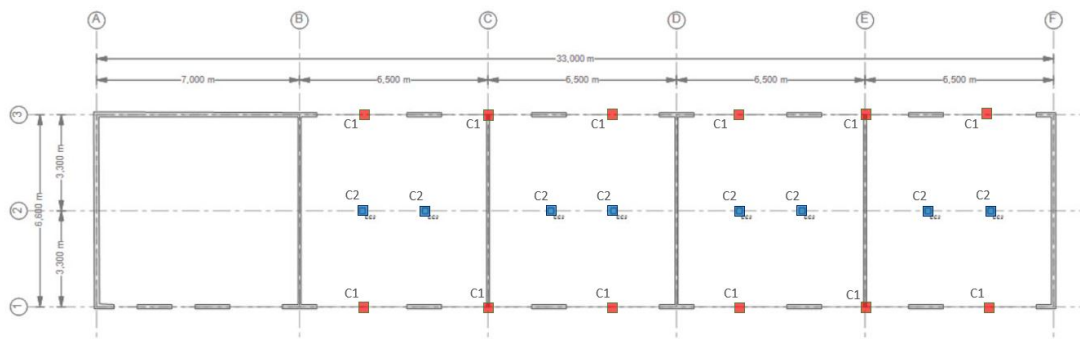


Figure K.1: Column layout of concrete building design

Table K.1: Governing column element details

Level	Element	Length (mm)	Height (mm)	Width (mm)	Cover (mm)
Storey2	C2	6000	200	200	40

Table K.2: Column: Design axial force and biaxial moment interaction

Column end	Design Axial force (kN)	Design Moment $M_2$ (kNm)	Design Moment $M_3$ (kNm)	Longi. Rebar (%)	Longi. Rebar ( $\text{mm}^2$ )
<b>Top</b>	2.12	5.16	53.42	1.0	400
<b>Bottom</b>	1.85	0.07	46.79	1.0	400

Table K.3: Column: Design shear force and reinforcement

Column end	Major Design shear (kN)	Minor Design shear (kN)	Major Shear rebar ( $\text{mm}^2/\text{m}$ )	Minor Shear rebar ( $\text{mm}^2/\text{m}$ )
<b>Top</b>	2.12	5.16	53.42	124.22
<b>Bottom</b>	1.85	0.07	46.79	0

### K.1.2 Beams

An overview of the beam elements of the concrete building structure is presented in figure K.2. Both types of beams have the same cross-sectional dimensions of 200 by 300 mm. The beams will however be performed with a different amount of longitudinal and shear reinforcement, because of the difference in span. Only one beam (of type B1) is worked out in depth in this report.

By making use of ETABS, axial force, biaxial moment and shear forces are checked and the required amount of reinforcement is determined. A summary of the checks and results can be found in tables K.4, K.5 and K.6. The beam with the largest bending moment is checked since that is the beam with the largest amount of required reinforcement. For this governing beam, LRFD7X is the leading load combination.

The resulting reinforcement ratio in the longitudinal direction of the beams is 0.31 percent. Based on this value a longitudinal reinforcement of  $6\phi 10\text{mm}$  is sufficient. The shear force acting on the beam is relatively low and can be transferred by the concrete itself. Therefore, no braces are required due to strength requirements. A practical bracing reinforcement will be applied of  $\phi 8-200\text{mm}$ .

Table K.4: Governing beam element details

Level	Element	Length (mm)	Height (mm)	Width (mm)	Cover top (mm)	Cover bottom (mm)
Storey2	B2	4600	300	200	60	60

Table K.5: Beam: Flexural design moment and reinforcement

	End-I Max. moment (kNm)	End-I Rebar (%)	Middle Max. moment (kNm)	Middle Rebar (%)	End-II Max. moment (kNm)	End-II Rebar (%)
<b>Top</b>	-26.44	0.28	-7.11	0.09	-28.48	0.29
<b>Bottom</b>	13.22	0.17	30.41	0.31	14.24	0.19

Table K.6: Beam: Design shear force and reinforcement

End-I Max. shear (kN)	End-I Rebar (%)	Middle Max. shear (kN)	Middle Rebar (%)	End-II Max. shear (kN)	End-II Rebar (%)
42.44	0.0	0.0	0.0	42.48	0.0

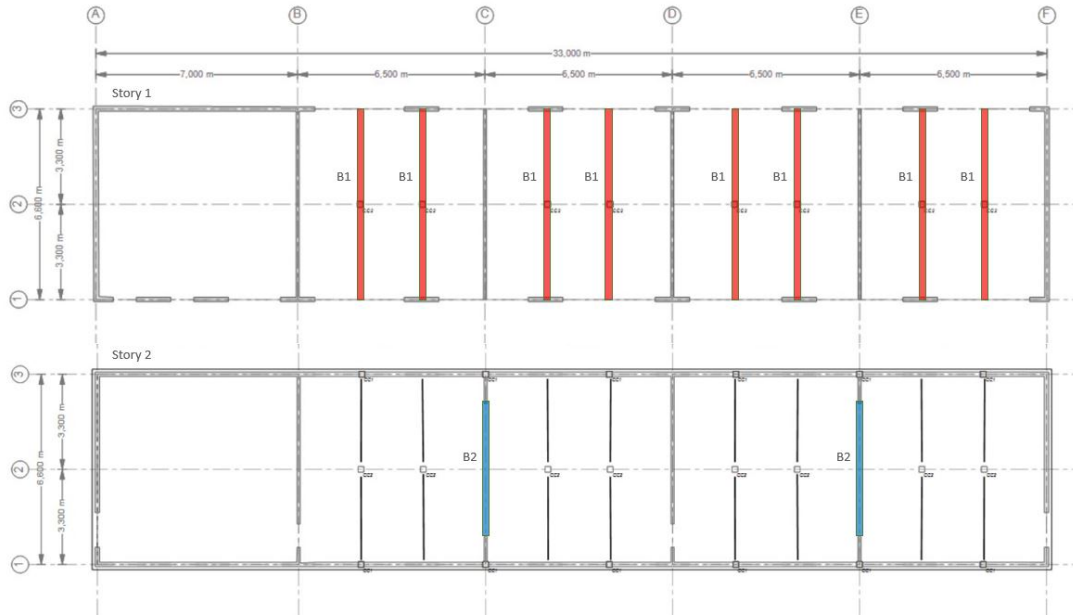


Figure K.2: Beam layout of concrete building design

### K.1.3 Walls

For the outer wall elements a wall thickness of 200mm will be used and 150mm for the inner walls. The thickness of the wall elements is governed by practical considerations, taking into account detailing of the rebar. By performing structural calculations and modeling, it is checked if the assumed dimensions fulfill the strength requirements. Additionally an estimation of the required amount of reinforcement is determined. To do this the structural walls are divided in several sections, with similar characteristics and dimensions. The calculation and results of just one governing wall section is presented below.

A summary of the checks and results can be found in tables K.7, K.8 and K.9. The resulting longitudinal minimum reinforcement ratio is the same for all wall elements: 0.25 percent. This value is not governed by strength requirements, but is equal to the minimum ratio prescribed in ACI 318-14. The governing load combination for the axial force and biaxial moment interaction check is LRFD7Y. For the shear force the leading load combination LRFD5X.

Table K.7: Governing wall element details

Level	Element	Length (mm)	Thickness (mm)	Cover (mm)
Storey1	P8	1200	200	50

Table K.8: Wall: Design axial force and bi-axial moment interaction

Wall end	Axial force (kN)	Design moment $M_2$ (kNm)	Design moment $M_3$ (kNm)	Required rebar ratio (%)	Required rebar area (mm <sup>2</sup> )
Top	-7.78	1.37	0.37	0.25	600
Bottom	-32.97	0.62	3.78	0.25	600

Table K.9: Wall: Design shear force and reinforcement

Wall end	Design axial force (kN)	Design moment (kNm)	Design shear force $V_u$ (kN)	$\Phi V_c$ (kN)	$\Phi V_n$ (kN)	Required rebar ratio (%)	Required rebar (mm <sup>2</sup> /m)
Top	49.47	-3.28	27.43	119.57	268.49	0.25	500
Bottom	91.21	91.21	42.83	155.15	304.08	0.25	500

#### K.1.4 Floor slab

The reinforcement in the 180mm thick concrete slab floor is determined by making use of the structural model in ETABS. ETABS performs design checks according to the American building standards (ACI 318-14 Concrete Strip Design) and generates a proposed amount of reinforcement based on the bending moment diagrams. These moment diagrams are obtained by assigning design strips in the model at governing locations. Because of the simple and constant wall configuration, just three design strips are considered. One in the longitudinal direction of the building and two in the transfers direction. The reinforcement resulting from this calculation serves as a quick design check to verify if the assumed slab thickness generates realistic results. By proper detailing a lower amount of reinforcement could be applied at certain parts of the slabs.

The figures below show the geometry of the one meter wide design strips, the moment diagrams and the proposed longitudinal reinforcement in mm<sup>2</sup>/m. The shear forces in the slab are relatively low and can be transferred by concrete shear stresses. From the required amount of reinforcement determined by ETABS, it can be concluded that a reinforcement of  $\phi 12$ -100 mm at the bottom and top of the slab will be sufficient. This amount of reinforcement should be applied in both the longitudinal, as well as the transfers direction. This is a realistic and practical amount of reinforcement and therefore it can be concluded that the design of the concrete slab floor is adequate.

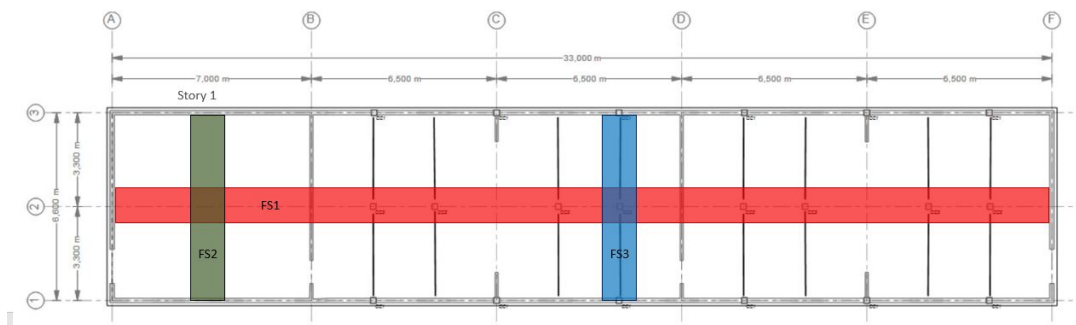


Figure K.3: Concrete floor slab: strip layout

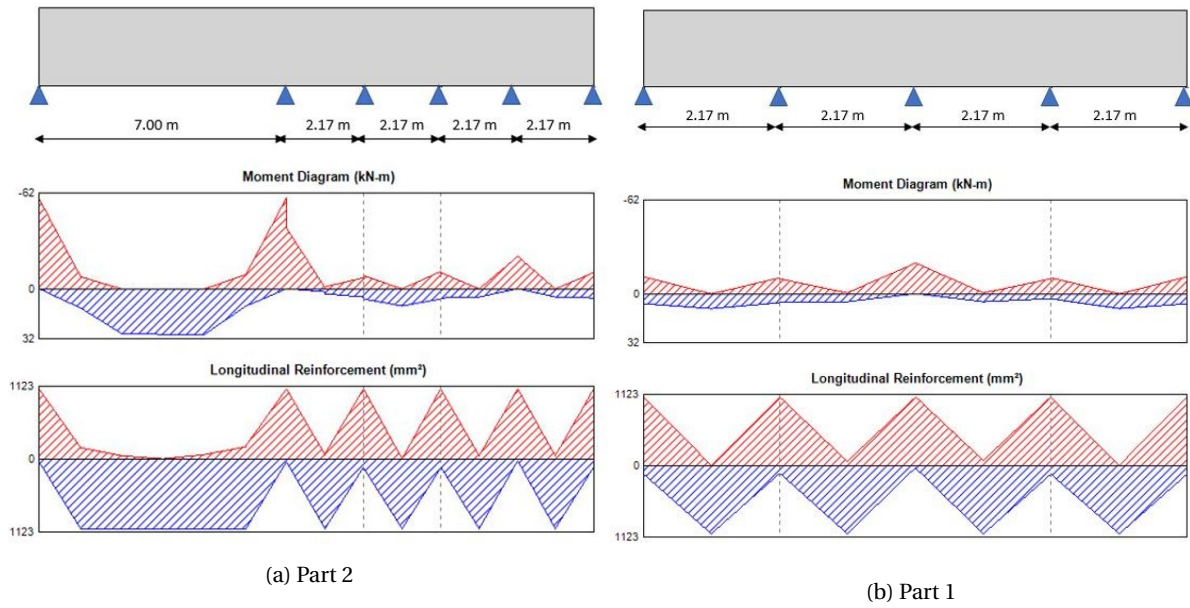


Figure K.4: Concrete floor slab (strip FS1): geometry, moment diagram and reinforcement

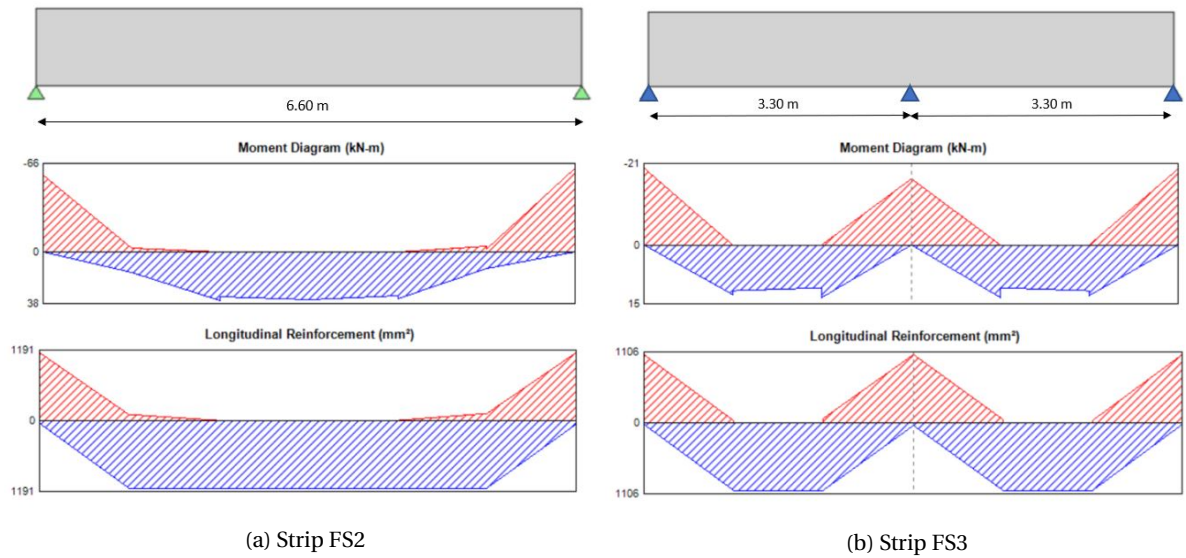


Figure K.5: Concrete floor slab (strip FS2 and FS3): geometry, moment diagram and reinforcement

### K.1.5 Roof slab

For the roof slab of 150mm thickness the same method is applied as described for the floor slab. By making use of ETABS an indication of the amount of reinforcement is generated. In the longitudinal direction of the slab 1400 mm<sup>2</sup>/m rebar is required and 1191 mm<sup>2</sup>/m in the transfers direction. This corresponds to a basic reinforcement of  $\phi 12$ -100 mm, in both directions. In the longitudinal direction, four additional reinforcement bars of  $\phi 12$ mm should be applied in the design strip RS1.

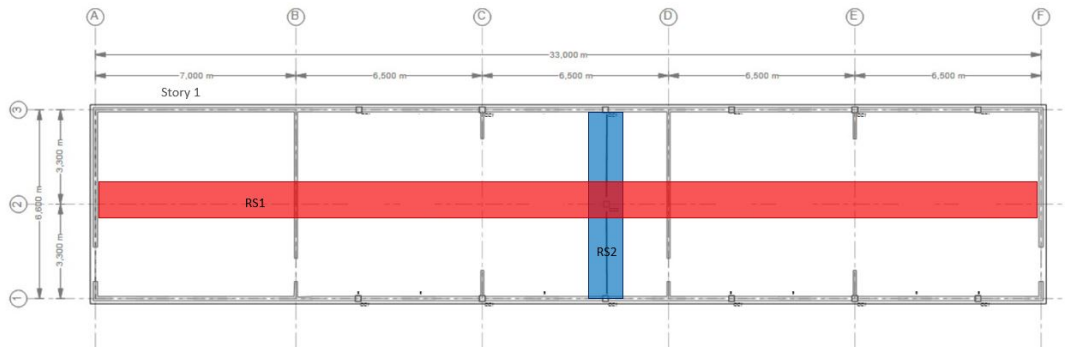


Figure K.6: Concrete roof slab: strip layout

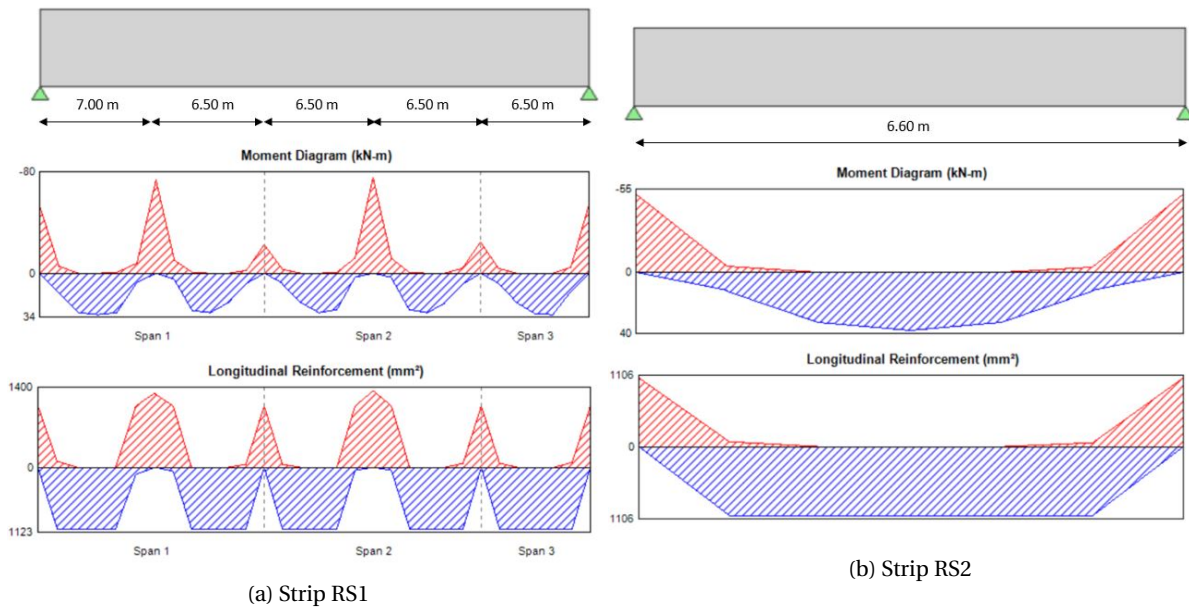


Figure K.7: Concrete roof slab strips: geometry, moment diagram and reinforcement

# L. Pavement Support Area

## L.1 Traditional concrete slab design

### L.1.1 Design parameters

#### Equivalent Single Axle Load

The loads that the pavement must support are expressed in equivalent single axle loads (ESALs) during the design life period. It is assumed that the traffic load will be 20 design trucks per day. This results in a traffic load of  $1.1 \times 10^6$  ESALs.

#### Reliability

A table can be found in MCV3 which gives an relationship between the traffic load, variability and the reliability factors:  $Z_R$  and  $S_0$ . From the table can be concluded that a  $Z_R$  of -0.253 can be applied. However, since it is the surface of a port, and not a road as suggested by the manual, it is decided together with the DoP to work with a reliability factor of -0.841. This value is suggested for concrete pavements by the Surface Design Manual of the DoP.

Table L.1: Reliability level and value of  $S_0$

ESALs (millions)	Reliability (%)	$Z_r$ (-)	$S_0$ in function of soil and traffic variability				
			15%	20%	30%	40%	50%
15	60	-0.253	0.35	0.36	0.37	0.39	0.40
15 to 30	60-70	-0.253 to -0.524	0.35	0.36	0.37	0.39	0.40
30 - 50	70 - 75	-0.524 to -0.674	0.34	0.35	0.36	0.38	0.39
50-70	75-80	-0.674 to -0.841	0.32	0.33	0.34	0.37	0.38
70-90	80-85	-0.841 to -1.037	0.30	0.31	0.32	0.35	0.36

#### Serviceability index

The serviceability of the pavement is implemented in the design formula in two different ways. An initial and a final serviceability has to be specified. The higher this value, the better the serviceability. The DoP did not specify any particular requirements concerning the serviceability thus the proposed values from the MCV3 are used. This means an initial serviceability index of 4.5 and a final serviceability index of 2.0.

#### Concrete properties

H30 concrete is used for the design and only the 28-day flexural resistance and the Young's modulus of the concrete are only relevant material properties. The chosen concrete has a flexural strength of 4.8 MPa and a Young's modulus of 29.000 MPa.

#### Subgrade reaction coefficient

The subgrade reaction coefficient is a parameter that is used to characterize the support capacity of the subgrade. MCV3 shows different theoretical or empirical methods to determine this parameter. If the CBR is known, which is the case since the backfilling soil can be chosen, it is possible to calculate the coefficient using the following formula:

$$k = 69.78 \log(CBR) - 10.16 \quad (L.1)$$

A backfilling with a CBR value of 40% results in a subgrade reaction coefficient of 102 MPa/m.

#### Properties base material

The Young's modulus of the base material and the friction coefficient between the pavement and the base are of importance for the design. MCV3 prescribes a friction coefficient of 0.7 between a granular base and an

concrete pavement, but a value of 0.5 is used due to the high rainfall in the area. A Young's modulus of 120 MPa is used.

### Berm factor

A standard berm factor is not perfectly applicable to the pavement in the support area, because the pavement does not have a berm like a normal road. However, a value of 0.94 for a concrete like berm is prescribed MCV3 and therefore this value is assumed.

### Temperatures and precipitation

The model required also some input related to the climate of the area. The meteorological data is obtained from a weather station from the general water directorate. The results are listed below:

- Wind speed 11.8 kts
- Average annual temperature 13deg C
- Average annual precipitation 1836 mm
- No. of days with more than 5 mm of rain 61

### Maximum tensile stress in the edge of the slab

The maximum tensile stress in the edge of a slab is used as input in the design formulas. This maximum stress takes into account the possible temperature differences. This stress is calculated using the following formula:

$$\sigma'_t = \sigma_l F_2 T B \left[ 1 + \left( \frac{5}{9} \right) b \Delta T (+) \right] \quad (L.2)$$

Where:

- $\sigma_l$  = Maximum tensile stress in the concrete slab for an edge load (MPa)
- $I$  = Relative stiffness ratio
- $E_c$  = Young's modulus of concrete
- $E_b$  = Young's modulus of the base
- $H_b$  = Thickness of the base
- $k$  = Subgrade reaction coefficient
- $\mu$  = Poisson's coefficient of concrete, 0.15
- $T B$  = Adjustment factor for type of berm
- $F_2$  = Friction factor

The unknowns that are listed above can be determined using the following formulas:

$$\sigma_l = \frac{8 \times 10^5}{D^2} \left[ 4.23 - 4.55 \left( \frac{180}{l} \right)^{0.2} - 1.58 \times 10^{-3} \left( \frac{E_b H_b}{k} \right)^{0.5} - 3.08 \times 10^{-2} \left( H_b \left( \frac{E_b}{E_c} \right)^{0.75} \right)^{0.5} \right] \quad (L.3)$$

$$I = 5.62 \sqrt[4]{\frac{E_c D^2}{12(1-\mu^2)k}} \quad (L.4)$$

$$F_2 = 1.12 - 2.46 \times 10^{-7} D E_b - 4.55 \times 10^{-4} D + 9.10 \times 10^{-5} E_b - 3.15 \times 10^{-4} f \quad (L.5)$$

$$\log b = -1.94 + 2.28 \frac{D}{I} + 91.7 \frac{L}{I} - 7.57 \times 10^8 \frac{D^2}{k I^4} + \frac{0.731}{I} \left( \frac{E_b H_b^{1.5}}{k} \right)^{0.5} - 119 \frac{D^2}{K I^2} - 8.71 \times 10^{10} \frac{D^3 L}{k I^6} \quad (L.6)$$

Where:

- $f$  = Coefficient of friction between slab and base
- $b$  = Adjustment factor for length of slab
- $L$  = Distance between two contradiction joints, 3.5 m
- $\Delta T(+)$  = Temperature factor

$$\Delta T(+) = 12.3 - \frac{339 \times 10^3}{D} + 0.707 \times WIND + 0.596 \times TEMP - 5.92 \times 10^{-4} \times PRECIP \quad (L.7)$$

$$\sigma_{L(AASHTO)} = \frac{8.00 \times 10^5}{D^2} \left( \frac{7.29}{D^{0.15}} \right) \quad (L.8)$$

$$F_{2(AASHTO)} = 1.19 - 4.97 \times 10^{-4} D \quad (L.9)$$

$$\log b_{(AASHTO)} = -1.94 + 0.134 D^{0.25} - 0 \quad (L.10)$$

From the equations follows a maximum tensile stress in the edge of the slab of 2.05 MPa.

#### Maximum tensile stress in the edge of a slab under AASHTO test conditions

The maximum tensile stress in the edge of a slab according AASHTO conditions is used as input in the design formulas. This maximum stress takes into account the possible temperature differences. The formula to determine the maximum tensile stress is the same as formula used in section L.1.1, but the used parameters are now calculated using the AASHTO test conditions, instead of the one that were calculated using MCV3.

$$\sigma_t = \sigma_{I(AASHTO)} F_{2(AASHTO)} \left[ 1 + \left( \frac{5}{9} \right) b_{(AASHTO)} \Delta T(+)(AASHTO) \right] \quad (L.11)$$

Where:

$$\sigma_{I(AASHTO)} = \frac{8.00 \times 10^5}{D^2} \left( 4.13 - \frac{7.29}{D^{0.15}} \right) \quad (L.12)$$

$$F_{2(AASHTO)} = 1.19 - 4.97 \times 10^{-4} D \quad (L.13)$$

$$\log b_{(AASHTO)} = -1.94 + 0.134 D^{0.25} - 1.37 \times 10^{-2} D^{0.5} + \frac{29.1}{D^{0.75}} - \frac{30.2}{D} - \frac{5.46 \times 10^2}{D^{1.5}} \quad (L.14)$$

$$\Delta T(+)(AASHTO) = 25.3 - \frac{2.53 \times 10^3}{D} \quad (L.15)$$

From the equations follows a maximum tensile stress in the edge of the slab according the AASHTO test conditions of 1.49 MPa.

#### L.1.2 Design verification Ministry of Housing and Urban Development

The calculated slab thickness by the AASHTO method is verified by the proposed model of the Ministry of Housing and Urban Development. The following design equations are used in this model:

$$W_{18} = \left( \frac{D + 25.4}{25.9} \right)^{7.35} 10^\alpha B^{4.22 - 0.32 p_f} \quad (L.16)$$

$$\alpha = \frac{\log\left(\frac{p_i - p_f}{3}\right)}{1 + \left(\frac{181}{D+25.4}\right)^{8.46}} + Z_R S_0 \quad (\text{L.17})$$

$$B = \frac{S'_c C_d}{1.48J} \left( \frac{D^{0.75} - 12.8}{D^{0.75} - 83.2 \left(\frac{k}{K_c}\right)^{0.25}} \right) \quad (\text{L.18})$$

Where:

- $C_d$  = Drainage coefficient of the base, 0.9
- $J$  = Load transfer coefficient, 3.7

The only unknown in the design equations is the traffic capacity, and this value is equal to 2.8 million ESALS. This is more than twice the amount than the traffic load as determined in section 4.3.2

## L.2 Short concrete slab design

### L.2.1 Design parameters

A further evaluation of all the parameters shown in table 9.3 can be found in this section. Most parameters are already elaborated for the traditional slab design. The width of the square slabs is chosen to be 1.75 meters. This value is chosen, because the Optipave only allows the slab length to vary between 1.4m and 2.3m. Since the vehicles in the support area drive in all directions and not just in one in a traditional way, the slab dimensions are limited by a maximum diagonal length of 2.3 meter. This results in a width of 1.75m. The maximum allowable faulting is 5 millimeter, just like for the traditional slabs. The allowable IRI at the end of the design life is 3.5 m/km. This value was specified by the DoP. The design reliability is not specified by a code, but from discussion with the DoP was concluded that a reliability of 80% is acceptable.

### L.2.2 Output OptiPave 2

The following design checks are performed by OptiPave:

- Percentage of cracked slabs
- Average amount of faulting
- International roughness index (IRI)

The progression of these parameters is shown in figure: L.1, L.2 and L.3. A vertical line can be found at 20 years, which is the design life of the pavement. The horizontal line indicated the maximum value of that parameter at the design life. From the graphs can be concluded that all the parameters do not reach the maximum value in all cases.

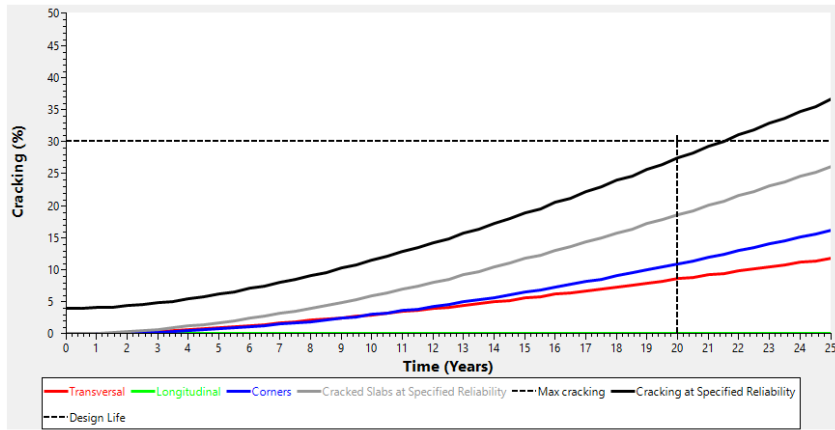


Figure L.1: Crack width design check

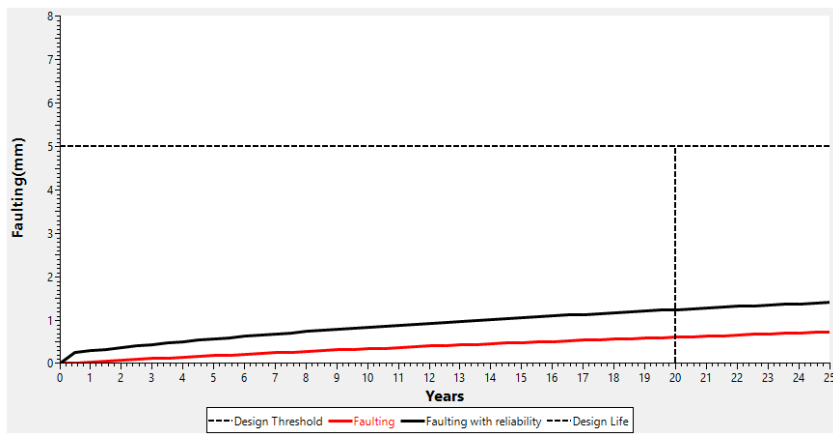


Figure L.2: Mean amount of faulting design check

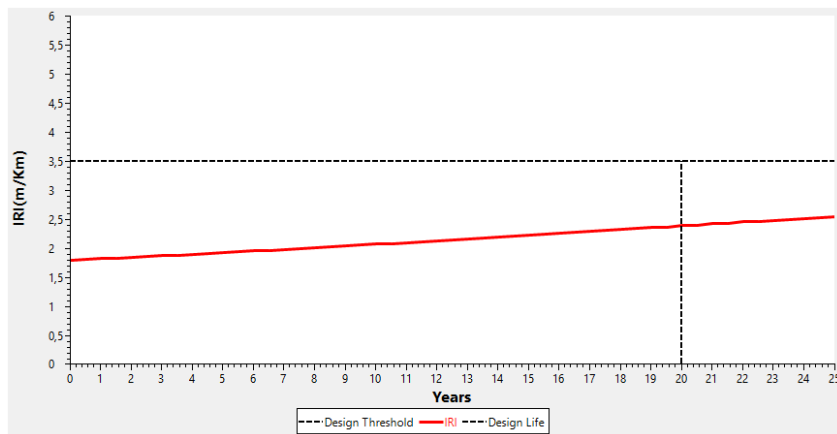


Figure L.3: IRI design check

# M. Pavement Access Road

## M.1 Surface treatment pavement design

### M.1.1 Design input: structural coefficients

Below the structural coefficients used for the design of the surface treatment pavement are given for the base, subbase and subgrade layer.

Table M.1: structural coefficient for bases between 0 and 250 mm

Base type	Structural coefficient
Stabilized with cement $R_7 > 4.6$ MPa	2.400
Stabilized with cement $R_7 > 2.8$ MPa	2.100
Stabilized with cement $R_7 < 2.8$ MPa	1.600
Stabilized with lime	1.400 - 1.600
Gravel CBR $\geq 100\%$	1.394
Gravel CBR = 90%	1.232
Gravel CBR = 85%	1.167
Gravel CBR = 80%	1.102
Gravel CBR = 75%	1.037
Gravel CBR = 70%	0.940
Gravel CBR = 60%	0.552
Gravel CBR = 50%	0.383

$R_7$  is the cylindrical compression resistance after 7 days.

Table M.2: Structural coefficients for subbases between 250 and 500 mm

Subbase type	Structural coefficient
Gravel CBR $\geq 40\%$	0.576
Gravel CBR = 35%	0.290
Gravel CBR = 30%	0.205
Gravel CBR = 25%	0.075

Table M.3: Structural coefficients for subgrade between 500 and 900 mm

Subgrade type	Structural coefficient
Gravel CBR $\geq 20\%$	0.481
Gravel CBR = 15%	0.357
Gravel CBR = 10%	0.212
Gravel CBR = 9%	0.183
Gravel CBR = 8%	0.133
Gravel CBR = 7%	0.084
Gravel CBR = 6%	0.053
Gravel CBR = 5%	0.033
Gravel CBR = 4%	0.020
Gravel CBR = 3%	0.015
Gravel CBR = 2%	0.010

### M.1.2 Design procedure

The basic design procedure to determine the thickness of the different layers, consists of 3 steps. First a required structural index (IER) is determined. Next, the minimum thickness of the base plus sub-base layer is determined and finally the thickness for all the separate layers is calculated. These steps are worked out below.

#### Step 1

The required structural index (IER) is a function of the equivalent number of axles (EE) that the pavement should be designed for, taking into account the design life time. Furthermore, the coefficient of variation (cv) is required as input. This value takes into account the variability in construction and is typically considered to be 25% in Chile. The formula used to determine the IER is:

$$IER(mm) = 1024cv^{0.354} \left( \frac{9.56}{11.49 - \log(EE)} - 1 \right) \quad (M.1)$$

#### Step 2

Depending on the CBR value of the subgrade, the minimum thickness of the base+subbase layer ( $e_{min}$ ) is determined, with equation M.2.

$$e_{min}(mm) = 592 - 308 \log(CBR) \quad (M.2)$$

#### Step 3

Finally, the thickness of each layer of the pavement structure is determined, such that the minimum required structural index (IER) requirement is fulfilled.

$$\sum_{i=1}^n e_i a_i \geq IER \quad (M.3)$$

$$e_{base} + e_{subbase} \geq e_{min} \quad (M.4)$$

Applying the three steps described above and by using an iterative procedure, a final design is made for the relevant design conditions. This design is presented in chapter 9 table 9.5.

## M.2 Asphalt concrete design

### M.2.1 Design parameters

The design parameters required as input in the design process of the asphalt pavement, are explained below. A summarizing table including a short description of the parameters and the final values is presented in Chapter 9 table 9.6.

#### Equivalent Single Axle Load (ESALs)

The stresses acting on the pavement are expressed as accumulated EE (ESALs) during the design life time of the structure. The calculation of these EE is already shown in previous sections. The values used in this analysis consider a design condition of 20 design trucks per day and the project life time of 20 years.

#### Reliability level

A table can be found in MCV3 which gives an relationship between the ESALs, variability and the reliability factors:  $Z_R$  and  $S_0$ . The table for flexible pavements, like the asphalt concrete pavement, is given below. The reliability factor  $Z_R$  is determined to be -1.037, based on a reliability percentage of 85%.

Table M.4: Reliability level and value of S<sub>0</sub> for flexible pavements

ESALs (millions)	Reliability (%)	Z <sub>r</sub> (-)	S <sub>0</sub> in function of soil and traffic variability				
			15%	20%	30%	40%	50%
<5	60	-0.253	0.45	0.46	0.47	0.49	0.50
15	60-70	-0.253 to -0.524	0.45	0.46	0.47	0.49	0.50
15 to 30	70-75	-0.524 to -0.674	0.45	0.46	0.47	0.49	0.50
30 - 50	75 - 80	-0.674 to -0.841	0.44	0.45	0.46	0.48	0.49
50-70	80-85	-0.841 to -1.037	0.42	0.43	0.44	0.47	0.48
70-90	85-90	-1.037 to -1.282	0.40	0.41	0.42	0.45	0.46

### Serviceability index

The serviceability of the pavement is implemented in the design formula in two different ways. First an initial serviceability has to be specified. The higher this value the better the serviceability. The final serviceability is the the lowest value that the index can reach at the end of the lifetime of the pavement. The DoP did not specify any particular requirements concerning the serviceability, therefore the proposed values from the MCV3 are used; an initial serviceability index of 4.2 and a final serviceability index of 2.0.

### Subgrade resilient modulus

The resilient effective subgrade modulus (M<sub>r</sub>) is the parameter characterizing the properties of natural soil at the project location, according to the design method AASHTO. M<sub>r</sub> represents the elastic modulus of the material after being subjected to cyclic loading. in this case this value is determined by considering the direct correlation with the CBR test value of the soil. The following equation is applied, valid for CBR between 12% and 80% :

$$Mr(MPa) = 22.1 (CBR)^{0.55} \quad (M.5)$$

### Minimum structural coefficient of layers

The minimum structural coefficient of the asphalt, base and subbase layer, is dependent on different factors, including the air temperature in the project area. The minimum NE for the asphalt layer (NE<sub>a min</sub>) and base+subbase layer (NE<sub>t</sub>-NE<sub>a min</sub>), can be determined by using the procedure prescribed in the MCV3. NE<sub>a min</sub> is determined to be 34.81 and (NE<sub>t</sub>-NE<sub>a min</sub>) is 23.95.

### Characterization of asphalt layer

For the asphalt layer of the pavement design, a single asphalt layer is considered because of the relatively low loading conditions. Resulting from the design procedure an asphalt concrete layer arises, whose Marshall Stability is not less than 9000N for all three design conditions. With the Marshall Stability value a structural coefficient of 0.43 is determined for the asphalt layer.

### Characterization of granular layer

For the granular layer, the use of a single layer base layer is considered, since it is expected that just the one layer will fulfill the design requirements. It is proposed to use a base layer of granular material with a CBR no less than 80%, for all three design conditions. This granular layer is associated with a structural coefficient of 0.13, calculated by the following relationship:

$$a_2 = 0.032(CBR)^{0.32} \quad (M.6)$$

The coefficient of drainage of the granular layer must be considered as well. For this the tables proposed in volume 3 of the Manual of Roads in Chile, are used. This manual differentiates the coefficients depending on the geographical area of the country, the fines content of the subgrade and the amount of precipitation in the project area. In this case the project is located in the VIII region of Chile, the fines content is below 10 percent and the average annual rainfall in Tirua is considered to be 1800mm. Considering the assumptions mentioned above, a coefficient of 1.15 is used.

### Calculating layer thickness

Considering the characteristics of the different layers as defined above, the thicknesses of the layers that make up the pavement are designed for the relevant design conditions:

Table M.5: Final design layer thickness and properties

Layer	Structural coefficient (a)	Drainage coefficient (m)	Thickness
Asphalt	0.43	-	90 mm
Base	0.13	1.15	170 mm

Table M.6: Minimum required and provided NE

NE	Minimum required	Provided value
NE Base	58.8	64.1
NE Asphalt	34.8	38.7
NE Total	23.9	25.4

## M.3 Short slab design

### M.3.1 Design parameters

#### Equivalent Single Axle Load

Similar to the previously worked out designs, it is assumed that the traffic load will be 20 design trucks per day, with a design life time of 20 years. This results in an equivalent number of axles of 1.1 million.

#### Soil parameters

Several parameters to be defined are the number of base layers, the erodibility of the base layer and the pavement-base friction coefficient. Furthermore, the resilient modulus during summer and winter of the subgrade layer and the poissons ratios of the different layers must be defined. All the parameters described above are defined by using the manual MCV3 and by discussion with the DoP. The final values are presented in table M.7.

Table M.7: Soil parameters required for short slab design

Number of base layers	1
Erodibility of base layer	1
Pavement-base friction coefficient	0.65
<b>Base</b>	
Resilient modulus	300 MPa
Poissons ratio	0.35
Thickness	150 mm
<b>Subgrade</b>	
Resilient modulus during winter	114 MPa
Resilient modulus during summer	137 MPa
Poissons ratio	0.4

#### Climate parameters

The model required also some input related to the climate of the area. The meteorological data is obtained from a weather station from the general water directorate. The results are listed below:

- Wind speed 11.8 kts
- Mean temperature winter season is 10.6deg C

- Mean temperature summer season is 15.6deg C
- Average annual temperature 13deg C
- Average annual precipitation 1836 mm
- No. of days with more than 5 mm of rain 61
- 122.3 days with precipitation per year
- Freezing index of 1.4

**Concrete properties**

For the design, only the 28-day flexural resistance and the Young's modulus are of interest. The concrete type applied for the short slab design, has a flexural strength of 4.8 MPa and a Young's modulus of 29.000 MPa.

# N. Meetings, Presentations and Lectures

## N.1 Meetings and presentations in chronological order

During our project we had four different general meetings with the DoP. The main purpose of these meetings was to have an open discussion with our clients and to present the obtained results. Detailed discussions were almost impossible during those general meetings. Therefore, next to the general meetings, we also had some specialized meetings with fewer people. The purpose of these meetings is to go more into depth to a particular problem. Next to those meetings some lectures were given by professors, to provide useful background information. A chronological overview of all meetings is shown in table N.1.

Table N.1: Overview meetings in chronological order

<b>Date</b>	<b>Type</b>	<b>Remarks</b>
17-Nov-17	General meeting	Introduction to project
24-Nov-17	General meeting	First presentation
24-Nov-17	Lecture	Earthquake general
01-Dec-17	General meeting	Second presentation
06-Dec-17	Site visit	Tumbes and Talcahuano
07-Dec-17	Lecture	Pavements
07-Dec-17	Lecture	Earthquake engineering
11-Dec-17	Lecture	Sheet pile wall
11-Dec-17	Specialized meeting	Breakwater configuration
13-Dec-17	Specialized meeting	Onshore building
15-Dec-17	General meeting	Third presentation
19-Dec-17	Specialized meeting	Discussion with fisherman
05-Jan-17	General meeting	Final presentation
10-Jan-17	General meeting	Follow-up meeting final presentation

## N.2 Summary meetings, presentations and lectures

### N.2.1 Abbreviation attendees

A short summary of each meeting is provided in this chapter. To keep the list of attendees as short as possible, abbreviations are used for each person.

Table N.2: Abbreviations of attendees

<b>Initials</b>	<b>Full Name</b>	<b>Specialization</b>
AN	Alfonso Neumann	Geotechnical Specialist (UdeC)
AS	Alvaro Sanhueza Orias	Student Udec
BC	Boris Castro Valdes	Student UdeC
CF	Cristian Figueroa de la Hoz	Project Engineer (DoP)
EA	Eriberto Arévalo	President of 1st Quidico Fishermans Union
FH	Fabian Fernandez Herrera	Architect (DoP)
FM	Fernando Matamala Cabezas	Project Engineer (DoP)
FN	Falko Noortman	Student TU Delft
FR	Felipe Retamal	Business Administrator (DoP)
FS	Felipe San Martin Albornoz	Student UdeC
JV	Javiera Paz Martin Canaves	Student UdeC
JV	Jose Vargas	Hydraulic Engineering Professor
MM	Mathijs Mann	Student TU Delft
MP	Mauricio Pradena Miquel	Head Supervisor Project
MR	Mark Ruessink	Student TU Delft
MV	Mario Valenzuela	Geotechnical Engineering Professor
PD	Peter Dechent	Structural Engineering Professor
RV	Ronald Verlinde	Student TU Delft
SD	Sergio Diaz	President of 2nd Quidico Fishermans Union
TS	Tamara Santos	Marine Biologist municipality of Tirua
WS	Wouter Sonnema	Student TU Delft

### N.2.2 General meeting: Introduction to project

- Date: 17 November 2017
- Location: DoP
- Attendees: AN, CF, FM, FN, MM, MP, MR, MV, PD, RV, WS

This meeting started with an introduction of the group to the department of ports. Afterwards CF gave a presentation where he gave an overview of the situation in Quidico. Followed with a discussion between the students and the DoP concerning the boundary conditions of the project. The most important boundary conditions that were defined during this meeting are listed below:

- The main hydraulical problems are that there is too much sediment in the area and the waves are too high in the bay
- The draft that should be used for the design is 1.5m
- A solution which included two breakwaters is proposed by a consultancy company
- The area close to the breakwater can be dredged
- Lifetime of the design should be 25 years
- A jetty is not required



Figure N.1: All attendees at the first meeting at the DoP

### **N.2.3 General meeting: First presentation**

- Date: 24 November 2017
- Location: UdeC
- Attendees: AN, BC, CE, FM, FN, FS, JV, MM, MP, MR, MV, PD, RV, WS

Only one week has passed since the last presentation. Therefore, the preparation time for this presentation was pretty short. The main focus of this presentation was to explain to the DoP how we interpreted their assignment and show them our first thoughts about possible solutions. The conclusions which could be drawn after the presentation are listed below:

- It can be assumed that no rocks are present in the soil
- A sheet wall pile is required for the mooring facilities
- Confined masonry is the preferred building material for onshore building
- The influence of the river will probably be small, but it may influence the sediments
- A solution without the second breakwater can be investigated

### **N.2.4 Lecture: Earthquake general by prof. Valenzuela**

- Date: 24 November 2017
- Location: UdeC
- Attendees: AN, AS, BC, FN, JV, MV, RV, WS

Professor Valenzuela gave a lecture about earthquakes in general and about which Chilean codes are applicable to earthquake engineering in Chile. The first part of the lecture was an explanation of the general engineering philosophy. The main focus lies with ductile engineering versus earthquakes. The main topics that were discussed are listed below:

- Chili is divided in three different earthquake areas

- The ground peak acceleration that should be used in the calculations depends on the seismic zone
- The ground peak acceleration hugely depends in the soil type
- NCh431 can be used for earthquake engineering in Chile

### N.2.5 General meeting: Second presentation

- Date: 1 December 2017
- Location: DoP
- Attendees: AN, BC, CE, FM, FN, FS, MM, MP, MR, MV, PD, RV, WS

Three Chilean students joined the project group. From this moment the Chilean and Dutch students are working together. This presentation started with a recap of the information received last presentation from the DoP. Afterwards, the first concept designs were shown of the breakwater configuration and the confined masonry building. The main topics that were discussed are listed below:

- Cocinerias should not be implemented in the building design, because they are illegal
- Liquefaction should be taken into account.

### N.2.6 Site visit to reference project: Tumbes and Talcahuano

- Date: 6 December 2017
- Location: Tumbes and Talcahuano bay
- Attendees: AN, BC, FN, RV

To assist as reference for the design of the onshore building, the mooring facilities and the pavement, several fishermen harbours are visited and analyzed. Two of the most relevant fishermen harbours are the harbours of Tumbes and Talcahuano.

#### Talcahuano fishermen harbour

This fishermen harbour is part of the bigger harbour area of Talcahuano, including a harbour for the national navy and a large scale container port. The interesting part for our project was the onshore building including all supporting facilities. The project engineers of the Department of Ports, mentioned several times that this building would give a good idea of what is expected in Quidico Bay. Just like the future building in Quidico, this building includes storage units, office areas and public facilities like bathrooms and meeting rooms. The fishermen harbour building of Talcahuano is however of a larger scale.



Figure N.2: Reference building Talcahuano

Besides the building, also the mooring facility of Talcahuano was of interest for our project. The quay wall was performed as a concrete mass wall. Connected to this wall, a mooring place made from steel was present

to enable discharge activities. This mooring facility was accessible during both during high as low tide. The pavement applied in the support area was a concrete slab foundation, with a grid size of about 3.0 meters.



Figure N.3: Steel mooring facility Talcahuano

### **Tumbes fishermen harbour**

The bay of Tumbes was considerably different compared to the harbour of Talcahuano. The supporting facilities were much more basic. The fishermen of Tumbes did not have an onshore building including supporting facilities and also no paved support area was present. There was however a small jetty, including mooring places and a small crane to offload heavy catches. This jetty also served as mooring facility for touristic boat tours. Tumbes is a great example of a bay where artisinal fishery attracts visitors. They provide good food and create a special atmosphere.

Since the main supporting element for the fishermen is the jetty, the relevance for our project is small. There is jetty necessary in Quidico. An aspect of interest for us was the quay wall and the ramp. In Tumbes the wall was performed by concrete mass walls and the ramp was constructed as a concrete slab resting on a filling. This filling was contained by another concrete mass wall.



Figure N.4: Quay wall Tumbes

## **N.2.7 Lecture: Pavements by prof Pradena**

- Date: 7 December 2017
- Location: UdeC
- Attendees: AS, BC, FN, FS, JV, MP, RV, WS

Professor Pradena gave a lecture about pavements. Since the Dutch student hardly have any experience with pavement designs, the lecture was more like a brief introduction. Two different pavement designs were shown: asphalt and concrete. Different dimensions for the concrete slabs were presented and especially the short slabs are of interest for the project. The main topics are summarized below:

- Concrete pavements are way more common in Chile compared to the Netherlands

- The capacity of a concrete slab is hugely dependent on the size of the slab
- Short slabs should be taken into account for the pavement in the supporting area

### **N.2.8 Lecture: Earthquake engineering by prof Dechent**

- Date: 7 December 2017
- Location: UdeC
- Attendees: FN, FS, PD, RV, WS

Professor Dechent is the structural dynamics specialist of UdeC. He gave a lecture about basic design versus earthquakes. The most important lessons from professor Dechent are listed below:

- Never trust computers models and always make some calculations by hand
- When modelling an earthquake, always include the properties of different soil layers
- A symmetrical structure is always preferred in a structure is designed in an earthquake prone area.
- Torsion due an earthquake load should be taken into account

### **N.2.9 Lecture: Sheet pile wall by Alfonso Neumann**

- Date: 11 December 2017
- Location: UdeC
- Attendees: AN, FN, RV, WS

This lecture was requested by the students, because there were some uncertainties concerning the sheet pile wall design. The design for the sheet pile wall was already made, this design was discussed with AN. The basis of the design was acceptable, but AN told the advantages of more advanced calculation methods. This methods could be used in a later stage to optimize the design. The conclusions of the meeting were:

- One anchor is sufficient for the design conditions
- An extra 20 to 40% embedded depth is suggested as a safety factor
- The earthquake load of the active soil can be modeled as the weight of the sliding wedge times an acceleration factor.

### **N.2.10 Specialized meeting: Breakwater configuration**

- Date: 11 December 2017
- Location: DoP
- Attendees: AS, CF, FM, MM, MR

During the project we have had several presentations and discussions with people from Universidad de Concepcion and people from the Department of Ports. This day we had a meeting with only people involved in the Hydraulic part of this project. During this meeting Cristian Figueroa de la Hoz and Fernando from the Department of Ports were present. During this meeting, The Delft3D model was discussed and some other questions were asked. First, the model results were roughly presented and discussed. The conclusion was that the model seems to work relatively good near-shore. After a small discussion about the model, we had a good discussion about the breakwater and its configuration. The initial orientation of the breakwater was not satisfactory for the fishermen and, therefore some new directions were discussed. By drawing some layouts on a smart board, we came to new configurations. By using the programs Global Mapper and Google Earth, the best locations and directions for the breakwater were obtained. We checked the most unfavorable angle of the waves and their corresponding heights. There were also some new updates about the project. These design phases should be considered during the breakwater design:

1. First the outer breakwater is constructed, without any dredging.
2. Monitoring the processes for a certain period.
3. If there is too much sediment, construct the contramolo or apply dredging.
4. Construct the mooring places.
5. Construct the storage area and houses.

The main design requirements are set during this meeting and listed below:

- The stones in front of the bay must be used as foundation for the first part of the breakwater (figure 5.1)
- The end of the breakwater must be out of the breaking zone
- Protection of the mooring facility against the most unfavorable waves
- Consider the sediment movement around Quidico

We talked about the new configurations of the breakwater. With the models we already got, the ones Cristian has and the depth files. From this, we looked for an alternative of the configuration of the breakwater. This is done by looking at the most guiding waves for the fishermen and not only for the breakwater. From the wind and wave rose and the location of the Island, it became clear that waves coming from the West to North-West are most guiding for the fishermen, as can be seen in figure 4.17.

Finally, we came to three final designs. All with the first part in extension of the bay. Then the second part will be with an angle of around 45 degrees, number 2 in figure N.5b. The question is how long the construction of part 2 would be. That was our task for the coming time. To figure out what the length must be and what the influence of the return current and refraction/diffraction would be. Because we knew diffraction is not included in Delft3D, diffraction would be done with rules of thumb.



(a) Discussion with Cristian and Fernando from DoP



(b) Final design

Figure N.5: Meeting at the Department of Ports

After all it was a very useful and efficient meeting. For the next meeting the new configurations are investigated.

### N.2.11 Specialized meeting: Onshore building

- Date: 13 December 2017
- Location: DoP
- Attendees: CF, FM, FH, FN, JV, RV

The reason of this meeting was to discuss the exact building requirements concerning the functional design of the onshore supporting building. The architect showed some buildings that could function as reference projects. The building that was most similar, was the harbour building of Coliumo. This building also contains storage boxes on ground level and an office on the second floor. The first floor is constructed from concrete and the top floor from steel. Besides storage boxes and offices, the building also contains multiple bathrooms.

One of the bathrooms is accessible for disabled people. Furthermore, a large ramp is build on one side of the building to enable disabled people to enter the second floor of the building. This design of the ramp will be copied for the building design of Quidico.



Figure N.6: Reference building Coliumo

The design requirements that followed from the meeting are the following:

- The entire building has to be made from reinforced concrete
- The building should be accessible for disabled people
- The minimum dimensions of the bathrooms specified
- The office should be accessible from both sides of the building
- A ramp is required for disabled people

### **N.2.12 General meeting: Third presentation**

- Date: 15 December 2017
- Location: UdeC
- Attendees: AN, BC, CF, FM, FN, FS, MM, MP, MR, MV, PD, RV, WS

The goal of this presentation to show the concept design that every specialty made. The presentation started with the design and configuration of the breakwater. Afterwards this breakwater was modelled from Geo-technical point of view, mostly focused on the risk of liquefaction. The design of the mooring facility followed afterwards and the presentation ended with the design of the onshore buildings. The following conclusions were taken from the discussion with the DoP during the presentation:

- The breakwater solution without the contramolo looked promising
- The height of the anchor position was something that should be investigated
- A safety factor of 1.2 and of 1.1 should be used for safety against sliding and rotation respectively for the concrete mass wall
- The distribution of stiffness of the concrete building was not sufficient.

### **N.2.13 Specialized meeting: Discussion fisherman**

- Date: 19 December 2017
- Location: Quidico
- Attendees: AS, BC, CF, EA FR, JV, MR, SD, TS

During this meeting it became clear that the fishermen need the breakwater as fast as possible. They have seen that in the village next to Quidico, named Tirua, the breakwater works well. The fishermen want a harbour with more mooring places. In the current situation, the boats are stored at the beginning of the river. For these mooring places, also a breakwater is necessary. Further the problem with the existing cocinerias was discussed again. The fishermen do not think this is their responsibility. Also, the Department of Ports is not in charge of this. A solution is not made during this meeting. Also, the question who is responsible for the illegal cocinerias and how to get them away is still open.

As already stated in the report, the fishermen were not satisfied with the first proposal from the Department of Ports. With the results of the Delft3D model and some common sense, we came to a new design which is a breakwater which is 90 meters long in northern direction than makes a 45 degree turn in the eastern direction. This second part which is also 90 meters long, will therefore point in north-eastern direction. They were quite enthusiastic about this proposed design.

When visiting the bay, the fishermen were pointing in the direction where they want the breakwater. This direction corresponded with the direction of our new proposal. During this site-visit, the ocean was rough, and it became clearer why a breakwater is necessary in this area. Waves were estimated by the fishermen around 4 meters near the shore. During these conditions they will never go out for fishing. The maximum wave height that they will go fishing is around 2.5 meters if the wind is not too strong.



(a) Rough wave conditions



(b) Breaking waves

Figure N.7: Waves just outside Quidico Bay

## N.2.14 General Meeting: Final Presentation

- Date: 5 January 2018
- Location: UdeC
- Attendees: AN, BC, CE, FM, FN, FS, MM, MR, MV, PD, RV, WS

The main goal of the final presentation was to show the final results without too many discussions. In the prior presentations, there was time reserved for discussion during the presentation. This time was skipped during this presentation. The comments of the DoP and other attendees at the final presentation are listed below:

- The DoP would like to see more results of what would happen with the currents and waves in the bay
- The thickness of the sheet pile wall was too thin
- The different building phases of the sheet pile wall should also be used as load cases
- The thickness of the slab in the concrete building design was too thick
- A steel roof is the preferred solution in the concrete building instead of a concrete slab



Figure N.8: Final presentation for the DoP

## N.2.15 Follow-up meeting final presentation

- Date: 10 January 2018
- Location: DoP
- Attendees: AS, BC, CE, FM, FN, JV, MM, MR, RV, WS

The DoP had some questions after the final presentation. Through the fact that they are going to read and probably use this report, they had some recommendations. During this meeting the following subjects were discussed concerning the breakwater:

- Circulation and the return current were not visible in the model
- It was concluded that some processes near-shore were not modelled well,
- A Boussinesq model could be an option for further research
- It was not entirely clear why was chosen for the 100 meter breakwater
- Wave height at the mooring facility should still be calculated
- Waves from south to south-west contain more energy, influence of these waves should be investigated
- Toe diameter should be 1 ton according calculations, but maybe larger stones are more practical

The following subjects were discussed concerning the sheet pile wall:

- The diameter of the anchors still needs to be worked out
- An anchor spacing of 1.8-2 meter is used in practice and a bar thickness of 1.25 inch
- A thickness of 7.5mm is acceptable and used in practice
- Larssen 601 is a typically used sheet pile wall in Chile
- Profiles of Arcelon should also be checked

The following conclusions could be considered for the onshore building:

- A floor slab thickness of 150 milimeter should be considered
- The roof should be made out of steel instead of timber, due to durability reasons
- An area of especially made for the selling of goods should be included in the design

After the meeting we received a list from the DoP, that the following points should be included in the report:

1. Include modelling results of natural conditions in the current situation and with a breakwater and/or contramolo.
2. Include operational analysis of the sheltered area.
3. Include recommendations about if a contramolo will be needed.
4. Include a quantitative analysis of accretion/erosion product of the breakwaters (e.g., annual rate).
5. Analyse what will happen with the depth in the bay.
6. Include an analysis of the construction work in phases, considering the changes in the sedimentological dynamics.
7. Consider increasing the size of the rock at the toe of the breakwater section due to its proximity to the low tide level.
8. Think about using commercial diameters in sheet pile anchoring bars.
9. Complement the information of short slabs for the paving of the esplanade.
10. Design the building considering the guidelines of the building in Coliumo.

# O. Relevant Rules and Regulations

The Chilean standards are largely based on the standards of the United States. The Chilean codes are applied in all cases where applicable. When an appropriate check could not be found in the Chilean codes, the American codes are used. The European codes are only used as reference.

<b>Code</b>	<b>Description</b>
AISC 2010	Specification for structural steel buildings
MCV3	Manual de Carreteras, Volumen 3 (Chilean highway manual)
NEN-EN 1993	Design of steel structures
NEN-EN 1994	Design of composite steel and concrete structures
NEN-EN 1998	Design of structures for earthquake resistance
NCh 427	Specification for calculating steel structures
NCh 430	Specification for reinforced concrete
NCh 431	Calculation of snow loads on buildings
NCh 432	Calculation of wind load on buildings
NCh 433	Seismic design of buildings
NCh 1508	Specification for soil mechanics
NCh 1517-1	Calculation of the liquid limit
NCh 1517-2	Calculation of the plastic limit
NCh 1537	Permanent load and life load
NCh 3171	Load combinations

# Bibliography

- [1] M. Adriles. “La Serie Occidental del basamento metamorfoico, centro sur de la Cordillera de Nahuelbuta, Chile, area Quidico-Capitan Pastene. Petrografia, mesoestructura y analysis microtectonico.” Thesis degree. Universidad de Concepcion, Department of Earth Sciences, Chile, 2003.
- [2] R. D. Andrus and K. H. Stokoe. *Liquefaction resistance based on shear wave velocity*. Tech. rep. 1997.
- [3] BMT Argoss. *Coordinate Systems Worldwide*. Dec. 2017. URL: <http://www.waveclimate.com>.
- [4] ASTM-International. *ASTM D2487-06, Standard Practice for Classification of Soils for Engineering Purposes (USCS)*. Tech. rep. 2006.
- [5] ASTM-International. *ASTM D6066-96, Standard Practice for Determining the Normalized Penetration Resistance of Sands for Evaluation of Liquefaction Potential*. Tech. rep. 2004.
- [6] A. P. Blake. *Forecast Error Bounds by Stochastic Simulation*. National Economic Review, 1996.
- [7] S. Bonnefoy-Claudet et al. “H/V ratio: a tool for site effects evaluation. Results from 1-D noise simulations”. In: *Geophysical Journal International* 167.2 (Nov. 2006), pp. 827–837.
- [8] Judith Bosboom and Marcel J.F. Stive. *Coastal Dynamics 1*. Delft University of Technology, 2015.
- [9] M. J. Briggs et al. “Wave diffraction around Breakwater”. In: *JOURNAL OF WATERWAY, PORT, COASTAL, AND OCEAN ENGINEERING* (1995).
- [10] CATDS. *Sea Surface Salinity Remote Sensing at CATDS Ocean Salinity Expert Center*. Dec. 2017. URL: <http://www.salinityremotesensing.ifremer.fr/>.
- [11] K. Cihan and Y. Yuksel. “Deformation of breakwater armoured artificial units under cyclic loading.” In: *Applied Ocean Research* 42.1 (2013), pp. 79–86.
- [12] K. Cihan, Y. Yuksel, et al. “Behavior of homogenous rubble mound breakwaters materials under cyclic loads.” In: *Soil Dynamics and Earthquake Engineering* 34.1 (2012), pp. 1–10.
- [13] CIRIA, CUR, and CETMEF. *The Rock Manual. The use of rocks in hydraulic engineering*. C683, CIRIA, London. 2007.
- [14] Deltares. *Delft3D-FLOW Manual*. Deltares, 2014.
- [15] EPSG. *Coordinate Systems Worldwide*. Dec. 2017. URL: <https://epsg.io/32718>.
- [16] GeographyPhotos. *Large breakwater concrete groyne Newhaven, East Sussex, England*. Dec. 2017. URL: <https://geographyphotos.photoshelter.com/image/I0000t5VdvArBxTo>.
- [17] J. Glodny et al. “Differential Late Paleozoic active margin evolution in South-Central Chile (37S-40S) the Lanalhue Fault Zone.” In: *South American Earth Sciences* 26.4 (Dec. 2008), pp. 397–411.
- [18] Google-Earth. *Google*. Dec. 2017. URL: <http://https://www.google.com/intl/es/earth/>.
- [19] Leo H. Holthuijsen. *Waves in Oceanic and Coastal Waters*. Cambridge University Press, 2007.
- [20] I. M. Idriss. *Seed Memorial Lecture*. University of California at Berkeley, 1995.
- [21] I. M. Idriss and R. W. Boulanger. *Semi-empirical procedures for evaluating liquefaction potential during earthquakes*. Tech. rep. 2004.
- [22] I. M. Idriss and R. W. Boulanger. *SPT Based Liquefaction Triggering Procedures*. Department of Civil and Environmental Engineering, University of California at Davis., Dec. 2010.
- [23] IOC. *SEA LEVEL STATION MONITORING FACILITY*. Dec. 2017. URL: <http://www.ioc-sealevelmonitoring.org>.
- [24] R. Kaznbach, F. Clauss, and S. Rochee. “Recent developments in procedures for estimation of liquefaction potential of soils.” In: *18th International Conference on Soil Mechanics* (2013).

- [25] A. Krueger and E. Gilbert. “Deepwater Fold Thrust Belts Not All the Beasts Are Equal”. In: *Search and Discovery Article* (2009).
- [26] S. S. C. Liao and R. V. Whitman. “Overburden Correction Factors for SPT in Sand.” In: *Journal of Geotechnical Engineering* 112.3 (Mar. 1986), pp. 272–377.
- [27] M. A. A. N. Mahmoud. “Reliability of using standard penetration test (SPT) in predicting properties of silty clay with sand soil.” In: *International Journal of civil and structural engineering* 3.3 (2013), pp. 545–556.
- [28] Navionics. *Chart Viewer*. Dec. 2017. URL: [https://webapp.navionics.com/?lang=en#boating@6&key=b\\_y\\_Fnqz%7CL](https://webapp.navionics.com/?lang=en#boating@6&key=b_y_Fnqz%7CL).
- [29] Ingenieria Civil Oceanica. *Atlas de Oleaje de Chile*. Dec. 2017. URL: <http://www.oleaje.uv.cl/regiones.php>.
- [30] Donghong Pei. “Modeling and Inversion of Dispersion Curves of Surface Waves in Shallow Site Investigations.” PhD thesis. University of Nevada, Aug. 2007.
- [31] A. F. Rauch. “Evaluating Cyclic Liquefaction Potential Using Cone Penetration Test”. In: *Canada Geotechnical Journal* 35.3 (Apr. 1998), pp. 442–459.
- [32] G. J. Schiereck and H. J. Verhagen. *Introduction to bed, bank and shore protection*. VSSD, 2016.
- [33] H. B. Seed and I. M. Idriss. “Simplified procedure for evaluating soil liquefaction potential”. In: *Journal of the Soil Mechanics and Foundations Division* 107.9 (Apr. 1971), pp. 1249–1274.
- [34] Sernageomin. *Mapa geologico de Chile*. Tech. rep. 2000.
- [35] *Sheet Piling Handbook*. 3rd ed. ThyssenKrupp GfT Bautechnik. Apr. 2010.
- [36] *Steel Sheet Piling Design Manual*. United States Steel. July 1984.
- [37] K. Terzaghi and R. B. Peck. *Soil Mechanics in Engineering Practice*. Wiley, 1948.
- [38] The-Geological-Society. *PLate Tectonics*. Dec. 2017. URL: <https://www.geolsoc.org.uk>.
- [39] USGS. *EarthExplorer*. Dec. 2017. URL: <https://earthexplorer.usgs.gov/>.
- [40] USGS. *The Tectonic Plates of the World*. Sept. 2011. URL: <https://pubs.usgs.gov/gip/dynamic/slabs.html>.
- [41] E. Vossenaar. “The effects of induced earthquakes on the breakwaters in Groningen.” Master thesis. Delft Technical University, 2017.
- [42] Wikipedia. *Ocean currents*. Dec. 2017. URL: [https://en.wikipedia.org/wiki/Ocean\\_current](https://en.wikipedia.org/wiki/Ocean_current).
- [43] Wikiwand. *Properties of water*. Dec. 2017. URL: [http://www.wikiwand.com/en/Properties\\_of\\_water](http://www.wikiwand.com/en/Properties_of_water).
- [44] T. L. Youd and I. M. Idriss. *Proceedings of the NCEER Workshop on Evaluation of Liquefaction Resistance of Soils*. Tech. rep. Dec. 1997.
- [45] T. L. Youd, I. M. Idriss, and R. D. Andrus. “Liquefaction Resistance of Soils: Summary Report from the 1996 NCEER and 1998 NCEER NSF Workshops on Evaluation of Liquefaction Resistance of Soils.” In: *Journal of Geotechnical and Geoenvironmental Engineering* 127.10 (Oct. 2001), pp. 817–833.
- [46] T. L. Youd, Member, et al. “Liquefaction Resistance of Soils: Summary of the 1996 NCEER and 1998 NCEER NSF Workshops on Evaluation of Liquefaction Resistance of Soils.” In: *Journal of Geotechnical and Geoenvironmental Engineering* 127.10 (Apr. 2011), pp. 817–833.